2017 | Faculty of Medicine and Life Sciences

▶▶

UHASSELT

KNOWLEDGE IN ACTION

Maastricht University

Doctoral dissertation submitted to obtain the degree of
Doctor of Biomedical Science, to be defended by

Jacobine Kuijlaars

DOCTORAL DISSERTATION
Neuronal networks *in vitro*:
from rat to men

BIOMED
BIOMEDICAL
RESEARCH INSTITUTE

▶▶ **UHASSELT**

Promoter: Prof. Dr Bert Brône | UHasselt

Co-promoters: Prof. Dr Theo Meert | UHasselt
                   Dr Rony Nuydens | Janssen Pharmaceutical Companies
                        of Johnson & Johnson

Members of the jury

Prof. Dr Marcel Ameloot	Hasselt University, Diepenbeek, Belgium, chairman
Prof. Dr Bert Brône	Hasselt University, Diepenbeek, Belgium, promotor
Prof. Dr Theo Meert	Hasselt University, Diepenbeek, Belgium and
	Janssen R&D, Beerse, Belgium, co-promotor
Dr Rony Nuydens	Janssen R&D, Beerse, Belgium, co-promotor
Prof. Dr Jean-Michel Rigo	Hasselt University, Hasselt, Belgium
Prof. Dr Ivo Lambrichts	Hasselt University, Diepenbeek, Belgium
Prof. Dr Sven Hendrix	Hasselt University, Diepenbeek, Belgium
Prof. Dr Winnok H. de Vos	Antwerp University, Antwerp, Belgium and
	Ghent University, Ghent, Belgium
Prof. Dr Sally A. Cowley	University of Oxford, Oxford, United Kingdom

Contents

3. Neuronal networks in a tau overexpression model in primary rodent and hiPSC-derived cortical cultures 63

Scientific Curriculum Vitae

Dankwoord

List of abbreviations

AAV6	adeno-associated viral serotype 6
AD	Alzheimer's disease
AM	acetoxymethyl
ApoE	apolipoprotein E
APP	amyloid precursor protein
BDNF	brain derived neurotrophic factor
BiFC	bimolecular fluorescence complementation
CNQX	6-Cyano-7-nitroquinoxaline-2,3-dione
CSF	cerebrospinal fluid
D-AP5	D-(-)-2-Amino-5-phosphonopentanoic acid
DAPT	N-[N-(3,5-Difluorophenacetyl)-L-alanyl]-S-phenylglycine t-butyl ester
DIV	day in vitro
DM	double mutant
DTT	1,4-dithiothreitol
E1, E2, …	exon 1, exon 2, …
fAD	familial Alzheimer's disease
FBS	fetal bovine serum
FDG	fluorodeoxyglucose
FTD	frontotemporal dementia
GDNF	glial derived neurotrophic factor
GECI	genetically encoded calcium indicator
GFP	green fluorescent protein
HBSS	Hanks balanced salt solution
HCS	high-content screening
HGPS	Hutchinson-Gilford Progeria syndrome
hiPSC	human induced pluripotent stem cell
HTS	high-throughput screening
ICC	immunocytochemistry
K18P301L	P301L mutated tau fibrils
LTD	long-term depression
LTP	long-term potentiation
MAPT	microtubule associated protein tau
MCI	Mild Cognitive Impairment
MEA	multi-electrode array
MEM	minimal essential medium
mGRASP	mammalian GFP Reconstitution Across Synaptic Partners
MOI	multiplicity of infection
MTBD	microtubule-binding domain
MW6, MW96	multiwell 6, multiwell 96
NFT	neurofibrillary tangle
NMDA	N-methylD-aspartate
NPC	neural precursor cell
NT	neurotransmitter
P301L hTau	human mutant P301L tau
PDL	poly-D-lysine
PEI	polyenimine
pFTAA	pentameric formyl thiophene acetic acid
PHF	paired helical filament
PLO	poly-L-ornithine
PS1	presinilin 1
PS2	presinilin 2
PSD	postsynaptic density
ROI	region of interest

sAD	sporadic Alzheimer's disease
SEM	standard error of the mean
SER	Spot-Edge-Ridge
SM	single mutant
sPSC	spontaneous synaptic current
TTX	tetrodotoxin
WT hTau	wildtype human tau
ZFN	Zinc Finger Nuclease

1

General introduction

1.1 Neuronal networks and cognition

According to the Oxford dictionary [1] cognition is "the mental action or process of acquiring knowledge and understanding through thought, experience, and the senses", which is an essential function of our brain for survival. The underlying mechanisms of cognition have been studied for many years and a key process in cognition is synaptic transmission. Synapses are the defining feature of neurons, enabling communication between these cells and eventually within and between neuronal circuits or networks. The idea of synaptic transmission was first illustrated by Santiago Ramón y Cajal in 1894, who described that electrical signals are transferred from the presynaptic to postsynaptic element via chemical neurotransmission. He also postulated that changes in strength of connections between neurons could be the mechanism of memory formation [2], called synaptic plasticity. In 1949, this idea was further expanded by the hypothesis that simultaneous activation of two neurons strengthens their connection, while separate activation weakens their connection [3]. Molecular understanding of synaptic plasticity was elucidated almost 25 years later by Bliss and Gardner-Merwin, who described long-term potentiation (LTP) and long-term depression (LTD) [4]. In the healthy adult brain, synaptic plasticity is the proposed neurochemical and structural basis of learning and memory, with essential roles for the hippocampus and neocortex [5].

The formation of neuronal networks involved in cognitive tasks such as learning and memory is driven by molecular pathways that are encoded by developmental programs. During embryonic and early post-natal development neurons start to form neurites that will develop in either axons or dendrites and eventually interconnect via synaptic contacts to form neuronal networks. Specialized presynaptic structures will form at the axonal terminals where neurotransmitters (NTs) will be transmitted to postsynaptic terminals on the dendrites of connected neurons via the synaptic cleft (Fig. 1.1). These structures are not rigid and continuous remodeling of pre- and postsynaptic elements is involved in synapse function and maturation. Presynaptic terminals include active zones where molecular components are present involved in synaptic vesicle loading, turnover, docking, fusion and endocytosis. Postsynaptic machinery is present on dendritic shafts and dendritic spines contain the active zones involved in glutamatergic signaling. These dendritic spines are known to change density and shape in response to synaptic transmission. The dynamic synaptic transmission involves many different steps that can be physiologically regulated or pathologically dysregulated (Fig. 1.1) [6]. Presynaptic vesicles are loaded with NTs, followed by transport towards and fusion with the presynaptic membrane as a result of electrical stimulation. This process highly depends on vesicular transporters (for example vGLUT and vGAT), ion channels involved in propagation of voltage signals and subsequently proteins involved in vesicle fusion, like SNARE complex proteins. Voltage-gated calcium channels allow the entrance of calcium into the presynaptic terminal. This calcium signal triggers

vesicle fusion, followed by NT release into the synaptic cleft, with an associated loss of protons from the vesicle when the acidic vesicle lumen fuses with the neutral environment of the synaptic cleft. Finally, NT molecules bind to postsynaptic receptors in order to activate postsynaptic signaling cascades.
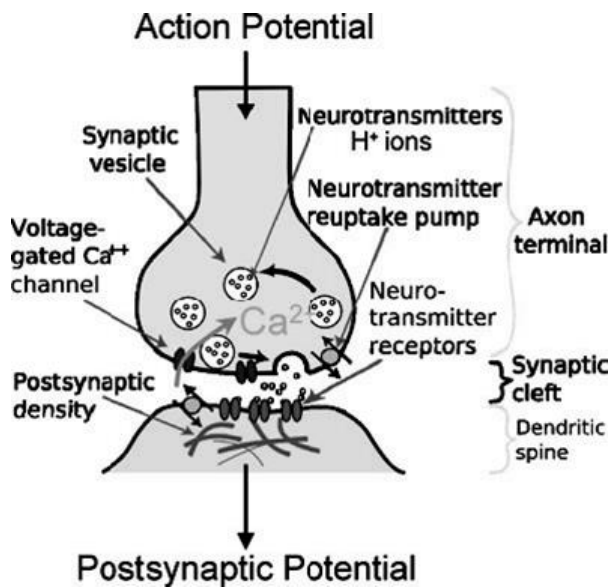
Figure 1.1 Schematic representation of synaptic transmission. This diagram represents some of the key steps in synaptic transmission, for example changes in membrane potential induced by an action potential, influx of calcium ions into the presynaptic element, synaptic vesicle fusion, and subsequent release of neurotransmitters into the synaptic cleft, followed by the generation and propagation of the postsynaptic potential. Adopted from Dreosti and Lagnado 2011 [6].

During development neurons show sporadic electrical activity. Robust neuronal network activity develops over time when electrical activity synchronizes. Pruning of the neuronal network is necessary for fine tuning and highly depends on spontaneous and experience-driven electrical activity stimulating synaptic connectivity and maturation [7-9]. These highly synchronized bursting patterns have been shown in different brain regions *in vivo* [8,10], *in vitro* in brain slices [11,12], and even in dissociated primary neuronal cultures [7,13]. Therefore, spontaneous activity is thought to be an intrinsic property of neurons, regulating synaptic transmission efficacy and cytoplasmic protein and membrane receptor trafficking [8,9,14]. This functional development of biological networks is often exemplified by live cell calcium imaging and clearly shows the maturation of neuronal networks *in vitro* [13]. Similarly, *in vitro* data show that structural correlates of *in vivo* network formation can be recapitulated in cultures of dissociated rodent neurons [13]. Verstraelen and colleagues showed that neurite outgrowth and synapse formation occur exponentially in the first week subsequent to dissociation after which the network expansion slowed down. Synaptogenesis continued and

dendritic spines emerged, indicating further maturation of the neuronal networks. Obviously, these cultured neuronal networks do not resemble the complexity of biological neuronal networks. An *in vitro* network is not influenced by other brains regions or feedback-loops and lacks the three-dimensional structure for example. But aspects of neuronal network function, such as synaptic transmission, can be studied in these networks *in vitro* in a controlled manner.

However, synaptic transmission is not straightforward and is underlain by complex mechanisms at molecular level. At a single neuron excitatory and inhibitory synaptic inputs are combined and transmitted to other neurons via synaptic contacts. The process of synaptic transmission itself can transform signals [6], for example via changes in postsynaptic receptor composition. Synapses are plastic, allowing these transformations to be changed on the shorter and longer term, and thereby adjusting input-output relationships of the network. These processes operate on largely differing dimensions of time, e.g. the basic synaptic transmission occurs in milliseconds, while processes as neuromodulation and neurodegeneration require minutes to days [15]. To understand neuronal network (dys)function, different time scales have to be studied, but also different levels of the network in varying dimensions (e.g. ranging from synaptic receptors to connections within local networks or between brain regions) [15]. Over the last decades different tools have been developed to study this multistep process, providing useful insights in synaptic transmission [6].

Tools for monitoring neuronal networks
One experimental strategy to look at neuronal networks *in vitro* is through microscopic imaging, which allows studying both synaptic morphology and functionality (or morphofunction). Immunocytochemistry (ICC) can be used to study neurons and their connections structurally. Using antibodies, specific cellular structures can be identified and quantified. However, ICC often requires fixation of cells and therefore dynamic processes are much harder to study. This can be resolved by ectopic expression of fluorescently labeled markers in living neurons. These fluorescent proteins can be targeted to subcellular locations (for example the pre- or postsynaptic compartments). Although immuno-cytochemistry with specific antibodies and the right image analysis paradigms can provide useful information about synapses (reviewed in ref. [16]), there is no guarantee that connected neurons or actual synapses are being quantified. Several options for imaging true connections between synaptic partners have been developed during the last decades (reviewed by Wickersham and Feinberg [17]). An elegant example of this principle is the mGRASP technique (mammalian GFP (green fluorescent protein) Reconstitution Across Synaptic Partners) [18], which allows the localization of synapses to be studied in living cells. This technique is based on split-GFP, i.e. the functional complementation between two nonfluorescent GFP fragments. One of those GFP fragments is coupled to a part of the presynaptic protein neurexin, the other GFP fragment to a part of the postsynaptic protein neuroligin, to achieve delivery to synaptic locations.

Synapse formation reconstitutes GFP across the synaptic cleft, which can be imaged in living cells and this way the appearance of synapses can be followed over time (Fig. 1.2). Since it has not been proven that reconstituted GFP is removed with synapse removal, caution has to be taken when interpreting mGRASP results.
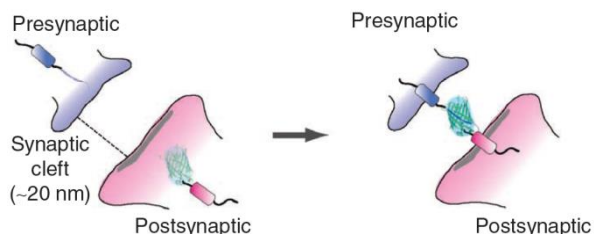
Figure 1.2 Schematic representation of the mechanism of action of mGRASP in the synapse. Presynaptic expression of pre-mGRASP produces mCerulean fluorescence (blue) and postsynaptic expression of post-mGRASP produces dTomato fluorescence (red). When synaptic partners are reconstituted GFP fluorescence (green) appears. Adopted from Kim *et al*., 2012 [18].

At the level of the synapse many more processes play pivotal roles in synaptic transmission besides the physical formation and structural fine-tuning of synapses. One important player is calcium. Following depolarization of the presynaptic neuron different voltage-gated calcium channels open, resulting in a transient calcium influx leading to synaptic vesicle release [19]. Using calcium indicators Smetters and Majewska showed that action potentials can be detected with calcium imaging [20]. Many different indicators of intracellular Ca^{2+} concentrations have been developed and have been used to study these processes. Initially, chemically synthesized Ca^{2+} indicators were developed, but these indicators have limitations. First of all, although loading into cells is accomplished as acetoxymethyl (AM) esters (as first described by Tsien in 1981[21]), this does not enable targeting to specific cells. Furthermore, AM esters tend to leak out of cells and compartmentalize into organelles, thereby limiting imaging duration to several hours. The limitations of synthetic calcium dyes do not exist for genetically encoded calcium indicators (GECIs), for example the family of GCaMPs [22]. These indicators were developed by a fusion of green fluorescent protein (GFP), calmodulin, and M13. Further development and optimization of these proteins was done in order to increase dynamic ranges and Ca^{2+} affinity. Examples of these optimized probes are GCaMP3 [23] and GCaMP6 [24]. Advantages of these GECIs are that GECIs can be used to follow a living cell culture over time, without decrease of functionality. Furthermore, expression can be targeted to specific cells (by incorporating a cell type specific promoter) or even specific cellular structures (by coupling the indicator to protein fragments). An example of the last property of GECIs is the fusion of GCaMP3 with PSD95 in order to target the calcium indicators to the postsynaptic compartment. Subcellular localization of this fusion protein is dependent on PSD95, which localizes to the postsynaptic density of excitatory synapses.

Several studies have shown that the calcium signal can give robust information about subtle changes in neuronal networks [13]. By using an imaging based approach, combined with automated analysis [25] additional network features can provide useful insights in neuronal network function and dysfunction.

A related pivotal event in neuronal network function is activity-dependent synaptic vesicle exocytosis, occurring at the presynaptic membrane. In the last two decades probes have been developed to study these processes as well. In 1998 Miesenböck and colleagues described pHluorin [26] which is a GFP based pH sensing protein. The fusion of pHluorin with the second intravesicular loop of synaptophysin, a membrane protein that localizes to synaptic vesicles, was developed and named sypHy [27]. This enabled specific probing of presynaptic vesicles, since the sypHy moiety faces the vesicle lumen, such that loss of protons with vesicle fusion can be imaged. In the acidic lumen of a synaptic vesicle, sypHy has very low fluorescence intensity. However, upon activity dependent fusion of synaptic vesicles with the synaptic plasma membrane, the probe faces the extracellular environment of the synaptic cleft where the neutral pH causes a strong increase in fluorescence intensity (Fig. 1.3). Further development of this indicator family created the red sypHtomato probe [28], enabling the combined imaging of presynaptic function (in red) with (postsynaptic) calcium dynamics (in green). Although presynaptic calcium influx is necessary for presynaptic vesicle exocytosis, these processes do not depend on each other in a 1:1 ratio [19]. Therefore, the probe could give additional valuable information about synaptic transmission. By combining the red sypHtomato with a green calcium indicator the relationship between these two processes can be questioned too [28,29].
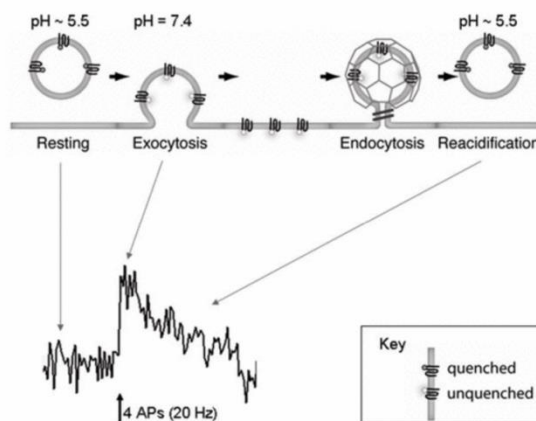
Figure 1.3 Schematic representation of the mechanism of action of sypHtomato. The pHtomato is quenched in the acidic environment inside the vesicle (pH ~5.5). Upon action potential (AP) firing, vesicles fuse with the plasma membrane, protons are lost and the environmental pH of the probe increases to pH 7.4 thereby increasing its fluorescence. After endocytosis and re-acidification fluorescence is quenched again. Adopted from Royle et al., 2008 [30].

Another widely used experimental approach to study neuronal function is electrophysiology. Single cells can be characterized using patch clamp techniques, while network function can be studied with multi-electrode arrays (MEAs). Both approaches share the advantage of a high temporal resolution, but give less spatial information, i.e. it is more difficult to identify the origin and location of the inputs on the cell that has been patched or the network that is interrogated with MEAs. The ongoing advancements in multi-electrode or micro-electrode technology focus on increasing the spatial resolution of this technique facilitating the understanding of single neurons or complete networks [31]. MEA technology can give complementary information to calcium imaging and morphological read-outs via immunocytochemistry. Ideally, electrophysiological data should be combined with calcium imaging to study the relationship between electrical and chemical signaling events in *in vitro* cultures.

1.2 Neuronal networks in neuropathology

Since cognitive functions of the brain badly need synaptic transmission for integration of signals, it is not surprising that synapses are affected in cognitive disorders. Cognitive decline is a hallmark of dementias, a symptom occurring in many neurodegenerative disorders. Alzheimer's disease (AD) is the most common form of dementia in elderly. Together with other dementias AD is an important global public health problem with an estimated prevalence of about 30 million and an expected increase in numbers worldwide [32]. The extremely high costs of care but also the impact for patients and their relatives underline the need for (more) effective therapies.

Cognitive disorders, including AD, schizophrenia and frontotemporal dementia (FTD), reflect marked disruptions in the processing of information, impaired neuronal connectivity and reduced cognition. Synapses play an important role in these disorders. For example, during AD progression normal synaptic function becomes impaired, synapses are eliminated and pathological proteins are transported through synapses (reviewed in ref. [33]). In AD the strongest correlate with cognitive decline is synapse loss in hippocampus and cortex [34], underlining the importance of synaptic function and structure in the disease. Not only loss of synapses and spines has been shown, but changes occur in morphology as a compensatory mechanism, for example increased size of the remaining spines [35]. Recently, several research groups have focused on the "synaptic hypothesis" for dementias including AD (e.g. reviewed in ref. [33,36,37]). Many of the synaptic changes seem to be reversible, which is an important finding regarding drug development for these cognitive disorders. Synapse loss appears to be an early event in pathogenesis of dementias, since synaptic changes have been shown in patients with only mild cognitive impairment and early AD [38,39]. Recent advances in biomarker identification in AD have made it possible to detect aspects of neuropathology in cognitively normal individuals, such as buildup of misfolded proteins, one or even two decades before onset of clinical dementia [40,41]. Figure 1.4 shows a hypothetical model representing the pathological cascade of AD with

the temporal pattern of biomarkers that can be used for tracking pathophysiological processes during this disease. These initial events are indicative for potential pathways to target for intervention, because they may underlie the start of pathology.
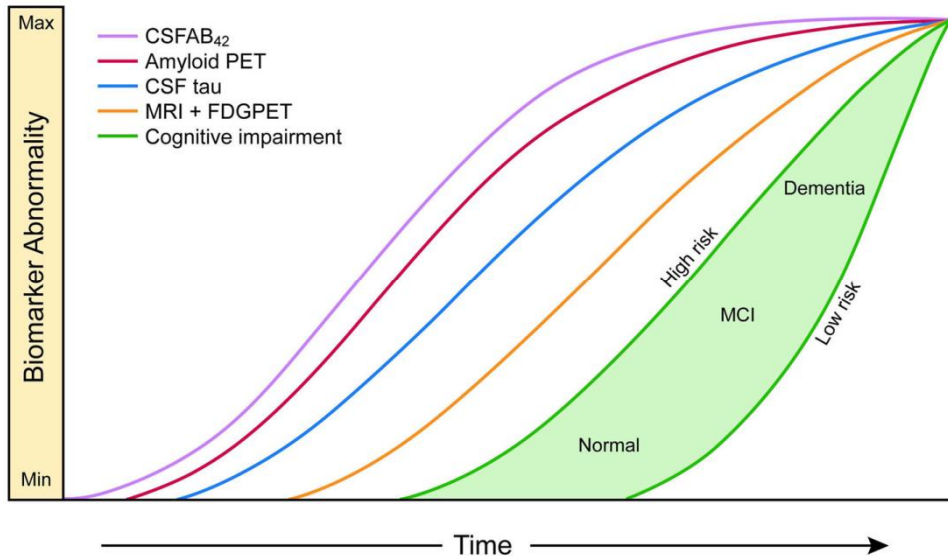
Figure 1.4 Dynamics of biomarkers for AD in a pathological cascade model. This model shows a possible order of biomarkers occurring during the pathological cascade of AD. The first identified feature is Aβ amyloid, identified by CSF Aβ42 (purple) or PET amyloid imaging (red). Next, elevated CSF tau levels (blue) can be measured. Neurodegeneration is measured by FDG (fluorodeoxyglucose) PET (reflecting increased metabolism by inflammatory responses) and structural MRI (orange). Markers increase over time (presented on the horizontal axis) and converge at the top right-hand corner of the plot at the point of maximum abnormality. Cognitive performance is depicted as a zone (green filled area) since high risk and low risk cases respond differentially. High risk subjects show a response curve that is shifted to the left, while for subjects with a lower risk profile the curve is shifted to the right, illustrating that two subjects with the same biomarker levels can show different cognitive outcomes. Adopted from Jack *et al.*, 2013 [41].

1.3 Tauopathies as an example of neuronal network dysfunction

As previously mentioned, Alzheimer's disease is the most common form of dementia. The incidence of this and other neurodegenerative disorders is expected to rise dramatically since life expectancy increases, causing a serious economic and social burden. Although AD was described already in 1907 by Alois Alzheimer [42], and despite major efforts in research towards the cause of the disease, no disease-modifying treatment is available yet.

Alzheimer's disease

In 1907 Alois Alzheimer reported the first case of AD [42]: the 51-year old Auguste Deter presented with progressive memory loss, cognitive decline, and adverse behavioral changes. Post-mortem examination of her brain showed abnormal histopathological hallmarks now being identified as plaques (accumulation of extracellular aggregates of insoluble beta-amyloid) and neurofibrillary tangles (NFTs, intraneuronal filaments of hyperphosphorylated tau protein), and are used for the definitive diagnosis of AD. Probably diagnoses are based on measurements of cognitive decline. The first signs of dementias are often attributed to normal aging and present themselves as difficulties in remembering recent events and information. The first stage, called Mild Cognitive Impairment (MCI), reflects gradual deterioration giving problems with subjective and objective memory, but does not convert to AD per se [43]. During disease progression, semantic memory for learned facts and implicit memory of the body become affected and eventually language and other cognitive abilities. In advanced AD, patients need help with basic activities of daily living, including eating and personal hygiene, while they do not recognize their close relatives anymore.

Structural changes in AD brains are characterized by "positive lesions", being the accumulation of plaques, tangles, neuropil threads, dystrophic neurites and "negative lesions", that is massive atrophy due to neuronal loss and degeneration of neurites and synapses [44]. Spread of these lesions throughout the brain typically occurs in a characteristic pattern [45], providing useful information about disease progression and symptoms. The two key proteins involved in AD are amyloid precursor protein (APP) and microtubule binding protein tau, eventually resulting in abnormal aggregates of misfolded proteins in the disease. Therefore, AD is called a proteinopathy. Genetic defects are observed in only about 5% of all patients diagnosed with Alzheimer's disease. These patients suffer from early onset familial AD (fAD), showing cognitive decline already before the age of 65. Inheritant dominant mutations in genes encoding either APP, presinilin 1 (PS1) or presinilin 2 (PS2) increase the level of amyloid peptide in the brain, thereby initiating AD pathology. However, the etiology of the other 95% of so-called sporadic AD (sAD) cases is complicated, which is due to a variety of (early-life) risk factors such as aging, gender, education, and genotype of apolipoprotein E (ApoE) [46].

Since genetic mutations in the APP pathway lead to development of Alzheimer's disease, the amyloid hypothesis for AD has received a lot of attention. APP is an integral membrane protein present in many tissues including neurons. Depending on the posttranslational sequential cleavage of APP by secretase proteins including PS1 and PS2 monomeric Aβ is produced. These enzymes cleave APP at different positions, creating a variety of Aβ peptides, of which Aβ43, Aβ42, Aβ40, Aβ38 and Aβ37 variants are detected in cell cultures and body fluids (Aβ numbering indicates the number of amino acids comprising the

peptide). These peptides form a heterogeneous mixture having different solubility, stability and biological and toxic properties. Aβ40 is the most common amyloid peptide present in the healthy and AD brain, while other peptides are present at lower levels. Aβ42 species are found to be significantly increased in cells expressing fAD mutations, but recent efforts also show quantitative changes in other Aβ peptide levels. Therefore, not the quantity but the balance between the different peptides seems to play a major role in the aggregation of amyloid, the formation of plaques and the pathology of AD. Neurons close to amyloid plaques show dystrophic neurons and synapse loss (reviewed in ref. [47]).

Historically, synaptic dysfunction in AD was attributed to amyloid pathology, because appearance of tau pathology was thought to occur later in disease progression and genetic defects in the APP pathway are responsible for fAD cases. Although plaques are typical hallmarks of AD, no correlation has been found with cognitive impairment, while tangles do correlate with cognitive impairment, neuronal cell death and synapse loss [48,49]. The demonstration that tau deposits closely correlate with cognitive decline [45,50] increased the interest for tau as possible mediator of synaptic dysfunction. The strongest correlate with cognitive decline is actually synapse loss in hippocampus and cortex [34]. In mouse models of AD, synaptic dysfunction is observed earlier than neuronal loss and coincides with the onset of memory deficiencies [51]. These findings led to the hypothesis that synaptic transmission is highly affected in AD (review in ref. [33,36]). Moreover, tau pathology causes neurological problems and dementias in many described tauopathies without amyloid or other proteinopathies and colocalisation of tau and amyloid at the synapse was proposed to explain their functional interaction in cognitive decline in AD patients [52,53]. Different animal models have been used to gain insight in synaptic dysfunctions caused by tau. For example rTg4510 mice, overexpressing human P301Ltau, showed alterations in synaptic function and structure [54-59]. Tangle bearing neurons are reported to contain less synaptic proteins and receive fewer synapses [60-62]. Furthermore, tau pathology showed to induce hyperexcitability of the glutamatergic system via increased presynaptic vesicle release and decreased glutamate clearance from the synaptic cleft by astrocytes. Both processes correlated well with memory performance of these mice, and occurred while tau pathology was still subtle without significant neuronal loss[63]. An increasing number of studies found that soluble forms of tau protein act at the synapse to cause neural network dysfunction rather than (insoluble) tangles (reviewed in ref. [54]). Next to animal models, dissociated rodent primary neuronal culture models have proven to provide valuable information about synaptic deficiencies. Hoover and colleagues showed in dissociated rodent primary neuronal cultures that early tau-induced deficits develop within the dendritic spines, by disrupting glutamate receptor trafficking or synaptic anchoring, thereby impairing synaptic function. By creating pseudophosphorylated and phosphorylation-deficient tau protein they showed that tau phosphorylation plays a critical role in mediating synaptic deficiencies in this model [64]. The distribution of tau pathology in time and space

correlates well with nerve cell degeneration and clinical symptoms in AD. However, the exact mechanisms and cause of synaptic dysfunction in neurodegenerative disorders like AD is not known yet.

Tauopathies

Tauopathies are a group of neurodegenerative disorders characterized by the accumulation and aggregation of the pathological tau protein in human brains [65]. In AD, Parkinson's disease, FTD, Pick's disease and progressive supranuclear palsy tau aggregation and formation of NFTs is a common pathological feature [66]. These NFTs were first described by Alois Alzheimer about a century ago[42], but not earlier than three decades ago the major component of tangles was identified as a hyperphosphorylated, filamentous form of the tau protein [67]. AD and other tauopathies unequivocally demonstrated that dysfunction of tau protein can drive neurodegeneration. Because multiple tau mutations are pathogenic in FTDP-17 patients and tau polymorphisms seem to be genetic risk factors for progressive supranuclear palsy, tau pathology is directly linked to etiology of neurodegenerative diseases including AD. Due to the variety in disease manifestations of these tauopathies, other factors such as additional genetic and epigenetic factors are involved, but the common factor is tau pathology.

Tau protein in physiology

Microtubule associated protein tau (*MAPT*) is primarily expressed in the central and peripheral nervous system and can be subdivided in 4 regions: the N-terminal projection region, a proline-rich domain, a microtubule binding domain and a C-terminal part [68]. The *MAPT* gene is encoded by sixteen exons on chromosome 17q21 [69] and alternative splicing results in six different isoforms with different physiological roles [68,70] (see Fig. 1.5). Inclusion or exclusion of exons two and three (E2 and E3) gives rise to isoforms containing 0, 1, or 2 N-terminal inserts. Exon ten (E10) encodes one of the four microtubule-binding domains (MTBD) in the C-terminal half of tau. Alternative splicing of E10 results in tau isoforms containing either 3 (3R tau) or 4 (4R tau) MTBDs, resulting in an increased microtubule-binding affinity of 4R tau. The expression of *MAPT* isoforms is developmentally regulated. Fetal and early post-natal neurons only express the shortest *MAPT* isoform 0N3R, whereas in the adult human brain all isoforms are expressed with a 3R:4R ratio close to one [71,72]. The amino-terminal insertions are not equally expressed in the adult brain, with respective percentages of about 37%, 54%, and only 9% for 0N, 1N and 2N isoforms. The rates of microtubule assembly are mainly influenced by the number of C-terminal repeats, rather than by the amino-terminal insertions.
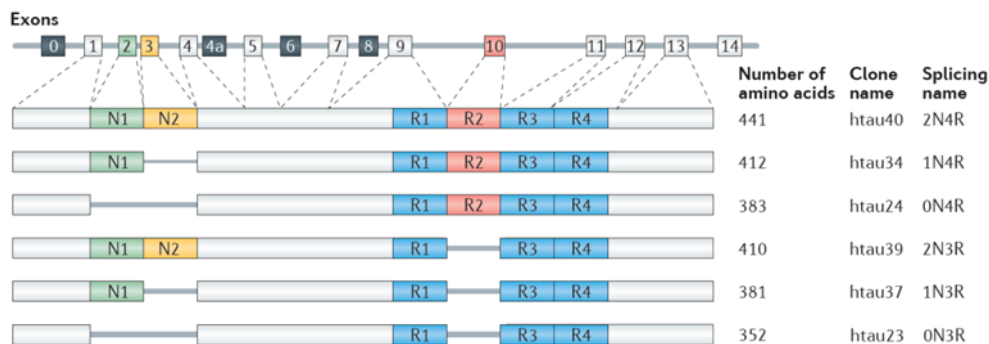
Figure 1.5 Schematic representation of the human *MAPT* gene and the splice isoforms of tau protein. *MAPT*, the gene encoding human tau, consists of 16 exons and intermediate introns. Exons 1 (E1), E4, E5, E7, E9, E11, E12 and E13 are always expressed, while E2, E3, and E10 are subject to alternative splicing. E0 is part of the promoter, which is transcribed but not translated. E4a, E6 and E8 are transcribed only in peripheral tissue. The six human brain tau isoforms contain 0, 1 or 2 near-amino-terminal inserts (0N, 1N or 2N, respectively) and 3 or 4 carboxy-terminal repeat domains (3R or 4R, respectively), depending on the presence or absence of R2. Adopted from Wang and Mandelkow 2015 [70].

Microtubule assembly was found to be 2.5-3.0 times faster and more efficient for isoforms containing four repeats when compared with three-repeat containing isoforms [71]. The function of the N-terminal inserts is less clear. However, the inserts are thought to influence the attachment or spacing between microtubules [73,74], the subcellular distribution of tau in neurons [75] and rate and extent of tau aggregation [76]. *MAPT* splicing and expression are differentially regulated between brain regions as well. For example, general tau, but more specifically 3R tau levels are higher in the neocortex than in white matter and cerebellum. The frontal and temporal cortex are most highly affected by tauopathy, suggesting that regional variation in *MAPT* expression might contribute to variation in susceptibility for tau pathology [77]. Since a lot of research on tau is done in transgenic mouse models, it is important to note that the adult rodent brain actually exclusively produce 4R tau [78].

Microtubule binding protein tau is a naturally unfolded and very soluble protein, involved in microtubule stabilization and assembly (Fig. 1.6), and more specifically in regulation of microtubule dynamics allowing cytoskeleton reorganization [79-81], neurite outgrowth, axonal transport, and maintenance of cellular viability [70]. Additionally, tau was found to play a role in maintenance of RNA and DNA integrity, regulation of neurogenesis, neuronal activity, and synaptic plasticity (reviewed in ref. [70]). Its function is not only regulated by alternative splicing, but also by phosphorylation and other posttranslational modifications, for example acetylation and glycosylation (reviewed in ref. [70]). Phosphorylation is the most prominent modification, which regulates the binding affinity of tau to microtubules. High tau phosphorylation occurs at embryonic stages when neurons still are very plastic while at later stages phosphorylation

is reduced compared to the embryonic brain [82]. Tau has many phosphorylation sites, and location and overall degree of phosphorylation highly determine its function with the interplay between kinases and phosphatases maintaining the balance between phosphorylation and dephosphorylation [83,84].

a Healthy neuron

Microtubules

Stabilizing Tau molecules

b Diseased neuron

Disintegrating microtubules

Microtubule subunits fall apart

Tangled clumps of Tau proteins
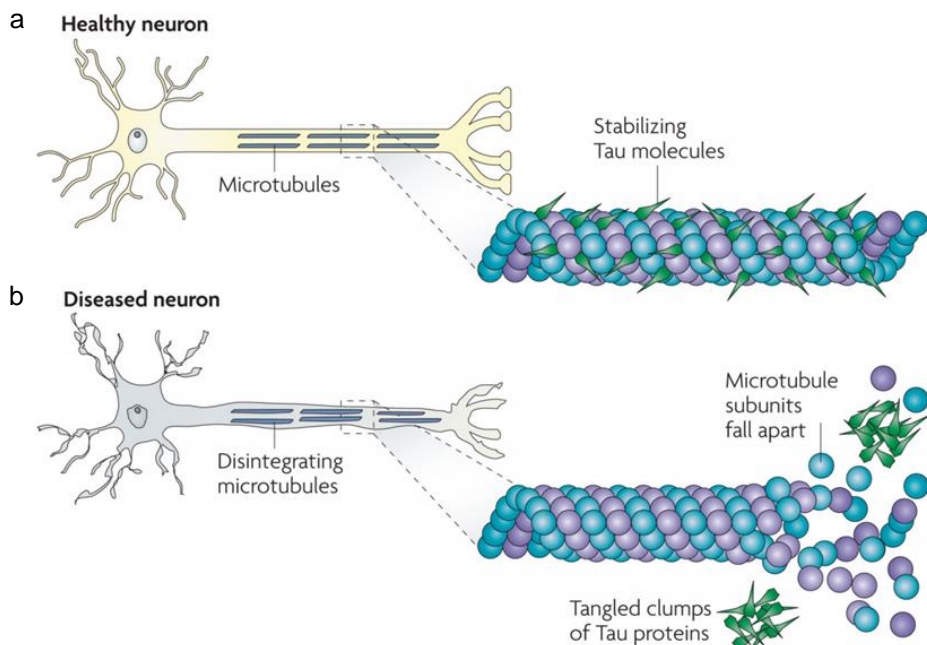
Figure 1.6 Schematic representation of tau function in healthy and diseased neurons. a) Tau is a microtubule stabilizing protein and is particularly enriched in neurons. Microtubules provide a course along which cellular cargo can travel through the lengthy axonal projections of neurons. b) Tau function is compromised in tauopathies, probably resulting both from tau hyperphosphorylation and from the sequestration of hyperphosphorylated tau into NFTs thereby reducing the microtubule binding capacities of tau. The loss of functional tau leads to microtubule instability, reduced axonal transport, and microtubule disintegration, which could contribute to neuropathology. Adopted from Brunden, Trojanowski, and Lee, 2009 [81].

Tau protein in pathology

In the healthy brain tau contains between two and three mole of phosphate per mole of protein, which increases threefold in AD brains [85]. These abnormal phosphorylation levels result in loss of its physiological function by decreasing microtubule-binding affinity, but also initiate gain of toxicity by increasing the self-aggregating and misfolding potency of the protein, eventually forcing the formation of highly organized insoluble paired helical filaments (PHF) and NFTs [86-88] which are the typical postmortem hallmark of tauopathies. Significant accumulation of NFTs coincides with oxidative stress, inflammation, synaptic and network dysfunction and ultimately neuronal loss, but not before stages of moderate to severe dementia [32]. However, coincidence does not necessarily

mean a causative relationship. Similar to other aggregating proteins such as amyloid beta, alpha-synuclein and prions, tau protein can form aggregates ranging from dimers, to bigger oligomers, and higher order multimers that eventually end up in insoluble fibrils (reviewed in ref. [89]). In the last decade, accumulating evidence has shown that tangles exert negligible neurotoxicity compared to soluble tau [87,90,91], either as single molecules or small oligomers. The exact mechanisms remain unclear and urge for more research.

The inherited forms of FTDP-17 are caused by intronic and exonic mutations in the *MAPT* gene on chromosome 17 [66,92], either changing the coding sequence of the gene, or the alternative splicing of *MAPT*. More than 30 mutations have been found in the *MAPT* gene of these patients. For example, tau proteins with a P301L mutation (identified in FTDP-17 families) showed a reduced affinity for microtubules and an increased tendency for aggregation [93]. Patients with the clinically more aggressive P301S mutation showed aggregation of hyperphoshorylated tau at young age already [94]. In contrast, no mutations in *MAPT* gene were found to cause or increase the risk for AD. However, distribution of tau pathology in time and space correlates well with nerve cell degeneration and clinical symptoms in AD. Therefore, interactions with other genes and epigenetics are thought to influence tau functionality. In AD cases, SNPs in the PPP3R1 gene encoding the regulatory subunit of calcineurin, a Ser/Thr phosphatase acting on tau, were associated with higher CSF concentrations of tau and phospho-tau, increased tangle pathology, and a more rapid disease progression [95]. Kauwe and colleagues also found SNPs in the *MAPT* gene affecting disease progression [96]. Altered splicing of the *MAPT* gene were found in other neurodegenerative tauopathies as well. Increased 4R/3R tau ratios have been described in patients with FTD, progressive supranuclear palsy, and Alzheimer's disease [92,97]. In the latter disorder an altered ratio can be caused by either an increase of 4R tau isoform production, or decreased 3R tau production, resulting in an approximately doubled 4R/3R ratio [98,99].

The precise contribution of tau phosphorylation, altered 4R/3R ratios, tau microtubule stabilization, tau aggregation and ultimately cognitive decline is unknown. Many aspects of tauopathies have been unraveled already, but additional research is necessary in order to clarify the exact mechanisms leading to cognitive impairment.

1.4 Modeling neurodegenerative diseases

Although many years of research clarified a multitude of mechanisms underlying neurodegenerative disorders, no disease-modifying treatments are available for most diseases. Until now only symptomatic treatment alleviates the disease manifestation in some patients. For example, based on the cholinergic deficit hypothesis [100], which attributes cognitive deficits to the lack of acetylcholine, currently three cholinesterase inhibitors are available for the treatment of AD (rivastigmine, galantamine and donepezil) leading to a temporary delay of

cognitive decline. Additionally, memantine, an NMDA (N-methylD-aspartate) receptor antagonist, is available for the treatment of moderate to severe AD, protecting neuronal cells from glutamate-mediated excitotoxicity by blocking pathologic stimulation of NMDA receptors [101]. However, preclinical and clinical research puts tremendous efforts in finding a cure for this group of disorders, but with high attrition rates (e.g. for AD reviewed in ref. [102]) due to severe side effects, lack of therapeutic efficacy or effectiveness in mild but not severe cognitive decline. It seems to be essential to prevent or delay the onset of the disorders, because in progressed state at later time points some aspects are irreversible already because neurodegeneration involves irreversible loss of neurons. For example, extensive preclinical and clinical research on AD (with over two hundred compounds reaching phase II clinical trials since 2003) still did not produce novel drugs that have been approved for use in AD patients [102].

What could be the reason for this poor outcome, while so much time and money is invested? The pathogenesis of neurodegenerative disorders is complex and fraught with open questions. The hypothesis that final pathology is rather the effect than the cause of neurodegenerative disorders indicates that many other factors might be involved in pathogenesis, including genetic factors, incidence of the disorder in the patient's family, cerebrovascular disease, traumatic brain injury, depression, hormonal disturbance, inflammation, hyperlipidemia and hyperglycemia [103]. Additionally, cognitive disorders often show highly heterogeneous symptoms and clinical etiologies with different disease progression and therapeutic responses as a result [104]. Lack of knowledge about the underlying mechanisms of pathology hampers the development of effective treatments and highly demands for additional research.

Animal models have proven to be a valuable tool to mimick certain aspects of these diseases as previously described. For example, in P301S tau transgenic mice (PS19), filamentous tau lesions were present at 6 months of age which progressively accumulated in association with neuronal loss and hippocampal and cortical atrophy by 9-12 months of age [105]. The APP23 mouse model expresses human APP with the Swedish mutation, and shows clear amyloidosis [106]. However, these two models only represent parts of the AD pathology. A promising rodent model for AD is the triple transgenic APP/tau/PS1 mouse model showing amyloid plaques and neurofibrillary tangles similar to human AD pathology. Synaptic dysfunction was even present before plaques and tangles in this model [107,108]. However, transgenic models never cover all aspects of human disease, for example because choices of transgenes have to be made. Although simplified aspects of human brain function can be modelled in the laboratory using *in vitro* and *in vivo* models, its complexity is difficult to reproduce. Many aspects of human neural development are similar to mechanisms unraveled in (mammalian) animal models, because they are evolutionary preserved. However, important brain regions in complex cognitive diseases, such as the cerebral cortex, are less developed in rodents and timing of brain development is

different in humans. New cell types and cortical layers have emerged when compared to rodents and human-specific migratory pathways have been identified. Clearly visible is the considerable increase of the relative size of the human brain and its increased gyration. This increased complexity has major impact on the acquisition of higher cognitive functions [109-113].

Another example of the complexity of the human brain is its variety in astrocytes. The human cortex contains at least four distinct types of astrocytes while only two types have been found in rodents. Astrocytes play an important role in supportive functions of the brain, such as ion and water homeostasis, energy and metabolism, neurotransmitter production, removal and breakdown and blood-brain barrier maintenance. Through secreted factors and physical contact astrocytes also regulate synaptic connectivity and transmission in the brain [114-116]. Besides their physiological functions, astrocytes play important roles in pathology as well [116-118]. Reactive astrogliosis is associated with various pathological conditions, such as trauma, ischemia, and neurodegenerative disorders including Alzheimer's disease. It is still unclear if reactive astrogliosis is beneficial or detrimental in many cases. Astrocytes are thought to form neuroprotective barriers to wall off misfolded and aggregating proteins such as beta amyloid, and reports show that reactive astrocytes can take up and degrade extracellular deposits of Aβ42. However, other studies indicate that astrocytes contribute to pathology, either via loss of function or gain of detrimental effects. Excitotoxic neurodegeneration can be caused by dysfunctional astrocytes that no longer take up glutamate out of the synaptic cleft, for example [63]. Furthermore, exacerbations of inflammation and production of neurotoxic levels of reactive oxygen species by astrocytes can be detrimental. Differences between species might cause differences in astrocytic responses and thus research on neuronal network function and dysfunction. Therefore it is difficult to simply extrapolate from animal models to human beings [119,120].

1.5 Human iPSC-derived neurons

Until recently it was impossible to obtain live neurons from patients with neurodegenerative disorders in order to model the disease *in vitro* [121]. However, in 2007 human induced pluripotent stem cells (hiPSCs) have been generated from somatic cells to overcome this hurdle [122]. hiPSCs are pluripotent cells produced by reprogramming somatic cells obtained from any individual, which can be differentiated into cells from all three germ layers when using specific differentiation protocols. These hiPSCs can be differentiated into neurons, glial cells or any other relevant cell type through culture protocols using different kinds of growth factors and conditions. hiPSC-derived cells can potentially be used for the development of autologous cell therapies for degenerative diseases, but suitable applications still have to be evaluated in order to minimize risks associated with hiPSC-derived cell therapies, such as tumorigenesis (e.g. reviewed in ref. [123]). Additionally, the availability of hiPSCs allows the study of previously inaccessible human neurons which is specifically interesting for

cognitive disorders. This enables the use of patient-derived cells, directly providing the genetic background of that person in (almost) any relevant cell type [124,125] (Fig. 1.7). Human iPSC-derived cells offer the only practical way to study the development and function of human brain cells *in vitro*, thereby circumventing developmental differences with animal models [112]. Strikingly, the temporal appearance of cortical development in iPSCs was shown to differ greatly between rodents and humans, which could be reminiscent of the *in vivo* developmental differences between species [126]. Therefore, hiPSCs show high potential to develop translational models that can complement or even replace animal studies, either by highlighting differences between species, or by further confirming results from animal studies.

The last decade different methods have been developed and optimized to generate human iPSCs starting from different tissues (e.g. fibroblasts, keratinocytes from hair, and cord blood cells). After that reprogramming factors are introduced to induce and keep cells in the pluripotent state, for example OCT4, SOX2 and NANOG which are expressed during early embryonic development. Additionally, cell proliferation factors like MYC and KLF4 positively contributed to generation of pluripotency. The delivery methods for these factors are very diverse as well, ranging from integration of exogenous genetic material to non-integrative methods using proteins. However, all methods have their pros and cons, for example variation in reprogramming efficiency or left-overs from integrative methods (reviewed in ref. [127]). Since the focus of this project was not on hiPSC generation, we used two completely different existing commercially available hiPSC lines, that is IPSC0028 (Sigma) and ChiPSC6b (Cellectis). Both cell lines were obtained from different tissues (epithelium and fibroblasts respectively), from different gender (female and male respectively), and were reprogrammed using different factors and different methods (retroviral vector containing OCT4, SOX2, KLF4 and MYC and episomal vectors encoding OCT4, SOX2, KLF4, LIN28, and L-MYC respectively).

Although the establishment of hiPSC technology happened no more than one decade ago many differentiation protocols to produce hiPSC-derived neurons have been described. Ranging from dopaminergic cells [128] to forebrain interneurons [129] and motor neurons; all cell types available have their own applications in research. It is highly important to select the right differentiation protocol to address specific research questions, since neuronal subtypes differ tremendously in functionality, gene expression and morphology. For example, production of 4R tau in hiPSC-derived dopaminergic and mixed neuronal populations appears already after 4 to 10 weeks of differentiation [128,130], while it might take up to 365 days in cortical neurons [131].
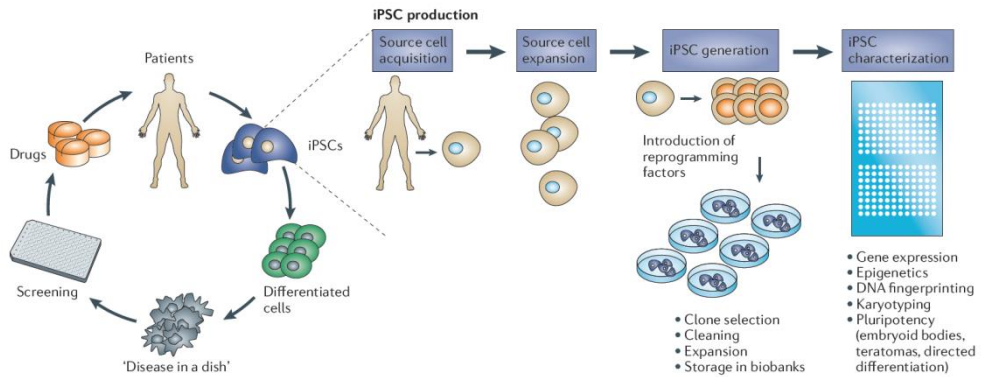
Figure 1.7 The availability of hiPSCs provides the opportunity to study previously inaccessible human cells as a "disease in a dish". A schematic representation of the iPSC technology platform shows a new approach in drug discovery (circle diagram on the left). Starting from patient sample for the derivation of induced pluripotent stem cells (iPSCs), directed differentiation of these cells into cells that have a crucial role in the disease generates a "disease in a dish". A schematic diagram of iPSC production is shown on the right. After cell collection from a patient the cells are expanded and iPSCs are derived; the process is followed by a thorough characterization of the hiPSCs, and their expansion and storage in a biobank. Adopted from Grskovic *et al.*, 2011 [125].

For this project, with the focus on neuronal network function in cognitive disorders, we have chosen for generation of hiPSC-derived cortical neurons. The cerebral cortex is the integrative and executive center of the human brain and plays an essential role in learning and memory [5]. In AD patients the strongest correlate with cognitive decline is synapse loss in the cortex and hippocampus [34]. In this project a specific group of neurodegenerative disorders called tauopathies will be discussed in more detail. In these pathologies the cortex is highly involved, as signified by the loss of synapses, spines, and decreased function of cortical projections [132]. In 2012 Shi and colleagues described the directed differentiation of hiPSCs to cerebral cortex neurons and neural networks [133] which was used as a starting point for the hiPSC-derived models used in this project. Rodent models have taught us a lot about fundamental features of cerebral cortex development, function and dysfunction. However, the human cerebral cortex is different from that of rodents in many ways [111], for example the increased size, complexity and nature of its developing stem cell populations [110], and the diversity of neuronal subtypes [109]. The latter two characteristics are of specific interest when developing a hiPSC-derived cortical model to model human cortical dysfunction. The cerebral cortex mainly consists of two classes of neurons, that is approximately 80% of excitatory glutamatergic projection neurons (that are generated by cortical stem and progenitor cells) and 20% of GABAergic interneurons that migrate during development because they are generated outside the cortex [134]. The development of deep layer (expressing markers such as *TBR1* and *CTIP2*) and upper layer (expressing markers such as *SATB2*) glutamatergic projection neurons follows a stereotypic temporal order [135], creating highly organized (micro)circuits [136-138]. The correct final neuronal

subtype of glutamatergic projection neurons and their characteristics are thus highly dependent on the differentiation via cortical stem and progenitor cells. The protocol described by Shi and colleagues is based on key milestones for cortical development recapitulating the proportions of cell populations, terminal neuronal differentiation, synaptogenesis and network formation [133,139]. Figure 1.8 schematically shows the temporal and spatial patterning of cortical neuron neurogenesis [140].

Various examples of studies using hiPSC-derived neuronal cultures for investigating neurodegenerative disorders have been published already. Israel and colleagues used hiPSCs from both fAD and sAD patients to show that neuronal derivates exhibited significantly higher levels of pathological markers amyloid beta and phosho-tau compared to non-demented controls [121]. In another study using fAD patient-derived hiPSCs comparable findings were reported, with increased amyloid beta secretion [141]. In an elegant study comparing a patient-derived hiPSC line containing the *MAPT* A152T mutation and an isogenic hiPSC line with the corrected mutation, this mutation was found to increase tau fragmentation and phosphorylation leading to axonal degeneration [142]. However, none of these reports investigated neuronal network dysfunction in hiPSC-derived neuronal models mimicking human neurodegenerative pathologies. To study the complete genetic background of AD, but also other tauopathies, somatic cells from patients with different tauopathies could be used to find common mechanisms underlying different tauopathies, or the other way around to find phenotypes specific for a certain disorder. To initiate this line of research we have used examples of known *MAPT* mutations to set up a phenotypic screening method.
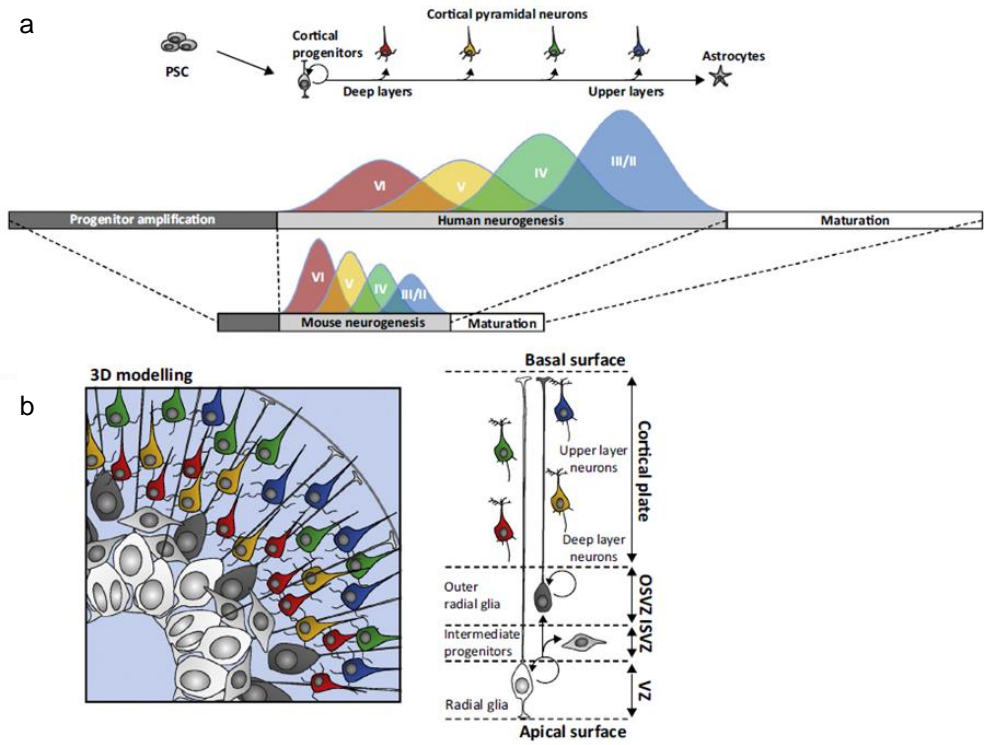
Figure 1.8 Temporal and spatial patterning of cortical neuron neurogenesis from pluripotent stem cells. a) Pluripotent stem cells (PSCs) differentiate towards cortical progenitors. Subsequent differentiation towards cortical pyramidal neurons first generates deep layer neurons, then upper layer neurons and eventually astrocytes. This temporal pattern is similar to *in vivo* situations, also recapitulating the difference in time-course with mouse tissue. b) A three-dimensional representation of the various cell types and their relationships as found *in vivo* can be recapitulated using pluripotent stem cells. This provides unique tools to study spatial patterning of cortical circuits. Adopted from Anderson and Vanderhaeghen 2014 [140].

1.6 Aims of the study

Efforts in drug development and discovery contribute to the increased life-expectancy in developed and developing countries. Fatal diseases from the past become manageable and people live longer. However, these accomplishments increase the prevalence and burden of chronic disorders, neurodegenerative and aging-related pathologies, thereby demanding for new drug development directions. Neurodegenerative disorders are a broad group of highly detrimental health problems, often with a complex and heterogeneous character. Although decades of research provided useful clues on disease etiology, symptoms and progression, for many of these disorders no disease-modifying treatment is available. Preclinical research often clearly points into certain treatment directions, but clinical trials are aborted or fail to reach effectiveness (e.g. ref. [102]), raising questions about the translational value of preclinical models. Therefore, there are ongoing attempts to bridge the gap between models used for drug development and human disease progression.

The goal of this PhD project is the development of a humanized cellular model to study neuronal networks *in vitro* in order to bridge this gap. Until the recent discovery of human induced pluripotent stem cells live human neurons were hardly available for research, while with the advent of hiPSC technology an almost endless source of patient-derived human neurons of different kinds becomes available. Since the technique of using hiPSC-derived neuronal cultures for studying neuronal networks *in vitro* is quite new, optimization of differentiation protocols is our starting point. Until recently no robust and workable protocol was described that provided highly connected hiPSC-derived functional cortical neuronal networks *in vitro*. Time-consuming protocols recapitulating human cortical development are very valuable for research, but are less attractive for drug development purposes. Thorough characterization and validation of control cultures is needed before the model can be used for development of drug discovery assays. The system preferably recapitulates some of the morphological and functional characteristics of the *in vivo* situation. Additionally, the use of these human neuronal networks for disease-modeling has to be explored.

Neurodegenerative disorders form a high social and economic burden. Therefore, we will specifically investigate synaptic function and dysfunction involved in neurodegenerative disorders. AD is the most common form of dementia and clearly represents tau pathology, supporting the application of the hiPSC-derived neuronal model on tauopathies in this project. Although no mutations in *MAPT* gene were found to cause or increase the risk for AD, amyloid-driven early-onset familial AD patients always show comorbid tau pathology and tau dysfunction is directly linked to cognitive decline in AD patients, while amyloid pathology is not. The final stage of tau dysfunction is the formation of neurofibrillary tangles, but earlier events in the disease cascade seem to cause cognitive deficits. Finally other tauopathies than AD, for example FTD, are cumbersome as well but do not

show additional amyloid pathogenesis, all pointing into the direction of tau protein as an important factor in cognitive decline.

Induced pluripotent stem cells have been recently generated to bridge the gap between human tissue and animal models and are used here to create a human 'disease in a dish' model. Optimization and validation of a robust and reproducible differentiation protocol towards cortical neuronal networks *in vitro* is necessary before disease-related changes can be investigated. Current protocols often show high variability affecting reproducibility implying that newly-formed neurons are still not well-characterized [124]. In **chapter 2** we aimed to adapt a previously published differentiation protocol in order to obtain a robust and workable model. The choice for cortical neurons was made because of the relevance for neurodegeneration and tauopathies: cortical regions are highly affected by these pathologies and are highly involved in complex cognitive tasks affected in patients. Thorough characterization and description of techniques to probe hiPSC-derived neuronal networks in a dish will provide a valuable base for subsequent disease modeling.

After establishment of a workable differentiation protocol towards a functional neuronal network *in vitro* we explored the use of a human tau overexpression model to study tauopathy-related changes in neuronal networks in **chapter 3**. The development and spreading of tau aggregates in this overexpression model in primary rodent and hiPSC-derived neuronal cultures was reported already, but not the effect of tau pathology on synaptic transmission. The small soluble tau oligomers seem to be more toxic than neurofibrillary tangles; by following the cultures over time using functional and morphological readouts we aimed to examine the formation of tau oligomers and tangles and their influence on neuronal networks *in vitro*. In order to further substantiate the use of either *in vitro* approach for the study of human (cognitive) diseases the comparison of hiPSC-derived neuronal networks with transgenic rodent cultures has to be made.

Furthermore, we investigated the use of engineered hiPSC lines to model tauopathies. In contrast to rodent models, it is relatively easy to induce targeted mutations in genes expressed by hiPSCs and their derivatives. **Chapter 4** aims at the creation, validation and thorough functional characterization of four mutated hiPSC lines, containing either a *MAPT* splicing variant mutation or the combination of the first with an exonic P301S mutation. Overexpression or engineered hiPSC models were used rather than patient hiPSCs as a proof of concept to test effect windows and compare with rodent models.

In **chapter 5** we aimed to optimize more tools to study neuronal networks *in vitro*. In order to retrieve a complete view of the ongoing processes, a combination of imaging based approaches with electrophysiology would provide a complete toolbox to interrogate function as well as morphology of the

networks. Tools were chosen to examine different levels of spatial and temporal resolution in order to get a complete overview of synaptic transmission.

In conclusion, the following aims were achieved in the presented PhD project:

- A robust reproducible differentiation protocol from hiPSCs towards functional cortical networks *in vitro* was optimized and thoroughly characterized;
- Tauopathy-related changes in synaptic transmission were studied using human *MAPT* overexpressing hiPSC-derived neuronal networks that were challenged with preformed tau fibrils. Several phenotypic differences in morphofunction (i.e. structural and functional differences) were identified;
- Creation and characterization of engineered hiPSC lines gained additional insights in tauopathy-related processes.

References

1   Dictionary, O. E. Oxford English dictionary online. *Mount Royal College Lib., Calgary* **14** (2004).

2   Cajal, S. R. Y. The Croonian Lecture: La fine structure des centres nerveux. *Proceedings of the Royal Society of London* **55**, 444-468 (1894).

3   Hebb, D. O. The organization of behavior: A neuropsychological theory. *New York* **4** (1949).

4   Bliss, T. V. & Lømo, T. Long-lasting potentiation of synaptic transmission in the dentate area of the anaesthetized rabbit following stimulation of the perforant path. *The Journal of physiology* **232**, 331-356 (1973).

5   Dudai, Y. & Morris, R. G. Memorable trends. *Neuron* **80**, 742-750 (2013).

6   Dreosti, E. & Lagnado, L. Optical reporters of synaptic activity in neural circuits. *Exp. Physiol.* **96**, 4-12 (2011).

7   Cohen, E., Ivenshitz, M., Amor-Baroukh, V., Greenberger, V. & Segal, M. Determinants of spontaneous activity in networks of cultured hippocampus. *Brain Res.* **1235**, 21-30 (2008).

8   Ben-Ari, Y. Developing networks play a similar melody. *Trends Neurosci.* **24**, 353-360 (2001).

9   Zhang, L. I. & Poo, M.-m. Electrical activity and development of neural circuits. *Nat. Neurosci.* **4**, 1207-1214 (2001).

10   Kandel, E. & Spencer, W. Electrophysiology of hippocampal neurons: II. After-potentials and repetitive firing. *J. Neurophysiol.* **24**, 243-259 (1961).

11   Miles, R., Traub, R. D. & Wong, R. Spread of synchronous firing in longitudinal slices from the CA3 region of the hippocampus. *J. Neurophysiol.* **60**, 1481-1496 (1988).

12   Silva, L. R., Amitai, Y. & Connors, B. W. Intrinsic oscillations of neocortex generated by layer 5 pyramidal neurons. *Science* **251**, 432 (1991).

13   Verstraelen, P. *et al.* Pharmacological characterization of cultivated neuronal networks: relevance to synaptogenesis and synaptic connectivity. *Cell. Mol. Neurobiol.* **34**, 757-776 (2014).

14   Katz, L. C. & Shatz, C. J. Synaptic activity and the construction of cortical circuits. *Science* **274**, 1133-1138 (1996).

15   Aramuni, G. & Griesbeck, O. Chronic calcium imaging in neuronal development and disease. *Exp. Neurol.* **242**, 50-56 (2013).

16   Detrez, J. R. *et al.* Image Informatics Strategies for Deciphering Neuronal Network Connectivity. *Adv. Anat. Embryol. Cell Biol.* **219**, 123-148, doi:10.1007/978-3-319-28549-8_5 (2016).

17   Wickersham, I. R. & Feinberg, E. H. New technologies for imaging synaptic partners. *Curr. Opin. Neurobiol.* **22**, 121-127 (2012).

18   Kim, J. *et al.* mGRASP enables mapping mammalian synaptic connectivity with light microscopy. *Nat. Methods* **9**, 96-102 (2012).

19   Dodge Jr, F. & Rahamimoff, R. Co-operative action of calcium ions in transmitter release at the neuromuscular junction. *The Journal of physiology* **193**, 419 (1967).

20   Smetters, D., Majewska, A. & Yuste, R. Detecting action potentials in neuronal populations with calcium imaging. *Methods* **18**, 215-221 (1999).

21   Tsien, R. Y. A non-disruptive technique for loading calcium buffers and indicators into cells. (1981).

22   Nakai, J., Ohkura, M. & Imoto, K. A high signal-to-noise $Ca2+$ probe composed of a single green fluorescent protein. *Nat. Biotechnol.* **19**, 137-141 (2001).

23   Tian, L. *et al.* Imaging neural activity in worms, flies and mice with improved GCaMP calcium indicators. *Nat. Methods* **6**, 875-881 (2009).

24   Chen, T.-W. *et al.* Ultrasensitive fluorescent proteins for imaging neuronal activity. *Nature* **499**, 295-300 (2013).

25   Cornelissen, F. *et al.* Quantitation of chronic and acute treatment effects on neuronal network activity using image and signal analysis toward a high-content assay. *J. Biomol. Screen.*, 1087057113486518 (2013).

26   Miesenböck, G., De Angelis, D. A. & Rothman, J. E. Visualizing secretion and synaptic transmission with pH-sensitive green fluorescent proteins. *Nature* **394**, 192-195 (1998).

27   Granseth, B., Odermatt, B., Royle, S. J. & Lagnado, L. Clathrin-mediated endocytosis is the dominant mechanism of vesicle retrieval at hippocampal synapses. *Neuron* **51**, 773-786 (2006).

28   Li, Y. & Tsien, R. W. pHTomato, a red, genetically encoded indicator that enables multiplex interrogation of synaptic activity. *Nat. Neurosci.* **15**, 1047-1053 (2012).

29   Jackson, R. E. & Burrone, J. Visualizing presynaptic calcium dynamics and vesicle fusion with a single genetically encoded reporter at individual synapses. *Front. Synaptic Neurosci.* **8** (2016).

30   Royle, S. J., Granseth, B., Odermatt, B., Derevier, A. & Lagnado, L. Imaging phluorin-based probes at hippocampal synapses. *Membrane Trafficking*, 293-303 (2008).

31   Obien, M. E. J., Deligkaris, K., Bullmann, T., Bakkum, D. J. & Frey, U. Revealing neuronal function through microelectrode array recordings. *Front. Neurosci.* **8**, 423 (2015).

32   Holtzman, D. M., Morris, J. C. & Goate, A. M. Alzheimer's disease: the challenge of the second century. *Sci. Transl. Med.* **3**, 77sr71-77sr71 (2011).

33   Spires-Jones, T. L. & Hyman, B. T. The intersection of amyloid beta and tau at synapses in Alzheimer's disease. *Neuron* **82**, 756-771 (2014).

34   Terry, R. D. *et al.* Physical basis of cognitive alterations in Alzheimer's disease: synapse loss is the major correlate of cognitive impairment. *Ann. Neurol.* **30**, 572-580 (1991).

35   Fiala, J. C., Spacek, J. & Harris, K. M. Dendritic spine pathology: cause or consequence of neurological disorders? *Brain research reviews* **39**, 29-54 (2002).

36   Cochran, J. N., Hall, A. M. & Roberson, E. D. The dendritic hypothesis for Alzheimer's disease pathophysiology. *Brain Res. Bull.* **103**, 18-28 (2014).

37   Penzes, P., Cahill, M. E., Jones, K. A., VanLeeuwen, J.-E. & Woolfrey, K. M. Dendritic spine pathology in neuropsychiatric disorders. *Nat. Neurosci.* **14**, 285-293 (2011).

38   Scheff, S. W. & Price, D. A. Alzheimer's disease-related alterations in synaptic density: neocortex and hippocampus. *J. Alzheimers Dis.* **9**, 101-115 (2006).

39   Masliah, E. *et al.* Altered expression of synaptic proteins occurs early during progression of Alzheimer's disease. *Neurology* **56**, 127-129 (2001).

40   Perrin, R. J., Fagan, A. M. & Holtzman, D. M. Multimodal techniques for diagnosis and prognosis of Alzheimer's disease. *Nature* **461**, 916-922 (2009).

41   Jack, C. R. *et al.* Tracking pathophysiological processes in Alzheimer's disease: an updated hypothetical model of dynamic biomarkers. *The Lancet Neurology* **12**, 207-216 (2013).

42   Alzheimer, A. Uber eine eigenartige Erkrankung der Hirnrinde. *Allgemeine Zeitschrife Psychiatrie* **64**, 146-148 (1907).

43   Petersen, R. C. *et al.* Mild cognitive impairment: clinical characterization and outcome. *Arch. Neurol.* **56**, 303-308 (1999).

44   Serrano-Pozo, A., Frosch, M. P., Masliah, E. & Hyman, B. T. Neuropathological alterations in Alzheimer disease. *Cold Spring Harb. Perspect. Med.* **1**, a006189 (2011).

45   Braak, H. & Braak, E. Neuropathological stageing of Alzheimer-related changes. *Acta Neuropathol.* **82**, 239-259 (1991).

46   Borenstein, A. R., Copenhaver, C. I. & Mortimer, J. A. Early-life risk factors for Alzheimer disease. *Alzheimer Dis. Assoc. Disord.* **20**, 63-72 (2006).

47   Benilova, I., Karran, E. & De Strooper, B. The toxic A [beta] oligomer and Alzheimer's disease: an emperor in need of clothes. *Nat. Neurosci.* **15**, 349-357 (2012).

48   Giannakopoulos, P. *et al.* Tangle and neuron numbers, but not amyloid load, predict cognitive status in Alzheimer's disease. *Neurology* **60**, 1495-1500 (2003).

49   Ingelsson, M. *et al.* Early Aβ accumulation and progressive synaptic loss, gliosis, and tangle formation in AD brain. *Neurology* **62**, 925-931 (2004).

50   Braak, H. & Del Trecidi, K. Neuroanatomy and pathology of sporadic Alzheimer's disease. *Adv. Anat. Embryol. Cell Biol.* **215**, 1-162 (2015).
51   Mucke, L. *et al.* High-level neuronal expression of Aβ1–42 in wild-type human amyloid protein precursor transgenic mice: synaptotoxicity without plaque formation. *The Journal of neuroscience* **20**, 4050-4058 (2000).
52   Takahashi, R. H., Capetillo-Zarate, E., Lin, M. T., Milner, T. A. & Gouras, G. K. Co-occurrence of Alzheimer's disease β-amyloid and tau pathologies at synapses. *Neurobiol. Aging* **31**, 1145-1152 (2010).
53   Fein, J. A. *et al.* Co-localization of amyloid beta and tau pathology in Alzheimer's disease synaptosomes. *The American journal of pathology* **172**, 1683-1692 (2008).
54   Crimins, J. L., Pooler, A., Polydoro, M., Luebke, J. I. & Spires-Jones, T. L. The intersection of amyloid beta and tau in glutamatergic synaptic dysfunction and collapse in Alzheimer's disease. *Ageing research reviews* **12**, 757-763 (2013).
55   Crimins, J. L., Rocher, A. B. & Luebke, J. I. Electrophysiological changes precede morphological changes to frontal cortical pyramidal neurons in the rTg4510 mouse model of progressive tauopathy. *Acta Neuropathol.* **124**, 777-795 (2012).
56   Crimins, J. L. *et al.* Homeostatic responses by surviving cortical pyramidal cells in neurodegenerative tauopathy. *Acta Neuropathol.* **122**, 551-564 (2011).
57   Kopeikina, K. J. *et al.* Synaptic alterations in the rTg4510 mouse model of tauopathy. *J. Comp. Neurol.* **521**, 1334-1353 (2013).
58   Kopeikina, K. J. *et al.* Tau causes synapse loss without disrupting calcium homeostasis in the rTg4510 model of tauopathy. *PLoS One* **8**, e80834 (2013).
59   Rocher, A. *et al.* Structural and functional changes in tau mutant mice neurons are not linked to the presence of NFTs. *Exp. Neurol.* **223**, 385-393 (2010).
60   Callahan, L. M., Vaules, W. A. & Coleman, P. D. Quantitative decrease in synaptophysin message expression and increase in cathepsin D message expression in Alzheimer disease neurons containing neurofibrillary tangles. *J. Neuropathol. Exp. Neurol.* **58**, 275-287 (1999).
61   Ginsberg, S. D., Hemby, S. E., Lee, V. M., Eberwine, J. H. & Trojanowski, J. Q. Expression profile of transcripts in Alzheimer's disease tangle-bearing CA1 neurons. *Ann. Neurol.* **48**, 77-87 (2000).
62   Katsuse, O., Lin, W.-L., Lewis, J., Hutton, M. L. & Dickson, D. W. Neurofibrillary tangle-related synaptic alterations of spinal motor neurons of P301L tau transgenic mice. *Neurosci. Lett.* **409**, 95-99 (2006).
63   Hunsberger, H. C., Rudy, C. C., Batten, S. R., Gerhardt, G. A. & Reed, M. N. P301L tau expression affects glutamate release and clearance in the hippocampal trisynaptic pathway. *J. Neurochem.* **132**, 169-182 (2015).
64   Hoover, B. R. *et al.* Tau mislocalization to dendritic spines mediates synaptic dysfunction independently of neurodegeneration. *Neuron* **68**, 1067-1081 (2010).
65   Lee, V. M., Goedert, M. & Trojanowski, J. Q. Neurodegenerative tauopathies. *Annu. Rev. Neurosci.* **24**, 1121-1159 (2001).
66   Spillantini, M. G. & Goedert, M. Tau protein pathology in neurodegenerative diseases. *Trends Neurosci.* **21**, 428-433 (1998).
67   Grundke-Iqbal, I. *et al.* Microtubule-associated protein tau. A component of Alzheimer paired helical filaments. *J. Biol. Chem.* **261**, 6084-6089 (1986).
68   MANDELKOW, E. M. *et al.* Structure, Microtubule Interactions, and Phosphorylation of Tau Proteina. *Ann. N. Y. Acad. Sci.* **777**, 96-106 (1996).
69   Neve, R. L., Harris, P., Kosik, K. S., Kurnit, D. M. & Donlon, T. A. Identification of cDNA clones for the human microtubule-associated protein tau and chromosomal localization of the genes for tau and microtubule-associated protein 2. *Molecular Brain Research* **1**, 271-280 (1986).
70   Wang, Y. & Mandelkow, E. Tau in physiology and pathology. *Nature Reviews Neuroscience* (2015).
71   Goedert, M. & Jakes, R. Expression of separate isoforms of human tau protein: correlation with the tau pattern in brain and effects on tubulin polymerization. *EMBO J.* **9**, 4225 (1990).

72   Takuma, H., Arawaka, S. & Mori, H. Isoforms changes of tau protein during development in various species. *Developmental brain research* **142**, 121-127 (2003).

73   Chen, J., Kanai, Y., Cowan, N. & Hirokawa, N. Projection domains of MAP2 and tau determine spacings between microtubules in dendrites and axons. *Nature* **360**, 674-677 (1992).

74   Frappier, T. F., Georgieff, I. S., Brown, K. & Shelanski, M. L. τ Regulation of Microtubule-Microtubule Spacing and Bundling. *J. Neurochem.* **63**, 2288-2294 (1994).

75   Liu, C. & Götz, J. Profiling murine tau with 0N, 1N and 2N isoform-specific antibodies in brain and peripheral organs reveals distinct subcellular localization, with the 1N isoform being enriched in the nucleus. *PLoS One* **8**, e84849 (2013).

76   Zhong, Q., Congdon, E. E., Nagaraja, H. N. & Kuret, J. Tau isoform composition influences rate and extent of filament formation. *J. Biol. Chem.* **287**, 20711-20719 (2012).

77   Trabzuni, D. *et al.* MAPT expression and splicing is differentially regulated by brain region: relation to genotype and implication for tauopathies. *Hum. Mol. Genet.* **21**, 4094-4103 (2012).

78   Larcher, J. C., Boucher, D., Ginzburg, I., Gros, F. & Denoulet, P. Heterogeneity of Tau proteins during mouse brain development and differentiation of cultured neurons. *Dev. Biol.* **154**, 195-204 (1992).

79   Mandelkow, E.-M. & Mandelkow, E. Biochemistry and cell biology of tau protein in neurofibrillary degeneration. *Cold Spring Harb. Perspect. Med.* **2**, a006247 (2012).

80   Feinstein, S. C. & Wilson, L. Inability of tau to properly regulate neuronal microtubule dynamics: a loss-of-function mechanism by which tau might mediate neuronal cell death. *Biochimica et Biophysica Acta (BBA)-Molecular Basis of Disease* **1739**, 268-279 (2005).

81   Brunden, K. R., Trojanowski, J. Q. & Lee, V. M.-Y. Advances in tau-focused drug discovery for Alzheimer's disease and related tauopathies. *Nature reviews Drug discovery* **8**, 783-793 (2009).

82   Lee, G. *et al.* Phosphorylation of tau by fyn: implications for Alzheimer's disease. *The Journal of neuroscience* **24**, 2304-2312 (2004).

83   Martin, L. *et al.* Tau protein kinases: involvement in Alzheimer's disease. *Ageing research reviews* **12**, 289-309 (2013).

84   Martin, L. *et al.* Tau protein phosphatases in Alzheimer's disease: the leading role of PP2A. *Ageing research reviews* **12**, 39-49 (2013).

85   Köpke, E. *et al.* Microtubule-associated protein tau. Abnormal phosphorylation of a non-paired helical filament pool in Alzheimer disease. *J. Biol. Chem.* **268**, 24374-24384 (1993).

86   Ding, H. & Johnson, G. V. The last tangle of tau. *J. Alzheimers Dis.* **14**, 441-447 (2008).

87   Crespo-Biel, N., Theunis, C. & Van Leuven, F. Protein tau: prime cause of synaptic and neuronal degeneration in Alzheimer's disease. *International Journal of Alzheimer's Disease* **2012** (2012).

88   Kidd, M. Paired helical filaments in electron microscopy of Alzheimer's disease. (1963).

89   Cowan, C. M. & Mudher, A. Are tau aggregates toxic or protective in tauopathies? *Tau oligomers*, 6 (2014).

90   Santacruz, K. *et al.* Tau suppression in a neurodegenerative mouse model improves memory function. *Science* **309**, 476-481 (2005).

91   Oddo, S. *et al.* Reduction of soluble Aβ and tau, but not soluble Aβ alone, ameliorates cognitive decline in transgenic mice with plaques and tangles. *J. Biol. Chem.* **281**, 39413-39423 (2006).

92   Hutton, M. *et al.* Association of missense and 5'-splice-site mutations in tau with the inherited dementia FTDP-17. *Nature* **393**, 702-705 (1998).

93   Hong, M. *et al.* Mutation-specific functional impairments in distinct tau isoforms of hereditary FTDP-17. *Science* **282**, 1914-1917 (1998).

94   Bugiani, O. *et al.* Frontotemporal dementia and corticobasal degeneration in a family with a P301S mutation in tau. *J. Neuropathol. Exp. Neurol.* **58**, 667-677 (1999).

95   Cruchaga, C. *et al.* SNPs associated with cerebrospinal fluid phospho-tau levels influence rate of decline in Alzheimer's disease. *PLoS Genet* **6**, e1001101 (2010).

96   Kauwe, J. S. *et al.* Variation in MAPT is associated with cerebrospinal fluid tau levels in the presence of amyloid-beta deposition. *Proceedings of the National Academy of Sciences* **105**, 8050-8054 (2008).

97   Ingelsson, M. *et al.* Increase in the relative expression of tau with four microtubule binding repeat regions in frontotemporal lobar degeneration and progressive supranuclear palsy brains. *Acta Neuropathol.* **114**, 471-479 (2007).

98   Conrad, C. *et al.* Single molecule profiling of tau gene expression in Alzheimer's disease. *J. Neurochem.* **103**, 1228-1236 (2007).

99   Ginsberg, S. D., Che, S., Counts, S. E. & Mufson, E. J. Shift in the ratio of three-repeat tau and four-repeat tau mRNAs in individual cholinergic basal forebrain neurons in mild cognitive impairment and Alzheimer's disease. *J. Neurochem.* **96**, 1401-1408 (2006).

100   Davies, P. & Maloney, A. Selective loss of central cholinergic neurons in Alzheimer's disease. *The Lancet* **308**, 1403 (1976).

101   Robinson, D. M. & Keating, G. M. Memantine. *Drugs* **66**, 1515-1534 (2006).

102   Godyń, J., Jończyk, J., Panek, D. & Malawska, B. Therapeutic strategies for Alzheimer's disease in clinical trials. *Pharmacol. Rep.* **68**, 127-138 (2016).

103   Castellani, R. J. & Perry, G. The complexities of the pathology–pathogenesis relationship in Alzheimer disease. *Biochem. Pharmacol.* **88**, 671-676 (2014).

104   Iris, F. in *Biomarkers for Psychiatric Disorders*   473-522 (Springer, 2008).

105   Yoshiyama, Y. *et al.* Synapse loss and microglial activation precede tangles in a P301S tauopathy mouse model. *Neuron* **53**, 337-351 (2007).

106   Sturchler-Pierrat, C. *et al.* Two amyloid precursor protein transgenic mouse models with Alzheimer disease-like pathology. *Proceedings of the National Academy of Sciences* **94**, 13287-13292 (1997).

107   Oddo, S. *et al.* Triple-transgenic model of Alzheimer's disease with plaques and tangles: intracellular Aβ and synaptic dysfunction. *Neuron* **39**, 409-421 (2003).

108   Oddo, S., Caccamo, A., Kitazawa, M., Tseng, B. P. & LaFerla, F. M. Amyloid deposition precedes tangle formation in a triple transgenic model of Alzheimer's disease. *Neurobiol. Aging* **24**, 1063-1070 (2003).

109   Hill, R. S. & Walsh, C. A. Molecular insights into human brain evolution. *Nature* **437**, 64-67 (2005).

110   Rakic, P. Evolution of the neocortex: a perspective from developmental biology. *Nature Reviews Neuroscience* **10**, 724-735 (2009).

111   Finlay, B. L. & Darlington, R. B. Linked regularities in the development and evolution of mammalian brains. *Science* **268**, 1578 (1995).

112   Clowry, G., Molnár, Z. & Rakic, P. Renewed focus on the developing human neocortex. *J. Anat.* **217**, 276-288 (2010).

113   Suzuki, I. K. & Vanderhaeghen, P. Is this a brain which I see before me? Modeling human neural development with pluripotent stem cells. *Development* **142**, 3138-3150 (2015).

114   Kucukdereli, H. *et al.* Control of excitatory CNS synaptogenesis by astrocyte-secreted proteins Hevin and SPARC. *Proceedings of the National Academy of Sciences* **108**, E440-E449 (2011).

115   Oberheim, N. A., Wang, X., Goldman, S. & Nedergaard, M. Astrocytic complexity distinguishes the human brain. *Trends Neurosci.* **29**, 547-553 (2006).

116   Sofroniew, M. V. & Vinters, H. V. Astrocytes: biology and pathology. *Acta Neuropathol.* **119**, 7-35 (2010).

117   Nagele, R. G., D'Andrea, M. R., Lee, H., Venkataraman, V. & Wang, H.-Y. Astrocytes accumulate Aβ42 and give rise to astrocytic amyloid plaques in Alzheimer disease brains. *Brain Res.* **971**, 197-209 (2003).

118   Nagele, R. G. *et al.* Contribution of glial cells to the development of amyloid plaques in Alzheimer's disease. *Neurobiol. Aging* **25**, 663-674 (2004).

119   Van Dam, D. & De Deyn, P. P. Drug discovery in dementia: the role of rodent models. *Nature Reviews Drug Discovery* **5**, 956-970 (2006).

120   Kaiser, T. & Feng, G. Modeling psychiatric disorders for developing effective treatments. *Nat. Med.* **21**, 979-988 (2015).

121   Israel, M. A. *et al.* Probing sporadic and familial Alzheimer/'s disease using induced pluripotent stem cells. *Nature* **482**, 216-220 (2012).

122   Takahashi, K. *et al.* Induction of pluripotent stem cells from adult human fibroblasts by defined factors. *Cell* **131**, 861-872 (2007).

123   Kumar, D., Anand, T. & Kues, W. A. Clinical potential of human-induced pluripotent stem cells. *Cell Biol. Toxicol.*, 1-14.

124   Dolmetsch, R. & Geschwind, D. H. The human brain in a dish: the promise of iPSC-derived neurons. *Cell* **145**, 831-834 (2011).

125   Grskovic, M., Javaherian, A., Strulovici, B. & Daley, G. Q. Induced pluripotent stem cells—opportunities for disease modelling and drug discovery. *Nature reviews Drug discovery* **10**, 915-929 (2011).

126   Espuny-Camacho, I. *et al.* Pyramidal neurons derived from human pluripotent stem cells integrate efficiently into mouse brain circuits in vivo. *Neuron* **77**, 440-456 (2013).

127   González, F., Boué, S. & Belmonte, J. C. I. Methods for making induced pluripotent stem cells: reprogramming a la carte. *Nature Reviews Genetics* **12**, 231-242 (2011).

128   Hartfield, E. M. *et al.* Physiological characterisation of human iPS-derived dopaminergic neurons. *PLoS One* **9**, e87388 (2014).

129   Nicholas, C. R. *et al.* Functional maturation of hPSC-derived forebrain interneurons requires an extended timeline and mimics human neural development. *Cell stem cell* **12**, 573-586 (2013).

130   Iovino, M., Patani, R., Watts, C., Chandran, S. & Spillantini, M. G. Human stem cell-derived neurons: a system to study human tau function and dysfunction. *PLoS One* **5**, e13947 (2010).

131   Sposito, T. *et al.* Developmental regulation of tau splicing is disrupted in stem cell-derived neurons from frontotemporal dementia patients with the 10+ 16 splice-site mutation in MAPT. *Hum. Mol. Genet.* **24**, 5260-5269 (2015).

132   Gomez-Isla, T., Spires, T., De Calignon, A. & Hyman, B. T. Neuropathology of Alzheimer's disease. *Handb. Clin. Neurol.* **89**, 233-243 (2008).

133   Shi, Y., Kirwan, P. & Livesey, F. J. Directed differentiation of human pluripotent stem cells to cerebral cortex neurons and neural networks. *Nat. Protoc.* **7**, 1836-1846 (2012).

134   Wonders, C. P. & Anderson, S. A. The origin and specification of cortical interneurons. *Nature Reviews Neuroscience* **7**, 687-696 (2006).

135   Caviness, V., Takahashi, T. & Nowakowski, R. Numbers, time and neocortical neuronogenesis: a general developmental and evolutionary model. *Trends Neurosci.* **18**, 379-383 (1995).

136   Fame, R. M., MacDonald, J. L. & Macklis, J. D. Development, specification, and diversity of callosal projection neurons. *Trends Neurosci.* **34**, 41-50 (2011).

137   Douglas, R. J. & Martin, K. A. Neuronal circuits of the neocortex. *Annu. Rev. Neurosci.* **27**, 419-451 (2004).

138   López-Bendito, G. & Molnár, Z. Thalamocortical development: how are we going to get there? *Nature Reviews Neuroscience* **4**, 276-289 (2003).

139   Shi, Y., Kirwan, P., Smith, J., Robinson, H. P. & Livesey, F. J. Human cerebral cortex development from pluripotent stem cells to functional excitatory synapses. *Nat. Neurosci.* **15**, 477-486 (2012).

140   Anderson, S. & Vanderhaeghen, P. Cortical neurogenesis from pluripotent stem cells: complexity emerging from simplicity. *Curr. Opin. Neurobiol.* **27**, 151-157 (2014).

141   Yagi, T. *et al.* Modeling familial Alzheimer's disease with induced pluripotent stem cells. *Hum. Mol. Genet.* **20**, 4530-4539 (2011).

142   Fong, H. *et al.* Genetic correction of tauopathy phenotypes in neurons derived from human induced pluripotent stem cells. *Stem cell reports* **1**, 226-234 (2013).

2

Optimization of neuronal network formation in hiPSC-derived cortical neuronal cultures

Based on:

Sustained synchronized neuronal network activity in a human astrocyte co-culture system

Jacobine Kuijlaars [a], Tutu Oyelami [b], Annick Diels [b], Jutta Rohrbacher [b], Sofie Versweyveld [b], Giulia Meneghello [b], Marianne Tuefferd [b], Peter Verstraelen [c], Jan R. Detrez [c], Marlies Verschuuren [c], Winnok H. De Vos [c,d], Theo Meert [a,b], Pieter J. Peeters [b], Miroslav Cik [b], Rony Nuydens [b], Bert Brône [a*], An Verheyen [b*].

[a] Hasselt University, Biomedical Research Institute, 3590 Diepenbeek, Belgium
[b] Janssen Research & Development, a division of Janssen Pharmaceutica N.V, 2340 Beerse, Belgium
[c] Antwerp University, Department of Veterinary Science, 2020 Antwerp, Belgium
[d] Ghent University, Department of Molecular Biotechnology, 9000 Ghent, Belgium

[*] Contributed equally

Abstract

Impaired neuronal network function is a hallmark of neurodevelopmental and neurodegenerative disorders such as autism, schizophrenia, and Alzheimer's disease and is typically studied using genetically modified cellular and animal models. Weak predictive capacity and poor translational value of these models urge for better human derived *in vitro* models. The implementation of human induced pluripotent stem cells (hiPSCs) allows studying pathologies in differentiated disease-relevant and patient-derived neuronal cells. However, the differentiation process and growth conditions of hiPSC-derived neurons are non-trivial. In order to study neuronal network formation and (mal)function in a fully humanized system, we have established an *in vitro* co-culture model of hiPSC-derived cortical neurons and human primary astrocytes that partially recapitulates neuronal network synchronization and connectivity within three to four weeks after final plating. Live cell calcium imaging, electrophysiology and high content image analyses revealed an increased maturation of network functionality and synchronicity over time for co-cultures compared to neuronal monocultures. The cells produce GABAergic and glutamatergic markers and respond to inhibitors of both neurotransmitter pathways in a functional assay. The combination of this co-culture model with quantitative imaging of network morphofunction is amenable to high throughput screening for lead discovery and drug optimization for neurological diseases.

2.1 Introduction

Neurons form connections driven by molecular pathways that are encoded by developmental programs. Refinement of this neuronal network highly depends on spontaneous and experience-driven electrical activity stimulating synaptic connectivity and maturation [1-3]. As a result, spontaneous neuronal activity, most often exemplified by intracellular calcium bursting behavior, synchronizes during central nervous system development to form robust neuronal network activity via synaptic contacts. Highly synchronized bursting has been observed in different brain regions *in vivo* [2,4], but also *in vitro* in brain slices [5,6], and even in dissociated primary neuronal cultures [1,7]. Therefore, spontaneous activity is thought to be an intrinsic property of neurons, regulating synaptic transmission efficacy and cytoplasmic protein and membrane receptor trafficking [2,3,8].

Various neurodevelopmental and neurodegenerative disorders are associated with cognitive deficits. A characteristic trait of these disorders is that the morphofunction (i.e. structural and functional differences) of neuronal networks underlying cognition becomes compromised [9] (reviewed in [10]). For example, synaptic degeneration, network remodeling, and abnormal synchronization of neuronal network activity are underlying cognitive deficits in Alzheimer's disease [11,12]. In epilepsy increasing neuronal excitability and hypersynchrony disrupt normal brain function [13,14], while hyposynchrony during development is suggested to underlie the pathology observed in schizophrenia patients [15].

Sensitive assays have been developed for measuring morphofunctional connectivity of neuronal networks, including synchronized calcium bursting behavior in primary cultures of rodent neurons [7,16,17]. Such assays have been exploited to assess various pharmacological and genetic interventions [18]. Additionally electrophysiology studies *in vivo* as well as on acute brain slices have shown their importance, as they mimic aspects of particular brain areas and the (patho-) physiologically developed wiring of these structures. However, animal models often fail to mimic all features of human disease and to date translational value remains poor [19,20], potentially due to species-specific features of particularly those brain structures like the cerebral cortex that are thought to be essential for human-specific cognitive functions (reviewed in [21]). Therefore, fully human-derived models would be extremely valuable for studying disease mechanisms and identifying new therapeutic targets for neurodevelopmental and neurodegenerative diseases. The discovery of human induced pluripotent stem cells (hiPSCs) [22] has enabled the study of genetic diseases in a lineage-specific context using patient-derived cells [23]. Human-derived models facilitate a better understanding of complex genetic disorders or polygenic diseases in contrast to most animal models which are often artificially mimicking only some aspects of a certain disorder [24]. They provide a valuable addition to cells derived from animal models, which are currently the mainstay for disease modeling and drug discovery. Patient-derived cells can also serve as powerful tool for

identification of new therapeutic targets and optimization of drug treatments in personalized medicine [24].

Experimental models using hiPSC-derived neurons could be of particular relevance for neurodevelopmental and neurodegenerative disorders with complex etiologies like autism, schizophrenia, and Alzheimer's disease [25,26], as the complex genetic background is difficult to mimic using mutant animal models. However, the currently available protocols to study robust functional network activity and connectivity in hiPSC-derived cortical neurons are often time-consuming and highly variable [20,27-30].

Functional maturation of human neurons has been shown to be improved when co-cultured with rodent astrocytes [29,31,32]. However, rodent astrocytes significantly differ from human astrocytes [33,34] and a co-culture model of human iPSC-derived cortical neurons with human primary astrocytes is currently not described to our knowledge. This co-culture model could be further exploited to study functional interactions between patient iPSC-derived astrocytes and neurons.

In this study we describe the morphofunctional characterization of a fully human iPSC-derived neuron-astrocyte co-culture model. We show that optimal co-culture conditions allow the formation of synchronized neuronal network activity, within a timespan of four weeks after final plating. These neurons express both GABAergic and glutamatergic markers and respond to inhibitors of both neurotransmitter pathways. Passaging and upscaling of neural precursor cells before final plating decreased the ability to form functional neuronal networks. We present a robust and convenient protocol based on 96 multi-well format to obtain functionally connected networks of hiPSC-derived cortical neurons demonstrating sustained synchronized network activity.

2.2 Methods and Materials

2.2.1 Cell culture conditions

All work with human-derived cells was done in accordance with the Belgian guidelines and regulations and informed consent was obtained from the subjects according to manufacturers. hiPSC lines ChiPSC6b_m1 (Cellectis) and iPSC0028 (Sigma) derived from healthy individuals were cultured in Matrigel™ (BD Biosciences) coated 6 multiwell (MW6) plates (Nunc) in mTeSR™1 medium (Stem Cell Technologies) and passaged with EDTA (Gibco) when confluent [35]. hiPSCs were upscaled by passaging for a maximum of 6 times and cryopreserved until further use. Pluripotency was checked before the start of differentiation.

For differentiation into neural precursor cells (NPCs) an adapted version of the protocol from Shi and colleagues [25] was used. Briefly, confluent hiPSCs were Accutase passaged and plated at 500,000 cells / cm^2 on Matrigel™ coated MW6 plates in mTeSR™1 complete medium supplemented with 10 µM ROCK inhibitor for 1 day (days in vitro (DIV) -2). The day after medium was changed completely with mTeSR™1 complete medium (DIV -1). At DIV0, neural induction was started by changing the medium into N2B27 (Neurobasal medium and DMEM:F12 Glutamax medium in a ratio 1:1, 1% B27 supplement, 1 mM Glutamax, 0.5x Pen/Strep, 0.5% N2 supplement, 2.5 µg/ml insulin (Sigma), 50 µM 2-mercaptoethanol, 0.5x MEM NEAA, 500 µM sodium pyruvate (all Thermo Fisher Scientific, unless stated otherwise) supplemented with 10 µM SB431542 (Sigma), and 1 µM dorsomorphin (Tocris Bioscience) for a total of 12 days. At DIV 12, the neuroepithelial sheet was mechanically broken into large aggregates and replated onto laminin (Sigma) coated MW6 plates. At DIV 13 and 15 medium was replaced with N2B27 medium supplemented with 20 ng/ml FGF2 (Stem Cell Technologies) for neural precursor cell (NPC) expansion. Neural rosettes were purified on DIV 18 using dispase (Sigma, 10 mg/ml in PBS, 1/10 diluted in medium). Large rosette clumps were maintained for another week with 1 or 2 more dispase passages depending on purity of the rosettes. Around day 25 of neural induction, cells were passaged with accutase (Thermo Fisher Scientific) to dissociate cell clumps into a single-cell suspension followed by plating on laminin-coated MW6 plates with N2B27 medium changes every other day. NPCs (DIV 27-30, passage 0) were cryopreserved, further proliferated/passaged in N2B27 medium with 10 ng/ml FGF2, or used for final plating and differentiation into cortical neurons.

Final plating was done between DIV 28 and 31 of differentiation on poly-L-ornithine (PLO) plus laminin (10 µg/ml, both Sigma) coated multiwell plates or coverslips with or without primary human astrocytes (1:4 ratio astrocytes to NPCs). Since different batches of laminin from two suppliers (Biolamina and

Sigma) seemed to cause a lot of variation in the attachment and balance between proliferation and differentiation of cells, we only used laminin from Sigma (three different batches) for all experiments described in this study, unless stated otherwise.

To exit the cell cycle for all neurons at the same time point, N-[N-(3,5-Difluorophenacetyl)-L-alanyl]-S-phenylglycine t-butyl ester (DAPT, 10 µM, Sigma) was added 3 times to the described cultures, every other day after final plating [36,37]. After final plating cells were grown in N2B27 medium supplemented with 1 mM dibutyryl cAMP (Sigma) from final plating onwards and furthermore supplemented with 10 ng/ml brain derived neurotrophic factor (BDNF) and 10 ng/ml glial derived neurotrophic factor (GDNF, both R&D Systems) after incubation with DAPT.

Cerebral cortex fetal primary human astrocytes (ScienCell™) were cultured and passaged according to the manufacturer's instructions (in human astrocyte medium, ScienCell™).

2.2.2 Cell culture conditions - primary rat astrocytes

Cerebral cortices from E18-19 Wistar rat embryos were dissected in HEPES (7 mM, Sigma) -buffered Hanks Balanced Salt Solution (HBSS) and cells were dissociated enzymatically with trypsin and mechanically triturated through two fire-polished glass pipettes with decreasing diameter. After centrifugation the pellet was resuspended in Minimal Essential Medium (MEM) supplemented with 10% heat-inactivated normal horse serum and 30 mM glucose (Merck) (MEM-horse medium). Cells were grown in cell culture flasks in MEM-horse medium for 12 – 14 days with medium changes every 2 - 3 days. With every medium change loosely attached cells were dislodged and removed. All cell culture supplies were purchased from Thermo Fisher Scientific, unless stated otherwise.

2.2.3 Immunocytochemistry

Cells were fixed for 15 minutes using 4% paraformaldehyde with 4% sucrose in TBS (TrisHCl pH 7.5, NaCl and MilliQ), washed and permeabilized for 15 minutes with Triton-X100 (0.25%) in TBS. After 30 minutes blocking with donkey serum in TBS-Triton (0.25%), cells were incubated overnight at 4°C with the following antibodies: rabbit or mouse anti-β3 tubulin, rabbit anti-PAX6 (all Covance), mouse anti-HuCHuD, rabbit anti-OCT4, rabbit anti-GS1 (all Thermo Fisher Scientific), chicken anti-MAP2 (Aves), rabbit anti-Nestin, rabbit anti-TBR1, rat anti-CTIP2, mouse anti-SATB2 (all Abcam), rabbit anti-vGLUT1, mouse anti-GAD65 (both Synaptic Systems), mouse anti-S100B (BD transduction laboratories), mouse anti-NANOG, rabbit anti-OTX2, or mouse anti-GFAP (all Millipore). Subsequently, cells were washed and incubated for 1 hour at room temperature with Alexa secondary antibodies (Thermo Fisher Scientific). DAPI was used to counterstain the nuclei. Images were taken either manually with a Leica DMI 4000B microscope or Zeiss LSM 510 (confocal) or automated with the

C7000™ High Content Imaging System (confocal, Yokogawa) or Opera Phenix™ High Content Screening System (confocal, Perkin Elmer).

An overview of antibodies is given in the next table.

antigen	supplier	clone	species	isotype	catalog number
β3-tubulin	Covance	TUJ1	rabbit	IgG2a	MMS-435P
β3-tubulin	Covance	Poly18020	mouse	IgG	PRB-435P
CTIP2	Abcam	25B6	rat	IgG2a	ab18465
HuCHuD	Thermo Fisher Scientific	16A11	mouse	IgG2b, kappa	A-21271
GAD65	Synaptic Systems	26H1	mouse	IgG3	198 111
GFAP	Millipore	G-A-5	mouse	IgG1	IF03L
GS1	Thermo Fisher Scientific	7HCLC	rabbit	IgG	PA5-29737
MAP2	Aves		chicken	IgY	MAP
NANOG	Millipore	7F7.1	mouse	IgG2a, kappa	MABD24
nestin	Abcam		rabbit	IgG	ab92391
OCT4	Thermo Fisher Scientific	C30A3	rabbit	IgG	A13998
OTX2	Millipore		rabbit		AB9566
PAX6	Covance	Poly19013	rabbit	IgG	PRB-278P
S100B	BD Biosciences	19/S100B	mouse	IgG1	612 376
SATB2	Abcam	SATBA4B10	mouse	IgG1	ab51502
TBR1	Abcam		rabbit	IgG	ab31940
vGLUT1	Synaptic Systems		rabbit		135 303

2.2.4 RNA extraction and microarray analyses

RNA extraction was performed using the RNeasy mini kit (Qiagen). cDNA targets were prepared and labelled using the IVT express kit and then hybridized on Affymetrix® Human Genome U219 array plate in the GeneTitan® instrument (Affymetrix) according to the manufacturer's protocol. Microarray analysis was performed using the Bioconductor package version 2.12 (working with R version 3.0.1) [38]. Target transcripts of probes were annotated using Entrez Gene based alternative cdf version 15.1.0 [39], assigning probes to 18567 unique transcripts. RMA algorithm was used for pre-processing [40].

2.2.5 Live cell calcium imaging

Cells were loaded with 1 µM Fluo-4-AM (Thermo Fisher Scientific) in recording buffer, containing (in mM): $CaCl_2$ 1.2; KCl 2.67; NaCl 138; KH_2PO_4 1.47; Na_2HPO_4 8; D-glucose 5.6 (adapted from [41]). Cultures were incubated at 37°C and 5% CO_2 for 30 minutes and then imaged with an inverted confocal laser scanning microscope (Axiovert 100M Carl Zeiss, combined with Zeiss LSM510 software) using a Plan-NEOFLUAR 20x objective lens (NA 0.50), used in widefield imaging mode. 450 frames (61 frames per minute) were recorded per well, of which the first 200 frames represent baseline recordings, followed by 200 frames after acute pharmacological stimulation. Finally, 30 µM glutamate (50 frames) was added to distinguish neurons from non-neuronal cells [42]. Traces of non-neuronal cells, showing only a transient increase in fluorescent intensity upon glutamate addition, were discarded.

A custom-made MATLAB script (based on ref. [16], available via www.uantwerpen.be/cell-group) was used to analyze live cell calcium traces and derive various parameters reflecting characteristics of neuronal activity. In brief, regions of interest (ROIs) were drawn based on time projection images of the recordings. For each ROI traces of fluorescence intensity over time were created and used as substrate for subsequent analyses. Fluorescence traces were normalized to the initial fluorescence intensity (F/F_0) and average calcium bursting frequency and amplitude were calculated for active cells. Active cells were defined as cells showing at least one peak (i.e. calcium burst) in the fluorescence signal. Fluorescence signals of individual active neurons per well were compared to calculate an average correlation score, indicative of synchronicity of calcium signals (Pearson correlation; -1 up to 1).

To study the influence of voltage-gated sodium channels on calcium oscillations, 100 nM tetrodotoxin (TTX) was added acutely to cultures after 200 frames. To study glutamatergic and GABAergic contributions to calcium signals and neuronal activity, a combination of 20 µM 6-Cyano-7-nitroquinoxaline-2,3-dione (CNQX, competitive AMPA/kainate receptor antagonist, Sigma) and 50 µM D-(-)-2-Amino-5-phosphonopentanoic acid (D-AP5, competitive NMDA receptor antagonist, Abcam), or 50 µM picrotoxin (GABA$_A$ receptor inhibitor, Tocris Bioscience) respectively was added acutely to the cultures after 200 frames. Calcium analysis of these recordings was done by splitting the analysis in two time stretches (before and after the pharmacological intervention), after which calcium parameters from both stretches were compared.

2.2.6 Electrophysiology – patch clamp

For recording membrane and evoked potentials neurons were cultured on coverslips. In the set-up, coverslips were continuously perfused with extracellular solution containing (in mM) NaCl 125; NaHCO$_3$ 25; NaH$_2$PO$_4$ 1.25; KCl 3; CaCl$_2$ 2; MgCl$_2$ 1; glucose 25; pyruvic acid 3, pH 7.2–7.4. Extracellular solution was maintained at a temperature of approximately 35^{0}C and bubbled with 95% O$_2$, 5% CO$_2$. Glass capillaries (Harvard Apparatus) were pulled with a Flaming/Brown micropipette puller (Sutter Instrument) (tip resistance 3-10 MΩ) and filled with intracellular solution containing (in mM) potassium gluconate 135; NaCl 7; HEPES 10; Na$_2$ATP 2; Na$_2$GTP 0.3; MgCl$_2$ 2, pH 7.2 – 7.4. The voltage clamp technique in whole cell configuration using an EPC10 patch clamp amplifier (HEKA) was performed on cells with documented images. After a cell was successfully patched the resting membrane potential was recorded in zero current clamp mode before starting the experiments. To record action potentials (in current clamp mode), cells were injected with current to maintain the cells at a holding potential of -65 mV. Steps of 50 pA were applied to evoke spiking within a range of -200 to 400 pA. Evoked responses were recorded from 4 time points (week 1: 7-12 days after final plating; week 2: 13-17 days after final plating; week 3: 21-24 days after final plating; week 4-5: 30-36 days after final plating), in order to monitor the progressive maturation of the neuronal culture.

Analysis of these experiments was carried out manually using the Fitmaster software®. Frequencies of action potential firing are reported as the computed mean of the highest frequency observed in each neuron. Depolarizing spikes were considered as action potentials when they were short lasting (shorter than 10 ms at half amplitude) and when the amplitude reached 0 mV. Frequencies of action potentials were calculated as the number of action potentials divided by the current pulse time, also when only one spike was recorded. Rheobase was calculated as the mean of the minimal current injected to evoke an action potential.

Recordings of spontaneous synaptic currents (sPSCs) were made at room temperature using the voltage clamp technique in whole cell configuration using an EPC10 patch clamp amplifier (HEKA). Synaptic activity was sampled at 20 kHz and stored on a PC and subsequently filtered at 1 kHz with a Bessel filter using Patchmaster software (HEKA), running on a PC. Coverslips were placed into petri dishes and fixed on the stage of a Patch Clamp Tower (Luigs and Neumann). An inverted microscope (Olympus IX-50; Luigs and Neumann) was used to observe the cells. Patch pipettes were pulled from borosilicate glass capillaries (outside diameter 1.5 mm, inside diameter 0.87 mm; Hilgenberg) using a horizontal Flaming/Brown micropipette puller (Sutter P-97; Science Products). The pipettes were filled with (in mM) NaCl 10; KCl 120; MgATP 2; HEPES 10; D-glucose 25; GTP 0.1; pH 7.2 with KOH. Spontaneous synaptic activity was recorded in cells maintained in culture for 5 weeks at a holding potential of -80 mV in the presence of extracellular solution containing (in mM) NaCl 141.5; KCl 3; $CaCl_2$ 2; HEPES 10; D-glucose 25; pH 7.4 with NaOH.

The number of postsynaptic currents and the number and duration of quasi rhythmic events were analyzed using Clampfit (Molecular Devices). Cells were classified based on their activity pattern. Cells showing no sPSCs at all or up to five single sPCSs per minute were labeled with "no activity", cells showing 5 or more single events or less than one burst per minute were labeled with "sparse activity" and cells bursting at a frequency higher than one burst per minute were labeled with "frequently bursting". sPSC bursting frequency was defined as bursts per minute.

2.2.7 Network morphology

Images of neuronal networks were automatically analyzed using a custom made script (Neuronal Maturation, available via www.uantwerpen.be/cell-group) for Fiji, image processing freeware [43], which is available upon request. In brief, multidimensional image data sets are read and projected along the Z-axis according to the maximum intensity, after which objects of interest – i.e., nuclei, neurites and synaptic puncta – are detected and quantified.

Nucleus detection is performed by applying an automatic intensity threshold [44] on DAPI stained images after background subtraction and Gaussian blurring, followed by a watershed-based separation of touching nuclei. To determine the cellular subtype, the mean intensity for each particle was measured in the TBR1, CTIP2, SATB2 and HuC/HuD images. For every neuronal marker an empirical cut-off value was determined, above which cells were considered to belong to a specific neuronal subtype.

To measure neurite outgrowth (MAP2), a multi-tier approach was used, which was based on a dedicated in-house developed analysis for dense neuronal networks, named MorphoNeuroNet [45]. The procedure selectively segments high and low-intensity features in the image and combines them into a single mask.

Synaptic *puncta* (vGLUT1, GAD65) were pre-processed by means of a rolling ball background subtraction, Laplace filtering, automated thresholding [17,46], particle size filtering and counting of the *puncta*. Density of *puncta* was expressed as the number of positive *puncta* per mm² MAP2-positive surface.

2.2.8 Statistics

Data are shown as mean + or ± standard error of the mean (SEM). The number of differentiations per experiment refers to the differentiation procedure from hiPSCs to NPCs (either from the same hiPSC line or from a different hiPSC line), while the number of samples refers to the number of wells or cells differentiated towards neurons starting from a single batch of NPCs.

For electrophysiology experiments the differences over time were calculated using one-way ANOVAs considering equal variances. For multiple comparisons between separate time points, Holm-Sidak's multiple comparisons tests were performed.

For calcium imaging experiments overall differences between groups were calculated using two-way ANOVAs considering equal variances. For multiple comparisons, Dunnett's *t* tests were performed to detect differences compared to control (for difference between culture conditions: control represents NPCs without co-culture without DAPT; for differences between human and rat astrocytes: control represents rat co-cultures; for difference between passage numbers: control represents p0 NPCs in human astrocyte co-cultures) per time point.

2.3 Results

2.3.1 Differentiated hiPSC-derived cortical neurons associate in dense clusters on laminin coated surfaces

In order to study neuronal function and connectivity *in vitro*, we adapted a previously established cortical differentiation protocol (Fig. 2.1a) [25] for differentiating hiPSCs into cerebral cortex neurons. Starting from commercially available hiPSCs (Sigma or Cellectis) (Fig. 2.1b) neural differentiation was induced. Neural progenitor phenotype was confirmed by PAX6, Nestin and OTX2 staining (Fig. 2.1c) at 25 days after starting neural induction. After proliferation and purification, neural precursor cells (NPCs) were cryopreserved until further use. Final plating of NPCs in neural maintenance medium on a laminin-coated surface further differentiated cells into cortical neurons producing neuronal marker class III β-tubulin and cortical markers TBR1, CTIP2, and SATB2 (Fig. 2.1d) at 80 days after neural induction (7 weeks after final plating). However, also non-differentiated progenitor cells were still present in the cultures. Furthermore, the cells clustered and detached easily (Fig. 2.1d), thereby complicating downstream analyses.

2.3.2 Astrocyte co-cultures and Notch signaling inhibition increase the homogeneity of hiPSC-derived cortical neurons

Different research groups have already shown that rodent astrocytes improve the maturation of hiPSC-derived neurons [29,31]. Hence, in order to reduce cell clustering and detachment of hiPSC-derived cortical neuronal networks, we established co-cultures with primary human fetal astrocytes provided by ScienCell™. Previously, gene expression of these astrocytes has been analyzed thoroughly [47]. Immunocytochemistry and microarray data (Fig. 2.2) on different passage numbers of these human primary astrocytes revealed that the levels of astrocyte markers GFAP and S100B (mRNA expression and protein production) decreased with increasing passage numbers. Therefore, only astrocytes passaged for a maximum of three times were used for co-cultures. These neuron/astrocyte co-cultures effectively reduced neuronal clumping and detachment *in vitro* (Fig. 2.3b).

Since studies of stem cell derived neuronal cultures can be impeded by ongoing progenitor proliferation and neurogenesis creating a culture with heterogeneous neuronal identities, a Notch signaling inhibitor (N-[N-(3,5-Difluorophenacetyl)-L-alanyl]-S-phenylglycine t-butyl ester, DAPT) was used to synchronize the cultures by stimulating differentiation and inhibiting proliferation of all NPCs at the same time [36,37].
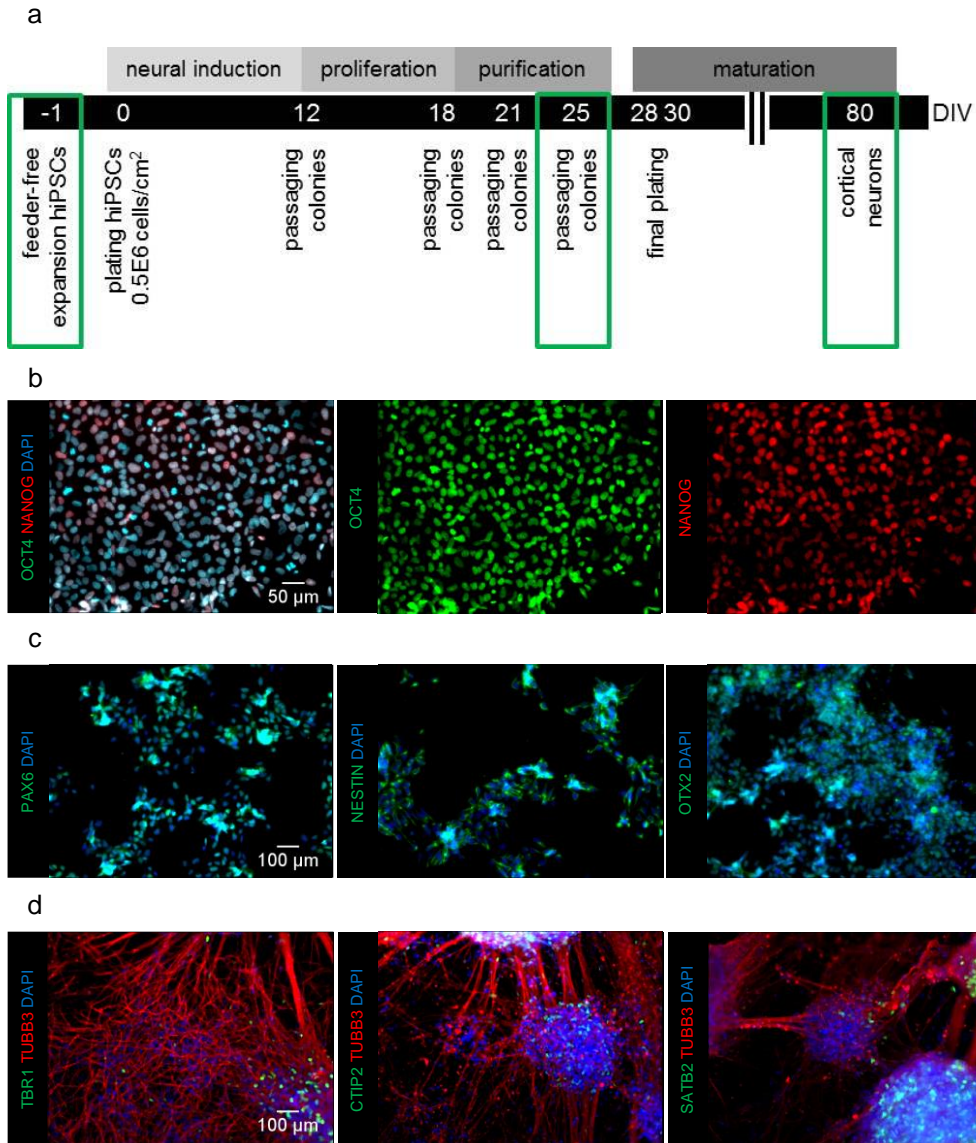
Figure 2.1 Characterization of hiPSC (-derived) cells during different steps of the differentiation protocol on laminin coated surface. a) Schematic overview of the differentiation protocol towards hiPSC-derived cortical neuronal cultures. b) hiPSCs produce pluripotency markers OCT4 and NANOG before the start of differentiation. c) Neural precursor cells produce neural stem cell markers PAX6, nestin, and OTX2 at the 25th day of the differentiation protocol. d) Fully differentiated neurons produce neuronal marker class III β-tubulin and cortical markers TBR1, CTIP2, and SATB2. However, due to the heterogeneous nature of the cultures, not all cells are immuno-positive for all markers (also undifferentiated neural precursor cells and potentially some astrocytes are present in the cultures).
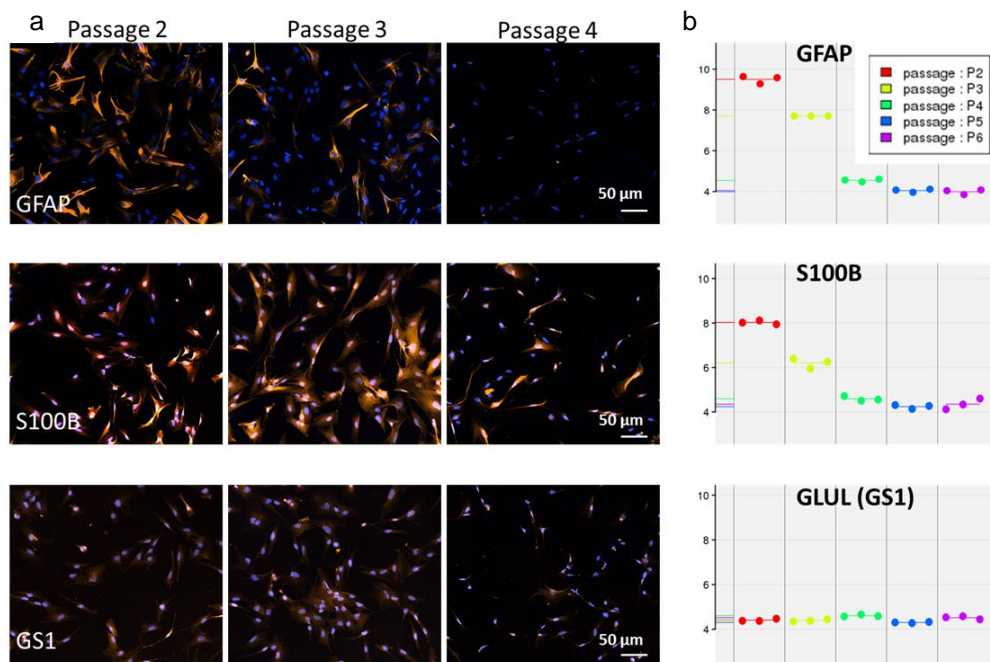
Figure 2.2 Primary human astrocytes lose primary cell identity over several passages. a) Immunocytochemistry for astrocyte markers GFAP and S100B shows a decrease in protein production over increasing number of passages of primary human astrocytes, GLUL (GS1) levels are unaltered. Astrocyte markers are shown in orange and DAPI (nuclei) in blue. b) Micro-array data show a decrease in expression of *GFAP* and *S100B* over increasing number of passages of primary human astrocytes, *GLUL* (*GS1*) expression is unaltered. Each datapoint represents 1 biological replicate from the same plate (n = 3).

In order to confirm preservation of cortical fate of the neuronal co-cultures, immunocytochemical stainings for cortical markers TBR1, CTIP2, and SATB2 were performed (Fig. 2.3c). Three weeks after final plating the cultures contain – next to the added astrocytes and undifferentiated NPCs – about 60% neurons (HuCHuD positive nuclei 62% ± 11%), of which 38% (± 6%) were TBR1 positive, 41% (± 3%) CTIP2 positive, and 12% (± 4%) SATB2 positive, suggesting that early generated deep layer neurons were predominantly present.

2.3.3 Functional maturation of hiPSC-derived neurons co-cultured with human astrocytes

Electrophysiological recordings were performed to test functionality and maturity of hiPSC-derived cortical neurons in co-cultures treated with DAPT. Whole-cell patch clamp recordings showed a gradual maturation of single cells within the network over time (Fig. 2.3d), as evident by a more negative resting membrane potential (p = 0.0113). In support of the progressive maturation, an increase in

rheobase was observed [48] (i.e. the minimal current sufficient to induce an action potential) at the second and third week after final plating (p = 0.0112). The number of neurons firing action potentials (wk1: 52%, wk2: 55%, wk3: 64%, wk4-5: 100% of all neurons recorded) and the respective firing frequency also increased over time (p = 0.0187) confirming maturation of cortical neurons [48].
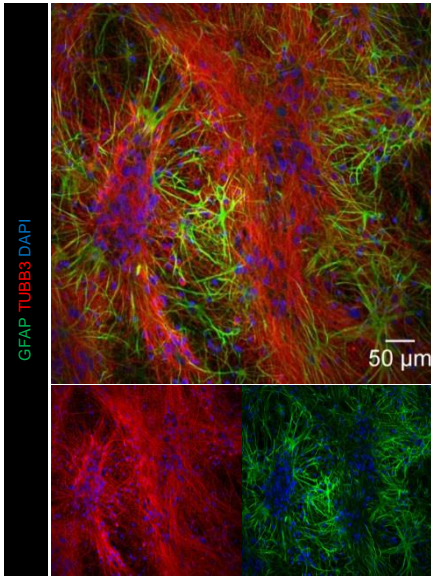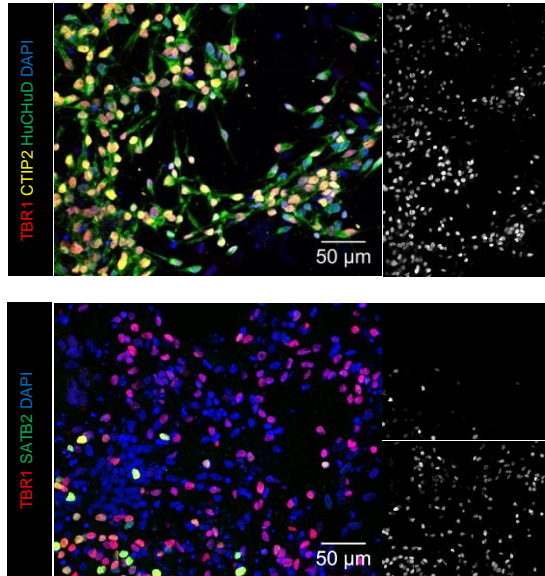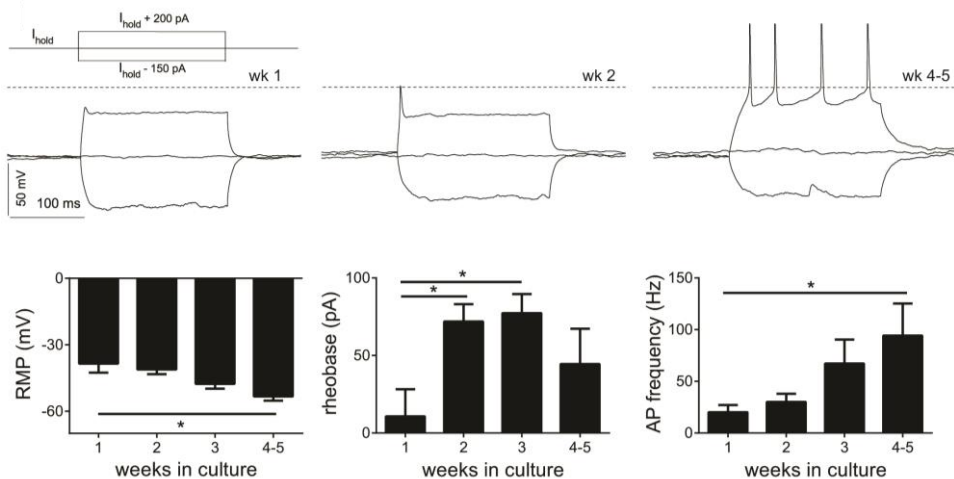
Figure 2.3 Functional maturation of hiPSC-derived cortical neurons in a short time frame via co-culture with astrocytes and treatment with DAPT. a) Cortical neurons are differentiated from NPCs after final plating on top of an astrocyte monolayer. During the first week of differentiation DAPT is added. Functional and morphological assays are performed at 2 – 8 weeks after final plating. b) hiPSCs differentiated towards cortical neurons in co-culture with primary human astrocytes are stained with neuronal marker class III β-tubulin, astrocyte marker GFAP and nuclear marker DAPI. c) Cortical fate of hiPSC-derived neurons grown in human astrocyte co-cultures is confirmed by immunocytochemistry for cortical markers TBR1 (bottom), CTIP2 (top), and SATB2 (top) in combination with the nuclear marker DAPI. d) Functional maturation of neurons analyzed using whole cell patch clamp. Traces of evoked potentials (protocol scheme included) show a clear difference between early (wk1 and wk2 respectively firing no action potentials or only one) and later time points (wk4-5 firing repetitive action potentials) of differentiation. The left graph shows a more negative resting membrane potential over time (One-way ANOVA, p=0.0113). The middle graph shows an increasing maximum action potential frequency over time (One-way ANOVA, p = 0.0187). An increased rheobase is observed as well two and three weeks after final plating (One-way ANOVA, p = 0.0112). n ≥ 9 from ≥ 1 differentiation, mean + SEM, * p<0.05.

2.3.4 Human neuron/astrocyte co-culture in combination with simultaneous differentiation of NPCs improves synchronization of calcium oscillations and network activity

In addition to electrophysiological recordings on single cells we studied the development of neuronal connectivity on neuronal network level with live cell calcium imaging. Using an in-house optimized assay (Fig. 2.4a) [16], functionality of differentiating hiPSC-derived neuronal networks was followed over a time course of 2 - 5 weeks after final plating. Neural precursor cells were plated with or without human astrocytes in the presence or absence of DAPT (Fig. 2.4b). We focused on the percentage of active neurons, bursting frequency and synchronicity (i.e. the mean Pearson's correlation between calcium indicator traces of single cells [16]). All conditions were compared to the initial protocol, which is monoculture without DAPT (Fig. 2.4b). When neurons were co-cultured with primary human astrocytes in the presence of DAPT, the percentage of active neurons was significantly increased at all time points measured while bursting frequency and synchronicity were significantly higher from week 3 onwards compared to monocultures (Fig. 2.4b). All measured parameters reached a plateau 4 to 5 weeks after final plating and remained high at least up to week 8 (Fig. 2.4c). The individual contributions of DAPT treatment and astrocyte co-culture were questioned further. Co-culture with astrocytes (without DAPT) did not improve any of the parameters, while DAPT treatment (without astrocytes) only increased the amount of active neurons. Therefore, the optimal condition is co-culturing with DAPT.
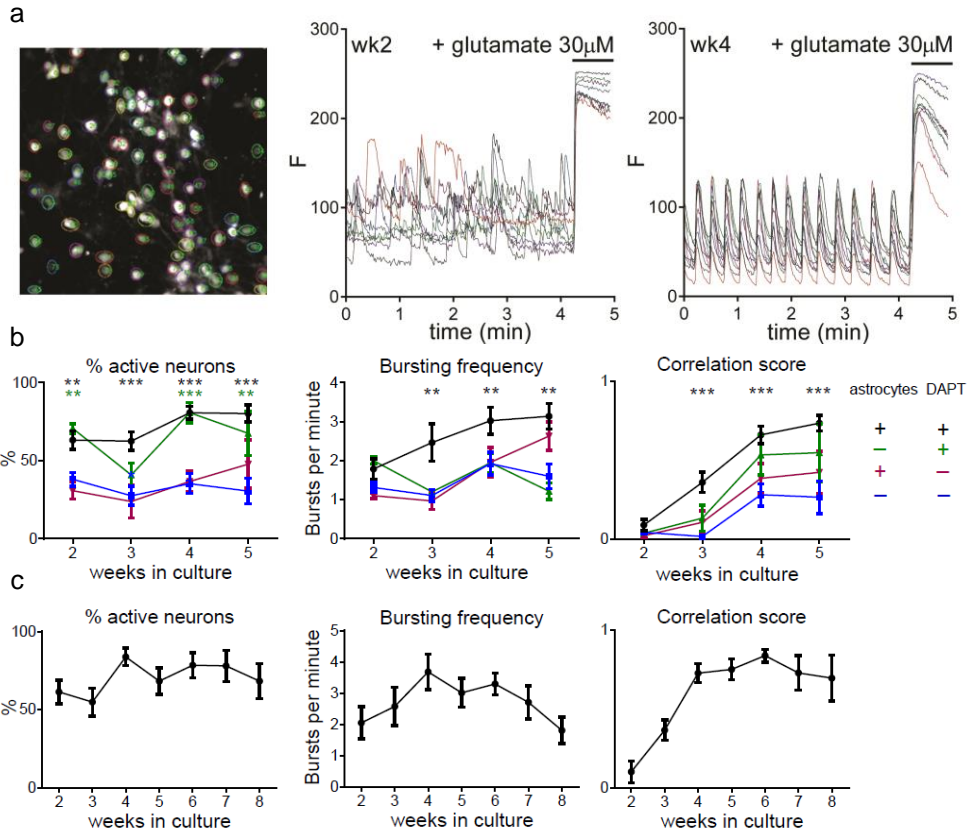
Figure 2.4 Optimization of conditions for synchronized neuronal calcium oscillations. a) Image showing automated identification of FLUO-4 loaded cells by color-coded regions of interest (ROIs) and representative traces (each trace represents fluorescence of one cell) of co-cultures with DAPT two weeks after final plating (left, no synchronicity) and four weeks after final plating (right, highly synchronized calcium influxes). After 250 frames (61 frames per minute) 30 μM glutamate was added, resulting in a large calcium influx and used to distinguish neurons from astrocytes. b) Co-culturing with primary human astrocytes and treatment with DAPT significantly increases the percentage of active neurons (Two-way ANOVA, $p < 0.0001$), bursting frequency (Two-way ANOVA, $p < 0.0001$) and synchronicity (Two-way ANOVA, $p < 0.0001$) compared to cultures without DAPT and astrocytes. $n \geq 4$ from ≥ 2 differentiations, mean ± SEM, ** $p<0.01$,***$p\leq0.0001$. c) Synchronized activity sustains up to 8 weeks after final plating in human astrocyte co-cultures with DAPT. $n \geq 5$ from ≥ 2 differentiations, mean ± SEM.

Because the use of different laminin batches seemed to cause some variation, we have further examined the four cell culture conditions on four different laminin batches (all from Sigma). As shown in Figure 2.5a live cell calcium imaging revealed that the co-culture with astrocytes and DAPT treatment gives the least variation in outcome when cultured on different laminin batches. Thus, this culture condition remains the best condition independent of the laminin

batch. When looking at the culture morphology, we showed that cell culture conditions significantly influenced the number of nuclei, the neurite surface per field, and the neurite surface per nucleus. The most stable conditions on different laminin batches were achieved either when co-cultured with astrocytes and DAPT or in case of monocultures without DAPT, but the neurite surface per nucleus was highest in case of the co-cultures with DAPT treatment.
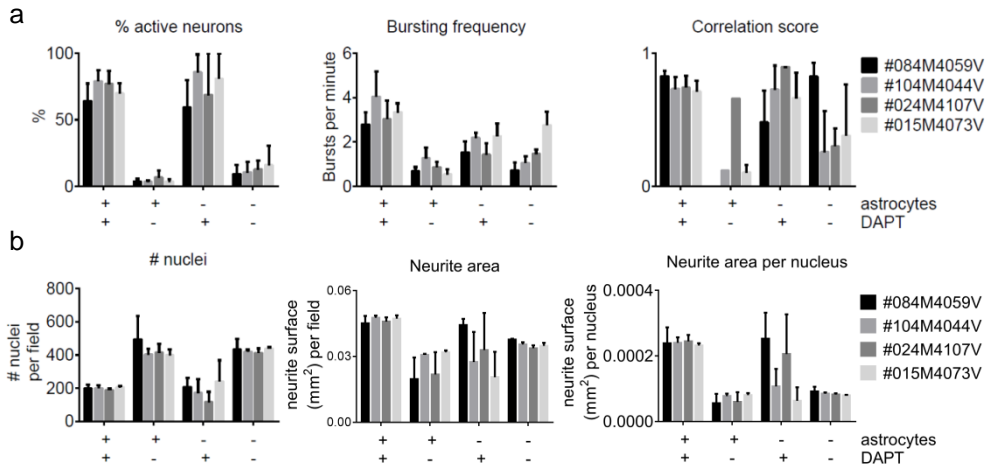
Figure 2.5 Comparison of laminin batches to optimize cell culture conditions. a) Live cell calcium imaging revealed that co-culturing with human astrocytes and DAPT treatment gives the least variation and highest outcomes in percentage active neurons, bursting frequency, and correlation score when cultured on different laminin batches. b) Cell culture conditions significantly influenced the number of DAPI positive nuclei (Two-way ANOVA, $p < 0.0001$), the neurite surface per field (Two-way ANOVA, $p = 0.0030$), and the neurite surface per nucleus (Two-way ANOVA, $p < 0.0001$). The most stable conditions on different laminin batches were achieved either when co-cultured with astrocytes and DAPT or in case of monocultures without DAPT, but the neurite surface per nucleus was highest in case of the co-cultures with DAPT treatment.

In order to compare fully human co-cultures with mixed rodent/human co-cultures (as previously described [29,31]), we cultured our hiPSC-derived neurons with freshly dissected rat primary astrocytes in the presence of DAPT. Mixed rat/human co-cultures showed an increased percentage of active neurons, bursting frequency and synchronization of neuronal calcium oscillations (Fig. 2.6) 2 to 5 weeks after final plating compared to monocultures, which is much faster than in previous studies (> 2 months) [29,31]. Additionally, there is a significantly increased percentage of active neurons, bursting frequency and correlation score in mixed co-cultures compared to fully human co-cultures at the earliest time points (wk2 and 3), while the percentage of active neurons decreased significantly at the latest time point measured (wk5). Nevertheless, with our aim to generate a fully human model, we only focus on human astrocytes for all further co-culture experiments.

2.3.5 Passaging and upscaling of NPCs before final plating decreases network activity

Increasing the amount of FGF2 passages of neural precursor cells has been shown to increase the yield of the neural induction [49]. Hence we explored the possibility of using higher passage numbers of NPCs by a limited amount of FGF2 passages (6 or 12 passages, passaging twice a week) before cryopreservation and final plating. Notably, live cell calcium imaging showed that even a limited amount of FGF2 passages (for 6 or 12 times) decreased neuronal network functionality (Fig. 2.7), lowering the percentage of active neurons ($p < 0.0001$), bursting frequency ($p < 0.0001$) and synchronicity ($p < 0.0001$). Therefore, FGF2 passaging is not recommended and we did not use passaged NPCs for other experiments in this study.

a

b
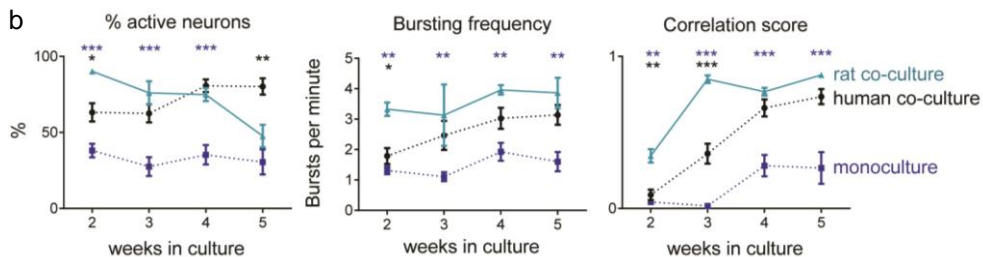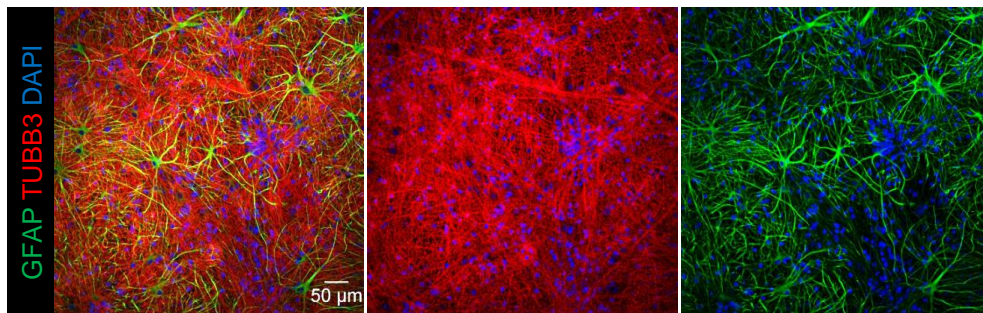
Figure 2.6 Primary rodent astrocytes induce synchronized neuronal calcium oscillations in human cortical neurons. a) hiPSCs differentiated towards cortical neurons in co-culture with primary rat astrocytes are stained with neuronal marker class III β-tubulin (TUBB3), astrocyte marker GFAP and nuclear marker DAPI. b) Co-cultures of hiPSC-derived cortical neurons with primary rat astrocytes (+ DAPT) have been compared to fully human co-cultures and monocultures. Rat co-cultures show an increased percentage of active neurons (Two-way ANOVA, $p < 0.0001$), bursting frequency (Two-way ANOVA, $p < 0.0001$) and synchronization (Two-way ANOVA, $p < 0.0001$) of neuronal calcium oscillations compared to monocultures over a time course of 2 – 5 weeks. When comparing rat and human co-cultures, there is a significant increase in the percentage of active neurons (wk2), bursting frequency (wk2) and correlation score (wk2 and wk3) at early time points, while there is a significant decrease in the amount of active neurons at the latest time point measured (wk 5). The comparison between monocultures and human co-cultures is shown in Figure 2.4b. n ≥ 3 from ≥ 2 differentiations, mean ± SEM. * $p<0.05$, ** $p<0.01$, ***$p≤0.0001$.
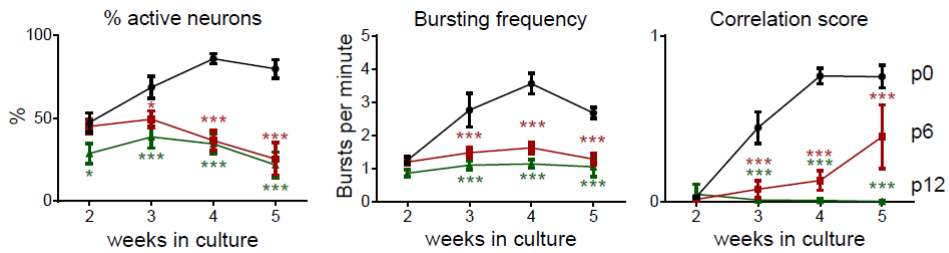
Figure 2.7 Optimization of conditions for synchronized neuronal calcium oscillations. Limited FGF2 passaging significantly reduces the percentage of active neurons (Two-way ANOVA, p<0.0001), bursting frequency (Two-way ANOVA, p<0.0001) and synchronicity (Two-way ANOVA, p<0.0001). n ≥ 4 from ≥ 2 differentiations, mean ± SEM, * p<0.05, ***p≤0.0001.

2.3.6 Synchronized calcium oscillations likely represent neuronal network activity

In order to explore the nature of the recorded calcium oscillations, we performed additional experiments. First, treatment of co-cultures with tetrodotoxin, an inhibitor of voltage-gated sodium channels, completely blocked all calcium oscillations (Fig. 2.8a), suggesting that calcium oscillations are a secondary effect to voltage-gated sodium channel mediated action potentials. Moreover, this observation excludes astrocyte-induced calcium oscillations in our model [50]. Furthermore, we measured spontaneous postsynaptic currents (sPSCs, Fig. 2.8b) in co-cultures compared to monocultures. The spontaneous electrical activity represented synaptic events because the burst firing was completely abolished in 5 out of 7 cells by combined application of the competitive AMPA/kainate receptor antagonist CNQX (20 µM) and competitive NMDA receptor antagonist DAP5 (50 µM) in the recording buffer during 5 minutes (data not shown). Co-cultures displayed more bursts of postsynaptic events (86.4% of cells) than monocultures (7.9% of cells) 5 weeks after final plating (Fig. 2.8c). More specifically, monocultures were mainly inactive (47.4% of cells compared to only 4.5% in co-cultures) or only showed sparse activity (44.7% of cells compared to 9.1% in co-cultures). These patch clamp experiments confirm that bursts of activity increase as cultures become more mature [51]. Finally, the frequency of sPSC bursts is similar to the frequency of calcium oscillations in both conditions (Fig. 2.8d), while there is a clear difference in frequency between the two cell culture conditions (Fig. 2.8d). These findings strongly suggest that synaptic network activity underlies the synchronicity of the calcium oscillations in the iPSC-derived neuronal co-culture network.
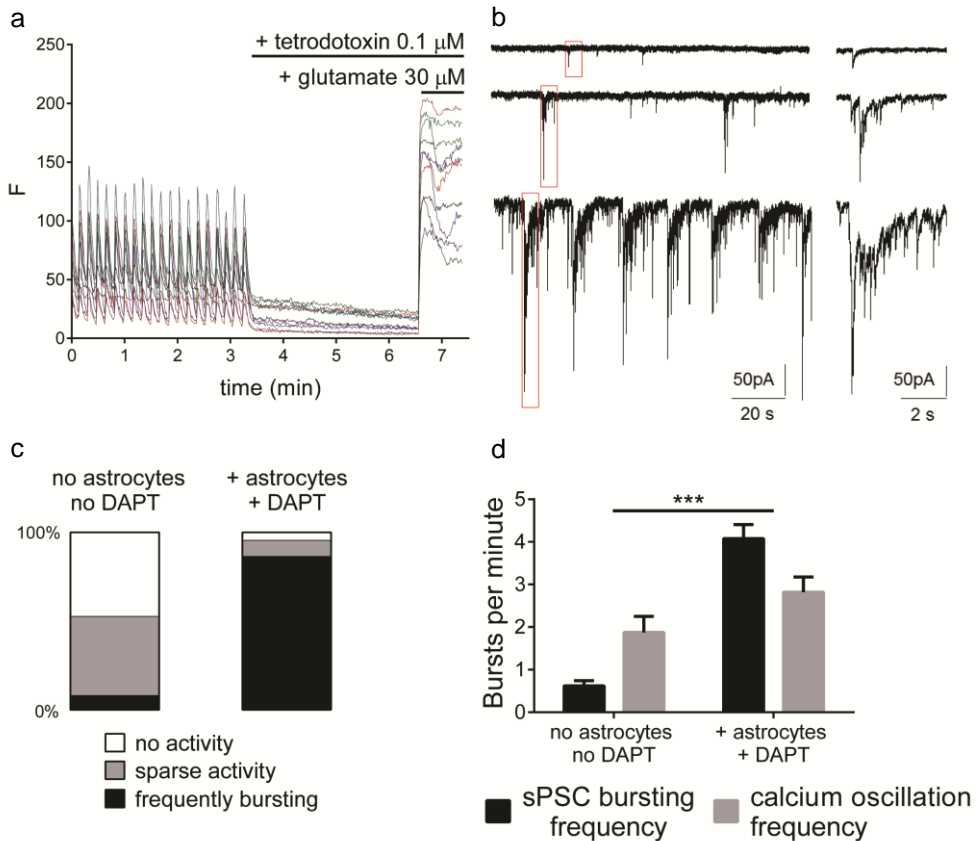
Figure 2.8 Synchronized calcium oscillations represent neuronal network activity.
a) Representative traces of live cell calcium imaging recordings in 5 week old cortical neuronal co-cultures, FLUO-4 intensity is shown over time (61 frames per minute). After 200 frames cells are exposed to tetrodotoxin (0.1 µM) followed by addition of glutamate (30 µM) after 200 frames, resulting in a large calcium influx. b) Representative traces of patch clamp recordings of sPSCs showing sparse sPSCs (upper trace), sparse bursts of sPSCs (middle trace) and frequent bursting (lower trace). c) Co-culture with primary human astrocytes + DAPT increases the percentage of cells with sPSC bursts compared to control (no DAPT, no astrocytes). "No activity" represents up to five single sPCSs per minute, "sparse activity" reflects 5 or more single events or less than one burst per minute and cells bursting at a frequency higher than one burst per minute are labeled with "frequently bursting". Number of cells per cell culture condition n ≥ 22, from ≥ 2 differentiations. d) Frequency of sPSC bursts per minute in co-cultures with primary human astrocytes + DAPT or neuron-only cultures equals the calcium oscillation frequency (Two-way ANOVA, p = NS for the respective cell culture conditions), while culture conditions induce significantly different bursting frequencies (Two-way ANOVA, p ≤ 0.0001). sPSC frequency: number of patched cells per cell culture condition ≥ 22 , from ≥ 2 differentiations, calcium oscillation frequency: n ≥ 6 from ≥ 2 differentiations. Mean + SEM, ***p≤0.0001.

2.3.7 GABAergic and glutamatergic contribution to network function in human astrocyte co-cultures

A balanced contribution of GABAergic and glutamatergic transmission to neuronal activity has been shown to be crucial for proper network function. Presence of sufficient glutamatergic neurons seems to be critical for maturity and function of a network [52]. However, GABAergic signaling has been shown to be as important for maturation and network development [53]. Therefore, the contribution of GABAergic and glutamatergic transmission to the neuronal activity in our co-cultures was studied using live cell calcium imaging. GABAergic and glutamatergic neurotransmission was studied at 3, 5, and 7 weeks after final plating by inhibiting their respective contributions. Responses were analyzed after recording baseline activity for 200 frames (61 frames per minute) by acute addition of respectively $GABA_A$ receptor inhibitor picrotoxin (50 µM) into the recording buffer or the combination of NMDA and AMPA receptor blockage with CNQX (20 µM) and DAP5 (50 µM) into the recording buffer. The effect of glutamatergic and GABAergic inhibition was recorded for another 200 frames.

Glutamatergic inhibition of network activity significantly reduced the percentage of active neurons ($p < 0.0001$ for all time points) and their synchronicity ($p < 0.05$ for all time points). The bursting frequency was reduced as well, although only at week 5 ($p < 0.001$) while the bursting amplitude remained unaffected on all time points ($p = NS$) (Fig. 2.9a). Representative traces are shown in Figure 2.9b.

On the other hand, GABAergic inhibition significantly reduced the percentage of active neurons ($p = 0.0015$), but the decrease was only significant at week 3 ($p < 0.01$). Synchronicity was unaffected ($p = NS$). Addition of picrotoxin also affected the bursting frequency (overall $p = 0.0302$) and the bursting amplitude (overall $p = 0.0125$) with a significant increase at week 5 ($p < 0.05$) (Fig. 2.9c). Representative traces are shown in Figure 2.9d.

2.3.8 Human astrocyte co-cultures show presence of both GABAergic and glutamatergic vesicular proteins

To verify whether the functional activity is also reflected by morphological correlates of connectivity we performed an automated analysis of synaptic marker levels in hiPSC-derived cortical neurons (Fig. 2.10a and 2.10b). Presence of glutamatergic and GABAergic vesicular proteins vGLUT1 and GAD65 complemented the contribution of both neurotransmitter pathways to the observed neuronal network function (Fig. 2.10c). At all three time points, similar levels of vGLUT1 and similar levels of GAD65 per neurite surface were observed.
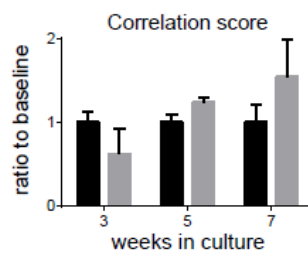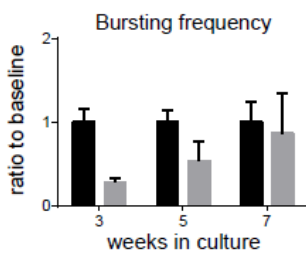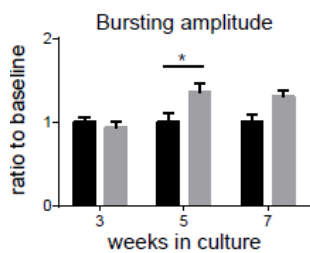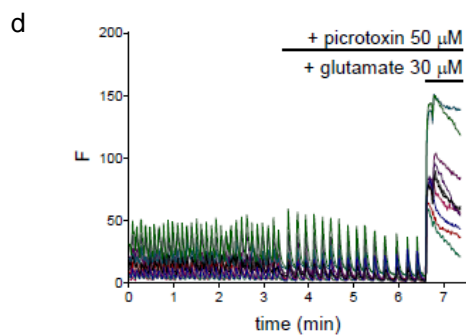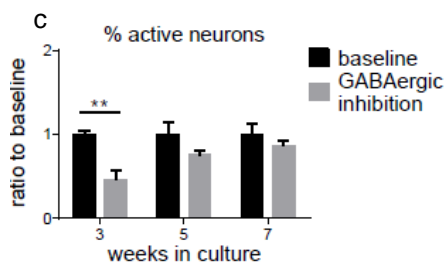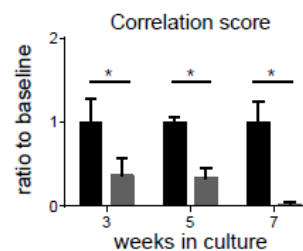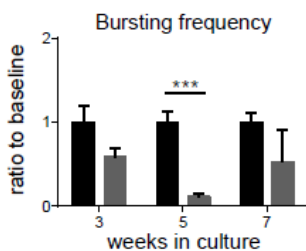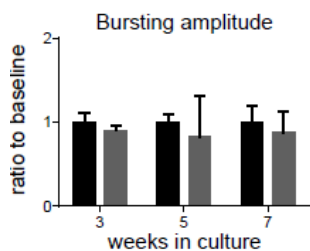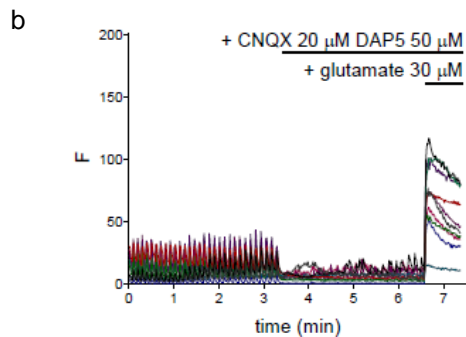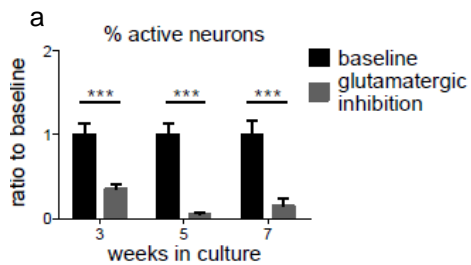
Figure 2.9 GABAergic and glutamatergic contribution to neuronal network function for cortical neurons in co-culture. a) Graphs showing a clear contribution of glutamatergic transmission to the calcium signal. Percentage of active neurons (One-way ANOVA, $p < 0.0001$), frequency (One-way ANOVA, $p = 0.0002$) and synchronicity (One-way ANOVA, $p = 0.0004$) significantly change compared to baseline. Mean + SEM, $n \geq 3$, from 3 differentiations. * $p<0.05$, ***$p \leq 0.0001$ on the different time points. b) Representative traces of live cell calcium imaging recordings in 5 week old cortical neuronal co-cultures, FLUO-4 intensity is shown over time (61 frames per minute). After 200 frames cells are exposed to DAP5 (50 µM) and CNQX (20 µM) followed by exposure to glutamate (30 µM) after 200 frames, resulting in a large calcium influx. c) Graphs showing the contribution of GABAergic transmission to the calcium signal. The percentage of active neurons (One-way ANOVA, $p = 0.0015$), bursting frequency (One-way ANOVA, $p = 0.0302$) and burst amplitude (One-way ANOVA, $p = 0.0125$) are significantly changed after addition of picrotoxin. Mean + SEM, $n \geq 3$, from 3 differentiations. * $p<0.05$, ** $p<0.01$ on the different time points. d) Representative traces of calcium imaging. After 200 frames, the cells are exposed to the GABAergic inhibitor picrotoxin (50 µM), followed by glutamate exposure (30 µM) after 200 frames.

a

vGLUT1 GAD65 MAP2 DAPI

50 µm

GAD65 DAPI

vGLUT1 DAPI

vGLUT1 - magnification

b

DAPI – nucleus selection

MAP2 - neurite area

vGLUT1 - synaptic puncta

c

Spot density

puncta / mm² MT area

80,000

0

3   5   7
weeks in culture
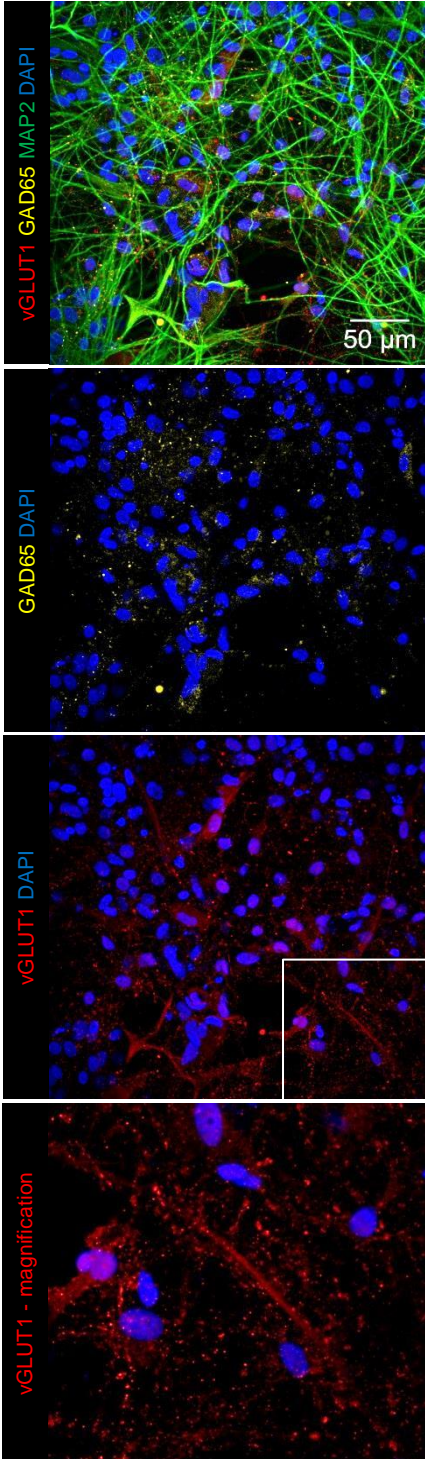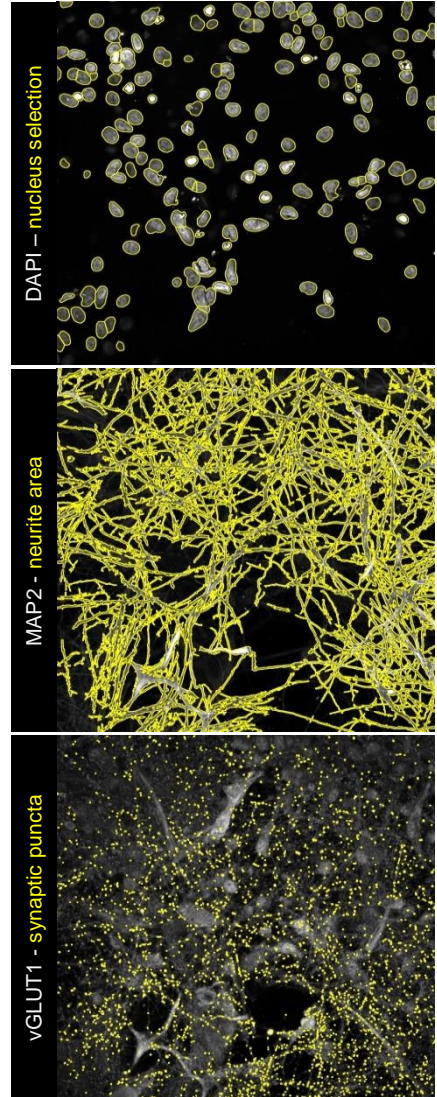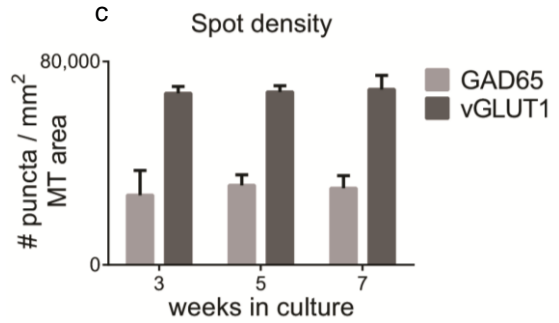
GAD65
vGLUT1

Figure 2.10 Astrocyte co-cultures are suitable for HCI and analyses. a) hiPSCs differentiated towards cortical neurons in co-culture with primary human astrocytes show presence of glutamatergic marker vGLUT1, GABAergic marker GAD65, and neuronal marker MAP2. b) Image analysis based on raw data files from a plate scanner. Masks (in yellow) are drawn per channel to identify the number of nuclei (based on DAPI staining), neurite area (based on MAP2 staining) and the number of puncta per marker (either based on vGLUT1 or GAD65). c) Quantification of glutamatergic marker vGLUT1 and GABAergic marker GAD65 per neurite area in human astrocyte co-cultures. Mean + SEM, n ≥ 4, from 3 differentiations.

2.4 Discussion

In the present study we report a fully human iPSC-derived cortical neuron/primary astrocyte co-culture system with sustained synchronized network activity. We found that differentiating hiPSC-derived neuronal cells in co-cultures progressively displayed more negative resting membrane potentials to a level sufficient to remove voltage-dependent inactivation of sodium channels and to fire repetitive action potentials. An increasing percentage of hiPSC-derived neurons fired action potentials over time, consistent with the extensive electrophysiological characterization of hiPSC-derived neurons that was published previously [54]. Besides the more negative resting membrane potential, a maturation-induced increase of the sodium channel density could contribute to the gradual increase in action potential firing capacity of the hiPSC-derived neurons. Moreover, simultaneously differentiated neurons in a human astrocyte co-culture system revealed increased activity, bursting frequency and calcium oscillation synchronization over time, representative of neuronal network activity. Human iPSC-derived neurons produced cortical markers TBR1, CTIP2, and SATB2, indicative of both deep and upper layer cortical neurons and reached a purity of about 60% of the total cell population.

Development of the central nervous system is characterized by the occurrence of spontaneous synchronized neuronal activity [8]. To study cortical network connectivity, synchrony, and function, mostly rodent brain slices and primary cortical neuronal cell cultures are used. For example, *ex vivo* population synchrony was found in hippocampal and cortical slices [5,6], and synchronized bursts were recapitulated using dissociated primary neuronal cultures *in vitro* [1,7]. More recently, hiPSC-derived cortical neurons have been shown to display bursts of synchronized network activity as well, within a specified time span of differentiation [30]. We were not able to reproduce these data, which might be due to subtle differences in the differentiation protocol, usage of different hiPSC lines, reprogramming methods or methods to measure spontaneous calcium activity. When co-culturing our hiPSC-derived neurons with primary human astrocytes in the presence of the Notch signaling inhibitor DAPT the most reproducible and sustained synchronized network activity was achieved, starting three weeks after final plating of neurons (~DIV50) and sustainable up to 8 weeks (~DIV90) *in vitro,* with neglectable variation between two different hiPSC lines, different experiments or different laminin batches. The support of primary human astrocytes, via released growth factors and physical contact [31], in combination with forced (DAPT) simultaneous differentiation of NPCs into neurons probably leads to more homogenous and mature networks in a shorter time frame. This way, there is no need to wait for the delayed emergence and development of astrocytes from NPCs, which causes slow but progressive maturation of the network [55]. Although we did not exclude the presence of spontaneously produced hiPSC-derived astrocytes in these cultures as previously described by Shi and colleagues [25,56], the calcium imaging data showed a highly beneficial

effect of the added astrocytes. The direct addition of astrocytes possibly accelerates the stimulation of synaptic connectivity and transmission in these cultures [57-59]. Further exploration of this hypothesis by comparison of hiPSC-derived neuronal networks with and without added astrocytes in immunocytochemical or electrophysiological experiments will contribute to our understanding of neuronal network function and dysfunction.

Furthermore, we were able to obtain mature networks using rodent astrocytes in about three weeks after final plating, which is much faster than in previously published work (2 months after final plating) [29,31]. This difference can result from differences in hiPSC lines, passage numbers before final plating, neural differentiation protocols or methods to measure network maturation. Although synchronization of calcium oscillations appeared earlier in mixed co-cultures than in fully human co-cultures, the percentage of active neurons decreased over time reaching levels of monocultures at week 5. This difference might be due to a "species-specific 'clock'" regulating neuronal maturation for different species with different kinetics [21]. Rodent astrocytes potentially have faster kinetics than human astrocytes. In order to explore the difference between rodent and human astrocytes additional immunocytochemical or electrophysiological experiments could be done. The contribution of physical contact or humoral factors from both astrocyte types using conditioned medium might shed a light on differences between both species. However, with our aim to generate a fully human model, we only focused on human astrocyte co-cultures.

We confirm with our model that the balance between glutamatergic and GABAergic neurons plays an important role in the observed network activity. This might explain why it is challenging to obtain synchronized oscillations [32,52]. During early cortical development, GABA is predominantly excitatory [60], followed by a switch to inhibitory properties during further maturation [61,62]. This supports our observations that both glutamatergic and GABAergic inhibitors reduce the amount of active neurons, bursting frequency and synchronicity at three weeks post final plating while at later time points (5-7 weeks) only inhibition of excitatory glutamatergic activity seems to affect network activity, while protein levels do not change over time. Notably, a trend towards increased synchronicity is observed after addition of GABAergic inhibitor picrotoxin at later time points suggesting that inhibitory neurons play an important role in controlling network activity (reviewed in [63]). As shown in primary rodent cortical neurons before, burst amplitude was significantly increased at later time points by picrotoxin as well [64]. This is another important difference to the study conducted by Kirwan and colleagues [30], who were unable to show an effect of GABAergic inhibition on calcium oscillations.

Although further optimization and upscaling is necessary the presented neuron-astrocyte co-culture model could be used to screen for compounds that affect

network functionality, either acute or chronically, in the context of phenotypic neurotoxicity screening. Due to the high sensitivity of the calcium assay, subtle changes in network activity might be detected, while other readouts like neurite outgrowth are still unaffected [7]. These combined readouts, in high-content format, allow for gauging neuronal networks *in vitro*. Furthermore, the model might offer a valuable tool for preclinical research and to screen for compounds that restore proper network functionality and reduce the progression of neuronal pathologies that display disturbed network activity and connectivity. For example, the potential mechanisms underlying the lack of neural synchronicity observed in schizophrenia [15] could be explored. Increased bursting frequency and synchronized oscillations as seen in Parkinson's disease [65], FTD [66,67] and epilepsy [11,13,14] and more complex dysregulation of network function as reported in Alzheimer's disease [11,68] and autism (reviewed in [10]) could be studied as well.

However, future research will have to demonstrate if a fully human co-culture system can be used with patient iPSC-derived astrocytes and neurons and whether impaired functional networks can be reversed using compounds or gene editing technologies. Furthermore, the interaction between human astrocytes and neurons could be studied by culturing diseased astrocytes with healthy neurons or vice versa. Finally, by adding human iPSC-derived or primary microglia, a triple co-culture model could eventually be a tool to study neuro-inflammation.

In summary, we report that simultaneously differentiated hiPSC-derived cortical neurons in co-culture with human primary astrocytes show increasing maturation of network functionality and synchronicity over time when compared to cultures without primary human astrocytes. Our approach is exquisitely suited for sensitive high-content screening approaches such as neurotoxicity screening, target identification and validation, disease modeling, and phenotypic drug screening potentially leading to safer and more efficacious medicines.

Acknowledgements

References

1   Cohen, E., Ivenshitz, M., Amor-Baroukh, V., Greenberger, V. & Segal, M. Determinants of spontaneous activity in networks of cultured hippocampus. *Brain Res.* **1235**, 21-30 (2008).
2   Ben-Ari, Y. Developing networks play a similar melody. *Trends Neurosci.* **24**, 353-360 (2001).
3   Zhang, L. I. & Poo, M.-m. Electrical activity and development of neural circuits. *Nat. Neurosci.* **4**, 1207-1214 (2001).
4   Kandel, E. & Spencer, W. Electrophysiology of hippocampal neurons: II. After-potentials and repetitive firing. *J. Neurophysiol.* **24**, 243-259 (1961).
5   Miles, R., Traub, R. D. & Wong, R. Spread of synchronous firing in longitudinal slices from the CA3 region of the hippocampus. *J. Neurophysiol.* **60**, 1481-1496 (1988).
6   Silva, L. R., Amitai, Y. & Connors, B. W. Intrinsic oscillations of neocortex generated by layer 5 pyramidal neurons. *Science* **251**, 432 (1991).
7   Verstraelen, P. *et al.* Pharmacological characterization of cultivated neuronal networks: relevance to synaptogenesis and synaptic connectivity. *Cell. Mol. Neurobiol.* **34**, 757-776 (2014).
8   Katz, L. C. & Shatz, C. J. Synaptic activity and the construction of cortical circuits. *Science* **274**, 1133-1138 (1996).
9   Wen, Z. *et al.* Synaptic dysregulation in a human iPS cell model of mental disorders. *Nature* **515**, 414-418 (2014).
10   Schipul, S. E., Keller, T. A. & Just, M. A. Inter-regional brain communication and its disturbance in autism. *Front. Syst. Neurosci.* **5** (2011).
11   Noebels, J. A perfect storm: converging paths of epilepsy and Alzheimer's dementia intersect in the hippocampal formation. *Epilepsia* **52**, 39-46 (2011).
12   Braak, H. & Del Trecidi, K. Neuroanatomy and pathology of sporadic Alzheimer's disease. *Adv. Anat. Embryol. Cell Biol.* **215**, 1-162 (2015).
13   Holtkamp, M. *et al.* Status epilepticus induces increasing neuronal excitability and hypersynchrony as revealed by optical imaging. *Neurobiol. Dis.* **43**, 220-227 (2011).

14   Morelli, G. *et al.* Cerebral Cortical Circuitry Formation Requires Functional Glycine Receptors. *Cereb. Cortex*, bhw025 (2016).

15   Uhlhaas, P. J. & Singer, W. Abnormal neural oscillations and synchrony in schizophrenia. *Nat. Rev. Neurosci.* **11**, 100-113 (2010).

16   Cornelissen, F. *et al.* Quantitation of chronic and acute treatment effects on neuronal network activity using image and signal analysis toward a high-content assay. *J. Biomol. Screen.*, 1087057113486518 (2013).

17   Detrez, J. R. *et al.* Image Informatics Strategies for Deciphering Neuronal Network Connectivity. *Adv. Anat. Embryol. Cell Biol.* **219**, 123-148, doi:10.1007/978-3-319-28549-8_5 (2016).

18   Harrill, J. A., Robinette, B. L. & Mundy, W. R. Use of high content image analysis to detect chemical-induced changes in synaptogenesis in vitro. *Toxicol. In Vitro* **25**, 368-387 (2011).

19   Wallace, T. L., Ballard, T. M. & Glavis-Bloom, C. in *Cognitive Enhancement*   27-57 (Springer, 2015).

20   Kaiser, T. & Feng, G. Modeling psychiatric disorders for developing effective treatments. *Nat. Med.* **21**, 979-988 (2015).

21   Suzuki, I. K. & Vanderhaeghen, P. Is this a brain which I see before me? Modeling human neural development with pluripotent stem cells. *Development* **142**, 3138-3150 (2015).

22   Takahashi, K. *et al.* Induction of pluripotent stem cells from adult human fibroblasts by defined factors. *Cell* **131**, 861-872 (2007).

23   Park, I.-H. *et al.* Disease-specific induced pluripotent stem cells. *Cell* **134**, 877-886 (2008).

24   Inoue, H., Nagata, N., Kurokawa, H. & Yamanaka, S. iPS cells: a game changer for future medicine. *EMBO J.* **33**, 409-417 (2014).

25   Shi, Y., Kirwan, P. & Livesey, F. J. Directed differentiation of human pluripotent stem cells to cerebral cortex neurons and neural networks. *Nat. Protoc.* **7**, 1836-1846 (2012).

26   Yagi, T. *et al.* Modeling familial Alzheimer's disease with induced pluripotent stem cells. *Hum. Mol. Genet.* **20**, 4530-4539 (2011).

27   Israel, M. A. *et al.* Probing sporadic and familial Alzheimer/'s disease using induced pluripotent stem cells. *Nature* **482**, 216-220 (2012).

28   Belinsky, G. S. *et al.* Patch-clamp recordings and calcium imaging followed by single-cell PCR reveal the developmental profile of 13 genes in iPSC-derived human neurons. *Stem Cell Res.* **12**, 101-118 (2014).

29   Odawara, A., Saitoh, Y., Alhebshi, A., Gotoh, M. & Suzuki, I. Long-term electrophysiological activity and pharmacological response of a human induced pluripotent stem cell-derived neuron and astrocyte co-culture. *Biochem. Biophys. Res. Commun.* **443**, 1176-1181 (2014).

30   Kirwan, P. *et al.* Development and function of human cerebral cortex neural networks from pluripotent stem cells in vitro. *Development* **142**, 3178-3187 (2015).

31   Tang, X. *et al.* Astroglial cells regulate the developmental timeline of human neurons differentiated from induced pluripotent stem cells. *Stem Cell Res.* **11**, 743-757 (2013).

32   Johnson, M. A., Weick, J. P., Pearce, R. A. & Zhang, S.-C. Functional neural development from human embryonic stem cells: accelerated synaptic activity via astrocyte coculture. *J. Neurosci.* **27**, 3069-3077 (2007).

33   Oberheim, N. A. *et al.* Uniquely hominid features of adult human astrocytes. *The Journal of Neuroscience* **29**, 3276-3287 (2009).

34   Zhang, Y. *et al.* Purification and characterization of progenitor and mature human astrocytes reveals transcriptional and functional differences with mouse. *Neuron* (2015).

35   Beers, J. *et al.* Passaging and colony expansion of human pluripotent stem cells by enzyme-free dissociation in chemically defined culture conditions. *Nat. Protoc.* **7**, 2029-2040 (2012).

36   Borghese, L. *et al.* Inhibition of notch signaling in human embryonic stem cell–derived neural stem cells delays G1/S phase transition and accelerates neuronal differentiation in vitro and in vivo. *Stem Cells* **28**, 955-964 (2010).

37   Ogura, A., Morizane, A., Nakajima, Y., Miyamoto, S. & Takahashi, J. γ-secretase inhibitors prevent overgrowth of transplanted neural progenitors derived from human-induced pluripotent stem cells. *Stem Cells Dev.* **22**, 374-382 (2012).

38   Gentleman, R. C. *et al.* Bioconductor: open software development for computational biology and bioinformatics. *Genome Biol.* **5**, R80 (2004).

39   Dai, M. *et al.* Evolving gene/transcript definitions significantly alter the interpretation of GeneChip data. *Nucleic Acids Res.* **33**, e175-e175 (2005).

40   Irizarry, R. A. *et al.* Exploration, normalization, and summaries of high density oligonucleotide array probe level data. *Biostatistics* **4**, 249-264 (2003).

41   Wang, X.-s. & Gruenstein, E. I. Mechanism of synchronized Ca 2+ oscillations in cortical neurons. *Brain Res.* **767**, 239-249 (1997).

42   Pickering, M., Pickering, B. W., Murphy, K. J. & O'Connor, J. J. Discrimination of cell types in mixed cortical culture using calcium imaging: a comparison to immunocytochemical labeling. *J. Neurosci. Methods* **173**, 27-33 (2008).

43   Schindelin, J. *et al.* Fiji: an open-source platform for biological-image analysis. *Nat. Methods* **9**, 676-682 (2012).

44   Huang, L.-K. & Wang, M.-J. J. Image thresholding by minimizing the measures of fuzziness. *Pattern Recog.* **28**, 41-51 (1995).

45   Pani, G. *et al.* MorphoNeuroNet: An automated method for dense neurite network analysis. *Cytometry Part A* **85**, 188-199 (2014).

46   Zack, G., Rogers, W. & Latt, S. Automatic measurement of sister chromatid exchange frequency. *J. Histochem. Cytochem.* **25**, 741-753 (1977).

47   Malik, N. *et al.* Comparison of the gene expression profiles of human fetal cortical astrocytes with pluripotent stem cell derived neural stem cells identifies human astrocyte markers and signaling pathways and transcription factors active in human astrocytes. (2014).

48   Liao, C.-C. & Lee, L.-J. Evidence for structural and functional changes of subplate neurons in developing rat barrel cortex. *Brain Structure and Function* **217**, 275-292 (2012).

49   Boissart, C. *et al.* Differentiation from human pluripotent stem cells of cortical neurons of the superficial layers amenable to psychiatric disease modeling and high-throughput drug screening. *Transl. Psychiatry* **3**, e294 (2013).

50   Araque, A., Parpura, V., Sanzgiri, R. P. & Haydon, P. G. Glutamate-dependent astrocyte modulation of synaptic transmission between cultured hippocampal neurons. *Eur. J. Neurosci.* **10**, 2129-2142 (1998).

51   Wagenaar, D. A., Pine, J. & Potter, S. M. An extremely rich repertoire of bursting patterns during the development of cortical cultures. *BMC Neurosci.* **7**, 1 (2006).

52   Meneghello, G. *et al.* Evaluation of established human iPSC-derived neurons to model neurodegenerative diseases. *Neuroscience* **301**, 204-212 (2015).

53   Rushton, D. J., Mattis, V. B., Svendsen, C. N., Allen, N. D. & Kemp, P. J. Stimulation of GABA-induced Ca 2+ influx enhances maturation of human induced pluripotent stem cell-derived neurons. *PLoS One* **8**, e81031 (2013).

54   Prè, D. *et al.* A time course analysis of the electrophysiological properties of neurons differentiated from human induced pluripotent stem cells (iPSCs). *PLoS One* (2014).

55   Krencik, R., Weick, J. P., Liu, Y., Zhang, Z.-J. & Zhang, S.-C. Specification of transplantable astroglial subtypes from human pluripotent stem cells. *Nat. Biotechnol.* **29**, 528-534 (2011).

56   Shi, Y., Kirwan, P., Smith, J., Robinson, H. P. & Livesey, F. J. Human cerebral cortex development from pluripotent stem cells to functional excitatory synapses. *Nat. Neurosci.* **15**, 477-486 (2012).

57   Kucukdereli, H. *et al.* Control of excitatory CNS synaptogenesis by astrocyte-secreted proteins Hevin and SPARC. *Proceedings of the National Academy of Sciences* **108**, E440-E449 (2011).

58   Oberheim, N. A., Wang, X., Goldman, S. & Nedergaard, M. Astrocytic complexity distinguishes the human brain. *Trends Neurosci.* **29**, 547-553 (2006).

59   Sofroniew, M. V. & Vinters, H. V. Astrocytes: biology and pathology. *Acta Neuropathol.* **119**, 7-35 (2010).

60   Ben-Ari, Y. Excitatory actions of GABA during development: the nature of the nurture. *Nat. Rev. Neurosci.* **3**, 728-739 (2002).

61   Ben-Ari, Y., Gaiarsa, J.-L., Tyzio, R. & Khazipov, R. GABA: a pioneer transmitter that excites immature neurons and generates primitive oscillations. *Physiol. Rev.* **87**, 1215-1284 (2007).

62   Ganguly, K., Schinder, A. F., Wong, S. T. & Poo, M.-m. GABA itself promotes the developmental switch of neuronal GABAergic responses from excitation to inhibition. *Cell* **105**, 521-532 (2001).

63   Mann, E. O. & Paulsen, O. Role of GABAergic inhibition in hippocampal network oscillations. *Trends Neurosci.* **30**, 343-349 (2007).

64   Murphy, T. H., Blatter, L. A., Wier, W. G. & Baraban, J. Spontaneous synchronous synaptic calcium transients in cultured cortical neurons. *J. Neurosci.* **12**, 4834-4845 (1992).

65   Heimer, G., Rivlin, M., Israel, Z. & Bergman, H. in *Parkinson's Disease and Related Disorders*   17-20 (Springer, 2006).

66   Whitwell, J. *et al.* Altered functional connectivity in asymptomatic MAPT subjects A comparison to bvFTD. *Neurology* **77**, 866-874 (2011).

67   Stancu, I.-C. *et al.* Templated misfolding of Tau by prion-like seeding along neuronal connections impairs neuronal network function and associated behavioral outcomes in Tau transgenic mice. *Acta Neuropathol.* **129**, 875-894 (2015).

68   Sorg, C., Riedl, V., Perneczky, R., Kurz, A. & Wohlschlager, A. M. Impact of Alzheimer's disease on the functional connectivity of spontaneous brain activity. *Curr. Alzheimer Res.* **6**, 541-553 (2009).

3

Neuronal networks in a tau overexpression model in primary rodent and hiPSC-derived cortical cultures

Abstract

Neuronal network dysfunction is thought to be one of the underlying mechanisms of cognitive decline. In a specific group of neurodegenerative disorders, called tauopathies, this neuronal network dysfunction might be caused by disturbed function and expression of *MAPT* encoding microtubule binding protein tau. The physiological role of tau is microtubule stabilization involved in cytoskeleton reorganization, neurite outgrowth, axonal transport, and maintenance of cellular viability. Using primary rodent and hiPSC-derived cortical neuronal cultures we investigated the influence of tau aggregation on neuronal network morphofunction in order to develop a translational model suitable for screening. Robust tau aggregation was accomplished by AAV-induced human tau overexpression carrying the pro-aggregating P301L mutation triggered with K18P301L fibrils. No differences in overall network functionality were reported in this model, but hyperactivity was found specifically in cells overexpressing tau. Fibril seeding caused some morphological changes indicative of tauopathy-like phenomena in primary cultures, but not in hiPSC-derived neuronal cultures. Combined with the phenotype of tau aggregation in both cell culture systems these models might gain useful insights in tauopathy-associated processes. Species-related differences between both models might be used to bridge the gap between animal models and clinical research. Moreover, the underlying mechanisms of the observed phenotypes remain to be elucidated.

3.1 Introduction

In 1907, Alois Alzheimer reported the first case of Alzheimer's disease (AD) [1], in which he reported histopathological hallmarks now being identified as plaques (accumulation of extracellular aggregates of insoluble beta-amyloid) and tangles (intraneuronal filaments of hyperphosphorylated tau protein). The third major morphological feature of AD is neuronal loss. Although plaques are typical hallmarks of AD, no correlation has been found with cognitive impairment, while tangles do correlate with cognitive impairment, neuronal and synapse loss [2,3]. The strongest correlate with cognitive decline is actually synapse loss in hippocampus and cortex [4], as confirmed in mouse models of AD in which synaptic dysfunction is observed earlier than neuron loss and coincides with the onset of memory deficiencies [5]. These early events are important targets for intervention, because they underlie the start of pathology. Recent advances in biomarker identification in AD enabled detection of aspects of AD pathology in cognitively normal individuals, one or even two decades before onset of clinical dementia [6]. Examples of these biomarkers are increased levels of tau and phosphorylated tau in cerebrospinal fluid (CSF). An increasing number of studies found that soluble forms of both beta-amyloid and tau protein act at the synapse to cause neural network dysfunction rather than (insoluble) plaques and tangles (reviewed in ref. [7]). For example, Hunsberger and colleagues found tau induced excitotoxicity in a p301L tau mouse model, while pathology was still subtle and before detectable neuronal loss [8]. However, the exact mechanisms and cause of synaptic dysfunction in AD is not known yet.

About a century ago, Alois Alzheimer first described neurofibrillary tangles (NFTs) [1], but not earlier than three decades ago the major component of tangles was identified as a hyperphosphorylated, filamentous form of the tau protein [9]. AD and other tauopathies (i.e. a group of neurodegenerative disorders characterized by the accumulation and aggregation of the pathological tau protein in human brains), for example frontotemporal dementia, unequivocally demonstrated that dysfunction of tau protein can drive neurodegeneration. In individuals with familial frontotemporal dementia, more than 30 mutations, for example P301L, have been found in the *MAPT* gene, encoding the tau protein [10,11]. Tau is a microtubule binding protein, traditionally perceived as axonal protein, where it serves to stabilize microtubules. Upon phosphorylation, tau reduces its affinity for and dissociated from microtubules. However, recent studies suggest an important role for tau in dendrites as well, where tau targets kinases to the postsynaptic density (PSD)[12]. Tai and colleagues also observed tau in pre- and postsynaptic terminals of nondemented human controls as well as AD patients [13], strengthening the idea of postsynaptic presence of tau protein. However, the exact role of distinct phospho-species and isoforms in physiological and pathological context awaits elucidation. During the course of AD, tau becomes hyperphosphorylated, detaches from microtubules and accumulates in filaments [14-16]. Filamentous tau accumulates intracellularly as NFTs, one of AD's typical

hallmarks. Significant accumulation of NFTs coincides with oxidative stress, inflammation, synaptic and network dysfunction and ultimately neuronal loss, but not before stages of moderate to severe dementia [17]. But in the last decade, accumulating evidence has shown that tangles exert negligible neurotoxicity compared to soluble tau [18,19].

In AD cases, SNPs in the PPP3R1 gene, encoding the regulatory subunit of calcineurin, were associated with higher CSF concentrations of tau and phospho-tau, increased tangle pathology, and a more rapid disease progression [20]. Kauwe and colleagues found SNPs in the *MAPT* gene, encoding tau, affecting disease progression as well [21]. In human AD brains, accumulation of oligomeric, hyperphosphorylated tau has been found in synapses [22]. Furthermore, Perez-Nievas and coworkers found that total number of NFT was not associated with dementia, while increased levels of phosphorylated tau, specifically in the synaptic compartment, did [23]. In another study in AD subjects, immunofluorescence showed tau protein, hyperphosphorylated tau and misfolded tau in pre- and postsynaptic terminals. However, in synapses from non-demented elderly tau hyperphosphorylation and some misfolding was shown as well, implicating that synaptic terminals are one of the first, probably most sensitive, subcellular compartments affected by tauopathies [13]. Tau hyperphosphorylation and misfolding at synapses may represent early signs of AD pathology, mediators of synaptopathy, and substrates for tauopathy spreading, but the actual role of tau in these processes is not known yet.

Different animal models have been used to gain insight in tauopathies. For example rTg4510 mice, overexpressing human P301L tau, showed alterations in synaptic function and structure [7,24-28]. Tangle bearing neurons are reported to produce less synaptic proteins and receive fewer synapses [29-31]. The importance of the tripartite glutamatergic synapse (consisting of a pre- and postsynaptic terminal and an astrocytic process) in synaptic function in AD is studied by Hunsberger and colleagues (for review: [32]). They found that tau pathology induces hyperexcitability of the glutamatergic system via increased presynaptic vesicle release and decreased glutamate clearance from the synaptic cleft by astrocytes. Both processes correlated well with memory performance of these mice, and occurred while tau pathology was still subtle without significant neuronal loss [8].

Next to *in vivo* experiments in animal models for tauopathies, dissociated rodent primary neuronal culture models have proven to provide valuable information about tau pathologies. Hoover and colleagues showed in dissociated rodent primary neuronal cultures that early tau-induced deficits develop within the dendritic spines, by disrupting glutamate receptor trafficking or synaptic anchoring, thereby impairing synaptic function. By creating pseudo-phosphorylated and phosphorylation-deficient tau protein they showed that tau phosphorylation plays a critical role in mediating synaptic deficiencies in this

model [33]. Another useful *in vitro* model to study tauopathies will be used in this chapter. In this model, dissociated primary neurons overexpressing human P301L mutant tau form NFTs after addition of recombinant P301L mutant tau fibrils [34]. Initially, the intracellular conversion of highly soluble tau protein without a defined secondary structure into insoluble tau fibrils was studied using cell lines. Extracellular tau aggregates, but not monomers, showed to be taken up by cultured cells and induced fibrillization of intracellular full-length tau. These intracellular fibrils can seed fibril formation and can be transferred between cells [35]. Fibrils time-dependently recruit normal tau and induce neuritic tau pathology in post-mitotic neurons as well [34]. Additionally, evidence was provided that tau pathology is transmitted from cell to cell *in vitro* [36] as well as *in vivo* [37,38]. Initiation of tau spreading with fibrils and overexpression of human P301L mutant tau was used in order to develop controllable tau aggregation within the experimental time window. Overexpression causes an increase in the local production of tau, while non-transgenic neurons show a very diffuse pattern. Furthermore, developing rodent neurons mainly express *MAPT* with three C-terminal repeats which has a lower propensity to aggregate than the adult (and overexpressed) four-repeat tau isoform [39]. Recently, tau aggregation was shown in a similar fashion in hiPSC-derived cortical neurons [40]. We will use this hiPSC-derived cortical neuronal model of tau aggregation for functional phenotyping.

In this chapter we tested the hypothesis that human soluble tau species induce synaptotoxicity and subsequent changes in structure and function of synapses and neuronal network in primary rodent and hiPSC-derived cortical cultures. Previously, these models have proven to show tau aggregation, but overall network characteristics were not examined yet. We found that tau overexpression combined with fibril seeding did not affect overall calcium oscillations in our primary rodent and hiPSC-derived cortical cultures, neither network morphology in hiPSC-derived cortical cultures. However, network morphology was significantly changed in primary rodent cultures. Wildtype human tau (WT hTau) overexpression seems to cause some toxicity, as reflected by a decreased neurite area and number of nuclei. Addition of K18P301L fibrils increased the number of nuclei, which could be indicative for astrogliosis.

3.2 Methods and Materials

3.2.1 *In vitro* culture of hiPSC-derived cortical neurons

hiPSC-derived cortical cultures (iPSC0028, Sigma) were prepared as described in Chapter 2. All functional experiments were performed on human astrocyte co-cultures treated with DAPT, since this was the optimal condition as described in Chapter 2.

3.2.2 *In vitro* culture of rat primary neurons

Cultures of dissociated primary neurons were prepared according to a protocol adapted from Banker and Goslin [41]. Briefly, hippocampi or cortices were dissected from wild-type E18/19 Wistar Crl:WI rats (Charles River) in HEPES (7mM) buffered Hanks balanced salt solution (HBSS, both Gibco), and dissociated enzymatically and mechanically. Cells were resuspended in minimal essential medium (MEM, Gibco) supplemented with 10% heat-inactivated normal horse serum (Innovative Research) and 30mM glucose (Merck). Cells were plated in poly-D-lysin-precoated microclear multiwell plates (Greiner) and kept in a humidified CO_2 incubator (37^0C; 5% CO_2). After cell attachment, medium was replaced with B27 supplemented Neurobasal medium, containing L-glutamine (2 mM) (all Gibco). Neuronal cultures develop a network featuring synchronized activity within about a week [42].

3.2.3 Tau transduction

Cultures of hiPSC-derived NPCs were transduced at 1 day before final plating and primary rodent neuronal cultures at 2DIV with either AAV6-syn1-TAU-WT, AAV6-syn1-TAU-WT-GFP, AAV6-syn1-TAU-P301L or AAV6-syn1-TAU-P301L-GFP constructs overexpressing human (mutant P301L) tau [40]. Cells were transduced at MOI (multiplicity of infection) 100 (without inducing cytotoxicity (data not shown). cDNA for the longest isoform of human tau (WT hTau) or human mutant P301L tau (P301L hTau), either fused to GFP or without additional tag, were synthesized at GeneArt and subcloned into a pT-Rex™-DEST30 Vector (Thermo Fisher Scientific). TauWT and TauP301L were cloned into the adeno-associated viral serotype 6 (AAV6) backbone and expression is driven by the human synapsin-1 promoter (Genscript). Viral vectors were obtained and packing was performed by S. Kügler (University Medical Center Göttingen) [43].

3.2.4 Induced tauopathy model in primary neuronal cultures

In order to induce tauopathy in wild-type neuronal cultures, a combination of transgene expression and addition of recombinant tau fibrils was used. P301L mutated tau fibrils (K18P301L) were added to cultures to induce intracellular tau aggregation. Truncated human Tau fragments containing the four microtubule binding repeat domain (K18; residues Q244-E372 of the longest human Tau isoform) with a P301L mutation (K18P301L) were produced in Escherichia coli

(Tebu-bio). K18P301L fibrils were produced according to the protocol that was previously published by Guo and Lee [34]. For *in vitro* fibrillization, 40 μM recombinant monomeric tau was incubated with 40 μM low molecular-weight heparin and 2 mM DTT in 100 mM sodium acetate buffer (pH 7.0) at 37°C. Tau was incubated for 3-10 days without agitation in order to form fibrils. Before they were added to neurons, fibrillization mixtures were centrifuged at 100,000 g for 60 minutes at 4°C, and the resulting pellet was re-suspended in an equal volume of 100 mM sodium acetate buffer (pH 7.0). K18P301L fibrils were sonicated with 60 pulses of 2 seconds and added to culture medium at 7DIV (for primary rodent cultures) or 14DIV (for hiPSC-derived neuronal cultures) at a concentration of 25 nM.

3.2.5 Calcium imaging

To separate "diseased" neurons from "healthy" neurons in a network combined imaging of calcium and (aggregated) tau was used. Because the tau tracing techniques were visible in the 488 nm channel, another calcium dye than FLUO4 was used. As alternative CaSiR-1 ™ (GORYO Chemical) was used, which is a near-infrared fluorescence synthetic calcium probe with a maximum fluorescence wavelength at 664 nm. Cells were loaded with 1 μM CaSir-1 ™ in recording buffer, using the same protocol as described in Chapter 2 for FLUO4.

A custom-made MATLAB script (based on ref. [44], available via www.uantwerpen.be/cell-group) was used to analyze live cell calcium traces and derive various parameters reflecting characteristics of neuronal activity, as described in Chapter 2. However, an extra feature was added to the script in order to analyse two different populations. In brief, regions of interest (ROIs) were drawn based on time projection images of the calcium recordings. In the second image, showing the presence of (aggregated) tau, a threshold was set for detecting (aggregated) tau overexpressing cells within these ROIs. This way the two cell populations could be separated and all parameters were calculated for both populations separately (Fig. 3.1).

3.2.6 Live cell visualization of (aggregated) tau

Live cell visualization of tau was accomplished using GFP-fused human tau overexpression. This method only showed the exogenous tau, but not endogenous tau. On the other hand aggregated tau, either exogenous or endogenous, was visualized using pentameric formyl thiophene acetic acid (pFTAA) [45], a fluorescent pentameric oligothiophene which identifies filamentous tau (Fig. 3.1). 3 μM pFTAA, diluted in prewarmed recording buffer, was added to neurons for one hour prior to calcium dye incubation.

3.2.7 Immunocytochemistry

Cells were fixed for 15 minutes using 4% paraformaldehyde with 4% sucrose in TBS (TrisHCl pH 7.5, NaCl and MilliQ), washed, blocked with 5% donkey serum in TBS and incubated with mouse anti-GluA (Synaptic Systems) overnight at 4°C.

Then cells were permeabilized for 15 minutes with Triton-X100 (0.25%) in TBS. After 30 minutes blocking with donkey serum in TBS-Triton (0.25%), cells were incubated overnight at 4°C with the following antibodies: chicken anti-MAP2 (Aves) and rabbit anti-synaptophysin (Abcam). Subsequently, cells were washed and incubated for 1 hour at room temperature with Alexa secondary antibodies (Thermo Fisher Scientific). DAPI (Sigma) was used to counterstain the nuclei. Images were taken automated with the Opera Phenix™ High Content Screening System (confocal, Perkin Elmer).

An overview of antibodies is given in the next table.

antigen	supplier	clone	species	isotype	catalog number
GluA	Synaptic Systems	248B7	mouse	IgG2a	182 411
MAP2	Aves		chicken	IgY	MAP
synaptophysin	Synaptic Systems		rabbit	IgG	ab14692
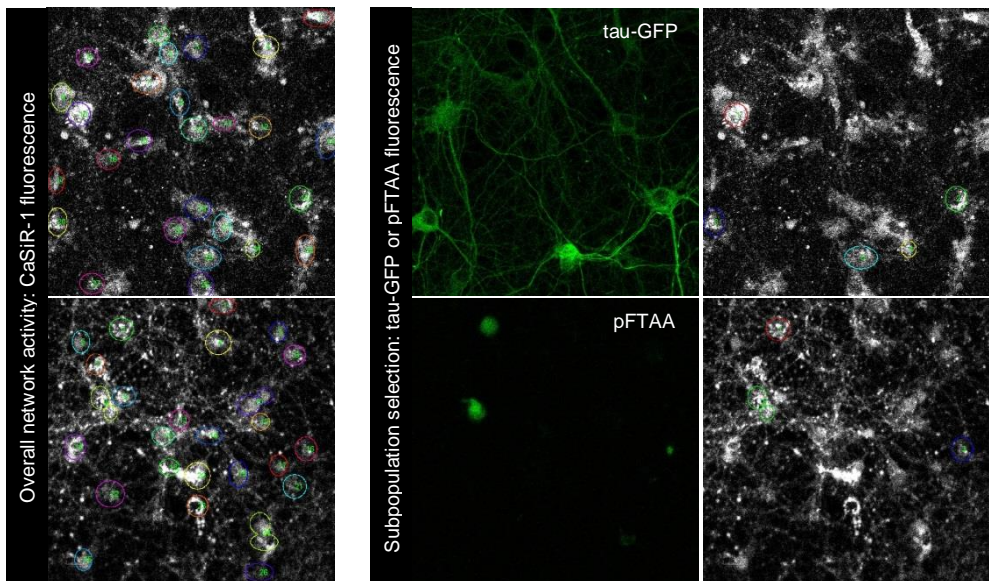
Fig. 3.1 Calcium analysis of tau (aggregate) positive subpopulations in primary neuronal cultures overexpressing P301L tau, treated with K18P301L fibrils. Overall network activity was analyzed based on CaSiR-1 fluorescence (left). Additionally, prior to live cell calcium recordings, corresponding images of GFP-fluorescent tau indicators (either tau-GFP or pFTAA) were captured and used as an overlay to create two subpopulations for live cell calcium imaging analysis: tau (aggregate) positive and negative subpopulations.

3.2.8 Network morphology

Images of neuronal networks were automatically analyzed using a custom made script (available via www.uantwerpen.be/cell-group), based on templates written by Evotec Technologies for Acapella™ 4.0 (PerkinElmer Inc.), implemented on an integrated Columbus™ server (PerkinElmer Inc.). In brief, multidimensional image data sets are read and preprocessed after which objects of interest – i.e. nuclei, neurites and pre- and postsynaptic puncta – are detected and quantified.

Nucleus detection is performed by projecting DAPI stained images along the Z-axis according to the maximum intensity, after which a median filter is applied. A user-defined intensity threshold is used to detect the nuclei, followed by a watershed-based separation of touching nuclei. To identify the neuronal nuclei, a user-defined area and circularity filter is applied.

To measure neurite outgrowth a similar approach is used. The network is identified by applying a user-defined intensity threshold after z-projection and Gaussian blurring of the images. The area of the identified network is expressed in μm^2. In addition, a skeleton of the network is generated based on the gradient image, after which the skeleton is pruned to remove all small fragments.

In order to detect pre- and post-synaptic *puncta* the sharpest z-slice of the respective channel is retained and spots are enhanced by a SER (Spot-Edge-Ridge) texture analysis implemented in Acapella. Spot maxima are identified in the enhanced image by applying a user-defined intensity threshold after which they are iteratively dilated and eroded based on the same threshold. To avoid detection of aspecific spots, the identified neurite network is used as a restrictive region after exclusion of the neuronal nuclei. Density of *puncta* was expressed as the number of *puncta* per μm^2 surface of the search region. To quantify colocalisation of pre- and post-synaptic spots, various object and intensity based colocalisation features are extracted. Additionally, the number of synapses is identified as the number of spots that show at least one pixel overlap between the two channels.

3.2.9 Statistics

Data are shown as mean + standard error of the mean (SEM). For hiPSC-derived cultures, the number of differentiations per experiment refers to the differentiation procedure from hiPSCs to NPCs (either from the same hiPSC line or from a different hiPSC line), while the number of samples refers to the number of wells differentiated towards neurons starting from a single batch of NPCs. For primary cultures, the number of differentiations per experiment refers to the differentiation procedure from cells collected from embryos from one pregnant female, while the number of samples refers to the number of wells from one dissection.

For general calcium imaging and network morphology experiments overall differences between groups were calculated using one-way ANOVAs. For multiple comparisons, Holm-Sidak's multiple comparisons tests were performed to detect differences between groups. For separated analysis of calcium imaging in function of tau (aggregation), overall differences between groups were calculated using two-way ANOVAs considering equal variances. For multiple comparisons, Sidak's multiple comparisons tests were performed to detect differences between tau (aggregation) positive and negative cells.

3.3 Results

3.3.1 Tau overexpression combined with fibril seeding does not affect overall calcium oscillations

In order to analyze the influence of aggregating tau on network functionality *in vitro*, control hiPSC-derived cortical neurons and primary rat cortical neurons were transduced with the longest human tau isoform (2N4R) with P301L mutation (whether or not coupled to GFP) or human 2N4R WT tau as a control for tau overexpression. Tau overexpression was confirmed previously by Western blot and quantitative RT-PCR [40]. Due to the lack of spontaneous aggregation transduced cultures were seeded with K18P301L fibrils, which has been shown to facilitate tau aggregation in P301L tau overexpressing primary rodent and hiPSC-derived neuronal cultures [34,40]. Six conditions providing the right controls for overexpression and aggregation were included in this experiment, that is control, WT hTau overexpressing, or P301L hTau overexpressing cultures, either with or without addition of K18P301L fibrils. Calcium imaging was done on both hiPSC-derived (at five weeks after final plating) and primary rat (at 15 DIV) cortical cultures. No significant differences in overall calcium oscillations were found between hiPSC-derived cultures whether or not transduced with either WT tau or P301L tau, whether or not seeded with K18P301L fibrils (Fig. 3.2a), neither in primary rat cortical cultures (Fig. 3.2b).
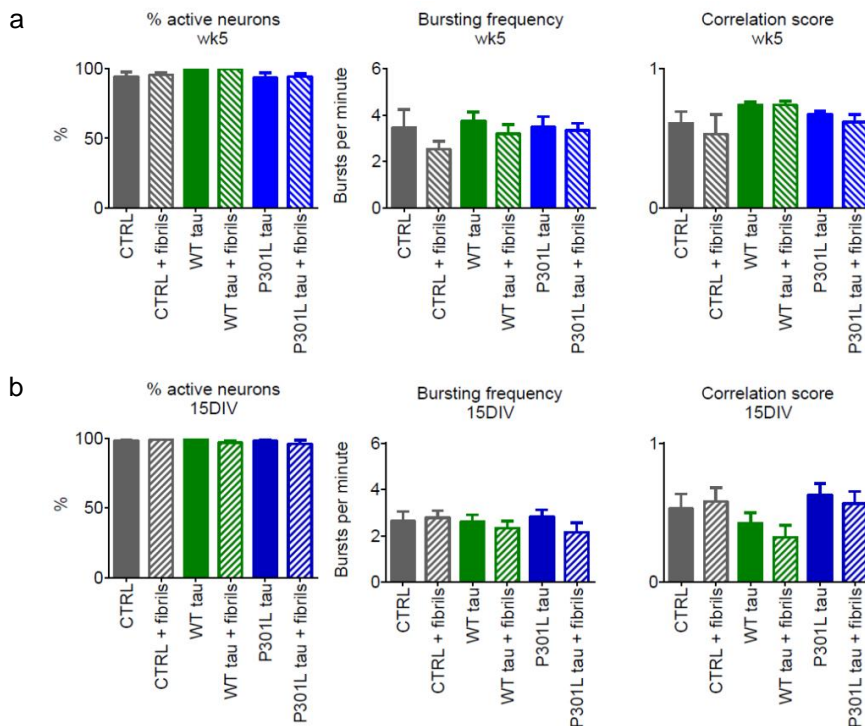
Figure 3.2 Tau overexpression combined with fibril seeding does not have major impact on calcium oscillations. a) Graphs show the effects of (mutated) tau overexpression and fibril seeding on calcium oscillations in hiPSC-derived cortical neurons (week 5). No significant differences in calcium oscillations were found between hiPSC-derived neurons whether or not transduced with either WT tau or P301L tau, whether or not seeded with K18P301L fibrils. Mean + SEM, n ≥ 2, from 2 differentiations. b) Graphs show the effects of (mutated) tau overexpression and fibril seeding on calcium oscillations in primary rat cortical neurons (15DIV). No significant differences in calcium oscillations were found between primary rat cortical neurons whether or not transduced with either WT tau or P301L tau, whether or not seeded with K18P301L fibrils. Mean + SEM, n ≥ 4, from 2 differentiations.

3.3.2 Tau overexpression rather than tau aggregation seems to influence functionality of impacted cells

Further analyses were done to characterize neuronal functionality in this model of induced tau aggregation. Due to the transduction methods both primary and hiPSC-derived cultures contain transduced and non-transduced cells, which might conceal a tauopathy-induced phenotype. By the addition of an extra mask in the calcium analysis script, we were able to distinguish tau-overexpressing cells (based on their GFP signal) from non-overexpressing cells. The percentage of GFP-positive tau overexpressing neurons per field was calculated and shows no differences between WT tau or P301L tau overexpressing cultures either with or without fibrils (for primary rodent cultures measured at 15DIV, for hiPSC-derived neuronal cultures at five weeks after final plating). However, primary rodent cultures clearly show a higher percentage of tau-overexpressing cells per field than hiPSC-derived neuronal cultures (Fig. 3.3a). Separate analysis of tau-coupled-GFP-positive and -negative neurons showed the difference in calcium oscillations between these two cell populations per well. For hiPSC-derived neurons (week 5) the percentage active neurons and synchronicity were significantly increased in the tau-overexpressing neurons (Fig. 3.3b). In primary rat cortical neurons (15 DIV) the bursting frequency and synchronicity were significantly increased in the tau-overexpressing neurons as well (Fig. 3.3c).

Using the same analysis script but a different labeling approach for discriminating two cell populations, we were able to quantify calcium oscillations in cell populations with and without detectable tau filaments. For this experiment primary neuronal cultures were incubated with pFTAA for one hour prior to calcium dye loading. pFTAA is a green fluorescent molecule which identifies filamentous tau. Separate analysis of pFTAA-positive and pFTAA-negative primary rat cortical neurons in P301L tau transduced cultures treated with K18P301L fibrils shows the difference in calcium oscillations between pFTAA-binding and non-binding neurons within one well. No significant differences were found between these two cell populations showing that tau fibrils do not correlate with changed calcium oscillations *in vitro* (Fig. 3.3d).

3.3.3 Morphology of primary cortical cultures overexpressing hTau and treated with K18P301L fibrils was significantly altered, but not hiPSC-derived cortical cultures

Network morphology was examined in the six conditions to elucidate the possible contributions of structural changes to network function. General neuronal structure was analyzed using anti-MAP2 staining, presynaptic vesicles were stained with anti-synaptophysin antibody and postsynaptic terminals were stained with anti-GluA antibody (Fig. 3.4a). The readouts were cell count, neurite area, and density of synapses per neurite area (co-localized staining of presynaptic and postsynaptic proteins were called synapses).
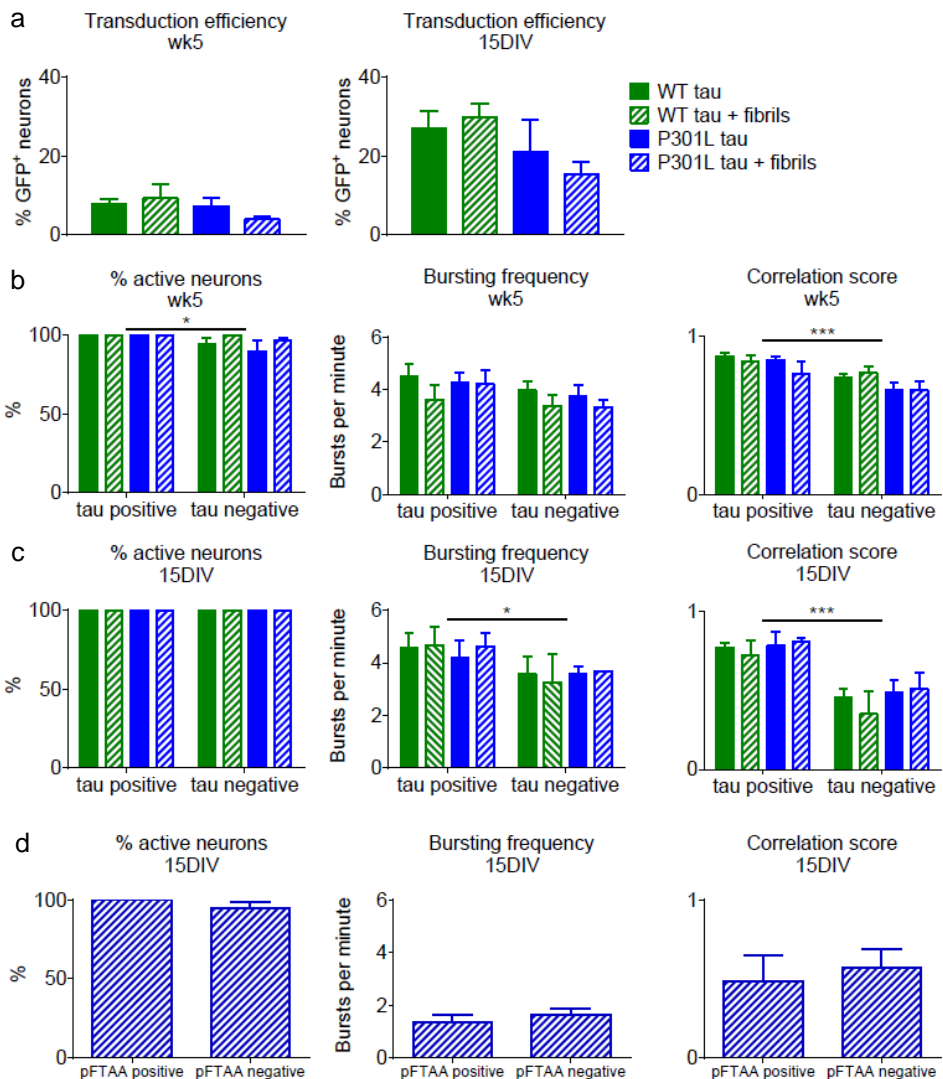
Figure 3.3 Separate analysis of tau-transduced neurons and non-transduced neurons shows the influence of tau overexpression on calcium oscillations rather than the influence of tau aggregation. a) The percentage GFP-positive tau overexpressing neurons per field was calculated. For both hiPSC-derived (left) and primary rodent (right) neuronal cultures no significant differences were found between WT and P301L tau overexpression either with or without fibrils (One-way ANOVA, p = 0.4640 and p = 0.4583 respectively). hiPSC-derived cultures: n ≥ 2 from 2 differentiations, primary rodent cultures: n ≥ 2 from 1 differentiation, mean + SEM. b) Separate analysis of tau-coupled-GFP-positive and -negative neurons shows the difference in calcium oscillations between two cell populations in one well. For hiPSC-derived neurons (week 5) the percentage active neurons (Two-way ANOVA, p = 0.0291) and synchronicity (Two-way ANOVA, p = 0.0006) are significantly increased in the tau overexpressing neurons. n ≥ 2 from 2 differentiations, mean + SEM, * p<0.05,***p≤0.0001. c) Separate analysis of tau-coupled-GFP-positive and -negative neurons shows the difference in calcium oscillations between two cell populations in one well. For primary rat cortical neurons (15 DIV) the bursting frequency (Two-way ANOVA, p = 0.0400) and synchronicity (Two-way ANOVA, p = 0.0001) are significantly increased in the tau-overexpressing neurons. n ≥ 2 from 1 differentiation, mean + SEM, * p<0.05,***p≤0.0001. d) Separate analysis of pFTAA-positive and pFTAA-negative primary rat cortical neurons in P301L tau transduced cultures treated with P301LK18 fibrils shows the difference in calcium oscillations between pFTAA-binding and non-binding neurons within one well. No significant differences were found between these two cell populations. n ≥ 2 from 2 differentiations, mean + SEM.

Overexpresssion of WT hTau in primary rat cortical neurons caused a significant decrease in neurite surface compared to both control and P301L hTau overexpressing neurons (Fig. 3.4b). Furthermore, K18P301L fibrils significantly increased neurite surface in P301L overexpressing primary neurons. Additional analyses showed that neurite length was changed rather than neurite width (data not shown). Total number of nuclei was significantly decreased by WT hTau overexpression, while K18P301L fibril addition significantly increased the number of nuclei in all three transduction conditions (Fig. 3.4c). In primary cultures synapse density was neither influenced by hTau transduction, nor by K18P301L fibril addition (Fig. 3.4d). Similar morphological analyses were done on hiPSC-derived cortical cultures. No significant differences were found in cell count, neurite area or synapse density (Fig. 3.5).
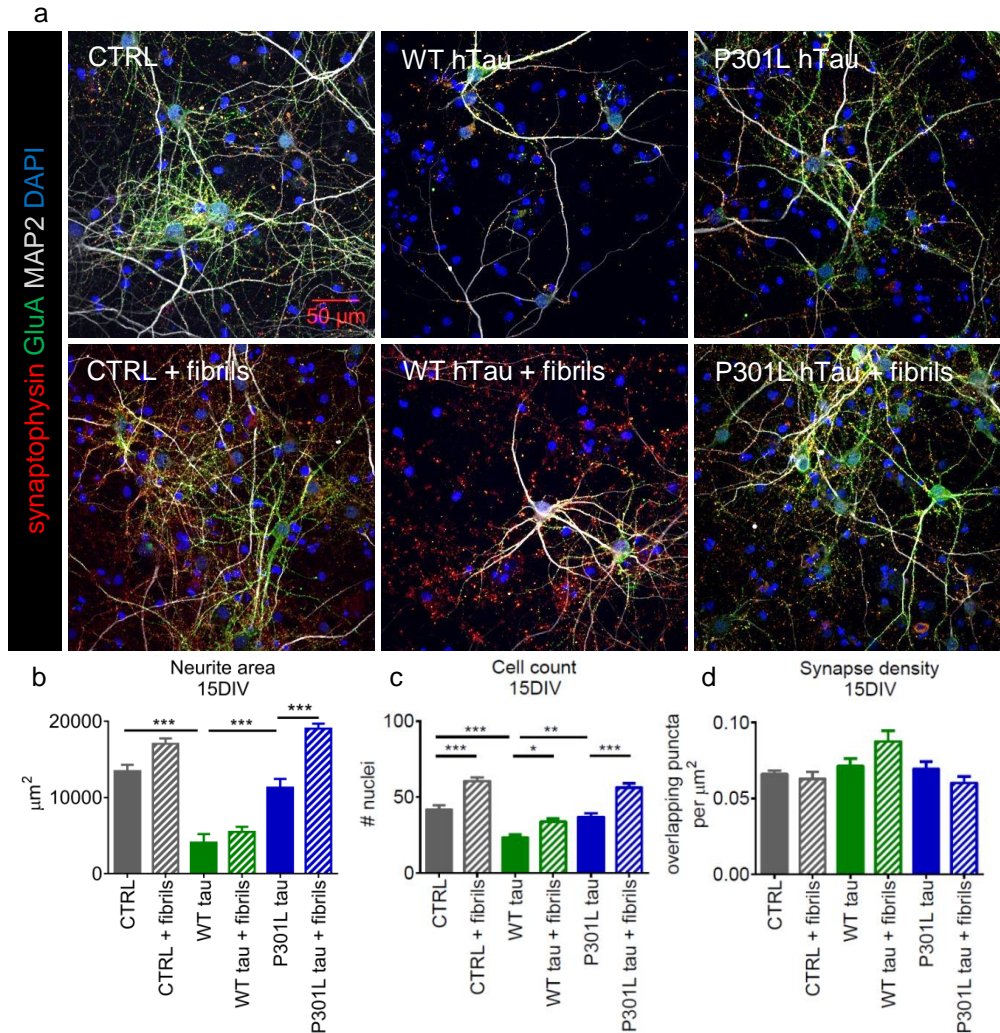
Figure 3.4 Decreased neurite surface in WT hTau overexpressing primary neurons, but not in P301L hTau overexpressing neurons. a) CTRL, WT hTau and P301L hTau overexpressing primary neurons, either treated with K18P301L fibrils or not were stained with anti-synaptophysin, anti-GluA, anti-MAP2 and DAPI. b) Neurite surface, based on the MAP2 staining, was analyzed automatically. WT hTau overexpresssion in primary rat cortical neurons (15DIV) caused a significant decrease in neurite surface (One-way ANOVA, $p < 0.0001$) compared to both control and P301L hTau overexpressing neurons. Fibril addition significantly increased neurite surface in P301L overexpressing primary neurons (One-way ANOVA, $p < 0.0001$). n = 12 from 1 differentiation, mean + SEM, ***$p \leq 0.0001$. c) Cell number, based on the DAPI staining, was analyzed automatically. Fibril addition significantly increased cell count in CTRL, WT hTau and P301L hTau overexpressing primary neurons while WT hTau overexpression decreased the number of cells per well (One-way ANOVA, $p < 0.0001$). n = 12 from 1 differentiation, mean + SEM, *$p < 0.05$, **$p < 0.01$, ***$p \leq 0.0001$. d) Synapse density was analyzed automatically. Synapses were defined as synaptophysin puncta overlapping with GluA puncta, density was calculated as number of overlapping puncta per neurite area in μm^2. No significant differences were found between the six conditions. n = 3 from 1 differentiation, mean + SEM.
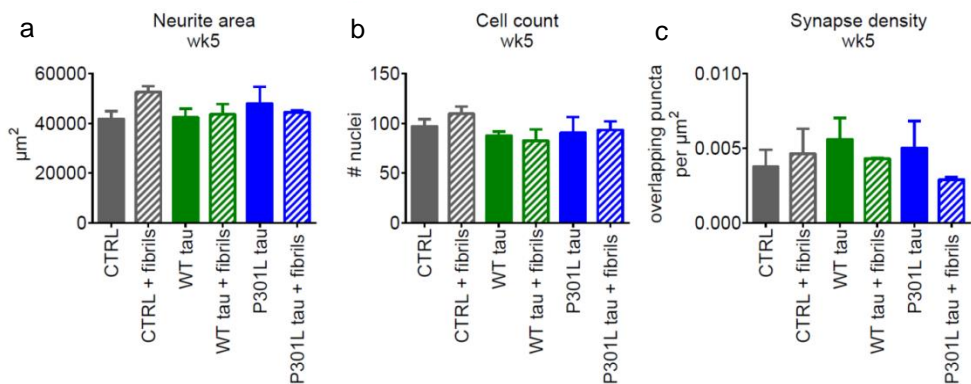
Figure 3.5 Unaltered network morphology in hiPSC-derived cortical neurons after tau overexpression and fibril addition. a) CTRL, WT hTau and P301L hTau overexpressing hiPSC-derived neurons, either treated with K18P301L fibrils or not were stained with anti-synaptophysin, anti-GluA, anti-MAP2 and DAPI. Neurite area, based on the MAP2 staining, was analyzed automatically. No significant differences were found between the six conditions. n ≥ 1 from ≥ 2 differentiations, mean + SEM. b) Number of nuclei, based on the DAPI staining, was analyzed automatically. No significant differences were found between the six conditions. n ≥ 1 from ≥ 2 differentiations, mean + SEM. c) Synapse density, based on co-localisation of synaptophysin- and GluA-positive puncta, was analyzed automatically. No significant differences were found between the six conditions. n ≥ 1 from ≥ 2 differentiations, mean + SEM.

3.4 Discussion

In this chapter we described the functional and morphological characterization of neuronal networks in a tauopathy model based on AAV-induced human (mutant P301L) tau overexpression in primary rat neuronal cultures and hiPSC-derived cortical cultures. The P301L mutation ultimately leads to aggregation of tau into NFTs, but robust tau aggregation could be triggered with K18P301L fibrils within a short time frame [34]. We found that human tau overexpression and K18P301L seeding does not have a significant influence on overall network calcium oscillations in both models. However, when studying transduced neurons separately from non-transduced neurons we found that the tau overexpressing neurons showed a significant increase in percentage active neurons, bursting frequency and/or synchronicity. When separating tau fibril containing (pFTAA-positive) cells from pFTAA-negative cells we found no differences between these two populations. Additionally we showed that WT hTau overexpression, but not P301L hTau, decreases the neurite surface and number of nuclei in primary rat cortical cultures, but not in hiPSC-derived cortical cultures. Other morphological changes in the primary neuronal model were induced by tau fibril addition, that is increased number of nuclei in all three transduction conditions and increased neurite area in P301L hTau overexpressing neurons. However, these findings were not replicated in the hiPSC-derived neuronal model.

The established functions of tau protein include the stabilization of microtubules, regulation of cytoskeleton organization, axonal transport. Recent studies found that nuclear tau seems to play a role in maintaining the integrity of DNA and RNA, and tau is implicated in regulation of neuronal activity, neurogenesis and synaptic plasticity (reviewed in ref. [46]). Previous research showed that tau pathology can induce neuronal calcium dysregulation. Hyperexcitability of the glutamatergic system, even while tau pathology was still subtle and significant neuronal loss was not yet visible, was reported in rTg(TauP301L)4510 mice [8], while 3R tau transgenic mice showed statistically significant decreases in spontaneous activity compared to non-transgenic mice [47]. Nonetheless, in our human tau overexpression models we found no significant differences in overall neuronal activity using live cell calcium imaging. We did find significant differences between tau overexpressing and non-overexpressing neurons, with an increased percentage of active neurons, bursting frequency and/or correlation score both in primary rodent and hiPSC-derived neuronal cultures. Various mechanisms might explain this hyperactivity. First of all, tau overexpressing neurons might react more strongly to equal inputs compared to non-overexpressing cells, resulting in hyperactive responses. For example, in P301L tau transgenic mice hyperactivity was recently found to be caused by decreased glutamate clearance from the synaptic cleft of tau-transgenic neurons [8], which might explain a stronger reaction of tau overexpressing neurons. Another explanation could be an overall increased excitatory input in our cultures. Non-transgenic, healthy cells might cope with this change, while transgenic neurons

cannot which could be reflected by increased activity. Thirdly, a difference in excitatory or inhibitory inputs between both cell groups might explain their functional disparity. A possible explanation could be an increased number of excitatory synapses or a decreased number of inhibitory synapses, although we could not detect any changes in synapse density in these cultures. Another mechanism could involve stronger excitatory synapses on transduced cells. Of course a combination of these three mechanisms might be involved. However, using the current readouts no decisive answer about the mechanism could be given. Future research using electrophysiological approaches might further clarify mechanisms involved in this functional difference.

Due to the usage of induced pathology by overexpression it might be possible that endogenous tau is still functioning normally, especially because endogenous 3R tau has a lower propensity to aggregate than (overexpressed) 4R tau [39]. This could cause low levels of recruitment of endogenous tau from hiPSC-derived and primary cortical neurons with a subsequent lack of effect on network function. As an alternative, targeted mutagenesis could produce a physiologically more relevant model for tauopathies in hiPSC-derived cultures. However, the imaging data, showing a significant decrease in neuronal network surface in WT tau overexpressing cells, suggest that the network is definitely changing. Therefore, it is debatable if the live cell calcium imaging technique is sensitive enough to identify subtle tauopathy-related network dysfunction. Other techniques, for example single cell electrophysiology, might shed a light on possible changes in synaptic transmission.

Additionally, the transduction efficiency in these experiments could be increased in order to induce an effect on total network function. Although tau-overexpression was high enough to induce tau aggregation as previously shown [36,40], transduction efficiencies were low, especially in the hiPSC-derived neuronal cultures (below 10%). Lentiviral transduction systems might be a more efficient transduction system in this case, as previously shown [48]. On the other hand the presence of tau aggregation in the absence of the P301L mutation in most neurons might be a more realistic model of tauopathies without mutations in the *MAPT* gene. Future efforts to increase the percentage of transgenic cells in cultures, or even use constitutive expression of transgenes might provide new insights in neuronal network function in tauopathies.

After comparing tau fibril-containing neurons with fibril-free neurons, as identified with pFTAA, we found no significant influence on calcium oscillations in tangle-bearing neurons, although these neurons were highly affected by tau pathology. This is consistent with previous studies in which NFT bearing neurons were able to functionally integrate in cortical circuits [49], and another study showing relatively normal electrophysiological properties in acute slice preparations of the human P301L tau overexpressing rTg4510 mice [28]. These results strengthen the hypothesis that tangles are not causing significant

disruption of network function. However, the fact that we did not detect variation between pFTAA-positive and pFTAA-negative cells does not mean that tau aggregates did not influence the neuronal network. pFTAA detects filamentous tau only [45], which are a later stage of aggregation, while smaller soluble tau aggregates are thought to be much more toxic [18,19]. Possibly soluble tau aggregates have exerted their effect on the cultures already, but are eventually deposited in less toxic NFTs. Future work is needed to elucidate how earlier stages of tau aggregation, such as soluble oligomeric tau aggregates, impact neuronal function. An additional identification method to detect tau aggregates in the pretangle stadium would enable following the aggregation process over time. FRET-based tau aggregation sensors or sensors based on the bimolecular fluorescence complementation (BiFC) technique (reviewed in ref. [50]) could provide valuable information about the formation and propagation of tau aggregates and their influence on neuronal network function.

Although we found no significant differences in overall network functionality in this tauopathy model, we found a significant impact of WT hTau overexpression on network structure in primary rodent cultures. As previously shown, tau-transfected cultures showed a lower overall neurite surface. This effect might be due to the microtubule-stabilizing properties of tau protein. Tau overexpression might cause taxol-like microtubule stabilization, possibly by downregulating microtubule destabilizing proteins, resulting in a reduction of neurite elongation [51]. Additionally, in their study Mandelkow and colleagues suggested that tau overexpression accounts for inhibition of transport of organelles and vesicle, thereby making neurites more sensitive to stress [52], which might be an explanation for the reduced cell count too. Therefore, it is important to consider that tau overexpression can lead to dramatic reorganization of the neuronal cytoskeleton, rather than modeling human tau pathology. However, overexpression of P301L tau only did not induce an effect on neurite surface, which might be due to an altered binding capacity or higher tau phosphorylation of P301L tau. These alterations reduce its affinity for microtubules, thereby dissociating from microtubules. When adding tau fibrils to these cultures there was a significant increase of the neurite area, which might suggest dystrophic neurite swellings that accumulate pathological tau, as previously reported in mouse models for AD [53,54]. However, additional image analyses revealed that neurite length was increased rather than neurite width, thereby excluding this hypothesis. The total cell number per well was influenced by tau fibrils as well. The increased number of nuclei might reflect neuroinflammation and astrogliosis, which is previously shown in tauopathy mouse models [55,56]. Additional immunocytochemical stainings, for example using astrocytic marker GFAP and neuronal marker neuronal class III tubulin, could clarify if the increased number of cells per field is caused by an increased number of astrocytes.

In contrast, we found no morphological changes in the hiPSC-derived neuronal model, although tau aggregation was clearly shown [40]. A major difference with

the primary rodent cultures is the transduction efficiency of hiPSC-derived neurons, which was previously reported to be lower [48]. Future morphological analysis of tau overexpressing neurons specifically can possibly unravel tauopathy-related changes as well. Another reason why tau overexpression caused varying effects in these two models might be the baseline levels of 3R and 4R tau isoforms. 4R tau isoforms are expressed in the human adult brain, but not yet in hiPSC-derived cortical neurons at 5 weeks after final plating [40,57], while rodent primary cultures at 15DIV show 3R and 4R tau in a ratio equal to one [58]. This may lead to an extraordinary overexpression of 4R tau in primary rodent cultures. Since 4R tau is more prone to aggregation (and even more when containing different mutations) [59] and is binding more stably to microtubules, the imbalance between 3R and 4R tau may lead to a more pronounced phenotype in the rodent system. Overexpression of 4R hTau in the hiPSC-derived cultures led to a 4R/3R ratio slightly higher than one [40], which is closer to physiological ratios in the human adult brain. Therefore, this model might be approaching human tauopathies more than the rodent model, although additional efforts have to be made to clarify tauopathy-related processes in this model.

To conclude, tau overexpression and fibril seeding did not cause differences in overall network functionality in these primary rodent and hiPSC-derived cortical models, using live cell calcium imaging at a fixed timepoint. Neurons specifically overexpressing tau did show hyperactivity in both models, but did not influence total networks *in vitro*. However, fibril seeding seemed to cause some tauopathy-like phenomena such as gliosis in primary rodent cultures. Further optimizations or adaptations of the model might increase tauopathy-related phenomena in these two cell culture systems. Combined with the phenotype of tau aggregation in both cell culture systems, these models might gain useful insights in tauopathy-associated processes. Moreover, the underlying mechanisms of the observed phenotypes remain to be elucidated.

References

1   Alzheimer, A. Uber eine eigenartige Erkrankung der Hirnrinde. *Allgemeine Zeitschrife Psychiatrie* **64**, 146-148 (1907).
2   Ingelsson, M. *et al.* Early Aβ accumulation and progressive synaptic loss, gliosis, and tangle formation in AD brain. *Neurology* **62**, 925-931 (2004).
3   Giannakopoulos, P. *et al.* Tangle and neuron numbers, but not amyloid load, predict cognitive status in Alzheimer's disease. *Neurology* **60**, 1495-1500 (2003).
4   Terry, R. D. *et al.* Physical basis of cognitive alterations in Alzheimer's disease: synapse loss is the major correlate of cognitive impairment. *Ann. Neurol.* **30**, 572-580 (1991).
5   Mucke, L. *et al.* High-level neuronal expression of Aβ1–42 in wild-type human amyloid protein precursor transgenic mice: synaptotoxicity without plaque formation. *The Journal of neuroscience* **20**, 4050-4058 (2000).
6   Perrin, R. J., Fagan, A. M. & Holtzman, D. M. Multimodal techniques for diagnosis and prognosis of Alzheimer's disease. *Nature* **461**, 916-922 (2009).
7   Crimins, J. L., Pooler, A., Polydoro, M., Luebke, J. I. & Spires-Jones, T. L. The intersection of amyloid beta and tau in glutamatergic synaptic dysfunction and collapse in Alzheimer's disease. *Ageing research reviews* **12**, 757-763 (2013).
8   Hunsberger, H. C., Rudy, C. C., Batten, S. R., Gerhardt, G. A. & Reed, M. N. P301L tau expression affects glutamate release and clearance in the hippocampal trisynaptic pathway. *J. Neurochem.* **132**, 169-182 (2015).
9   Grundke-Iqbal, I. *et al.* Microtubule-associated protein tau. A component of Alzheimer paired helical filaments. *J. Biol. Chem.* **261**, 6084-6089 (1986).
10   Spillantini, M. G. & Goedert, M. Tau protein pathology in neurodegenerative diseases. *Trends Neurosci.* **21**, 428-433 (1998).
11   Hutton, M. *et al.* Association of missense and 5'-splice-site mutations in tau with the inherited dementia FTDP-17. *Nature* **393**, 702-705 (1998).
12   Ittner, L. M. *et al.* Dendritic function of tau mediates amyloid-β toxicity in Alzheimer's disease mouse models. *Cell* **142**, 387-397 (2010).
13   Tai, H.-C. *et al.* Frequent and symmetric deposition of misfolded tau oligomers within presynaptic and postsynaptic terminals in Alzheimer's disease. *Acta neuropathologica communications* **2**, 1 (2014).
14   Stoothoff, W. H. & Johnson, G. V. Tau phosphorylation: physiological and pathological consequences. *Biochimica et Biophysica Acta (BBA)-Molecular Basis of Disease* **1739**, 280-297 (2005).
15   Spillantini, M. G. & Goedert, M. Tau pathology and neurodegeneration. *The Lancet Neurology* **12**, 609-622 (2013).
16   Kidd, M. Paired helical filaments in electron microscopy of Alzheimer's disease. (1963).
17   Holtzman, D. M., Morris, J. C. & Goate, A. M. Alzheimer's disease: the challenge of the second century. *Sci. Transl. Med.* **3**, 77sr71-77sr71 (2011).
18   Santacruz, K. *et al.* Tau suppression in a neurodegenerative mouse model improves memory function. *Science* **309**, 476-481 (2005).
19   Oddo, S. *et al.* Reduction of soluble Aβ and tau, but not soluble Aβ alone, ameliorates cognitive decline in transgenic mice with plaques and tangles. *J. Biol. Chem.* **281**, 39413-39423 (2006).
20   Cruchaga, C. *et al.* SNPs associated with cerebrospinal fluid phospho-tau levels influence rate of decline in Alzheimer's disease. *PLoS Genet* **6**, e1001101 (2010).
21   Kauwe, J. S. *et al.* Variation in MAPT is associated with cerebrospinal fluid tau levels in the presence of amyloid-beta deposition. *Proceedings of the National Academy of Sciences* **105**, 8050-8054 (2008).
22   Tai, H.-C. *et al.* The synaptic accumulation of hyperphosphorylated tau oligomers in Alzheimer disease is associated with dysfunction of the ubiquitin-proteasome system. *The American journal of pathology* **181**, 1426-1435 (2012).
23   Perez-Nievas, B. G. *et al.* Dissecting phenotypic traits linked to human resilience to Alzheimer's pathology. *Brain*, awt171 (2013).

24   Crimins, J. L., Rocher, A. B. & Luebke, J. I. Electrophysiological changes precede morphological changes to frontal cortical pyramidal neurons in the rTg4510 mouse model of progressive tauopathy. *Acta Neuropathol.* **124**, 777-795 (2012).

25   Crimins, J. L. *et al.* Homeostatic responses by surviving cortical pyramidal cells in neurodegenerative tauopathy. *Acta Neuropathol.* **122**, 551-564 (2011).

26   Kopeikina, K. J. *et al.* Synaptic alterations in the rTg4510 mouse model of tauopathy. *J. Comp. Neurol.* **521**, 1334-1353 (2013).

27   Kopeikina, K. J. *et al.* Tau causes synapse loss without disrupting calcium homeostasis in the rTg4510 model of tauopathy. *PLoS One* **8**, e80834 (2013).

28   Rocher, A. *et al.* Structural and functional changes in tau mutant mice neurons are not linked to the presence of NFTs. *Exp. Neurol.* **223**, 385-393 (2010).

29   Ginsberg, S. D., Hemby, S. E., Lee, V. M., Eberwine, J. H. & Trojanowski, J. Q. Expression profile of transcripts in Alzheimer's disease tangle-bearing CA1 neurons. *Ann. Neurol.* **48**, 77-87 (2000).

30   Callahan, L. M., Vaules, W. A. & Coleman, P. D. Quantitative decrease in synaptophysin message expression and increase in cathepsin D message expression in Alzheimer disease neurons containing neurofibrillary tangles. *J. Neuropathol. Exp. Neurol.* **58**, 275-287 (1999).

31   Katsuse, O., Lin, W.-L., Lewis, J., Hutton, M. L. & Dickson, D. W. Neurofibrillary tangle-related synaptic alterations of spinal motor neurons of P301L tau transgenic mice. *Neurosci. Lett.* **409**, 95-99 (2006).

32   Rudy, C. C., Hunsberger, H. C., Weitzner, D. S. & Reed, M. N. The role of the tripartite glutamatergic synapse in the pathophysiology of Alzheimer's disease. *Aging Dis.* **6**, 131-148 (2015).

33   Hoover, B. R. *et al.* Tau mislocalization to dendritic spines mediates synaptic dysfunction independently of neurodegeneration. *Neuron* **68**, 1067-1081 (2010).

34   Guo, J. L. & Lee, V. M. Neurofibrillary tangle-like tau pathology induced by synthetic tau fibrils in primary neurons over-expressing mutant tau. *FEBS Lett.* **587**, 717-723 (2013).

35   Frost, B., Jacks, R. L. & Diamond, M. I. Propagation of tau misfolding from the outside to the inside of a cell. *J. Biol. Chem.* **284**, 12845-12852 (2009).

36   Calafate, S. *et al.* Synaptic contacts enhance cell-to-cell tau pathology propagation. *Cell reports* **11**, 1176-1183 (2015).

37   Peeraer, E. *et al.* Intracerebral injection of preformed synthetic tau fibrils initiates widespread tauopathy and neuronal loss in the brains of tau transgenic mice. *Neurobiol. Dis.* **73**, 83-95 (2015).

38   Iba, M. *et al.* Synthetic tau fibrils mediate transmission of neurofibrillary tangles in a transgenic mouse model of Alzheimer's-like tauopathy. *The Journal of Neuroscience* **33**, 1024-1037 (2013).

39   Zhong, Q., Congdon, E. E., Nagaraja, H. N. & Kuret, J. Tau isoform composition influences rate and extent of filament formation. *J. Biol. Chem.* **287**, 20711-20719 (2012).

40   Verheyen, A. *et al.* Using Human iPSC-Derived Neurons to Model TAU Aggregation. *PLoS One* **10**, e0146127 (2015).

41   Banker, G. *Culturing nerve cells*. (MIT press, 1998).

42   Verstraelen, P. *et al.* Pharmacological characterization of cultivated neuronal networks: relevance to synaptogenesis and synaptic connectivity. *Cell. Mol. Neurobiol.* **34**, 757-776 (2014).

43   Taschenberger, G. *et al.* β-synuclein aggregates and induces neurodegeneration in dopaminergic neurons. *Ann. Neurol.* **74**, 109-118 (2013).

44   Cornelissen, F. *et al.* Quantitation of chronic and acute treatment effects on neuronal network activity using image and signal analysis toward a high-content assay. *J. Biomol. Screen.*, 1087057113486518 (2013).

45   Brelstaff, J. *et al.* The fluorescent pentameric oligothiophene pFTAA identifies filamentous tau in live neurons cultured from adult P301S tau mice. *Front. Neurosci.* **9**, 184 (2015).

46   Wang, Y. & Mandelkow, E. Tau in physiology and pathology. *Nature Reviews Neuroscience* (2015).

47   Overk, C., Rockenstein, E., Florio, J., Cheng, Q. & Masliah, E. Differential calcium alterations in animal models of neurodegenerative disease: reversal by FK506. *Neuroscience* **310**, 549-560 (2015).

48   Meneghello, G. *et al.* Evaluation of established human iPSC-derived neurons to model neurodegenerative diseases. *Neuroscience* **301**, 204-212 (2015).

49   Kuchibhotla, K. V. *et al.* Neurofibrillary tangle-bearing neurons are functionally integrated in cortical circuits in vivo. *Proceedings of the National Academy of Sciences* **111**, 510-514 (2014).

50   Lim, S., Haque, M. M., Kim, D., Kim, D. J. & Kim, Y. K. Cell-based models to investigate Tau aggregation. *Computational and structural biotechnology journal* **12**, 7-13 (2014).

51   Vega, I. E., Hamano, T., Propost, J. A., Grenningloh, G. & Yen, S.-H. Taxol and tau overexpression induced calpain-dependent degradation of the microtubule-destabilizing protein SCG10. *Exp. Neurol.* **202**, 152-160 (2006).

52   Mandelkow, E.-M., Stamer, K., Vogel, R., Thies, E. & Mandelkow, E. Clogging of axons by tau, inhibition of axonal traffic and starvation of synapses. *Neurobiol. Aging* **24**, 1079-1085 (2003).

53   Jackson, R. J. *et al.* Human tau increases amyloid b plaque size but not amyloid b-mediated synapse loss in a novel mouse model of Alzheimer's disease. (2016).

54   Spires, T. L. *et al.* Dendritic spine abnormalities in amyloid precursor protein transgenic mice demonstrated by gene transfer and intravital multiphoton microscopy. *The Journal of neuroscience* **25**, 7278-7287 (2005).

55   Wagner, J. *et al.* Reducing tau aggregates with anle138b delays disease progression in a mouse model of tauopathies. *Acta Neuropathol.* **130**, 619-631 (2015).

56   Yoshiyama, Y. *et al.* Synapse loss and microglial activation precede tangles in a P301S tauopathy mouse model. *Neuron* **53**, 337-351 (2007).

57   Sposito, T. *et al.* Developmental regulation of tau splicing is disrupted in stem cell-derived neurons from frontotemporal dementia patients with the 10+ 16 splice-site mutation in MAPT. *Hum. Mol. Genet.* **24**, 5260-5269 (2015).

58   Rodríguez-Martín, T. *et al.* Reduced number of axonal mitochondria and tau hypophosphorylation in mouse P301L tau knockin neurons. *Neurobiol. Dis.* **85**, 1-10 (2016).

59   Gamblin, T. C. *et al.* In vitro polymerization of tau protein monitored by laser light scattering: method and application to the study of FTDP-17 mutants. *Biochemistry* **39**, 6136-6144 (2000).

4

Neuronal network function in a model of human induced pluripotent stem cell-derived cortical neurons with induced tau mutations

Abstract

Alzheimer's disease and frontotemporal dementia are examples of tauopathies and are amongst the most common forms of dementia. This specific group of neurodegenerative disorders is characterized by the formation and deposition of abnormal tau protein in the brain. Various disease models have been used to study tauopathies, either *in vivo* or *in vitro*, and gained important insights about disease mechanisms, genetics, and possible treatments. However, translational value of many models remains poor as reflected by high attrition rates for clinical trials and the lack of disease-modifying drugs for most neuro-degenerative disorders. In order to bridge the gap between previous findings and human disease a new human induced pluripotent stem cell (hiPSC)-derived neuronal tauopathy model is proposed here. Zinc-finger nuclease technology induced mutations were used to create four mutant hiPSC lines containing the 10 + 16 *MAPT* splicing variant mutation only (increasing the inclusion of the second repeat domain (exon 10) and thus 4R tau production) or in combination with the pro-aggregating P301S mutation. The combination of these two mutations was necessary since the P301S mutation is located in exon 10 that is spliced out in control hiPSC-derived neuronal cultures at least until 100 DIV. Thorough characterization of hiPSC-derived cortical networks revealed that neuronal differentiation is highly affected by the splicing variant mutation showing characteristics of forebrain-type interneurons instead of cortical projection neurons. Additionally network activity was disrupted in these neuronal cultures. The P301S mutation further changed gene expression profiles, and promoted fibril seeding-induced tau aggregation in hiPSC-derived neuronal cultures, which is a common characteristic of tauopathies, suggesting that the model is a valuable approach to model human tauopathies *in vitro*. The combination of different tools to study these "neuronal networks in a dish" and the use of different hiPSC lines might eventually contribute to the knowledge about disease onset, progression and treatment options for tauopathies.

4.1 Introduction

Human induced pluripotent stem cell (hiPSC)-derived cell cultures have proven to be a useful tool to gain insights in disease mechanisms of neurodegenerative disorders (e.g. [1-3], and reviewed in ref. [4]). One of these models, which was proposed by Verheyen and colleagues, describes the overexpression of human tau harboring the pro-aggregating P301L mutation in hiPSC-derived neurons combined with seeding of preformed tau aggregates [2]. The functional characterization of this model has been shown in the previous chapter. However, the model is based on induced overexpression of 4R tau, which might hamper the pathophysiological development of tauopathy-like phenotypes, because tau overexpression might cause taxol-like microtubule stabilization and clogging of axons (as previously discussed in Chapter 3). Therefore, this chapter describes a new approach based on targeted genome engineering to study tauopathies in hiPSC-derived cortical cultures.

Not only in Alzheimer's disease, but also in other tauopathies, such as Parkinson's disease, frontotemporal dementia (FTD), Pick's disease and progressive supranuclear palsy, tau aggregation is a common pathological feature [5]. Tau protein is a microtubule stabilizing protein, involved in e.g. cytoskeleton (re)organization and axonal transport. The adult human brain contains six different tau isoforms which are generated by alternative splicing of exons 2, 3, and 10. Proper tau splicing seems to be crucial for neuronal health. During development, in different brain regions, and during pathology alternative splicing takes place. Exons 2 and 3 encode a varying number of 29-residue near-amino-terminal inserts: isoforms containing 0, 1, or 2 inserts are known as 0N, 1N and 2N, respectively. The presence of three or four carboxy-terminal repeat domains (3R or 4R respectively; the second repeat is encoded by exon 10 and is not included in 3R tau) further categorizes tau isoforms [6]. During development only the shortest tau (3R) isoform is expressed, while in adulthood all six isoforms are present and levels of 3R and 4R isoforms are roughly equal [7]. The alternative splicing of exon 10 is of particular interest, because quite some *MAPT* mutations are located on this exon. These mutations either change the coding sequence of the gene, or the alternative splicing of *MAPT*. A particular group of FTD patients exhibit the 10+16 mutation in the stem-loop structure of intron 10. As a consequence these patients show a more frequent inclusion of exon 10 during *MAPT* splicing and thus an increased proportion of four-repeat (4R) tau isoforms [8,9]. An example of a missense mutation is the P301L mutation (identified in FTDP-17 families) in which tau shows a reduced affinity for microtubules and an increased tendency for aggregation [10]. Patients with the clinically more aggressive P301S mutation showed aggregation of hyperphoshorylated tau at young age already [11] (Fig. 4.1).

However, when modeling tauopathies *in vitro* using hiPSC-derived neurons the correct splicing variants have to be expressed. Sposito and colleagues showed that exon 10 is (still) spliced out in 100-day old cortical neuronal cultures

derived from control hiPSCs, which would prohibit expression of *MAPT* mutations in this exon [12]. In contrast, neurons from FTD patients with a 10 + 16 intronic mutation in the *MAPT* gene expressed both 3R and 4R tau isoforms, suggesting that this mutation overrides the developmental regulation of exon 10. At later timepoints (365 DIV) control hiPSC-derived neurons showed a switch in tau splicing. Although this is recapitulating physiological development it is not feasible for drug discovery purposes. Therefore, we have developed different hiPSC lines containing two of these tauopathy-related mutations. Starting from a parental control hiPSC line the 10 + 16 mutation was introduced to enable expression of mutations located in exon 10. Additionally, the P301S mutation was added to these cell lines, because the early-onset of tauopathy in P301S carriers maximizes the chance of observing a cellular phenotype. The comparison of CTRL hiPSC-derived cortical neurons with 10 + 16 splicing variant mutations enables to study the effects of alternative splicing, while the comparison of the latter with the hiPSC-lines with the additional P301S mutation enables to study the effects of the missense mutation which are detectable only when alternative splicing causes (adult) 4R tau production.

In this chapter we tested the morphological and functional properties of these hiPSC-derived cortical neurons expressing P301S mutated tau as a model for tauopathies. We observed that the alternative splicing of *MAPT* significantly changed the differentiation process of these neurons, since gene expression profiles, proliferation markers, and cortical marker expression differed considerably from parental control hiPSC-derived neurons. Furthermore, live cell calcium imaging showed decreased network functionality of the 4R tau expressing neurons, while the P301S mutation did not alter the phenotype any further.

4.2 Methods and Materials

4.2.1 Generation of mutant hiPSC lines

Starting from parental control (CTRL) hiPSCs (iPSC0028, Sigma) Sigma created customized mutant hiPSC lines using Zinc Finger Nuclease (ZFN) Technology on request. Targeted mutations were induced at either the 10 + 16 location (intron 10: cytosine → uracil) and/or the P301S location (exon 10: cytosine → uracil) (Fig. 4.1a, b). Mono-allelic single mutant (SM(mono)), bi-allelic single mutant (SM(bi)), double mutant with mono-allelic P301S mutation (DM(bi, mono)), and double mutant with bi-allelic P301S mutation (DM(bi, bi)) hiPSC lines were created (Fig. 4.1c). An overview of hiPSC lines is given in the next table.

name	CTRL	SM (mono)	SM (bi)	DM (bi,mono)	DM (bi,bi)
mutations	-	IVS10+16 $^{+/-}$	IVS10+16 $^{+/+}$	IVS10+16 $^{+/+}$ P301S $^{+/-}$	IVS10+16 $^{+/+}$ P301S $^{+/+}$
clone	-	1D01-11	1F05-D12	7G4A8	7H6A1

4.2.2 Cell culture conditions

hiPSC-derived cortical cultures were prepared as described in Chapter 2. All functional experiments were performed on human astrocyte co-cultures treated with DAPT, since this was the optimal condition as described in Chapter 2. Samples for the microarray experiment, immunocytochemistry for cortical markers and proliferation assay were prepared without human astrocytes and DAPT to specifically look at effects on hiPSC-derived neurons and avoid masking of effects by astrocytes.

4.2.3 RNA extraction and microarray analyses

RNA extraction was performed using the RNeasy96 kit (Qiagen). cDNA targets were prepared and labelled using the IVT PLUS kit and then hybridized on Affymetrix® Human Genome U219 array plate in the GeneTitan® instrument (Affymetrix) according to the manufacturer's protocol. Microarray analysis was performed using R version 3.3.0 [13]. Target transcripts of probes were annotated using Entrez Gene based alternative cdf version 20.0.0 [14], assigning probes to 18660 unique genes. RMA algorithm was used for pre-processing [15]. KEGG pathway analyses were performed to detect changes in biological and signaling pathways [16,17]. Additionally, pair-wise comparisons between either CTRL and SM(bi) or SM(bi) and DM(bi, bi) were performed at different time points.

4.2.4 Immunocytochemistry

For the proliferation assay cells were stained using the Click-iT® Plus EdU imaging kit (Thermo Fisher Scientific) according to the manufacturer's guidelines. Afterwards cells were fixed for 15 minutes using 4% paraformaldehyde with 4% sucrose in TBS (TrisHCl pH 7.5, NaCl and MilliQ), washed, blocked with 5% donkey serum in TBS and permeabilized for 15 minutes with Triton-X100 (0.25%) in TBS. After 30 minutes blocking with donkey serum in TBS-Triton (0.25%), cells were incubated overnight at 4°C with mouse anti-β3 tubulin

(Covance). Subsequently, cells were washed and incubated for 1 hour at room temperature with Alexa secondary antibody (Thermo Fisher Scientific). DAPI (Sigma) was used to counterstain the nuclei. Images were taken automated with the Opera Phenix™ High Content Screening System.
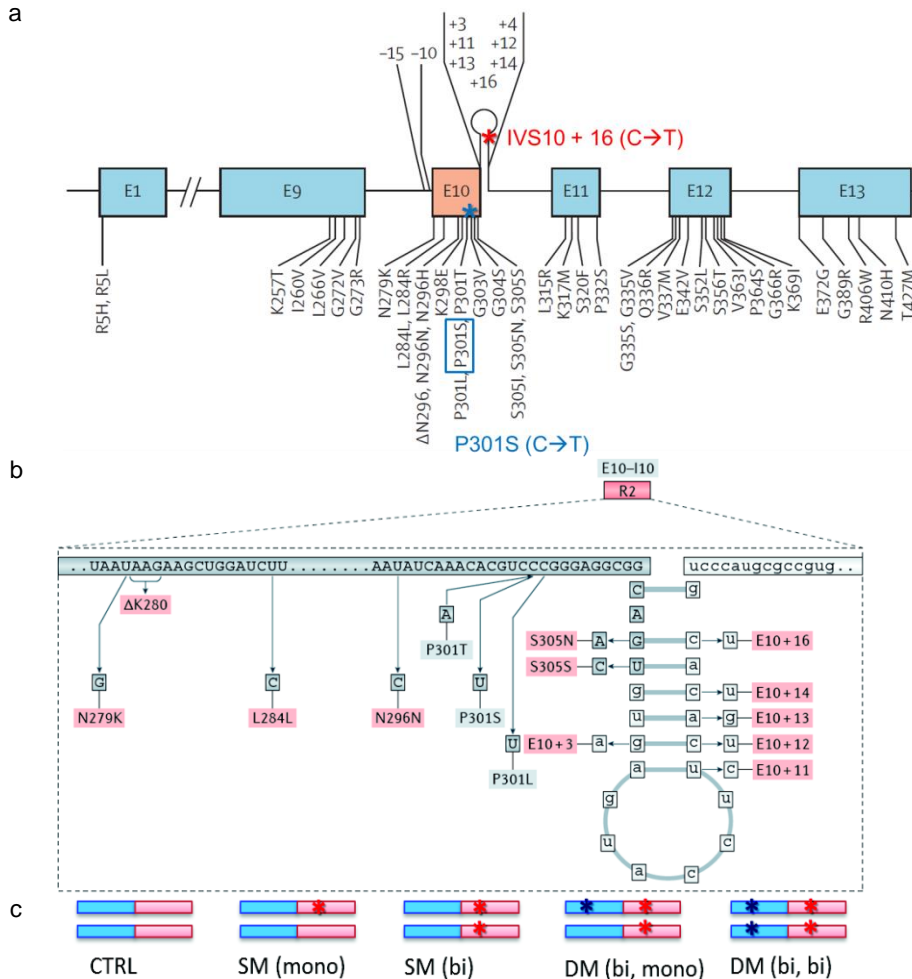
Figure 4.1 Generation of mutant hiPSC lines by ZFN-engineering. a) Schematic representation of the *MAPT* gene, showing the locations of the point mutations used to create mutant hiPSC lines. Blue asterisk represents P301S point mutation; red asterisk represents IVS10+16 point mutation. Figure was adapted from Spillantini *et al.*, 2013 [18]. b) Schematic representation of the mRNA sequence encoding part of exon 10 (E10, uppercase) and intron 10 (I10, lower case). Mutations that are located near the E10 – I10 interface affect splicing and expression of *MAPT*, which encodes tau protein. Mutations that alter *MAPT* splicing are shown in red boxes. Figure was adopted from Wang and Mandelkow 2016 [6]. c) Schematic representation of four mutant hiPSC lines generated from a parental control (CTRL). Single mutant (SM) lines contain mono- or bi-allelic point mutations ((mono) or (bi)), double mutant (DM) lines contain bi-allelic IVS10+16 point mutations (bi) and mono- or bi-allelic P301S mutations ((mono) or (bi)). Blue bars represent *MAPT* exon 10, red bars represent *MAPT* intron 10, blue asterisks represent P301S point mutations, and red asterisks represent IVS10 + 16 point mutations.

Cortical markers (TBR1 and CTIP2) were stained according to the protocol described in Chapter 2. In a similar fashion glumatergic vesicle marker vGLUT2 and GABAergic vesicle marker vGAT were stained in combination with neuronal specific β3 tubulin. For the morphological characterization of neuronal networks cells were stained according to the protocol previously described in Chapter 3.

An overview of antibodies is given in the next table.

antigen	supplier	clone	species	isotype	catalog number
β3-tubulin	Covance	Poly18020	mouse	IgG	PRB-435P
CTIP2	Abcam	25B6	rat	IgG2a	ab18465
GluA	Synaptic Systems	248B7	mouse	IgG2a	182 411
MAP2	Aves		chicken	IgY	MAP
synaptophysin	Synaptic Systems		rabbit	IgG	ab14692
TBR1	Abcam		rabbit	IgG	ab31940
vGAT	Synaptic Systems		rabbit		131 003
vGLUT2	Synaptic Systems		rabbit		135 403

4.2.5 K18

Truncated human tau fragments containing the four microtubule binding repeat domain (K18; residues Q244-E372 of the longest human Tau isoform) with a P301L mutation (K18P301L) were produced as described in Chapter 3. K18P301L fibrils were added to the culture medium 14 days after final plating at a concentration of 25 nM.

4.2.6 AlphaLISA

Cells in 96w plate were lysed in 40 µl / well RIPA buffer (ThermoFisher Scientific) with protease-and phosphatase inhibitors (Roche). After 20–30 minutes of gentle shaking at room temperature, 5 µl of sample was mixed with 20 µl biotinylated and acceptor bead-conjugated antibodies in an OptiPlate-384 (all Perkin Elmer). After two hours of incubation at room temperature, 25 µl of streptavidin donor beads were added for 30 minutes at room temperature followed by detection with the Envision plate reader (all Perkin Elmer). Raw values were normalized to control (no fibril) samples per plate.

To allow the detection of tau aggregates, the monoclonal JRF/hTAU/10 antibody (hTau10) was conjugated to both acceptor beads and biotin, this way developing the hTau10/hTau10 assay. At least a dimer or a bigger aggregate of tau proteins is needed in order to bind both acceptor bead-conjugated and -biotinylated antibodies and yield a signal upon excitation, since monomeric tau has only one hTAU10 epitope [2,19]. Detection of tau phosphorylation was assessed using the phospho-tau antibody AT8 (pSer202/Thr205, Innogenetics) [20]. Biotinylated AT8 was combined with acceptor bead-conjugated hTau10 in the AT8/hTAU10 assay, and total tau levels were assessed in the HT7/hTau10 assay. A biotinylated HT7 antibody (Innogenetics) was combined with acceptor bead-conjugated hTAU10 such that different epitopes are recognized by these 2 total tau antibodies.

4.2.7 Live cell calcium imaging

Live cell calcium imaging was performed using FLUO4, as previously described in Chapter 2. A custom-made MATLAB script (based on ref. [21], available via www.uantwerpen.be/cell-group) was used to analyze live cell calcium traces and derive various parameters reflecting characteristics of neuronal activity, as described in Chapter 2.

4.2.8 Image analysis

Images of neuronal cultures stained with DAPI and EdU were automatically analyzed using a custom made script (Neuronal Maturation, available via www.uantwerpen.be/cell-group) for Fiji, image processing freeware [22], which is available upon request and described in Chapter 3. In brief, nucleus detection is performed by applying an automatic intensity threshold [23] on DAPI stained images after background subtraction and Gaussian blurring, followed by a watershed-based separation of touching nuclei. To determine the number of overlapping EdU-positive nuclei, the mean intensity for each particle was measured in the EdU images. An empirical cut-off value was determined, above which cells were considered to be EdU-positive.

Network morphology was assessed as described in Chapter 3 after immunocytochemical staining of fixed samples with mouse anti-GluA (Synaptic Systems), chicken anti-MAP2 (Aves) and rabbit anti-synaptophysin (Abcam) as previously described in Chapter 3.

4.2.9 Statistics

Data are shown as mean + or ± standard error of the mean (SEM). The number of differentiations per experiment refers to the differentiation procedure from hiPSCs to neural precursor cells (NPCs, either from the same hiPSC line or from a different hiPSC line), while the number of samples refers to the number of wells differentiated towards neurons starting from a single batch of NPCs.

For general calcium imaging and network morphology experiments overall differences between groups were calculated using one-way ANOVAs. For multiple comparisons, Holm-Sidak's multiple comparisons tests were performed to detect differences between groups. For the proliferation assay (EdU) and alphaLISA experiments, overall differences between groups were calculated using two-way ANOVAs considering equal variances. For the proliferation assay Holm-Sidak's multiple comparisons tests were performed to detect differences between cell lines at the different time points. For alphaLISA experiments Sidak's multiple comparisons tests were performed to detect differences between cultures with and without added fibrils.

4.3 Results

4.3.1 Differentiation towards cortical neurons is different from parental control

In order to characterize the neuronal cultures derived from the four generated mutant cell lines, gene expression in the mutant lines was assessed using microarray. Microarray data (Table 4.1) showed that the 10+16 splicing variant significantly decreased the levels of *TBR1*, upper layer cortical marker *SATB2* and glutamatergic markers *vGLUT1* and *vGLUT2*, while *vGAT* was slightly upregulated when compared to controls. Although the differentiation protocol was equal for all five cell lines, immunocytochemistry confirmed that clear differences in the production of these markers were present. As shown in Figure 4.2, control neurons produced both deep layer cortical markers, while both SM(bi) and DM(bi,bi) neurons did not show TBR1 (Fig. 4.2a). Furthermore, glutamatergic marker vGLUT2 was not shown in SM(bi) and DM(bi,bi) neurons neither (Fig. 4.2b), while GABAergic marker vGAT was (Fig. 4.2c), indicating clear differences in the outcome of the differentiation protocol.

Furthermore, the 10+16 splicing variant induced a significant decrease in cell proliferation when compared to controls (Fig. 4.3). The total number of cells (Fig. 4.3b) and the number of proliferating cells (Fig. 4.3c) was significantly decreased at 3, 5, and/or 7 weeks after final plating. Data were normalized to the NPC stadium to correct for the plating density. Plating density was not significantly different between the three cell lines. However, when comparing the percentage of proliferating cells between the three cell lines, there was a significant decrease in proliferation at three weeks after final plating only (Fig. 4.3d), indicating that control cells are more proliferative at the beginning of the culture after which ratios are stabilized. The control cultures expanded more than the 10+16 splicing variant expressing cells, explaining the higher number of (proliferating) cells at later time points.

4.3.2 Microarray data show differences between parental control, single mutants and double mutants in several pathways

Further characterization of the hiPSC-derived NPCs and neurons was done using microarray analysis. Cell cultures from different time points during differentiation were lysed and analyzed. Table 4.1 shows the significant differences in gene expression induced by the bi-allelic 10+16 splicing compared to control in a number of specific pathways or protein groups. Several genes involved in neuronal differentiation and differentiation towards cortical neurons are down regulated in the mutants, while expression of genes involved in GABAergic neurotransmission and differentiation towards inhibitory neurons was increased. Additionally, genes in the tau and amyloid pathways are upregulated in the neurons carrying the 10+16 mutation. Similar data are shown in Table 4.2

for the significant differences between the DM(bi,bi) and SM(bi). In the P301S expressing neurons many differences were found in the expression of kinases and phosphatases. Furthermore, there was a down regulation of genes involved in many different pathways, including neuronal differentiation, GABAergic but also glutamatergic neurotransmission, and microtubule associated proteins.

bi-allelic E10+16 mutation compared to parental control		NPC			wk5			wk7		
	gene symbol	fold increase	fold decrease	p value	fold increase	fold decrease	p value	fold increase	fold decrease	p value
neuronal differentiation	NEUROD1		32.60	6.6819E-42		25.48	3.7791E-40		13.99	2.5166E-35
	NEUROD2		2.40	3.3421E-10		55.58	2.6404E-40		48.42	1.7897E-39
	NEUROD6		6.60	8.9723E-11		235.07	1.4294E-30		251.25	7.6197E-31
	PAX6		3.95	2.3965E-34		2.36	6.5418E-24		2.15	1.3892E-21
	NRN1		16.83	8.6161E-28		109.36	1.7963E-39		113.26	1.1959E-39
	NNAT		31.11	1.7364E-35		33.30	6.0619E-36		33.35	5.9157E-36
cortical development	EOMES (TBR2)		117.67	1.3824E-58		34.46	2.9153E-51		26.22	2.6824E-49
	TBR1		5.06	3.3352E-29		13.69	2.8738E-40		13.78	2.4782E-40
	SATB2					3.67	6.1754E-26		5.14	4.7743E-31
	BCL11B (CTIP2)				1.71		0.0006119		1.67	0.00101305
	DCX				2.05		1.7874E-17	1.47		1.8355E-08
differentiation and survival of inhibitory neurons in forebrain	DLX5	2.91		6.5105E-11	6.27		8.2796E-20	6.10		1.6533E-19
	DLX6	3.42		7.8186E-22	16.47		3.3235E-40	12.69		6.9016E-38
GABAergic neurotransmission	SLC32A1 (VGAT)	2.01		3.7281E-16	10.83		1.1436E-42	9.78		1.2826E-41
	GAD1 (GAD67)	2.11		1.0222E-09	5.02		1.6974E-22	2.48		2.445E-12
	GABRB1				4.05		2.2982E-15	3.31		6.8027E-13
	GABRA1	1.99		3.2933E-05	1.55		0.00555014	3.67		9.5622E-12
	GABRG3				1.88		1.1682E-05	1.80		3.6396E-05
	GABRA4				2.24		1.4486E-05	2.28		1.0131E-05
	GABRA2		4.49	1.8716E-19	3.29		2.9229E-15	2.82		4.3861E-13
	GABRA5		2.24	1.493E-08	4.25		5.3137E-17	3.04		1.1215E-12
	GABBR2		1.72	1.1017E-10	1.23		0.00352786	1.38		1.777E-05
	GABBR1		2.44	5.2822E-09	1.81		1.5219E-09			
glutamatergic neurotransmission	SLC17A7 (VGLUT1)		1.62	1.725E-08		15.71	5.8029E-42		16.73	1.6817E-42
	SLC17A6 (VGLUT2)	14.97		1.9617E-32		18.36	4.1989E-34		13.09	2.8534E-31
	GRM2				1.25		0.01024874			
	GRID1				1.20		0.0087664	1.32		9.5578E-05
	GRM4				1.23		0.00731727			
	GRM5				5.52		2.967E-20	3.31		5.9201E-14
	GRM7				9.78		3.7207E-19	3.26		4.7535E-09
	GRM8				3.03		1.3982E-07	4.08		2.8641E-10
	GRIA4				4.53		6.3774E-18	2.57		1.654E-10
potassium channels	KCNT2					1.69	9.5418E-07			
	KCNMB2					1.20	0.00410187		1.44	1.1153E-07
	KCNMB4					1.63	2.5898E-10		1.34	2.0346E-05
	KCTD6					1.69	1.812E-08			
	KCNJ3					1.23	0.00150732		1.30	9.182E-05
	KCNAB1				5.82		2.4064E-19	4.52		1.629E-16
	KCNA1				3.43		1.3325E-14	2.38		1.3335E-09
	KCNB1				2.41		3.2413E-13	2.38		5.3878E-13
	KCNC2				3.33		4.1627E-13	2.69		2.2995E-10
	HCN1				3.22		2.0687E-11	1.43		0.01354166
	KCNK3				1.68		5.6436E-08	1.69		4.0137E-08
	KCNH2				1.48		9.6189E-06	1.33		0.00081957
	KCNH8				1.82		2.8234E-10	2.41		5.0768E-16
	KCNH1				2.37		5.5223E-08	3.25		7.6688E-12
	KCNJ2				1.51		2.5062E-07	1.27		0.00119346
	KCNF1				1.63		0.00016893	1.55		0.00065777
	KCTD12				1.48		0.00041505	1.41		0.00187834
	KCTD2				1.25		0.00183636	1.24		0.00302052
	KCTD10				1.45		0.00661543	3.01		1.4514E-11
sodium channels	SCN3B				3.10		2.2741E-14	1.74		7.1721E-06
calcium binding proteins	CABP7					20.57	5.608E-31		9.28	2.6041E-24
	S100B					2.45	2.7434E-19		3.03	1.5209E-23
calcium channels	CACNA2D3				4.15		2.7981E-30	7.26		6.351E-38
	CACNG3				2.22		2.5192E-06	2.42		3.2277E-07
	CACNB3				1.73		3.849E-09	1.93		1.7131E-11
	CACNB4				1.86		1.5194E-07	1.35		0.00588167
	CACNG7				1.30		0.0072412			
	CACNG2				6.44		4.469E-15	6.67		2.1935E-15
	CACNA1D				1.79		6.7284E-10			
phosphodiesterases	PDE8B				3.95		3.8107E-20	2.98		6.0575E-16
	PDE5A		2.58	8.5781E-08	6.40		2.6293E-17	1.88		0.00013153
phosphatases	PPP2R2C				2.68		2.479E-10	3.06		4.4564E-12
	PTPRT				15.64		2.2598E-30	8.71		3.9044E-25
	PPP1R9A				4.68		3.5629E-24	2.81		2.0825E-16
tau pathway	MAPT				2.39		1.2289E-24	1.51		2.2523E-11
amyloid pathway	APP				1.38		5.3228E-05			
	BACE1				1.36		9.0638E-05	2.08		2.3417E-14

Table 4.1 10+16 splicing variant induces significant differences in gene expression. Gene expression was analyzed using microarray to do a pairwise comparison between SM(bi) and control hiPSC-derived NPCs (right before final plating) or neuronal cultures (five and seven weeks after final plating). Different gene groups are categorized in the first column, the second column shows the gene symbols of affected genes. Per time point (NPC, wk5 or wk7) up- (in green) and downregulated (in red) genes are shown, including the fold increase or decrease and p-value of significance.
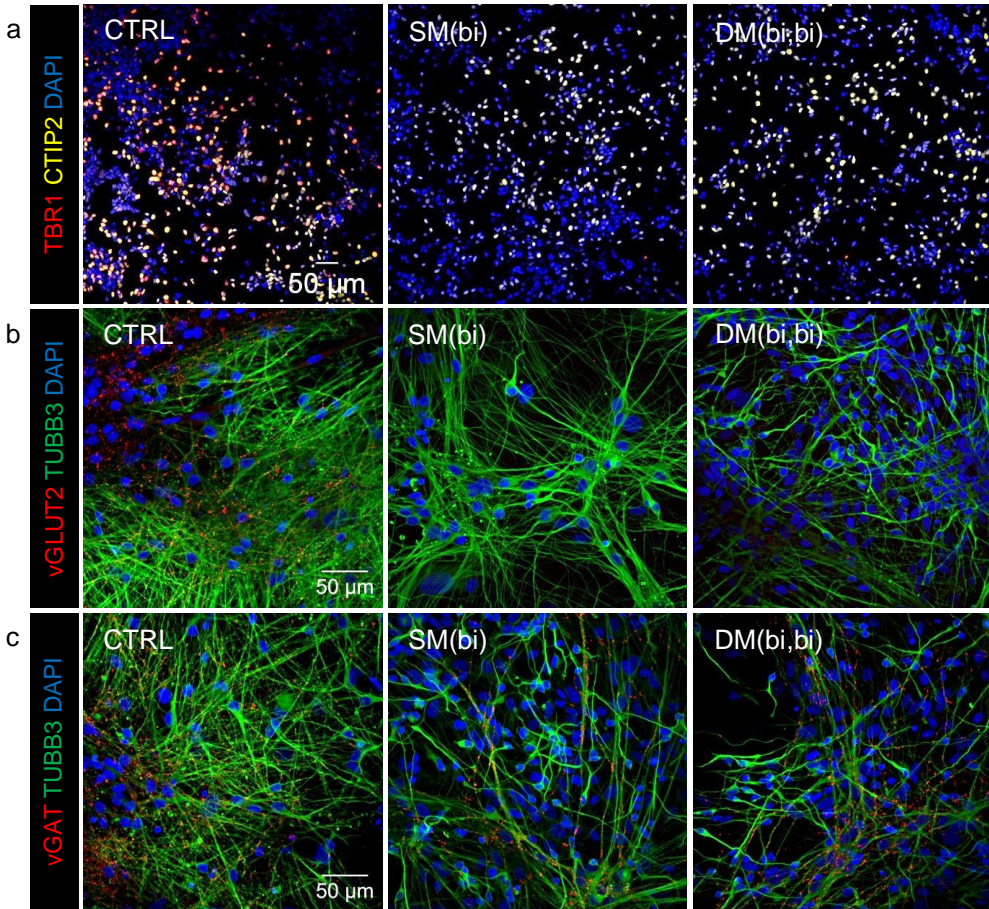
Figure 4.2 10+16 splicing variant alters differentiation towards cortical neurons. a) hiPSC-derived neuronal cultures from CTRL, SM(bi) and DM(bi,bi) lines were stained for deep layer cortical markers TBR1 and CTIP2. Fully differentiated hiPSC-derived neurons from CTRL showed both cortical markers TBR1 and CTIP2, neurons from the 10+16 splicing variant expressing cell lines (either SM(bi) or DM(bi,bi) did not produce sufficient TBR1. b) hiPSC-derived neuronal cultures from CTRL, SM(bi) and DM(bi,bi) lines were stained for vesicular glutamate transporter vGLUT2, neuronal marker class III β-tubulin, and DAPI. Fully differentiated hiPSC-derived CTRL neurons clearly showed vGLUT2, while fully neurons from the 10+16 splicing variant expressing cell lines (either SM(bi) or DM(bi,bi) did not. c) hiPSC-derived neuronal cultures from CTRL, SM(bi) and DM(bi,bi) lines were stained for vesicular GABA transporter vGAT, neuronal marker class III β-tubulin, and DAPI. hiPSC-derived neurons from all three cell lines clearly showed vGAT.

Additional KEGG analyses revealed the following interesting biological and signaling pathways to be altered by the tau mutations in the NPC stage: axon guidance, Hippo signaling pathway (involved in regulation of cell proliferation and apoptosis), cell cycle, signaling pathways regulating pluripotency of stem cells, and the Wnt signaling pathway. At 5 weeks after final plating axon guidance and pathways involved in the GABAergic and glutamatergic synapses were highly affected.
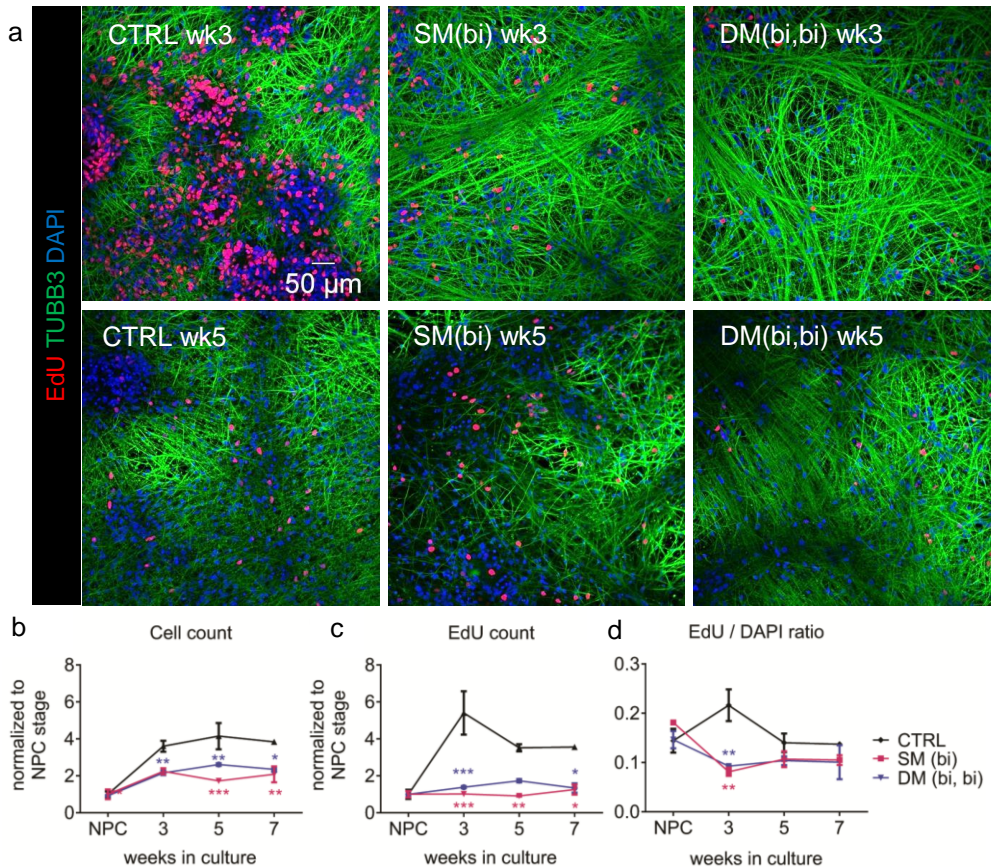
Figure 4.3 10+16 splicing variant decreases cell proliferation. a) hiPSC-derived neuronal cultures from CTRL, SM(bi) and DM(bi,bi) lines were stained for neuronal marker class III β-tubulin (in green), proliferation marker EdU (in red), and nucleus marker DAPI (in blue) at NPC stage (not shown) and wk3, wk5 and wk7 (not shown) after final plating. b) Number of cells, based on the DAPI staining, was analyzed automatically. After normalization to the number of cells that was plated in the NPC stage, the cells expressing the 10+16 mutation (SM(bi) and DM(bi,bi)) showed significantly reduced cell numbers after final plating when compared to CTRL (two-way ANOVA, $p < 0.0001$). n = 2 from 1 differentiation, mean ± SEM, *$p<0.05$, **$p<0.01$, ***$p≤0.0001$. c) The number of proliferating cells, based on the EdU staining, was analyzed automatically. To study the increase of proliferating cells over time, the number of EdU-positive cells was normalized to the NPC stage. The number of proliferating cells was significantly decreased in the cells with the 10+16 mutation compared to CTRL (two-way ANOVA, $p < 0.0001$). n = 2 from 1

differentiation, mean ± SEM, *p<0.05, **p<0.01, ***p≤0.0001. d) The ratio of proliferating cells was calculated after normalization of the Edu count to the number of cells per well. A significantly lower fraction of proliferating cells was present in the cells with the 10+16 mutation compared to CTRL at three weeks after final plating (two-way ANOVA, p = 0.0138). n = 2 from 1 differentiation, mean ± SEM, **p<0.01.

4.3.3 AlphaLISA shows tau aggregation in seeded double bi-allelic mutant

Since it was unknown if the induced tau mutations made cells prone to aggregation, alphaLISA was used to analyze aggregated tau, total tau and phospho-tau levels in lysates produced from neuronal cultures (as previously described [2]). Additionally, K18P301L fibrils were added to the cultures at two weeks after final plating to further facilitate tau aggregation. Ten conditions were compared, but only the bi-allelic double mutant showed significant tau aggregation, and only after K18P301L seeding (Fig. 4.4a), as shown by the hTau10/hTau10 assay. The HT7/hTau10 assay showed that total tau levels are similar for all cell lines (with or without K18P301L seeding), except that SM(bi) cortical neurons show slightly lower total tau levels than the DM(bi,mono) (Fig. 4.4b). Finally, phosphorylated tau levels are slightly different between non-seeded cortical neurons from different cell lines, with an increased level of phosphorylation in SM(mono) cells compared to control and SM(bi) cells and additionally an increased level in DM(bi,mono) cells when compared to SM(bi) cells. Earlier time points (three and five weeks after final plating) did not show any significant differences between the ten conditions on these three alphaLISA assays (data not shown).

4.3.4 The 10+16 splicing variant significantly decreases neuronal network function *in vitro*

Neuronal network functionality of the five different hiPSC-lines was assessed using live cell calcium imaging five weeks after final plating. There were clear differences between SM and CTRL neuronal cultures, since SM hiPSC-derived neuronal cultures show a significantly decreased percentage of active neurons, bursting frequency and correlation score compared to parental control cultures (Fig. 4.5a). In order to study the effect of the additional P301S mutation on neuronal network functionality, calcium oscillations in SM(bi) cultures were compared with both DM cell lines. The mono- or bi-allelic P301S mutation of the DM hiPSC-derived cortical cultures did not induce significant changes in any of the three readouts of the calcium assay when compared to SM(bi) neuronal cultures (Fig. 4.5b).

bi-allelic E10+16 mutation + P301S mutation compared to bi-allelic E10+16 mutation	gene symbol	NPC			wk5			wk7		
		fold increase	fold decrease	p value	fold increase	fold decrease	p value	fold increase	fold decrease	p value
neuronal differentiation	NNAT	23.97332		1.17E-33	56.93882		2.68E-39	35.28261		2.51E-36
neuronal differentiation	PAX6		1.297709	3.63E-06		1.553691	5.11E-12		1.53957	1.01E-11
differentiation and survival of inhibitory neurons in forebrain	DLX5		1.806576	4.34E-05						
differentiation and survival of inhibitory neurons in forebrain	DLX6		1.72867	7.32E-09						
GABAergic neurotransmission	GABRB3		1.26784	0.000797						
GABAergic neurotransmission	GABBR2		1.630064	1.99E-09						
GABAergic neurotransmission	GABRG2		1.297607	0.002					1.843679	1.64E-05
GABAergic neurotransmission	SLC32A1		1.62105	1.45E-10		1.352916	8.93E-06		1.2991	8.76E-05
glutamatergic neurotransmission	GRM3		1.722317	5.14E-05						
glutamatergic neurotransmission	SLC25A18					2.021688	1.73E-07		2.090151	5.97E-08
glutamatergic neurotransmission	GRIK2					1.99202	9.86E-16		1.269602	0.000348
microtubule-associated proteins	MAP2		1.365776	2.89E-07						
microtubule-associated proteins	MAPT		1.303563	1.78E-06						
microtubule-associated proteins	MAP1LC3A		1.794688	1.3E-10		1.340554	0.000239			
microtubule-associated proteins	MAP7D3	1.483609		1.01E-07						
microtubule-associated proteins	MAP7D2				1.738515		1.71E-08	1.606194		5.98E-07
kinases	DAPK1		1.208555	0.000237						
kinases	NTRK3		1.476421	0.000467						
kinases	CDK5R1		1.421278	0.001503						
kinases	MAPK8IP1		1.290937	0.002359						
kinases	CDK2AP2		1.285867	0.001665						
kinases	SKAP2		1.798287	2.43E-05						
kinases	STK32B		1.492623	0.001023						
kinases	DCLK1		1.376966	0.000347						
kinases	EFNB2		1.395	4.43E-06						
kinases	EFNA3		1.408143	0.000276						
kinases	PRKCZ		1.315173	2.41E-06						
kinases	PKIB		1.572932	0.000504		1.785627	1.56E-05			
kinases	NTRK2		1.416858	9.78E-06		1.312364	0.00037			
kinases	PRKCB		1.835454	6.53E-11		1.303481	0.00093			
kinases	PIM2					1.865019	0.000168		1.761295	0.000556
kinases	PIP5K1B		2.06146	1.4E-11		1.578972	1.88E-06		1.803505	5.48E-09
kinases	AUNIP	1.665504		8.4E-06						
kinases	NEK2	1.419831		0.002163						
kinases	NTRK1	2.028624		9.73E-06						
kinases	CIT	1.412171		4.52E-07						
kinases	TESK2	1.276988		0.001499						
kinases	NTPCR	1.227997		0.002613						
kinases	MAP3K4	1.329482		0.000161						
kinases	IRAK1	2.351941		3.34E-09						
kinases	ROCK2	1.217031		0.000731						
kinases	DYRK4	1.474732		3.77E-05	1.413444		0.000197			
kinases	STK26				2.162996		3.19E-09	1.946398		1.24E-07
kinases	SH3KBP1				1.672871		6.37E-09	2.546964		7.7E-18
kinases	MAP4K1				1.33438		0.000464	1.412394		4.07E-05
kinases	AKAP13				1.492369		0.000496	1.634772		3E-05
kinases	RPS6KA3	2.16422		1.51E-14	2.13222		3.11E-14	2.152547		1.96E-14
kinases	EFNB1	2.235552		5.53E-15	1.786012		3.40E-10	1.886911		2.16E-11
phosphatases	PPP2R5B		1.389466	0.000515						
phosphatases	PDP1		1.190788	0.000522						
phosphatases	PPP1R18		1.24695	0.000141						
phosphatases	PPP1R14C		1.783975	6.3E-05						
phosphatases	PDXP		1.228775	0.001481						
phosphatases	PTPRC		1.217787	6.08E-05						
phosphatases	PTPRD		1.356647	5.55E-05		1.282266	0.000776			
phosphatases	PTPRT					1.785338	1.23E-05		1.624599	0.000179
phosphatases	PTPMT1		1.586734	1.81E-09		1.532771	1.42E-08		1.329885	4.64E-05
phosphatases	DUT	1.311638		0.001105						
phosphatases	DUSP22	1.423942		0.000256						
phosphatases	DUSP23	1.364169		7.82E-05						
phosphatases	PTPDC1	1.359273		0.00014						
phosphatases	PSMD10				1.898069		3.15E-21	1.917961		1.5E-21
phosphatases	DUSP26	1.682565		4.18E-12	2.032159		4.13E-17	1.952798		4.28E-16
heat shock proteins	HSPA1A				11.21512		2.46E-15	14.08095		6.9E-17
calcium binding proteins and calcium channels	S100A10		1.772251	2.31E-06	1.453238		0.001129	1.470747		0.000805
calcium binding proteins and calcium channels	EFCAB2	1.506519		5.3E-09	1.263474		0.000243			
calcium binding proteins and calcium channels	CACNA2D3					2.116753	3.69E-17		1.591089	7.11E-10
mitochondria related proteins	TIMM17B					1.854313	2.49E-08		1.721598	4.7E-07
protein degradation related protein	ATG4A				1.963295		3.32E-10	1.804308		1.28E-08
chloride channel	CLCN4					2.150244	5.18E-10		2.064841	2.37E-09
sulfotransferase	HS6ST2	1.513521		5.25E-09	1.606293		1.18E-10	1.416304		3.45E-07

Table 4.2 P301S mutation induces significant differences in gene expression. Gene expression was analyzed using microarray to do a pairwise comparison between DM(bi,bi) and SM(bi) hiPSC-derived NPCs (right before final plating) or neuronal cultures (five and seven weeks after final plating). Different gene groups are categorized in the first column, the second column shows the gene symbols of affected genes. Per time point (NPS, wk5 or wk7) up- (in green) and downregulated (in red) genes are shown, including the fold increase or decrease and p-value of significance.
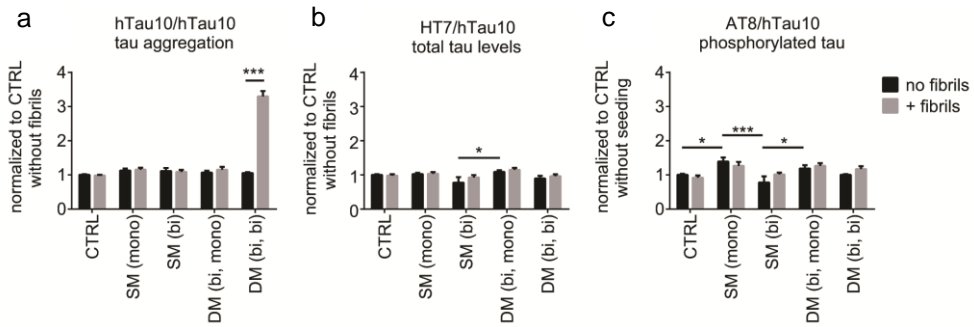
Figure 4.4 AlphaLISA shows tau aggregation in seeded double bi-allelic mutant. a) AlphaLISA data (hTau10/hTau10 assay) show that K18P301L seeding induces a significant increase in tau aggregation (Oneway ANOVA, p < 0.0001, Holm-Sidak's multiple comparisons test p < 0.0001) in DM(bi,bi) cortical neurons 7-9 weeks after final plating, while there are no significant differences for all other cell lines. Mean + SEM, n ≥ 6, from 3 differentiations. b) AlphaLISA data (HT7/hTau10 assay) show that total tau levels are similar for all cell lines (with or without K18P301L seeding), except that single mutant (bi) cortical neurons show slightly lower total tau levels than double mutant (bi,mono) cortical neurons (Oneway ANOVA, p = 0.0030, Holm-Sidak's multiple comparisons test p < 0.05). Mean + SEM, n ≥ 6, from 3 differentiations. c) AlphaLISA data (AT8/hTau10 assay) show that phosphorylated tau levels show some differences between non-seeded cortical neurons from different cell lines (Oneway ANOVA, p < 0.0001), with an increased level in SM(mono) cells compared to control and SM(bi) cells (respectively Holm-Sidak's multiple comparisons test p < 0.05, and p ≤ 0.0001) and an increased level in DM(bi,mono) when compared to SM(bi) cells (Holm-Sidak's multiple comparisons test p < 0.05). Mean + SEM, n ≥ 6, from 3 differentiations.

4.3.5 The 10+16 splicing variant increases synapse density of hiPSC-derived neurons

Finally, to verify whether the functional activity was also reflected by morphological correlates of neuronal network connectivity an automated analysis of synaptic marker production was performed in hiPSC-derived cortical co-cultures at five weeks after final plating. Cultures were stained with presynaptic marker anti-synaptophysin, post-synaptic marker anti-GluA, neurite marker anti-MAP2 and nuclear counterstain DAPI (Fig. 4.6a). Total cell number and neurite area were not affected by one or both mutations, while the bi-allelic 10+16 splicing variant significantly increased the synapse density (Fig. 4.6b).
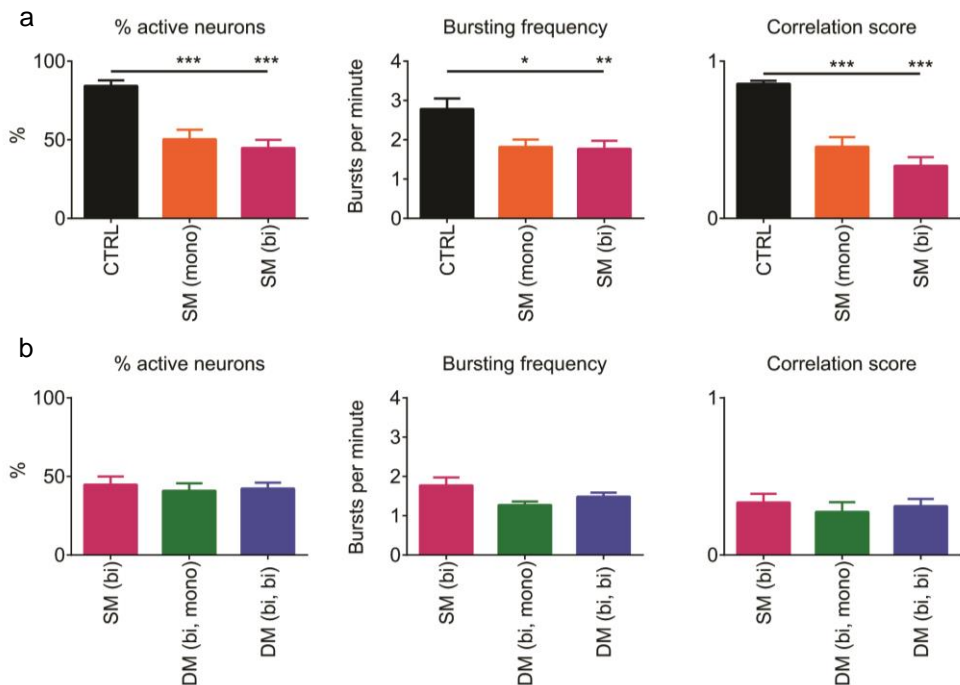
Figure 4.5 Live cell calcium imaging shows decreased functionality due to 10+16 but not P301S mutation. a) Using live cell calcium imaging, single mutant hiPSC-derived neuronal cultures show a significantly decreased percentage of active neurons (one-way ANOVA, $p < 0.0001$), bursting frequency (one-way ANOVA, $p = 0.0030$) and correlation score (one-way ANOVA, $p < 0.0001$) compared to parental control cultures. $n \geq 3$ from $\geq$ 3 differentiations, mean + SEM, *$p<0.05$, **$p<0.01$,***$p\leq0.0001$. b) The additional mono- or bi-allelic P301S mutation of the double mutant hiPSC-derived cortical cultures does not induce significant changes in the percentage active neurons, bursting frequency, or correlation score when compared to the bi-allelic single mutant neuronal cultures. $n \geq 3$ from $\geq$ 3 differentiations, mean + SEM.
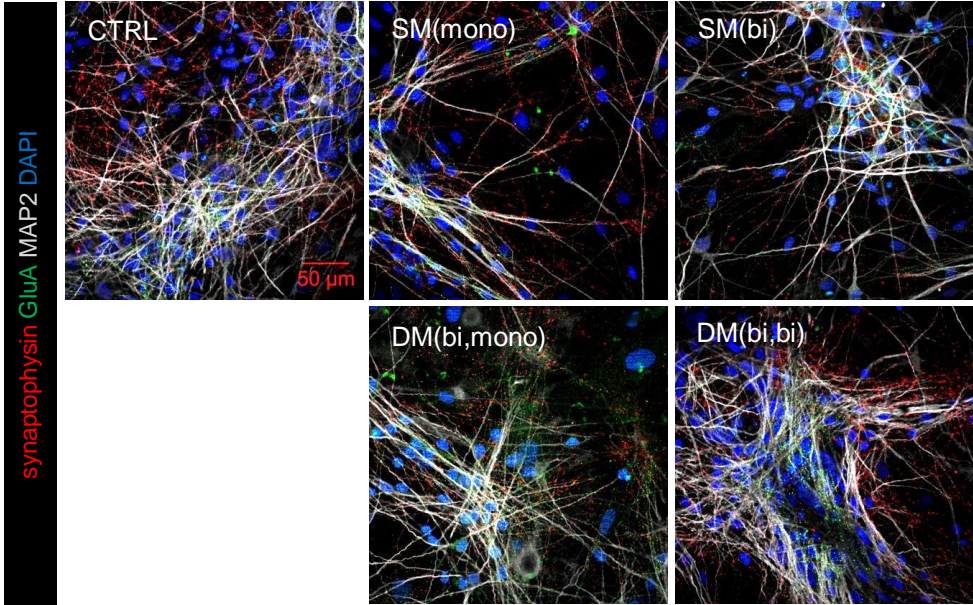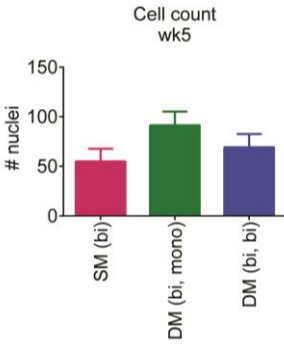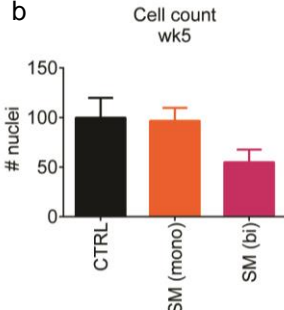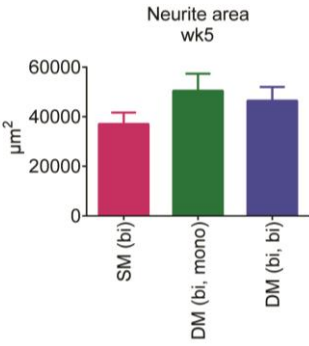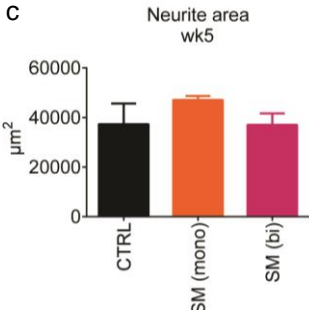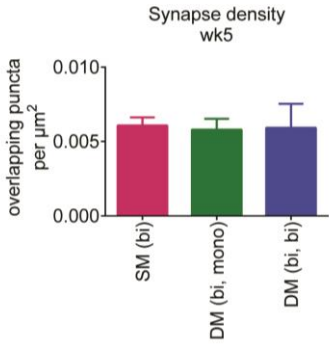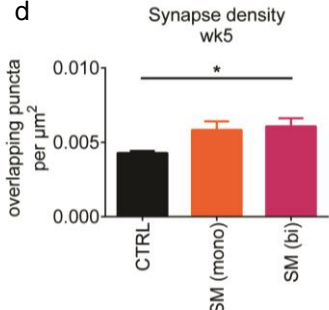
Figure 4.6 Analysis of neuronal network morphology reveals increased synapse density due to the 10+16 splicing variant. a) Neuronal co-cultures (five weeks after final plating) derived from all five hiPSC lines were stained with anti-synaptophysin, anti-GluA, anti-MAP2 and DAPI. b) Cell number, based on the DAPI staining, was analyzed automatically. Neither the 10+16 splicing variant, nor the P301S mutation induced changes in the total cell number. $n \geq 1$ from ≥ 1 differentiation, mean + SEM. c) Neurite area, based on the MAP2 staining, was analyzed automatically. Neither the 10+16 splicing variant, nor the P301S mutation changed the total neurite area. $n \geq 1$ from ≥ 1 differentiation, mean + SEM. d) Synapse density was analyzed automatically. Synapses were defined as synaptophysin *puncta* overlapping with GluA *puncta*, density was calculated as number of overlapping *puncta* per neurite area in μm^2. The bi-allelic 10+16 splicing variant significantly increased the synapse density (One-way ANOVA, $p = 0.0242$). $n \geq 1$ from ≥ 1 differentiation, mean + SEM, *$p<0.05$

4.4 Discussion

Many different models have been used to study tauopathies, either *in vivo* or *in vitro*, and learned us a lot about potential disease mechanisms, genetics, and possible treatments for these neurodegenerative disorders. However, translational value of many models remains poor, which is reflected by the high attrition rate in clinical trials for neurodegenerative disorders. In order to bridge the gap between animal models and human disease we have developed a new human iPSC-derived neuronal model to study processes involved in tauopathies. In this model, mature 4R tau production is obtained using the zinc-finger technology induced 10+16 *MAPT* splicing variant mutation as it is found in FTD patients [12]. This mutation, inducing alternative splicing of *MAPT*, includes the expression of exon 10 on which many exonic mutations are located. Additionally, hiPSC lines containing the P301S mutation (located on exon 10) were generated. The combination of these two mutations was necessary since the P301S mutation is located in exon 10 that is spliced out in CTRL hiPSC-derived neuronal cultures at least until 100 DIV. In this new tauopathy model, we found that cortical differentiation is significantly changed by the 10+16 splicing variant, supported by significantly altered gene expression. As a consequence, neuronal network function was decreased, while morphologically synapse density was increased. The P301S mutation further changed gene expression profiles, and enabled fibril seeding-induced tau aggregation in hiPSC-derived neuronal cultures.

In order to express the P301S mutation the additional 10+16 splicing variant mutation was needed. We will first discuss the effects of this mutation, which was present in all four mutant hiPSC lines. As shown by immunocytochemistry and microarray this mutation highly affected the differentiation of hiPSCs towards cortical neurons. First of all, 10+16 splicing variant expressing mutant lines showed a less proliferative, and probably more differentiating, phenotype than CTRL cells without the mutation. This might be explained by the fact that differentiation in these cells is forced towards a more mature phenotype, that is 4R tau production instead of gradual increase of the 4R/3R in normally developing neurons. CTRL cells did not express 4R tau before 365 DIV [12]. This is comparable to physiological expression of tau isoforms, since 4R tau is not expressed during early development but expression increases later in life reaching equal levels compared to 3R tau isoforms in adulthood. Secondly, projection neuron markers TBR1 and SATB2 were not produced in differentiated mutant neurons, and some important glutamatergic genes (e.g. *vGLUT1* and *vGLUT2*) were down regulated. GABAergic markers (e.g. *vGAT*, *GAD67* and several GABA receptor genes) were significantly upregulated as shown by the microarray data, as well as some markers linked to differentiation and survival of interneurons in the forebrain. Recently Nicholas and colleagues described the functional maturation of hiPSC-derived ganglionic eminence-like progenitors and subsequently forebrain-type interneurons that show coinciding gene expression

patterns, for example high *DLX* and *DCX* and decreased *PAX6* and *TBR1* levels [24]. The production of *CTIP2* was previously described in GABAergic neurons derived from ganglionic eminence progenitors as well [25]. This might suggest that the 10+16 mutants produce a different lineage of (cortical) neurons than the CTRL cells. Additional immunocytochemical assays using interneuron markers parvalbumin, calbindin or calretinin could further substantiate the hypothesis that interneurons evolve from mutant hiPSC differentiation.

Of particular interest is the involvement of the Wnt signaling pathway which was revealed by the KEGG analysis. The Wnt signaling (and its counterpart hedgehog) is highly involved in the establishment of the dorsoventral axis of the central nervous system [26]. During neural induction of human stem cells the addition of hedgehog agonist purmorphamine ventralizes the differentiation and avoids expression of cortical stem cell markers [27]. In addition Wnt signaling inhibition was used for directed differentiation of hiPSCs towards forebrain GABAergic interneurons [28] and GABAergic *CTIP2* expressing neurons [25], indicating the relevance of these pathways in neuronal differentiation. Interestingly, the Wnt signaling pathway was the only gene set significantly altered between 3R and 4R tau expressing neuronal cells [29] and is known to be involved in Alzheimer's disease (reviewed in ref. [30]). A possible approach to further study the effect of Wnt signaling on neuronal differentiation of mutant and CTRL hiPSCs would be the interference during differentiation with hedgehog antagonists such as cyclopamine [31] or agonists such as purmorphamine.

The altered balance between GABAergic and glutamatergic neurons might have major implications for neuronal network function. The shift towards a more GABAergic and thus inhibitory contribution to neurotransmission in 10+16 splicing variant expressing mutants might explain the decreased network function that was shown with live cell calcium imaging. Changes could be related to downregulation of the Wnt pathway resulting in increased differentiation towards GABAergic neurons [28]. Accumulating evidence indicates that GABAergic neurotransmission significantly alters during AD pathology [32]. For example, postsynaptic $GABA_A$ receptors were differentially expressed [33,34] with a preservation of β subunits but a upregulation of α1 and γ subunits [20,21]. Our microarray data showed similar differences with no influence on β subunits, but significant increases in α and γ subunits in the 10+16 mutant hiPCS-derived neurons, suggesting that functional remodeling was ongoing.

Finally, we analyzed the correlates of the decreased functionality in neuronal morphology. We found no significant differences in the cell count and neurite area induced by the splicing variant. This seems to be in contrast to the previously described decreased cell count in the proliferation assay. However, the morphological analysis was done on co-cultures with astrocytes since these were used for the functional assays as well. The addition of human astrocytes might have camouflaged the decreased level of neuronal proliferation. The

synapse density was significantly increased in the 10+16 splicing variant expressing neuronal cultures, although functional data might imply the opposite. However, the synapses are not characterized and might represent a different kind of synapse in the mutant cell lines. For example, inhibitory (GABAergic) cortical interneurons make local synapses while (glutamatergic) cortical pyramidal neurons project over long distances [35]. Additional immunocyto-chemical characterization or analysis of postsynaptic currents (PSCs) might further substantiate this increase.

Additionally, the double mutant (DM) hiPSC lines contained the P301S mutation in the *MAPT* gene (either mono-allelic or bi-allelic) as identified in FTD patients. No significant differences in proliferation and cortical marker immunoreactivity were found in these two lines. However, microarray analysis revealed further changes when compared to the single mutant lines. Many changes appeared in the expression of genes encoding kinases and phosphatases. This is of importance in view of the tau protein, since many of its amino acid residues are potential phosphorylation sites [36]. Dysregulation of kinase and phosphatase activity might cause tau hyperphosphorylation and as a consequence tau protein can become insoluble and self-aggregating. However, we did not observe any changes in tau phosphorylation using the AT8/hTau10 alphaLISA. Similarly, tau phosphorylation was found at comparable levels in FTD and control neurons in a previous study [12]. This might be due to high baseline phosphorylation levels due to microtubule dynamics for example, because these neuronal cultures are still in a rather developmental stage.

In order to further study the tendency of mutant lines to produce tau aggregation, which is the major characteristic of tauopathies, we used the alphaLISA assay that was previously described by Verheyen *et al*. [2]. We found that induction of tau aggregation was not possible within the time span of 10 weeks after final plating without addition of artificial fibrils. However, after adding K18P301L fibrils, the DM(bi,bi) neuronal cultures clearly showed a threefold increase in tau aggregation compared to all other conditions. Although it is thought that tau hyperphosphorylation precedes tau aggregation [37] no differences in phosphorylation levels were found in the cultures showing tau aggregation. However, due to the heterogeneity of phosphorylation sites in tau and the unknown influence of cofactors it is still a matter of debate if phosphorylation is a requisite for aggregation (as reviewed in ref. [6]).

While the additional P301S mutation was responsible for important tauopathy-related phenotypes was the impact of the 10 + 16 mutation on neuronal differentiation compelling as well. Both mutations are interesting targets to study since both are linked to tauopathies. However, altered differentiation caused by the 10 + 16 mutation might mask some of the effects of the P301S mutation. Therefore, it would be interesting to use an inducible gene editing system for the 10 + 16 mutation for future research.

To conclude, we propose a new tauopathy model, based on 4R tau isoform expression with the P301S mutation in hiPSC-derived neuronal cultures. Several characteristics of this model are recapitulating human tauopathy related phenomena, such as tau aggregation and impaired neuronal network functionality. Although additional efforts have to be made to clarify the exact mechanisms of tauopathy, the model can add useful information to the current knowledge about tauopathies. In addition to the study of mutations changing the coding sequence of the *MAPT* gene this model provides a valuable approach to study pathological alternative splicing of *MAPT in vitro*. Finally, the model could be used as a screening model for therapeutic approaches interfering with tau pathology.

References

1   Takamatsu, K. *et al.* Degradation of amyloid beta by human induced pluripotent stem cell-derived macrophages expressing Neprilysin-2. *Stem Cell Res.* **13**, 442-453 (2014).

2   Verheyen, A. *et al.* Using Human iPSC-Derived Neurons to Model TAU Aggregation. *PLoS One* **10**, e0146127 (2015).

3   Kondo, T. *et al.* Modeling Alzheimer's disease with iPSCs reveals stress phenotypes associated with intracellular Aβ and differential drug responsiveness. *Cell stem cell* **12**, 487-496 (2013).

4   Payne, N. L. *et al.* Application of human induced pluripotent stem cells for modeling and treating neurodegenerative diseases. *New biotechnology* **32**, 212-228 (2015).

5   Spillantini, M. G. & Goedert, M. Tau protein pathology in neurodegenerative diseases. *Trends Neurosci.* **21**, 428-433 (1998).

6   Wang, Y. & Mandelkow, E. Tau in physiology and pathology. *Nature Reviews Neuroscience* (2015).

7   Goedert, M. & Jakes, R. Expression of separate isoforms of human tau protein: correlation with the tau pattern in brain and effects on tubulin polymerization. *EMBO J.* **9**, 4225 (1990).

8   Connell, J. *et al.* Quantitative analysis of tau isoform transcripts in sporadic tauopathies. *Molecular brain research* **137**, 104-109 (2005).

9   Grover, A. *et al.* 5' splice site mutations in tau associated with the inherited dementia FTDP-17 affect a stem-loop structure that regulates alternative splicing of exon 10. *J. Biol. Chem.* **274**, 15134-15143 (1999).

10   Hong, M. *et al.* Mutation-specific functional impairments in distinct tau isoforms of hereditary FTDP-17. *Science* **282**, 1914-1917 (1998).

11   Bugiani, O. *et al.* Frontotemporal dementia and corticobasal degeneration in a family with a P301S mutation in tau. *J. Neuropathol. Exp. Neurol.* **58**, 667-677 (1999).

12   Sposito, T. *et al.* Developmental regulation of tau splicing is disrupted in stem cell-derived neurons from frontotemporal dementia patients with the 10+ 16 splice-site mutation in MAPT. *Hum. Mol. Genet.* **24**, 5260-5269 (2015).

13   Gentleman, R. C. *et al.* Bioconductor: open software development for computational biology and bioinformatics. *Genome Biol.* **5**, R80 (2004).

14   Dai, M. *et al.* Evolving gene/transcript definitions significantly alter the interpretation of GeneChip data. *Nucleic Acids Res.* **33**, e175-e175 (2005).

15   Irizarry, R. A. *et al.* Exploration, normalization, and summaries of high density oligonucleotide array probe level data. *Biostatistics* **4**, 249-264 (2003).

16   Goeman, J. J., Oosting, J., Cleton-Jansen, A.-M., Anninga, J. K. & Van Houwelingen, H. C. Testing association of a pathway with survival using gene expression data. *Bioinformatics* **21**, 1950-1957 (2005).

17   Goeman, J. J., Van De Geer, S. A., De Kort, F. & Van Houwelingen, H. C. A global test for groups of genes: testing association with a clinical outcome. *Bioinformatics* **20**, 93-99 (2004).

18   Spillantini, M. G. & Goedert, M. Tau pathology and neurodegeneration. *The Lancet Neurology* **12**, 609-622 (2013).

19   Calafate, S. *et al.* Synaptic contacts enhance cell-to-cell tau pathology propagation. *Cell reports* **11**, 1176-1183 (2015).

20   Goedert, M., Jakes, R. & Vanmechelen, E. Monoclonal antibody AT8 recognises tau protein phosphorylated at both serine 202 and threonine 205. *Neurosci. Lett.* **189**, 167-170 (1995).

21   Cornelissen, F. *et al.* Quantitation of chronic and acute treatment effects on neuronal network activity using image and signal analysis toward a high-content assay. *J. Biomol. Screen.*, 1087057113486518 (2013).

22   Schindelin, J. *et al.* Fiji: an open-source platform for biological-image analysis. *Nat. Methods* **9**, 676-682 (2012).

23   Huang, L.-K. & Wang, M.-J. J. Image thresholding by minimizing the measures of fuzziness. *Pattern Recog.* **28**, 41-51 (1995).

24   Nicholas, C. R. *et al.* Functional maturation of hPSC-derived forebrain interneurons requires an extended timeline and mimics human neural development. *Cell stem cell* **12**, 573-586 (2013).

25   Carri, A. D. *et al.* Human pluripotent stem cell differentiation into authentic striatal projection neurons. *Stem Cell Reviews and Reports* **9**, 461-474 (2013).

26   Ulloa, F. & Martí, E. Wnt won the war: Antagonistic role of Wnt over Shh controls dorso-ventral patterning of the vertebrate neural tube. *Dev. Dyn.* **239**, 69-76 (2010).

27   Shi, Y., Kirwan, P., Smith, J., Robinson, H. P. & Livesey, F. J. Human cerebral cortex development from pluripotent stem cells to functional excitatory synapses. *Nat. Neurosci.* **15**, 477-486 (2012).

28   Liu, Y. *et al.* Directed differentiation of forebrain GABA interneurons from human pluripotent stem cells. *Nat. Protoc.* **8**, 1670-1679 (2013).

29   Chen, S., Townsend, K., Goldberg, T. E., Davies, P. & Conejero-Goldberg, C. MAPT isoforms: differential transcriptional profiles related to 3R and 4R splice variants. *J. Alzheimers Dis.* **22**, 1313-1329 (2010).

30   Vallée, A. & Lecarpentier, Y. Alzheimer disease: crosstalk between the canonical Wnt/beta-catenin pathway and PPARs alpha and gamma. *Front. Neurosci.* **10** (2016).

31   Chen, J. K., Taipale, J., Cooper, M. K. & Beachy, P. A. Inhibition of Hedgehog signaling by direct binding of cyclopamine to Smoothened. *Genes Dev.* **16**, 2743-2748 (2002).

32   Li, Y. *et al.* Implications of GABAergic Neurotransmission in Alzheimer's Disease. *Front. Aging Neurosci.* **8** (2016).

33   Mizukami, K., Grayson, D. R., Ikonomovic, M. D., Sheffield, R. & Armstrong, D. M. GABA A receptor β2 and β3 subunits mRNA in the hippocampal formation of aged human brain with Alzheimer-related neuropathology. *Molecular brain research* **56**, 268-272 (1998).

34   Iwakiri, M. *et al.* An immunohistochemical study of GABAA receptor gamma subunits in Alzheimer's disease hippocampus: Relationship to neurofibrillary tangle progression. *Neuropathology* **29**, 263-269 (2009).

35   Markram, H. *et al.* Interneurons of the neocortical inhibitory system. *Nature Reviews Neuroscience* **5**, 793-807 (2004).

36   Hanger, D. P., Anderton, B. H. & Noble, W. Tau phosphorylation: the therapeutic challenge for neurodegenerative disease. *Trends Mol. Med.* **15**, 112-119 (2009).

37   Braak, F., Braak, H. & Mandelkow, E.-M. A sequence of cytoskeleton changes related to the formation of neurofibrillary tangles and neuropil threads. *Acta Neuropathol.* **87**, 554-567 (1994).

5

**Technical note:
Monitoring neuronal activity
*in vitro***

Abstract

Neuronal network dysfunction is a hallmark of many neurodevelopmental and neurodegenerative disorders which are characterized by cognitive deficits, including autism, schizophrenia and Alzheimer's disease. During development, neurons assemble into neuronal networks which become the primary mediators of cognition. Lacking knowledge about disease etiology and progression hampers the development of disease-modifying treatments and additional research concerning these neuronal networks and neurotransmission is necessary to unravel disease mechanisms. Development and maturation of neuronal networks can be partially recapitulated *in vitro*, including neurite outgrowth, formation of synaptic connections and development of spontaneous neuronal network activity and can be used as a model for neuronal network function and dysfunction. Thorough investigation of network pathologies requires complete dissection of not only network structure, but also its function. Neuronal networks can be studied structurally and functionally through different means allowing for different experimental approaches as previously discussed in the introduction. This technical note describes the exploration of different tools for studying primary rodent and hiPSC-derived cortical neuronal networks *in vitro*. For most tools described here more optimization is needed for successful implementation to study spontaneous network activity in hiPSC-derived cultures. However, the optimized approaches can be used to phenotype *in vitro* models and subsequently additional tools can be applied to confirm or scrutinize findings.

With the aim of studying neuronal networks *in vitro*, the optimization of tools to accomplish this is a legitimate first step. Our final goal was to study spontaneous network activity in hiPSC-derived cortical neurons with optical indicators of neural activity and structure and electrophysiology. However, most tool optimization was done in primary rodent neuronal cultures because optimization in hiPSC-derived neurons would have been very labor intensive due to long culture periods required to obtain functional networks. While primary rodent neuronal cultures show spontaneous network activity within one week, hiPSC-derived cortical neurons need at least 3 weeks before spontaneous network activity can be detected (as described in Chapter 2). Rat primary neuronal cultures were prepared and maintained as described in Chapter 3, hiPSC-derived neuronal cultures were prepared according to procedures described in Chapter 2, unless stated otherwise.

5.1 Optical indicators of neural activity and structure

Transgene expression of genetically encoded indicators of neural activity in primary cultures was accomplished via lentiviral or AAV- transduction. In order to test the optimal conditions of viral transduction of hiPSC-derived cortical neurons lentiviruses were generated from cDNA constructs of MISSION® pLKO.1-puro-CMV-TagRFP™ Positive Control Plasmid DNA and MISSION® pLKO.1-puro-CMV-TurboGFP™ Positive Control Plasmid DNA (Sigma). hiPSC-derived neurons were transduced with both viruses in order to study general transduction efficiency. However, due to the CMV promoter in both constructs many cells were transduced, not only mature neurons but also NPCs that were not yet differentiated and astrocytes, thereby overshadowing neurons. Therefore, the more specific neuronal human synapsin-1 promoter was used for studying neuronal function and optimizations were done for the specific constructs.

cDNA constructs with a human synapsin-1 promoter have been produced for GCaMP3 [1] (Fig. 5.1a), sypHtomato [2] (Fig. 5.2a), PSD95-GCaMP3, pre-mGRASP-mCerulean, post-mGRASP –dTomato [3] (both Fig. 5.3a), and GCaMP6f [4]. GCaMP3 and SypHtomato constructs were obtained respectively from Prof. Loren Looger (Janela Farm Research Campus, USA) and Prof. Yulong Li (School of Life Sciences, Beijing, China). The entire open reading frame of each chimera was amplified using PCR and cloned in the lentiviral transfer vector pLenti6.3/V5-DEST™ (Thermo Fisher Scientific), whose CMV promoter was replaced by the human synapsin-1 promoter [5,6]. For the PSD95-GCaMP3 construct two different forms of PSD95 were tested, that is PSD95α and PSD95β [7], thus two different constructs were created. Lentiviral particles were produced in HEK293T cells using 2nd generation packaging, and concentrated using centrifugation. Adeno-associated virus particles for GCaMP6 were produced using the AAV-6 Helper Free Packaging System according to manufacturer's guidelines (Cell Biolabs,

Inc.). The optimal amount of virus and day of transfection have been determined experimentally, since no absolute titers were determined.

Imaging of optical indicators was done with a LSM510 Meta Zeiss confocal microscope with multiphoton laser. This set-up allowed multicolour imaging using a two-photon Mai Tai laser which allowed the excitation wavelength to be varied between 650 and 1100 nm and 3 separate lasers with dedicated laser lines: an Argon laser (458, 477, 488, 514 nm excitation) and two HeNe lasers (respectively 543 and 633 nm excitation). Live-cell time-lapse imaging of multiple individual neurons and synapses was possible since this set-up was equipped with a heated chamber and CO_2 supply.

5.1.1 Live cell calcium imaging

Live cell calcium imaging was tested for different markers, that are the synthetic FLUO4 (green), Rhod-3, GFP certified Fluoforte (both red) and CaSiR-1 (far red), and genetically encoded GCaMP3 (green) and GCaMP6f (green). The use of those calcium indicators has been optimized in primary neuronal cultures, while only synthetic indicators were used successfully in hiPSC-derived neurons. GCaMP3 expression and functionality have been shown as well in hiPSC-derived neurons, but since GCaMP3 is a lot less sensitive than FLUO4 (and GCaMP6 [4]) it is not sensitive enough to pick up small changes in calcium levels in spontaneously firing hiPSC-derived neurons.

Synthetic calcium indicators were loaded to the cells on the day of the assay. Cells were loaded with either 1 µM Fluo4-AM, 2 µM Rhod-3 AM (Thermo Fisher Scientific), 1 µM GFP certified Fluoforte (Enzo Life Sciences, Inc) or 1 µM CaSiR-1 AM (Goryo Chemical) in recording buffer, containing (in mM): $CaCl_2$ 1.2; KCl 2.67; NaCl 138; KH_2PO_4 1.47; Na_2HPO_4 8; D-glucose 5.6 (adapted from [8]). Cultures were incubated at 37°C and 5% CO_2 for 30 minutes and then imaged with an inverted confocal laser scanning microscope (Axiovert 100M Carl Zeiss, combined with Zeiss LSM510 software) using a Plan-NEOFLUAR 20x objective lens (NA 0.50).

In order to optimize the use of genetically encoded calcium indicators in hiPSC-derived cortical neurons GCaMP3 transduction conditions were tested in primary rat neuronal cultures first to avoid time-consuming hiPSC-derived cultures. Lentiviral particles were added to the culture medium at 2DIV at different volumes (100µl - 0.2µl added to 200µl culture medium on top of either 10,000 cells of 20,000 cells per well) to determine the optimal amount of virus to be added. Production of fluorescent markers was visualized with a LSM510 microscope. The optimal expression levels were obtained with 2µl virus per well, but a 10-fold lower volume showed sufficient fluorescence too. However, spontaneous calcium oscillations were visible much better with the higher concentration. GCaMP3 fluorescence was visible from three days after addition up to at least two weeks after addition (Fig. 5.1). Furthermore, an additional

transduction time point was tested (6DIV), but the fluorescent signal was much weaker and these wells showed a lot more cell death.
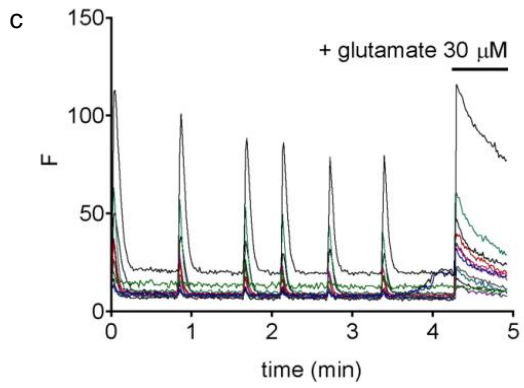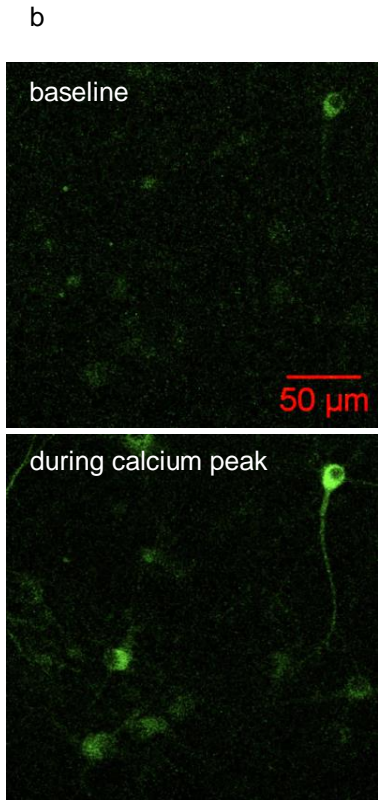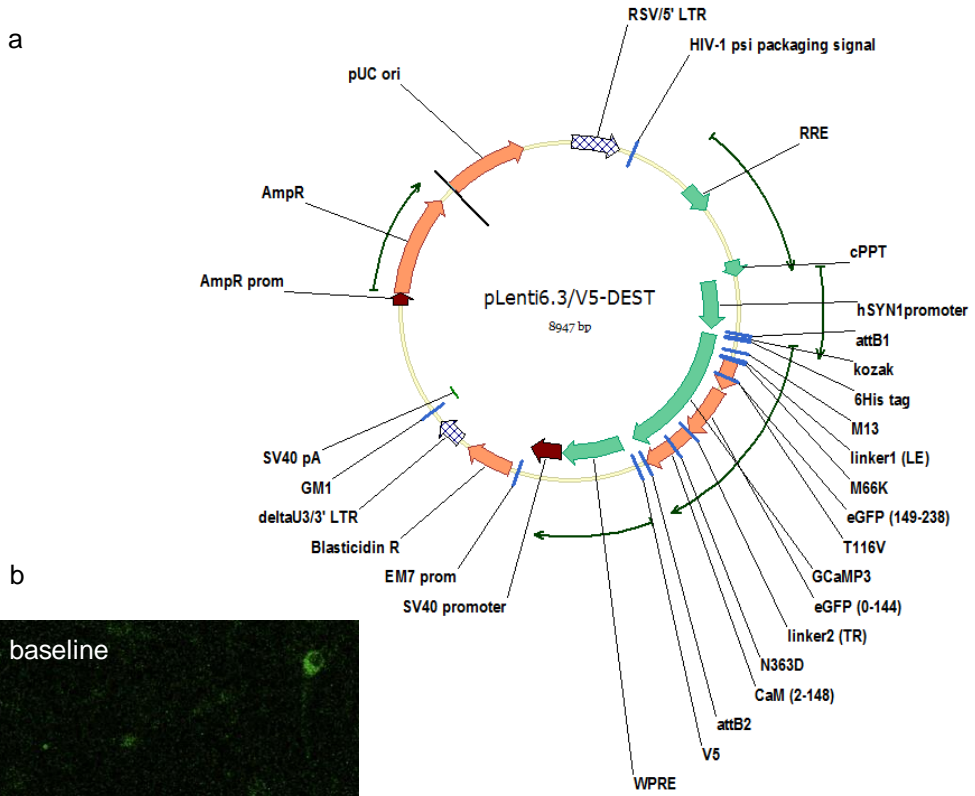
a

b

baseline

50 µm

during calcium peak

c

Figure 5.1 GCaMP3 expression in primary rodent cultures. a) Vector NTI image of GCaMP3 construct. All genes are named in black text, with protein coding genes indicated by orange arrows and ribosomal RNA genes indicated by green arrows. GCamP3: plasmid # 22692 (Addgene). b) Primary cortical neurons (14DIV) showing GCaMP3 fluorescence at baseline levels (left) and during a calcium burst (right). c) Representative traces of live cell calcium imaging recordings in 14DIV old primary rodent cortical cultures, GCaMP3 intensity is shown over time (61 frames per minute). After 250 frames cells are exposed to glutamate (30 μM), resulting in a large calcium influx.

After determination of optimal conditions in primary rat neuronal cultures, hiPSC-derived neuronal cultures were tested. Lentiviral particles were added to the culture medium at 2, 3, 4, or 5 weeks after final plating because of the difference in length of neuronal differentiation between primary and hiPSC-derived neurons. Different volumes (20μl - 0.2μl added to 200μl culture medium on top of 20,000 cells per well) were analyzed. Independent of the day of transduction GCaMP3 fluorescence was visible after three or more days after transduction without clearly affecting cell culture morphology or health. In some wells clear activity of neurons was shown, sometimes even with a trend towards synchronous activity, but imaging a complete network was almost impossible due to the small window. Furthermore, cells started clumping together some time after viral transduction.

Since GCaMP6 has been shown to be much more sensitive than GCaMP3 [4], GCaMP6f has been tested in hiPSC-derived neurons as well. Different viral vectors have been tested, but only lentivirus seemed to be effective in hiPSC-derived neuronal cultures. Experiments with AAV6 did not show clear fluorescence of the marker and AAV-DS seemed to cause some toxicity. An additional time point of transduction was tested, that was one day before final plating (meaning in NPC stadium). Although clear and abundant fluorescence from the lentiviral GCaMP6 was visible at early time points after transduction in NPC stadium, and even some spontaneous activity was observed, by the time cultures reached more mature conditions insufficient fluorescence was visible.

5.1.2 Imaging presynaptic vesicle release with sypHtomato

Presynaptic vesicle release can be studied with the genetically encoded, synaptophysin-coupled, pH-sensitive red marker sypHtomato. In order to optimize the use of sypHtomato in hiPSC-derived cortical neurons, transduction conditions were tested in primary rat neuronal cultures again to avoid time-consuming hiPSC-derived cultures. Lentiviral particles were added to the culture medium at 2, 6, or 9DIV at different volumes (20μl - 0.2μl added to 200μl culture medium on top of 10,000 or 20,000 cells per well). SypHtomato fluorescence was visualized with a LSM510 microscope. Transduction of primary rat neuronal cultures was most efficient when done at 2DIV. Images showed a clear vesicular fluorescent signal in neurites, although the most intense spots were found close to the nucleus (Fig. 5.2). Functionality of the pH sensing capacity of sypHtomato was tested by acute addition of NH_4Cl to the culture

medium, which increased overall fluorescent intensity of the marker (Fig. 5.2b). However, no clear response was detected due to spontaneous activity in primary neurons that were actively firing (as confirmed by co-expression with GCaMP3, data not shown), neither after stimulation with KCl.
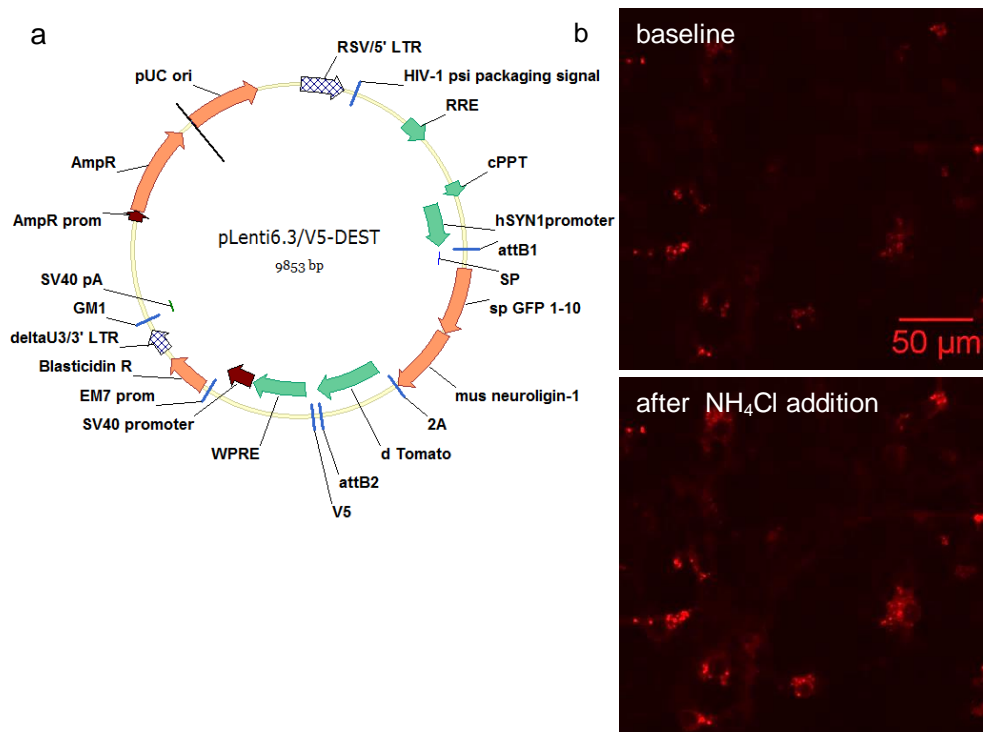
Figure 5.2 SypHtomato expression in primary hippocampal cultures. a) Vector NTI image of sypHtomato construct. All genes are named in black text, with protein coding genes indicated by orange arrows and ribosomal RNA genes indicated by green arrows. pHTomato: JQ966306 (GenBank) b) Primary hippocampal neurons (14DIV) expressing sypHtomato. Left image shows fluorescence at baseline, right image shows increased fluorescence after neutralization of the culture medium with NH_4Cl. High fluorescence in cell bodies might be due to organelles with a neutral pH, such as the endoplasmatic reticulum [9].

5.1.3 Imaging postsynaptic calcium dynamics with PSD95-GCaMP3

By coupling GCaMP3 to the postsynaptic density protein PSD95 it is possible to study calcium signaling more specifically in the postsynaptic element. Therefore, PSD95-GCaMP3 was developed and optimized in primary cultures. Lentiviral particles of both PSD95α-GCaMP3 and PSD95β-GCaMP3 were added to the culture medium at 2 or 6DIV at different volumes (20µl - 0.2µl added to 200µl culture medium on top of 10,000 or 20,000 cells per well). PSD95α-GCaMP3 was

clearly visible from 3 days after transduction and showed spontaneous activity (when transduced at 2DIV), in contrast to PSD95β-GCaMP3 which was not visible. PSD95α-GCaMP3 was very well visible in neurites as well, but not specific to synapse-like structures. However, baseline fluorescence was very low, making it more difficult to set the right focus when cells were inactive. As cultures grew older, cells transduced at 2DIV seemed to show some toxicity, in contrast to transduction at 5 or 6DIV.

5.1.4 Imaging bonafide synapses with mGRASP

The last genetically encoded indicator tested was mGRASP, which consists of two different constructs. That is the presynaptic mCerulean-coupled pre-mGRASP and the postsynaptic dTomato-coupled post-mGRASP. Upon reconstitution across synaptic partners a GFP signal should be visible. In order to verify the reconstitution of the two parts HEK cells were transduced with both pre-mGRASP and post-mGRASP (with CMV promo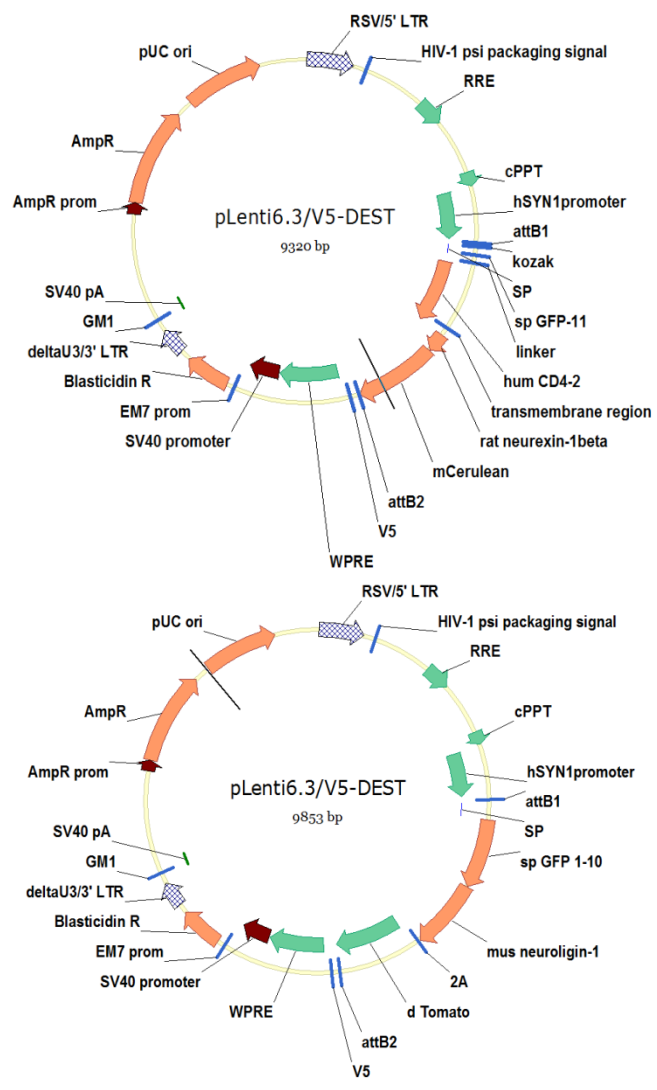ter), showing GFP fluorescence (Fig. 5.3). Briefly, human embryonic kidney (HEK293) cells were grown in Dulbecco's modified Eagle's medium supplemented with 10% heat-inactivated fetal bovine serum (FBS), 1% pyruvate (10 mM), 1% penicillin-streptomycin and L-glutamine (20 mM) (all Gibco). Cells were maintained in a humidified CO_2 incubator (37^0C; 5% CO_2). After one day *in vitro* (1DIV) DNA mixture containing pLenti CMV pre-mGRASP plasmid and pLenti CMV post-mGRASP plasmid was diluted in OptiMEM (Gibco) with FuGENE 6 Transfection Reagent (Roche Applied Science). The mixture was incubated for 10 minutes at room temperature and then added to the cells. After 24 h incubation, the growth medium was removed and replaced with fresh medium and cultures were visualized with a LSM510 microscope.

To optimize the use of mGRASP in hiPSC-derived cortical neurons, transduction conditions were tested in primary rat neuronal cultures again to avoid time-consuming hiPSC-derived cultures. Lentiviral particles of both pre-mGRASP and post-mGRASP were added to the neuronal culture medium at 2DIV at different volumes (100μl - 0.2μl added to 200μl culture medium on top of either 10,000 cells of 20,000 cells per well), but no expression of pre-mGRASP was detected and post-mGRASP fluorescence was observed in non-healthy cells and cell debris only.

5.2 Probing neural networks with electrophysiology

Another useful tool for studying network activity *in vitro* (or *ex vivo*) is a multi-electrode array (MEA). In this project a 60-6wellMEA chip and MW48 MEA plates were tested. 60-6wellMEAs (Multi Channel Systems) contain six wells with a surface comparable to MW96 wells. The diameter of the nine electrodes per well in these chips is 30 μm, the distance from centre to centre is 200 μm. Each well contains one additional electrode that is used as reference electrode. MEA wells

a

pLenti6.3/V5-DEST
9320 bp

RSV/5' LTR
HIV-1 psi packaging signal
RRE
cPPT
hSYN1promoter
attB1
kozak
SP
sp GFP-11
linker
hum CD4-2
transmembrane region
rat neurexin-1beta
mCerulean
attB2
V5
WPRE
SV40 promoter
EM7 prom
Blasticidin R
deltaU3/3' LTR
GM1
SV40 pA
AmpR prom
AmpR
pUC ori

pLenti6.3/V5-DEST
9853 bp

RSV/5' LTR
HIV-1 psi packaging signal
RRE
cPPT
hSYN1promoter
attB1
SP
sp GFP 1-10
mus neuroligin-1
2A
d Tomato
attB2
V5
WPRE
SV40 promoter
EM7 prom
Blasticidin R
deltaU3/3' LTR
GM1
SV40 pA
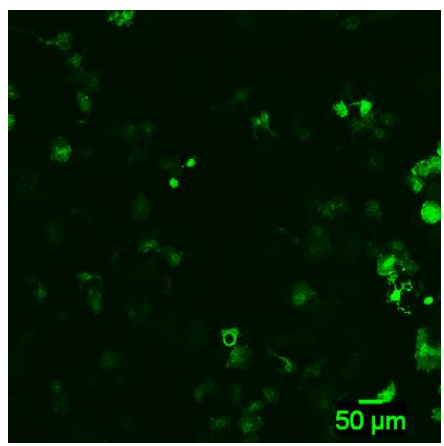AmpR prom
AmpR
pUC ori

b

50 µm

Figure 5.3 mGRASP reconstitution shown in HEK cells. a) Vector NTI images of both mGRASP constructs (top: pre-mGRASP, bottom: post-mGRASP). All genes are named in black text, with protein coding genes indicated by orange arrows and ribosomal RNA genes indicated by green arrows. Pre-mGRASP component fused with mCerulean: JN898961 (GenBank) and post-mGRASP component fused to 2A-dTomato: JN898960 (Genbank). b) HEK293 cells transduced with both pre-mGRASP and post-mGRASP show reconstituted GFP in the same cell two days after transduction (3DIV).

were coated with either 0.4mg/ml poly-D-lysine (PDL, Sigma, MW=30,000-70,000) in borate buffer overnight at 37^0C, or with 0.1% polyenimine (PEI, Sigma) in borate buffer for at least one hour (after which PEI solution was washed away and plates were air dried), followed by incubation with 10ug/ml laminin (Sigma) for 4 up to 24 hours. Primary cultures (75,000 – 100,000 cells/well) were grown in the wells in a humidified incubator (37^0C; 5% CO2). Recordings were made using MC_Rack software and Multi-Channel Systems hardware. MW48 MEA plates (Axion Biosystems) contain 48 wells with a surface comparable to normal MW48 plates. Each well contains sixteen electrodes. MEA wells were coated with 0.1% PEI (Sigma) in borate buffer for at least one hour after which PEI solution was washed away and plates were air dried, followed by incubation with 10ug/ml laminin (Sigma) for 2 hours. hiPSC-derived NPCs (40,000 per well) and primary human astrocytes (10,000 per well) were plated simultaneously in one cell suspension (comparable to cell densities used in MW96 plates). Recordings were made using the Maestro MEA system and AxIS software (Axion Biosystems).

For primary hippocampal neurons different coatings were tested (PEI, PDL, and PDL + laminin) from which the combination of PDL with laminin was the most stable condition. However, the PEI coating was suitable too. For the 60-6wellMEA increasing synaptic activity was measurable with increasing cell densities from 50,000 cells per well to 100,000 cells per well (in comparison neuronal networks in MW96 consist of 20,000 cells per well on an equal surface). However, there was quite some variation between wells cultured in the same way, probably because the separate 60-6wellMEA chips undergo different levels of mechanical stress due to movement and are more prone to medium evaporation due to limited possibilities to cover the wells. Therefore, MW48 MEA plates were tested to decrease the amount of variation. For primary neuronal cultures the combination of PEI coating with a cell density of 50,000 – 75,000 cells per well (in comparison neuronal networks in MW96 consist of 40,000 cells per well on an equal surface) gave network bursts and some synchronized activity. Fine-tuning the conditions for culturing hiPSC-derived neurons in MEAs was more difficult, but PEI coating combined with laminin coating gave actively firing neurons. However, the general protocol for co-cultures had to be adapted, since low plating volumes impede plating procedures. To avoid desiccation of cells during culturing, a mixed cell suspension of astrocytes (20%) and NPCs (80%) was plated instead of plating a monolayer of astrocytes before NPCs were added (as described as optimal condition in Chapter 2).

5.3 Discussion

As discussed by Rose and colleagues [10] a good genetically encoded calcium indicator (GECI), or in general a good genetically encoded indicator, has to meet several criteria. For example, the probe should be bright enough to identify cells that express it, even at rest and standard methods for gene transfer should be sufficient for obtaining satisfactory expression levels. Furthermore, probes should be sensitive enough to faithfully report spontaneous events due to firing of single action potentials and binding kinetics should be sufficiently fast to accurately follow neuronal dynamics. Finally, indicators should not perturb cells that express the probe anywise [10].

In order to have an extensive toolbox to study various steps in the process of neuronal network functionality this chapter describes different tools, all with their own advantages and disadvantages. Live cell calcium imaging has proven to be a useful tool to study general network properties *in vitro* [11]. Although synthetic calcium dyes such as FLUO4, Rhod3 or CaSir have shown to be effective in rendering network properties, the more recently developed GECIs are promising tools with several advantages over the synthetic dyes. Since GECIs can be expressed chronically, the same cultures can be revisited and studied over time. Furthermore, GECIs can be targeted to specific cell populations or even subcellular locations. This also provides the opportunity to combine different genetically encoded indicators in one experiment. However, no optimal conditions for the use of GCaMP3 in hiPSC-derived neurons were found in this study, because the dynamic range of the probe seemed to be too small for imaging spontaneous activity in these cells. As described by Chen and colleagues [4] GCaMP6 is much more sensitive, which seemed to be the case in our hiPSC-derived neurons too, but in our hands it was not possible to keep expression levels high until the neurons were mature enough for the functional tests required. The higher sensitivity of hiPSC-derived neurons for viral transduction might be due to the prolonged exposure and cultivation time of these cells. When compared with rodent neurons human neurons have more tedious patterns of neurite outgrowth and synaptogenesis [12-14] which might make them prone for external factors during prolonged periods of time. Keeping the iPSC-derived cells healthy during the whole procedure of transduction, maturation and interrogation was one of the major challenges that caused the lack of successful implementation of genetically encoded indicators in this part of the project.

When looking to the application of calcium imaging that was used in the different chapters of this thesis a fair trade-off has been made between accuracy and throughput, and this was aligned with the labelling procedure. Although more cell cultures were needed, the choice to use synthetic dyes was made instead of optimizing the use of GECIs in hiPSC-derived neurons. Wells with neuronal cultures were used for single experiments with acute pharmacology combined

with chronic analysis of cultures. Although synthetic dyes were taken up by all cells in the neuronal cultures, the separation between neurons and astrocytes could be made based on the differential response of both cell types on a glutamate stimulus at the end of each recording, as previously described [15]. The selection of neurons based on that distinction was incorporated in the analysis script that was used (based on [16]). The last advantage of the use of synthetic dyes was that there was no chronic calcium buffering by GECIs during the long cultivation period of hiPSC-derived neurons (as discussed by Rose and colleagues [10]).

The next genetically encoded indicator we described in this chapter was sypHtomato. Expression of sypHtomato was shown in primary rodent neuronal cultures, and functionality of the pH-sensing capacities of the probe was shown. However, with the experimental options we have tried, sypHtomato seems to be not sensitive enough to visualize single synaptic events of spontaneous activity in primary rodent neuronal cultures, and to our knowledge literature only shows examples of use of the probe with induced responses (e.g. by electric field stimulation) [17-20]. Since we would like to study spontaneous network activity, we did not use this genetically encoded indicator in hiPSC-derived neuronal cultures in previous chapters.

As an alternative to the widely used immunocytochemistry for synaptic proteins, the mGRASP technique was tested in primary rodent neuronal cultures. Although several attempts have been done to express the two constructs in primary neuronal cultures, no successful experiment was reported here due to toxicity of the post-mGRASP probe and failure to express the presynaptic probe. While *in vivo* studies have proven the value of this tool [3,21,22], to our knowledge no *in vitro* mammalian studies on neuronal cultures using mGRASP have been described previously.

Another valuable approach, not based on microscopic imaging, is electrophysiology using multi-electrode arrays. Optimization of cell culture conditions to avoid detachment and variability in cell functionality was the most challenging part for this approach. Further optimization is necessary before this approach can be used successfully in hiPSC-derived cortical networks.

The combination of different tools can be used to gain insight in neuronal networks. For most tools described in this chapter more optimization is needed, before it can be successfully used in hiPSC-derived cultures. However, with the aim of studying spontaneous neuronal network activity in hiPSC-derived neurons we only used one functional and one morphological tool in this thesis, that is calcium imaging with FLUO4 (or other synthetic dyes) for functional examination of the network and immunocytochemistry for neuronal structure. Future interrogation of neuronal network activity could be done with other tools in order to confirm and scrutinize findings.

Acknowledgements

References

1   Tian, L. *et al.* Imaging neural activity in worms, flies and mice with improved GCaMP calcium indicators. *Nat. Methods* **6**, 875-881 (2009).
2   Li, Y. & Tsien, R. W. pHTomato, a red, genetically encoded indicator that enables multiplex interrogation of synaptic activity. *Nat. Neurosci.* **15**, 1047-1053 (2012).
3   Kim, J. *et al.* mGRASP enables mapping mammalian synaptic connectivity with light microscopy. *Nat. Methods* **9**, 96-102 (2012).
4   Chen, T.-W. *et al.* Ultrasensitive fluorescent proteins for imaging neuronal activity. *Nature* **499**, 295-300 (2013).
5   Kügler, S., Kilic, E. & Bähr, M. Human synapsin 1 gene promoter confers highly neuron-specific long-term transgene expression from an adenoviral vector in the adult rat brain depending on the transduced area. *Gene Ther.* **10**, 337-347 (2003).
6   Hioki, H. *et al.* Efficient gene transduction of neurons by lentivirus with enhanced neuron-specific promoters. *Gene Ther.* **14**, 872-882 (2007).
7   Chetkovich, D. M. *et al.* Postsynaptic targeting of alternative postsynaptic density-95 isoforms by distinct mechanisms. *The Journal of neuroscience* **22**, 6415-6425 (2002).
8   Wang, X.-s. & Gruenstein, E. I. Mechanism of synchronized Ca 2+ oscillations in cortical neurons. *Brain Res.* **767**, 239-249 (1997).
9   Wu, M. M. *et al.* Organelle pH studies using targeted avidin and fluorescein–biotin. *Chem. Biol.* **7**, 197-209 (2000).
10   Rose, T., Goltstein, P. M., Portugues, R. & Griesbeck, O. Putting a finishing touch on GECIs. *Front. Mol. Neurosci.* **7**, 88 (2014).
11   Verstraelen, P. *et al.* Pharmacological characterization of cultivated neuronal networks: relevance to synaptogenesis and synaptic connectivity. *Cell. Mol. Neurobiol.* **34**, 757-776 (2014).
12   DeFelipe, J. The evolution of the brain, the human nature of cortical circuits, and intellectual creativity. *Front. Neuroanat.* **5**, 29 (2011).
13   Petanjek, Z. *et al.* Extraordinary neoteny of synaptic spines in the human prefrontal cortex. *Proceedings of the National Academy of Sciences* **108**, 13281-13286 (2011).
14   Suzuki, I. K. & Vanderhaeghen, P. Is this a brain which I see before me? Modeling human neural development with pluripotent stem cells. *Development* **142**, 3138-3150 (2015).
15   Pickering, M., Pickering, B. W., Murphy, K. J. & O'Connor, J. J. Discrimination of cell types in mixed cortical culture using calcium imaging: a comparison to immunocytochemical labeling. *J. Neurosci. Methods* **173**, 27-33 (2008).
16   Cornelissen, F. *et al.* Quantitation of chronic and acute treatment effects on neuronal network activity using image and signal analysis toward a high-content assay. *J. Biomol. Screen.*, 1087057113486518 (2013).
17   Kim, S. H. & Ryan, T. A. Synaptic vesicle recycling at CNS synapses without AP-2. *The Journal of Neuroscience* **29**, 3865-3874 (2009).

CHAPTER 5

18   Jackson, R. E. & Burrone, J. Visualizing presynaptic calcium dynamics and vesicle fusion with a single genetically encoded reporter at individual synapses. *Front. Synaptic Neurosci.* **8** (2016).
19   Arranz, A. M. *et al.* LRRK2 functions in synaptic vesicle endocytosis through a kinase-dependent mechanism. *J. Cell Sci.* **128**, 541-552 (2015).
20   Granseth, B. & Lagnado, L. The role of endocytosis in regulating the strength of hippocampal synapses. *The Journal of physiology* **586**, 5969-5982 (2008).
21   Feng, L., Kwon, O., Lee, B., Oh, W. C. & Kim, J. Using mammalian GFP reconstitution across synaptic partners (mGRASP) to map synaptic connectivity in the mouse brain. *Nat. Protoc.* **9**, 2425-2437 (2014).
22   Druckmann, S. *et al.* Structured synaptic connectivity between hippocampal regions. *Neuron* **81**, 629-640 (2014).

6

Summary, general discussion and future perspectives

In 2015 there were an estimated 46.8 million people worldwide suffering from dementia and this number will probably almost double every 20 years. Much of this increase will be in developing countries in which life expectancies are increasing due to the tremendous progress made in medicine. Dementia is not only highly impacting patients and their relatives, but also worldwide economy because the total estimated cost of dementia was 818 billion US dollar in 2015 (http://www.alz.co.uk/research/statistics; accessed December 15, 2016). Although enormous amounts of money and time are spent in drug discovery and development for these devastating disorders, disease-modifying treatments are not yet available for many of them. Preclinical and clinical research have provided many different targets to tackle the diseases, but clinical trial failure rates remain high [1]. Therefore new therapeutic but also research strategies have to be established.

Dementias are characterized by cognitive decline, which is the decreased capability to perform complex tasks of the brain, including learning and memory. Since cognitive functions of the brain rely on synaptic transmission, it is not surprising that synapses are affected in cognitive disorders. A particular group of cognitive disorders is called neurodegenerative disorders because of the progressive decline in neuronal integrity, especially in the brain. Alzheimer's disease is one of these neurodegenerative disorders and is the most common form of dementia [2]. One of the common features of many neurodegenerative diseases is the progressive and region-specific accumulation of misfolded proteins [3]. In case of a specific group of neurodegenerative disorders called tauopathies, such as Alzheimer's disease or frontotemporal dementia, microtubule-binding protein tau aggregates and eventually forms insoluble intracellular deposits of tau called neurofibrillary tangles. Although the final manifestation of the pathology is the precipitation of insoluble NFTs preceding smaller aggregates of tau seem to be more toxic [4-6]. While clinical research and research on animal models have provided a lot of information about disease mechanisms, no cure for the disease is available and additional research is a necessity.

Although techniques such as fMRI allow non-invasive interrogation of the human brain and provided useful insights, these approaches are costly and time consuming. Furtheremore, it is not possible to easily manipulate the human brain in order to study disease mechanisms. The complexity of the human brain and the inaccessibility of live human neurons force researchers to investigate physiological and pathophysiological processes of the brain by the use of models. Animal models have been indispensable for the current knowledge about the human brain, but the use of these models has several drawbacks, such as the lower complexity of brain structure, neuronal cells and protein and gene expression patterns. Especially when studying complex neurological disorders such as neurodegenerative disorders it is difficult to mimic the characteristics of

the complete human disease in animal models. The translational gap between these models and human disease is still too big.

The recent development of human induced pluripotent stem cells (hiPSCs) [7] might provide means to narrow this gap. The possibility to use patient-derived cells enables researchers to adopt the complete genetic background instead of choosing a set of transgenes in animal models. Using specific cell culture conditions these pluripotent cells can be differentiated towards almost all cell types of the body. These patient-specific cells might be amenable for cell therapy, but also provide tools for patient-specific drug screening *in vitro*. Culturing these cells as an *in vitro* system is scalable and controllable. Although the technical development of functional neuronal models included the (partial) characterization of differentiated cells, there is a remaining need to confirm functionality and authenticity of the newly generated neurons for many of the differentiation protocols. A prerequisite for functional neurons is their ability to generate action potentials and transmit neurotransmitter-mediated signals via synapses. The underlying neuronal properties permitting neurotransmission are developmentally regulated and changing during network formation (reviewed in ref. [3]). Additionally, their ability to express pathophysiologically relevant phenotypes has to be explored further.

To bridge the gap between models used for drug development and human disease progression this project aimed at developing an optimized differentiation protocol of hiPSCs towards functional cortical neuronal networks and characterize the morphofunction (i.e. structural and functional differences) of these neuronal networks *in vitro*. After establishment of functional neuronal networks we explored the usefulness of the hiPSC-derived model to study neuronal network dysfunction in view of tauopathies. We studied the influence of tau mutations and aggregation on neuronal network function using two different approaches in order to explore possibilities for modeling tauopathies using hiPSCs. The first one relies on tau aggregation induced by overexpression of mutated tau in combination with stimulation of pathology with artificial misfolded tau fibrils. The second model is based on targeted mutations in the *MAPT* gene encoding tau protein. The development of pathology was followed over time using a toolbox for neuronal function.

6.1 Robust neuronal network function can be recapitulated in hiPSC-derived neuronal co-cultures

Development of the central nervous system is characterized by the phenomenon of spontaneous synchronized neuronal network activity [8]. This process is partially recapitulated in slice preparations [9,10], primary rodent neuronal cultures [11,12] and recently in hiPSC-derived cortical neurons [13]. However, high variability and difficulties to reproduce these results underline the need for a more robust

protocol and a better characterization of these networks. Therefore we optimized the protocol recently published by Shi and colleagues [14], by the addition of two steps in the differentiation protocol. First of all, neurons were co-cultured with human astrocytes in order to stimulate maturation of the network, as previously shown for co-cultures with rodent astrocytes [15,16]. Additionally we treated our co-cultures with Notch signaling inhibitor DAPT in order to inhibit ongoing progenitor proliferation and stimulate neuronal differentiation [17,18]. This way we produced robust, reproducible, and highly synchronizing hiPSC-derived cortical networks *in vitro*, even when starting from different hiPSC sources. Therefore there is no need to wait for the delayed emergence and development of astrocytes from NPCs, which causes slow though progressive maturation of the network [19]. Further characterization of the networks revealed passive membrane properties, such as the more negative resting membrane potential and decreasing excitability of neurons [20] during ongoing neuronal maturation, and the presence of spontaneous postsynaptic currents, which are strong indicators of neuronal maturation [3]. Additionally we showed that GABAergic and glutamatergic neurotransmission were both contributing to network activity, thereby recapitulating the developmental switch from excitatory to inhibitory neurotransmission for the GABAergic activity and showing progressively increasing frequencies of activity indicative for developmental synaptogenesis [21,22]. Next to the functional characterization with electrophysiology and calcium imaging, immunocytochemistry confirmed the GABAergic and glutamatergic composition of the cultures showing both GAD65 and vGLUT1 immunoreactivity and showed that cortical markers TBR1, CTIP2, and SATB2, indicative of both deep and upper layer cortical neurons, were present. Furthermore, neurons were identified through microtubule-associated protein MAP2 immunoreactivity.

Although immense progress was made in the field of hiPSC-derived models many challenges still have to be dealt with [3]. One of these challenges in the scope of neuronal network function is the establishment of functional synaptic plasticity. To our knowledge there have been no studies reporting functional synaptic plasticity, which is an important process in cognition. An additional concern about the current status of hiPSC-derived neuronal models is the maturity of the final neuronal cultures. Although the neurons in our model express markers such as MAP2 and show electrophysiological properties of mature networks, several research groups showed that this does not guarantee the same level of maturity of neurons as present in adult human brains (e.g. reviewed in ref. [3]). When the gene expression profile of neurons differentiated from human iPSCs was compared to that available through the Allen Brain Atlas, the expression profile was found to be most similar to human neurons around the age of the first trimester of pregnancy [23] as was confirmed by Mariani and colleagues who came to a similar conclusion [24]. Additionally, the progressive maturation of neurons *in vitro* as shown in this project was similarly shown by Odawara and colleagues, who further continued to much longer culture periods with even more mature network properties [25]. Since several characteristics of

maturing but not yet fully mature networks, such as the developmental switch from GABAergic neurotransmission and the continuously increasing firing frequency, were present in our neuronal networks, this seems to be the beginning of maturation rather than the final stage as in the adult brain.

However, the use of combined readouts for characterization of the networks and their possible application in high-content format allow for gauging cultured neuronal networks at different levels. This approach seems highly suitable for sensitive screening applications such as neurotoxicity screening, target identification and validation and disease modeling. The model might offer a valuable tool for preclinical research and to screen for compounds that restore proper network functionality or reduce the progression of neuronal pathologies that result in disturbed network activity and connectivity, but the level of network maturity always has to be taken into account. Increased bursting frequency and synchronized oscillations as seen in Parkinson's disease [26] and FTD [27,28] and more complex dysregulation of network function as reported in Alzheimer's disease [29,30] can be studied. But also neurodevelopmental diseases such as epilepsy [29,31,32] show increased neuronal network oscillations and in autism [33] and schizophrenia [34] neuronal network dysfunction was reported as well. Examples of applications of this approach for disease modeling were described in Chapters 3 and 4. The model allows for acute or chronic testing of compounds on neuronal functionality, potentially leading to safer and more efficacious medicine and replacement of studies conducted on animal derived cultures. However, future research will have to demonstrate if impaired functional networks in this fully human system can be reversed using compounds or gene editing technologies.

Additionally this model is an interesting approach to study the interaction between human astrocytes and neurons by culturing diseased astrocytes with healthy neurons or vice versa. Eventually even the triple combination with microglia might be developed to study neuroinflammatory diseases, but also physiological processes involved in synapse degradation, called synaptic pruning [35-37], and microglia-related processes in neurodegenerative disorders. The role of microglia in neurodegenerative disorders has received more attention in the last decade [38], especially when microglia-related proteins, such as TREM2 or CD33 [39,40], were identified as susceptibility loci for neurodegenerative disorders. The possible advantages and challenges of a triple co-culture system will be discussed more thoroughly later.

6.2 Induced tau aggregation does not cause detectable changes in overall neuronal network function

After characterization of the control cultures we continued to study its possible application for disease modeling. Neurodegenerative disorders often display

cognitive decline as one of the major symptoms. Neuronal network dysfunction is thought to be one of the underlying mechanisms of this decline. In a specific group of neurodegenerative disorders, called tauopathies, this neuronal network dysfunction might be caused by disruptions in the function and expression of microtubule binding protein tau. Tau normally acts as microtubule stabilizing protein, allowing cytoskeleton reorganization, neurite outgrowth, axonal transport, and maintenance of cellular viability. However, all disorders in this group, for example Alzheimer's disease, frontotemporal dementia, or progressive supranuclear palsy, show aggregation of tau protein, which hampers its physiological function.

Therefore, we used a previously described hiPSC-derived neuronal model recapitulating tau aggregation [41] as a starting point to test the application of hiPSC-derived neuronal cultures to model neurodegenerative disorders. The model is based on virally induced overexpression of human tau either with or without the P301L MAPT mutation, because 4R tau was not detected in control hiPSC-derived cortical neurons within 5 weeks after final plating [41-43] and the lack of exon 10 (expressed in 4R tau) might hamper the aggregation of tau when pro-aggregating point mutations in this exon are present. However, in this hiPSC-derived neuronal model overexpression of tau carrying the pro-aggregating P301L mutation on its own failed to induce spontaneous tau aggregation as previously shown in other hiPSC-derived tauopathy models [43-45]. Therefore tau aggregation was triggered using preformed tau fibrils consisting of the tau-microtubule binding repeat (K18) with P301L mutation, which has been shown to facilitate tau aggregation in *in vitro* tauopathy models [46,47]. As a comparison we also tested functional and morphological network changes caused by tau aggregation in a primary rodent neuronal model. Although tau was aggregating over time in both models, we could not detect changes in overall calcium oscillations in these cortical cultures. However, when separately analyzed, tau-overexpressing neurons showed an increased percentage active neurons, bursting frequency and/or synchronicity when compared to non-overexpressing (hiPSC-derived or primary rodent) neurons. This might involve similar mechanisms as in a previously described rTg(TauP301L)4510 mice in which hyperexcitability of the glutamatergic system was shown [48]. The fact that we did not detect overall changes in network function might be due to an insufficient transduction efficiency or the fact that endogenous tau is still functioning normally. Consistent with previous studies we found no significant influence on network function in tau fibril-containing neurons [49,50], strengthening the hypothesis that not neurofibrillary tangles but smaller tau aggregates cause synaptotoxicity [5,6].

Structural analysis of the neuronal network in hiPSC-derived cultures did not show any morphological network changes either, while primary rodent neuronal cultures did. In the latter we showed a decreased neurite surface and number of nuclei in WT tau overexpressing cultures. In their study Mandelkow and

colleagues showed similar results, possibly caused by inhibition of transport of organelles and vesicles by increased microtubule binding, thereby making neurites more sensitive to stress [51]. However, overexpression of P301L tau only did not induce an effect on neurite surface, which is probably due to its reduced affinity for microtubules, thereby dissociating from microtubules. It is important to consider that tau overexpression can lead to clogging of axons and dramatic reorganization of the neuronal cytoskeleton, rather than modeling human tau pathology. Finally, in primary neuronal cultures tau fibril addition increased the number of nuclei in all three transduction conditions, indicative of neuroinflammation and gliosis as previously shown in tauopathy mouse models [52,53].

Although overall network function was not affected during tau aggregation in our overexpression models, several tauopathy-related processes were recapitulated. In order to be a good disease model the cultures have to meet some requirements (as reviewed in ref. [54]). First of all appropriate cell differentiation has to be recapitulated, in a cell type relevant for the disease. And the differentiation protocol has to be robust and reproducible. Since differentiation protocols are very time-consuming it would be useful to be able to differentiate in several separate steps. This first requirement has been met with the characterization of the cortical neuronal cultures in Chapter 2. Additionally, progression of disease pathogenesis has to be recapitulated. This model clearly showed some tau aggregation-related processes, although the underlying mechanisms of the observed phenotypes remain to be elucidated. Due to relatively long cultivation periods and subsequently high costs hiPSC-derived neuronal cultures might be less suitable for primary screening purposes, but the model can serve as a more relevant biological system to confirm hits from primary tau aggregation inhibition screens in cell lines. Additionally, the model allows identification of new targets and mechanisms involved in human tau aggregation [41].

Furthermore, the slight differences between primary rodent and human iPSC-derived cultures shed new light on the interpretation of previously reported findings in rodent tauopathy models. While no morphological differences on network level were detected in hiPSC-derived cultures, primary rodent cultures did. First of all, this might reflect a difference in transduction efficiency of hiPSC-derived neurons, which has been proven to be more difficult [55]. However, the baseline levels of 3R and 4R tau isoforms differ substantially between rodent and hiPSC-derived neuronal cultures. 4R tau isoforms are expressed in the human adult brain, but not yet in hiPSC-derived cortical neurons at 5 weeks after final plating [41,42], while rodent primary cultures at 15DIV show 3R and 4R tau in a ratio equal to one or even above [56]. This may lead to an extraordinary overexpression of 4R tau in rodent cultures, which is the tau isoform that is more prone to aggregation [57]. Therefore, the altered 4R/3R ratio might lead to a more pronounced phenotype in the rodent cultures while in hiPSC-derived

cultures the overexpression of 4R hTau led to a 4R/3R ratio slightly higher than one [41], which is closer to physiological ratios in the human adult brain.

6.3 Development of a new hiPSC model to study tauopathies

In order to develop a more physiological hiPSC-derived model for tauopathies another approach was used. Instead of overexpression of transgenes, which caused some unwanted side effects on neuronal function, this second model was based on a targeted point-mutation introducing the P301S mutation in *MAPT*. However, exon 10 of the *MAPT* gene is spliced out in CTRL hiPSC-derived neuronal cultures at least until 100 DIV. Therefore mature 4R tau expression was accomplished by the additional zinc-finger technology induced 10+16 *MAPT* splicing variant mutation that was found in FTD patients [42]. This was necessary for the expression of the P301S mutation which is located in exon 10. However, it was not known if this new model recapitulates tauopathy-like mechanisms and thorough characterization had to be performed.

Starting from one CTRL hiPSC line, four different mutant hiPSC lines were generated, expressing one (splicing variant 10+16, either mono- or bi-allelic) or two mutations (bi-allelic 10 + 16, either mono- or bi-allelic P301S). Immunocytochemistry and microarray data showed a major impact of the alternative *MAPT* splicing on neuronal differentiation. These neurons showed a less proliferative, probably more differentiating, phenotype than CTRL cells, possibly because cells are directly forced towards a more mature tau phenotype (4R tau expression) rather than a gradual increase in 4R/3R ratio as in normally developing neurons. Furthermore, mutant hiPSC-derived neurons seem to represent a different lineage of cortical neurons than CTRL cells, for example because of downregulation of projection neuron markers TBR1 and SATB2 and glutamatergic genes. In contrast, GABAergic markers were upregulated as well as some markers linked to differentiation and survival of interneurons in the forebrain. Additionally, high DLX and DCX and decreased PAX6 levels were shown. This altered gene and protein expression pattern in mutant neurons points into the direction of hiPSC-derived medial ganglionic eminence-like progenitors and subsequently forebrain-type interneurons that were previously described by Nicholas and colleagues [58]. The decreased network activity that was shown with live calcium imaging might be caused by this altered balance between GABAergic and glutamatergic neurons in neuronal cultures expressing the splicing variant. Morphological correlates of functional changes were analyzed as well. Although functional data might imply the opposite, the synapse density was significantly increased by the splicing variant compared to controls. However, the synapses were not characterized and might reflect again the change in neuronal lineage induced by the more mature 4R tau. For example, cortical interneurons make local synapses while cortical pyramidal neurons project over longer distances [59].

Additional effects on neuronal networks induced by the P301S mutation were investigated using the double mutant hiPSC lines. Microarray analysis revealed significant alterations in the expression of genes encoding kinases and phosphatases, which is important since many residues of the tau protein are potential phosphorylation sites [60]. Imbalance between kinase and phosphatase activity might cause tau hyperphosphorylation and as a consequence tau protein can become insoluble and self-aggregating. However, we did not observe changes in tau phosphorylation using alphaLISA, possibly because of high baseline phosphorylation levels due to microtubule dynamics for example, because these neuronal cultures are still in a rather developmental stage.

Finally, we studied the tendency of mutant lines to produce tau aggregation, which is the major characteristic of tauopathies, by using the alphaLISA assay that was previously described by Verheyen and colleagues [41]. Similar to the other tauopathy model that was described before, no spontaneous tau aggregation was shown in this model within the time span of 10 weeks after final plating. Therefore tau aggregation was triggered again using artificial tau fibrils consisting of the tau-microtubule binding repeat (K18) with P301L mutation. This way the double mutant cell line expressing both mutations bi-allelically clearly showed a threefold increase in tau aggregation compared to the other conditions.

Therefore, we showed that this new hiPSC-derived model recapitulated several tauopathy-related characteristics such as tau aggregation, an imbalance between GABAergic and glutamatergic neurotransmission, and impaired neuronal network functionality. The major changes compared to CTRL hiPSC-derived cultures were induced by the tau splicing variant, which is of particular interest for pathologies showing alternative splicing due to mutations in the *MAPT* gene, such as the 10+16 splicing variant mutation found in patients with FTD [42,61]. As a result, the 4R/3R ratio of tau is disrupted in these patients causing severe pathology. The alterations in neuronal differentiation induced by the splicing variant might be of importance for disease modeling as well, since both GABAergic and glutamatergic neurons are affected in tauopathies such as AD [62,63] and inhibitory interneurons play essential roles in network organization crucial for learning and memory [64,65]. Other mutations in the *MAPT* gene have been shown to alter neuronal differentiation and development as well. In a recent study using similarly differentiated hiPSC-derived cortical neurons both N279K and P301L mutations in the *MAPT* gene induced earlier electrophysiological maturation and altered mitochondrial transport compared to control neurons [43]. However, in our model tau aggregation was not accomplished in the mutant hiPSC lines only expressing the splicing variant. The additional P301S mutation (bi-allelic) was necessary to detect tau aggregation at later time points after triggering the cells with artificial fibrils. Gene expression altered by the P301S mutation probably contributed to tau aggregation, since dysregulation of phosphorylation-related genes was clearly visible.

Phosphorylation is one of the most important posttranslational modifications involved in tau function and dysfunction [66-68]. All mutations can possibly contribute to disease development but additional research is necessary to clarify its mechanisms.

6.4 Optimization of a toolbox to study neuronal networks *in vitro*

In order to investigate neuronal network function and dysfunction more throughly, various methodologies have been developed over the years. The choice for a specific technique depends on several factors: the level of resolution needed, either temporally or spatially; the possibility to manipulate experimental conditions; the amount of network perturbation allowed; the extent to which neuronal networks are intact; its robustness; and importantly the cost, time and difficulty of using the method [3,69]. In order to study the complete phenomenon of neuronal network function *in vitro* a combination of different methods is often required. Each method can be used to answer specific scientific questions. In order to have an extensive complementary toolbox to study various steps in the process of neuronal network functionality the optimization of different tools, all with their own advantages and disadvantages, has been evaluated as described in Chapter 5. In this project we have specifically chosen to study spontaneous network activity only, rather than evoked. Due to cost, time and ongoing optimization of hiPSC-derived neuronal networks we initiated the optimization of tools using primary rat neuronal cultures.

Calcium is an essential second messenger in mammalian neurons, highly involved in neuronal network function. The transient but steep rise of calcium concentration in the presynaptic element can cause synaptic vesicle release into the synaptic cleft [70] leading to chemical neurotransmission. Thus, live cell calcium imaging shows a fundamental step in synaptic transmission. Using automated analysis of calcium oscillations in a number of neurons we were able to study network formation and functionality [71]. We optimized calcium indicators from two different classes: chemical indicators (FLUO4-AM, Rhod3, and CaSiR) and protein-based genetically encoded calcium indicators (GECIs; GCaMP3 and GCaMP6). FLUO4 is widely used in neuroscience (e.g. ref. [12]) because they are relatively easy to introduce in different cellular models and provide large signal-to-noise ratios [72], thereby fulfilling all the requirements for our experiments in both rodent and hiPSC-derived neurons. We only studied calcium oscillations but not calcium concentrations, therefore not requiring ratiometric calcium dyes [72]. Furthermore, the approach using FLUO4 enabled the easy pharmacological manipulation of cultures. The more recently developed GECIs have some advantages when compared to chemical indicators. Their continuous expression enables to follow the same cultures chronically and to target their expression to specific cell populations or compartments. However, due to the low dynamic

range of GCaMP3 in hiPSC-derived neuronal cultures compared to primary cultures and difficulties to chronically express GCaMP6 in hiPSC-derived neurons, we did not use this tool in later characterizations of human neuronal networks. Additionally we tried to optimize sypHtomato [73] to study spontaneous presynaptic vesicle release in combination with calcium dynamics [74] since these processes do not depend on each other in a 1:1 ratio [75]. This red fluorescent marker was clearly present in synaptic vesicles of primary rodent cultures, but was not sensitive enough to visualize spontaneous vesicle fusion at the presynaptic membrane.

Another investigated approach to probe neuronal functionality was electrophysiology. The patch clamp technique [76] allows the study of single neurons, either single or multiple ion channels or the entire cell. A more recently developed tool is the use of multi-electrode arrays [77]. At the multicellular level extracellular recordings of local field potential provide information about collective activity of the neuronal network for *in vitro* cultures or *ex vivo* slice preparations. This tool has a higher temporal resolution than the imaging based approaches. Therefore, MEA can give additional information to imaging based functional readouts.

Relying on these functional methods alone to identify neuronal network dysfunction would give an incomplete answer to questions concerning cellular identity for example. The structural correlates of functional changes can provide complementary information, when analyzed with the right image analysis paradigms (reviewed in ref. [78]). GABAergic and glutamatergic markers have been optimized to confirm functional findings and synaptic markers such as GluA and synaptophysin were used to support the characterization of neuronal networks in this project. Immunocytochemistry can provide useful insights in network structure and synaptic connections, but might be misleading sometimes [3]. For example, postsynaptic markers have been shown without corresponding markers for the presynaptic element [79] and the other way around [80]. The localization of proteins alone might thus be insufficient to confirm pathologically related alterations, emphasizing the necessity for a combination of different tools. Therefore, use of another genetically encoded indicator to visualize synapses, called mGRASP, was investigated. This technique, based on GFP reconstitution across synaptic partners, only identifies bonafide synapses [81]. While this tool has been used *in vivo* [81-83], to our knowledge no *in vitro* mammalian studies on neuronal cultures using mGRASP have been described previously. In our hands the *in vitro* approach was not succesfull as we did neither manage to achieve appropriate expression of the two constructs in neurons nor reconstitution.

In previous chapters of this project we used FLUO4 for calcium imaging, the patch clamp technique for studying synaptic activity and immunocytochemistry for structural characterization of neuronal networks. Additional approaches such

as microarray analysis and alphaLISA were used for further characterization of disease-related phenotypes in order to acquire as much information as possible about the models. Additional functional and morphological tests may unravel disease mechanisms in the future.

6.5 Future perspectives

6.5.1 Recapitulation of neurodegeneration "in a dish"

Recapitulation of human neurodegenerative disorders using induced pluripotent stem cell-derived differentiation "in a dish" is still an enormous scientific challenge. Although research showed to be able to model neuronal circuits *in vitro* by confirmation of neuronal marker expression, recapitulation of electrophysiological functionality, neuronal maturation and tau developmental splicing, and stimulation of maturation by human astrocytes, we cannot conclude that these neuronal networks realistically represent neuronal connectivity and maturity present in the central nervous system. Since the technique of disease modeling using hiPSCs is not yet older than a decade it is not surprising that there still is the need to refine techniques to recapitulate (patho)physiology.

Of course the classical drawbacks of *in vitro* modeling such as the lack of native network structure, (brain) regions, feedback loops and connections between them apply for this approach. Additional differences with human (patho)physiology always have to be taken into account when using hiPSC-derived models such as the models described in this thesis. One of the major concerns of using hiPSC-derived systems for modeling neurodegenerative disorders is the maturity and age of the differentiated cells. Many neurodegenerative disorders manifest later in life and are inevitably associated with aging-related processes. Work by several research groups suggests that reprogramming somatic cells to iPS cells "resets" phenotypes associated with cellular aging, such as mitochondrial function and telomere length [84-86]. Additionally, differentiated neurons showing several properties of mature networks were shown to still represent gene expression profiles similar to human gestational age of eight to ten weeks [23,24]. Although transplantation studies of human NPCs into rodent brains have shown that human neural cells mature of a human, rather than rodent, timeline [87], simply allowing differentiating cells to age *in vitro* is very impractical and expensive. Therefore, several groups have explored options to accelerate hiPSC aging, for example by using hiPSCs expressing progerin which triggers fast aging in Hutchinson-Gilford Progeria syndrome (HGPS) [88,89], or hiPSCs from patients with Werner syndrome, an accelerated aging syndrome [90]. Although these approaches seem to provide useful tools to induce aging phenotypes, additional understanding of underlying mechanisms in these and neurodegenerative disorders is required. Therefore, it

remains challenging to researchers to provide neuronal models mature enough to be representative of adult neurons, but being abundant enough and practical to use for screening assays.

Another important aspect of *in vitro* disease modeling is the extent of simplification of cellular models. While pure neuronal cultures can form synapses and display connectivity, they might not reach the maturity of neurons in heterogeneous cultures containing co-cultured astrocytes for example [15,16]. These co-cultured astrocytes have proven to provide support to CTRL hiPSC-derived neurons, both via released growth factors and physical contact [31]. However, in differentiating hiPSC-derived neuronal cultures astrocytes will appear spontaneously about a hundred days after NPC plating in differentiation media [14,91], but faster differentiation with higher purity of astrocytes has been described as well [19,92]. Additionally, microglia have shown to be important for normal neuronal network development, since these cells are highly involved in synaptic pruning and clearance of apoptotic cells for example [35,37]. Recently, efficient derivation of microglia-like cells from hiPSCs has been reported as well [93], although it is unknown if these microglia represent with the same characteristics as microglia *in vivo*. The addition of astrocytes and microglia to hiPSC-derived neuronal cultures might not only contribute to neuronal network development, but might be relevant for disease modeling as well. Although it is not yet known if their role is causative or just represents a secondary effect and if their role is pro-inflammatory or neuroprotective, astrocytes and microglia are proposed to have important impact on disease progression in neurodegenerative disorders [48,94-96]. For example, in tauopathy-related mouse models synapse loss and microglia activation were reported as early markers of disease progression [53,97,98]. Assays on hiPSC-derived tauopathy models in this project were performed in the human astrocyte co-culture system that was optimized in Chapter 2. Astrocytes are known to be involved in the homeostasis of neuronal tissue. In case of tau aggregation, astrocytes could be involved in degradation of misfolded proteins, thereby preventing tauopathy-induced morphological or functional network alterations in our cultures. Interestingly, other research groups found detrimental neuro-inflammatory effects of astrocytes in neurodegenerative disorders. In our model, the co-cultures with human astrocytes would then mean an exaggeration of tau-induced pathology, while we did not observe explicit morphological or functional phenotypes due to tau aggregation. However, Notch signaling is essential for the proper formation of astrocytes and Notch-signalling inhibitor DAPT (used for proper neuronal network development, Chapter 2) has been shown to decrease astrocyte proliferation and production of pro-inflammatory factor IL-1B in response to stress [99]. Therefore, DAPT might hamper the physiological astrocyte proliferation and astrocyte-induced inflammation induced by pathology, thereby masking detrimental effects that are present *in vivo*. The future comparison of hiPSC-derived neuronal cultures with and without astrocytes, and even with and without diseased astrocytes, might unravel their involvement in neuronal

network morphofunction in tauopathies. The increased awareness of the role of inflammation in neurodegenerative disorders and the recent development of hiPSC-derived astrocytes and microglia promote and also demand the development of a triple co-culture system. This again initiates the debate about complexity of cellular models versus the simplification of systems to be amenable for applications such as drug screening. However, it will definitely be very informative to fully characterize heterogeneous hiPSC-derived models in order to understand human physiology and pathology.

An even more complex, but probably still more relevant, model system of human CNS is a three-dimensional cell culture system. Although the analysis of pure cell populations can give valuable information on characteristics of that specific cell type, it is often the interaction between different cell types that is important for modeling complete systems such as a neuronal network. The additional dimension compared to monolayer cultures provides a way for cells to compartmentalize in order to function properly. For example, astrocytes look and behave differently in the brain than in a monlayer culture [100,101]. Another concern which is specifically relevant in case of proteinopathies like tauopathies is that phenotypes of aberrant extracellular protein aggregation are lost in two-dimensional cultures because of the lack of compartmentalization and lack of interstitial fluid, thereby also losing local presence of metabolites [94]. Therefore, recent studies focused on the development of three-dimensional culture systems, for example using Matrigel of hydrogel as scaffolds for hiPSC-derived cells [102,103]. These 3D cultures were used to model Alzheimer's disease-like phenomena, such as extracellular amyloid plaques [104,105] and cytoskeletal abnormalities [106]. Unfortunaltely we were not able to further explore the use of triple or 3D culture systems in this project, since this was out of the scope of the project.

A last concern about the translation from hiPSC-derived models to human disease is the choice for the genetic background of hiPSC lines. In this project we have chosen to use the combination of CTRL hiPSCs with induced mutations, either via overexpression or via targeted mutations, as a first step in the development and validation of hiPSC-derived models. In order to get a more realistic representation of human disease, the use of a broad range of patient-derived hiPSC lines should be investigated, with a subsequent broad range in outcomes. However, the phenotypes displayed by cells bearing physiological mutations, such as in patient-derived hiPSC lines, may often be less robust than those obtained via the experimental overexpression of mutant proteins [94]. For example, Mertens and colleagues compared the effect of compound treatment on neuronal cells from familial AD (fAD) patients to either non-neuronal cell lines overexpressing fAD *APP*, or human control embryonic stem cell derived neural cells overexpressing mutant *APP*. They found that concentrations of the compounds that were effective in the non-neuronal cell lines were modestly effective in the APP-overexpressing human cells, but not in the cells derived from fAD patients [107]. Therefore, the use of isogenic lines with corrected disease

alleles (Fig. 6.1d) may allow detection of even modest phenotypes induced by that specific mutation [94] and is therefore a suitable approach to avoid variation in outcomes induced by other factors.

6.5.2 hiPSC-derived models can be used to bridge the gap with animal models

Statistics have clearly shown the high demand for new approaches to better translate observations from rodent models into clinical studies. While animal models have provided useful insights in human disease mechanisms and have served as screening tool for drug development, differences between rodent and human brains are inevitably clear. Starting from the observation that cognitive functions are less complex in animals than in humans, we cannot expect the same level of complexity in the brains of humans and animals. The human cerebral cortex has an increased size and shows a greater diversity in cellular subtypes and greater complexity in its organization compared to animal brains [108-113]. Specifically relevant when modeling tauopathies is the differential expression of tau isoforms in adult brains from rodents compared to humans. While human brains express all six isoforms of tau, adult mouse brains almost exclusively express the three isoforms of 4R tau [114,115]. Thus hiPSC-derived neurons, which clearly recapitulate developmental tau splicing [42] and various aspects of cortical development [14,87,91] more closely resemble human brain complexity and development and might bridge the gap between animal models and clinical outcomes, especially when studying cognition-related phenomena. The clear differences between both model systems might explain the discrepancies between rodent primary and hiPSC-derived neuronal cultures we found in Chapters 3 and 5. Additionally, the development of mature neurons *in vitro* from rodent tissue is much faster than differentiation from hiPSCs. Therefore, rodent primary cultures might be more suitable for initial compound screens. However, the "species-specific clock" probably causing this difference in the timeline of neuronal maturation for different species [116] is another important factor that bridges the gap between the model and human disease. In addition hiPSCs provide one of the few possibilities to study human neuronal development *in vitro*.

Next to the human background of hiPSC-derived models other factors promote the use of these models for studying neurodegenerative disorders. With the development of new gene editing approaches hiPSCs in pluripotent state are easier to manipulate than animal models in which mutant strains have to be generated by labor-intensive breeding programs. Furthermore, starting from a single hiPSC line different cell types can be easily generated, providing the possibility to study the interaction between healthy and diseased cells without adverse graft-versus-host reactions. Although differentiation protocols are more time-consuming than for primary rodent cultures, the infinite proliferation capacity of hiPSCs requires less work to obtain the material to begin with.

Because of the availability of hiPSCs and its relevance for studying neuronal networks *in vitro* it might be possible to replace part of the experiments currently performed on rodent primary cultures by hiPSC-derived cultures in order to reduce the use of laboratory animals. Additionally, hiPSC-derived models can be used to confirm findings previously reported in animal models, or the other way around hiPSCs can underscore differences between animal models and human (patho)physiology in order to reduce the gap with clinical research.

6.5.3 hiPSC-derived neuronal models can serve as a base for development of screening assays

Although the hiPSC-derived models described in the previous chapters are not a perfect representation of human (patho)physiology, these models can possibly serve as a base for development of screening assays that can be used to investigate pathology and to find new therapeutic targets to treat these pathologies (Fig. 6.1) [117].

The development of a robust reproducible differentiation protocol is a crucial starting point. As shown in Chapter 2 two different hiPSC lines were differentiated into cortical neuronal cultures with limited variation. This differentiation protocol has been successfully applied for modeling tauopathy-related phenotypes in Chapters 3 and 4. The automation of data analysis paradigms and the combination of different tools used in these chapters further allowed standardization of analyses and can possibly be used for development of high-throughput (HTS) and high-content screening (HCS) approaches. Using hiPSCs, HTS and HCS could allow for standardized analysis of many compounds and disease hallmarks, as well as various cellular contexts affecting drug efficiency or neurotoxicity. This can be done either in a cohort of patients and controls or by specifically choosing for one patient-derived or engineered hiPSC line clearly showing a certain phenotype. The hiPSC approach can then be used as a prescreening method before time-consuming preclinical animal studies and can hopefully reduce the number of failing clinical trials. After HTS, HCS could be used to further analyze relevant signaling pathways and disease mechanisms.
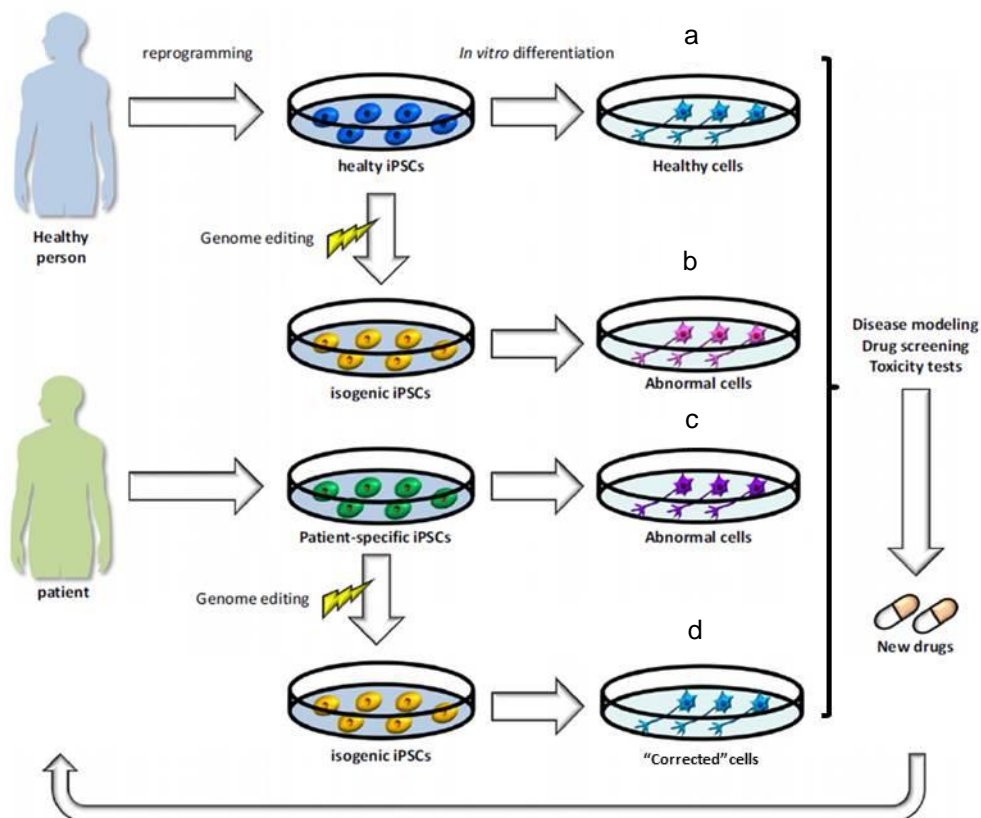
Figure 6.1 Schematic representation of the application of hiPSC technology in disease research. hiPSCs are established by introducing reprogramming factors into healthy human (a, b) and patient-derived (c, d) somatic cells. hiPSCs are induced to differentiate into target cells. The differentiated target cells can then be used for the analysis of disease pathology, drug screening and toxicity and efficacy testing of compounds. (b) Via genome editing technologies mutations can be induced in healthy hiPSCs to produce a disease model or make isogenic hiPSC lines to precisely analyze pathogenetic mechanisms that are attributable to the effects of the induced mutation. d) The other way around, via genome editing technologies mutations in patient-derived hiPSCs can be corrected to precisely analyze the pathogenetic mechanisms that are attributable to the effects of that specific mutation in the complete genetic background of the patient. Adapted from Imaizumi and Okano, 2014 [117].

Various examples of hiPSC-derived tauopathy-related models have been described in literature. In 2012 Israel and colleagues studied hiPSC-derived neurons from fAD and sAD patients, in which increased phospho-tau and activation of tau kinase GSK3β were shown. After manipulation of these cells with compounds they could significantly reduce this phenotype [118]. In another study using patient-derived hiPSCs carrying a heterozygous *MAPT* mutation several tauopathy-related phenotypes were identified. These phenotypes were absent in an isogenic control with the corrected mutation and were significantly exaggerated in isogenic controls with the homozygous mutation [44]. Additionally,

Verheyen and colleagues described the possible reduction of tau aggregation levels in their hiPSC-derived tauopathy model [41]. However, none of these studies reported changes in neuronal network functionality which is one of the first deficits reported in the disease progression of several tauopathies before the formation of tangles. But these models all represent valuable approaches to test the efficacy of tau-directed treatments. Various steps in the tau pathology cascade can be targeted (reviewed in ref.[119]). Although the causal role for tau phosphorylation in tau pathology is still a matter of debate, its strong correlation with tau pathology implicated it as target for intervention. Therefore, tau kinase inhibitors are one of the potential therapeutics. Based on the observation that tau detaches from microtubules resulting in loss of its physiological function, microtubule stabilizing agents have been proposed as possible intervention. The next step in the tauopathy cascade is the aggregation of tau, which might be inhibited by therapeutical interference as well. Another proposed approach is the reduction of tau levels, either by decreasing its gene expression, or by captivation of extracellular tau or by passive or active immunotherapy to increase tau clearance [119]. All these interventions can be experimentally tested on hiPSC-derived tauopathy models, thereby providing useful insights in possible mechanisms of action and therapeutical efficacy.

Studying the complete progression of tauopathies, but also other disorders, *in vitro* is impossible because many factors including other tissues and external influences play an important role in complex disorders. Therefore, modeling diseases requires the choice for a certain approach depending on the specific research question. Ideally, a large cohort of patient-derived material would be necessary to study the many different aspects of a disorder. For example for sporadic Alzheimer's disease currently no recurrent mutations are known, in contrast to fAD, although 60-80% of sAD might have genetic underpinnings [120]. The availability of patient-derived material from different sAD cases would enable identification of phenotypes in order to interrogate its etiology and it can also provide the option to develop personalized medicine. However, genetic variation within and between populations has major impact on the outcome of studies using this approach. Each hiPSC study is challenged by the question of to what extent observed variation between phenotypes is related to the disease being modeled or to other factors. To overcome this diversity and focus on the questions to be answered one can choose to use only a few phenotypes in a larger collection of patient-derived material or investigate robust phenotypes in a small cohort only. The previously mentioned option of generation of isogenic hiPSC lines provides another tool to address this variation, but that is only possible when the specific mutation is known. This approach enables to study causative mutations, but not other genetic variation such as SNPs because they may only be a risk factor in combination with their background (reviewed in ref. [94]). However, when studying the effect of therapeutic approaches on robust recurring phenotypes or end stages, such as tau aggregation for example, the (genetic) variation might be less important. Different tauopathies are associated

with different conformations of tau aggregates [121], but all tauopathies share the common factor of tau aggregation. The onset of neurodegenerative disorders can be influenced by the genetic background and may cause a long latency period *in vitro* [47] that may necessitate the use of exogenous reagents to induce tau aggregation for disease modeling. In the models described in Chapters 3 and 4 tau aggregation was clearly present, but only after being triggered by artificial fibrils. Of course this has clear consequences for the conclusions to be drawn from these models.

The models represented in this project are highly relevant to study aspects of neuronal networks in physiology and in the scope of certain aspects of tauopathies and other cognitive disorders. However, the research questions to be answered should guide researchers in choices to be made concerning simplification or comprehensiveness of their model. Culture protocol duration, the choice for mono- or co-cultures, the size of cohorts of patient-derived material, the possibility to trigger pathology artificially and many other aspects should be taken into account.

To conclude, in this project we presented a robust and reproducible differentiation protocol from hiPSCs towards functional cortical networks *in vitro*, which were characterized thoroughly. This protocol was fundamental for the development of two models that was used to study tauopathy-related changes in neuronal networks. The combination of different tools to study these "neuronal networks in a dish" and the use of different hiPSC lines might eventually contribute to the knowledge about disease onset and progression and treatment options for tauopathies, but also other cognitive disorders. However, the combination of different approaches seems inevitable but this might enable the replacement of certain experiments performed using animal models and might bridge the gap with clinical research.

References

1   Godyń, J., Jończyk, J., Panek, D. & Malawska, B. Therapeutic strategies for Alzheimer's disease in clinical trials. *Pharmacol. Rep.* **68**, 127-138 (2016).
2   Holtzman, D. M., Morris, J. C. & Goate, A. M. Alzheimer's disease: the challenge of the second century. *Sci. Transl. Med.* **3**, 77sr71-77sr71 (2011).
3   Chinchalongporn, V. *et al.* Connectivity and circuitry in a dish versus in a brain. *Alzheimers Res. Ther.* **7**, 44 (2015).
4   Crespo-Biel, N., Theunis, C. & Van Leuven, F. Protein tau: prime cause of synaptic and neuronal degeneration in Alzheimer's disease. *International Journal of Alzheimer's Disease* **2012** (2012).
5   Oddo, S. *et al.* Reduction of soluble Aβ and tau, but not soluble Aβ alone, ameliorates cognitive decline in transgenic mice with plaques and tangles. *J. Biol. Chem.* **281**, 39413-39423 (2006).
6   Santacruz, K. *et al.* Tau suppression in a neurodegenerative mouse model improves memory function. *Science* **309**, 476-481 (2005).
7   Takahashi, K. *et al.* Induction of pluripotent stem cells from adult human fibroblasts by defined factors. *Cell* **131**, 861-872 (2007).
8   Katz, L. C. & Shatz, C. J. Synaptic activity and the construction of cortical circuits. *Science* **274**, 1133-1138 (1996).
9   Miles, R., Traub, R. D. & Wong, R. Spread of synchronous firing in longitudinal slices from the CA3 region of the hippocampus. *J. Neurophysiol.* **60**, 1481-1496 (1988).
10   Silva, L. R., Amitai, Y. & Connors, B. W. Intrinsic oscillations of neocortex generated by layer 5 pyramidal neurons. *Science* **251**, 432 (1991).
11   Cohen, E., Ivenshitz, M., Amor-Baroukh, V., Greenberger, V. & Segal, M. Determinants of spontaneous activity in networks of cultured hippocampus. *Brain Res.* **1235**, 21-30 (2008).
12   Verstraelen, P. *et al.* Pharmacological characterization of cultivated neuronal networks: relevance to synaptogenesis and synaptic connectivity. *Cell. Mol. Neurobiol.* **34**, 757-776 (2014).
13   Kirwan, P. *et al.* Development and function of human cerebral cortex neural networks from pluripotent stem cells in vitro. *Development* **142**, 3178-3187 (2015).
14   Shi, Y., Kirwan, P. & Livesey, F. J. Directed differentiation of human pluripotent stem cells to cerebral cortex neurons and neural networks. *Nat. Protoc.* **7**, 1836-1846 (2012).
15   Odawara, A., Saitoh, Y., Alhebshi, A., Gotoh, M. & Suzuki, I. Long-term electrophysiological activity and pharmacological response of a human induced pluripotent stem cell-derived neuron and astrocyte co-culture. *Biochem. Biophys. Res. Commun.* **443**, 1176-1181 (2014).
16   Tang, X. *et al.* Astroglial cells regulate the developmental timeline of human neurons differentiated from induced pluripotent stem cells. *Stem Cell Res.* **11**, 743-757 (2013).
17   Borghese, L. *et al.* Inhibition of notch signaling in human embryonic stem cell–derived neural stem cells delays G1/S phase transition and accelerates neuronal differentiation in vitro and in vivo. *Stem Cells* **28**, 955-964 (2010).
18   Ogura, A., Morizane, A., Nakajima, Y., Miyamoto, S. & Takahashi, J. γ-secretase inhibitors prevent overgrowth of transplanted neural progenitors derived from human-induced pluripotent stem cells. *Stem Cells Dev.* **22**, 374-382 (2012).
19   Krencik, R., Weick, J. P., Liu, Y., Zhang, Z.-J. & Zhang, S.-C. Specification of transplantable astroglial subtypes from human pluripotent stem cells. *Nat. Biotechnol.* **29**, 528-534 (2011).
20   Spigelman, I., Zhang, L. & Carlen, P. L. Patch-clamp study of postnatal development of CA1 neurons in rat hippocampal slices: membrane excitability and K+ currents. *J. Neurophysiol.* **68**, 55-69 (1992).

21   Ben-Ari, Y., Gaiarsa, J.-L., Tyzio, R. & Khazipov, R. GABA: a pioneer transmitter that excites immature neurons and generates primitive oscillations. *Physiol. Rev.* **87**, 1215-1284 (2007).

22   Kavalali, E. T. *et al.* Spontaneous neurotransmission: an independent pathway for neuronal signaling? *Physiology* **26**, 45-53 (2011).

23   Brennand, K. *et al.* Phenotypic differences in hiPSC NPCs derived from patients with schizophrenia. *Mol. Psychiatry* **20**, 361-368 (2015).

24   Mariani, J. *et al.* Modeling human cortical development in vitro using induced pluripotent stem cells. *Proceedings of the National Academy of Sciences* **109**, 12770-12775 (2012).

25   Odawara, A., Katoh, H., Matsuda, N. & Suzuki, I. Physiological maturation and drug responses of human induced pluripotent stem cell-derived cortical neuronal networks in long-term culture. *Sci. Rep.* **6** (2016).

26   Heimer, G., Rivlin, M., Israel, Z. & Bergman, H. in *Parkinson's Disease and Related Disorders*   17-20 (Springer, 2006).

27   Stancu, I.-C. *et al.* Templated misfolding of Tau by prion-like seeding along neuronal connections impairs neuronal network function and associated behavioral outcomes in Tau transgenic mice. *Acta Neuropathol.* **129**, 875-894 (2015).

28   Whitwell, J. *et al.* Altered functional connectivity in asymptomatic MAPT subjects A comparison to bvFTD. *Neurology* **77**, 866-874 (2011).

29   Noebels, J. A perfect storm: converging paths of epilepsy and Alzheimer's dementia intersect in the hippocampal formation. *Epilepsia* **52**, 39-46 (2011).

30   Sorg, C., Riedl, V., Perneczky, R., Kurz, A. & Wohlschlager, A. M. Impact of Alzheimer's disease on the functional connectivity of spontaneous brain activity. *Curr. Alzheimer Res.* **6**, 541-553 (2009).

31   Holtkamp, M. *et al.* Status epilepticus induces increasing neuronal excitability and hypersynchrony as revealed by optical imaging. *Neurobiol. Dis.* **43**, 220-227 (2011).

32   Morelli, G. *et al.* Cerebral Cortical Circuitry Formation Requires Functional Glycine Receptors. *Cereb. Cortex*, bhw025 (2016).

33   Schipul, S. E., Keller, T. A. & Just, M. A. Inter-regional brain communication and its disturbance in autism. *Front. Syst. Neurosci.* **5**, 10 (2011).

34   Uhlhaas, P. J. & Singer, W. Abnormal neural oscillations and synchrony in schizophrenia. *Nat. Rev. Neurosci.* **11**, 100-113 (2010).

35   Kettenmann, H., Kirchhoff, F. & Verkhratsky, A. Microglia: new roles for the synaptic stripper. *Neuron* **77**, 10-18 (2013).

36   Stevens, B. *et al.* The classical complement cascade mediates CNS synapse elimination. *Cell* **131**, 1164-1178 (2007).

37   Paolicelli, R. C. *et al.* Synaptic pruning by microglia is necessary for normal brain development. *Science* **333**, 1456-1458 (2011).

38   Wes, P. D., Sayed, F. A., Bard, F. & Gan, L. Targeting microglia for the treatment of Alzheimer's Disease. *Glia* (2016).

39   Jonsson, T. *et al.* Variant of TREM2 associated with the risk of Alzheimer's disease. *N. Engl. J. Med.* **368**, 107-116 (2013).

40   Hollingworth, P. *et al.* Common variants at ABCA7, MS4A6A/MS4A4E, EPHA1, CD33 and CD2AP are associated with Alzheimer's disease. *Nat. Genet.* **43**, 429-435 (2011).

41   Verheyen, A. *et al.* Using Human iPSC-Derived Neurons to Model TAU Aggregation. *PLoS One* **10**, e0146127 (2015).

42   Sposito, T. *et al.* Developmental regulation of tau splicing is disrupted in stem cell-derived neurons from frontotemporal dementia patients with the 10+ 16 splice-site mutation in MAPT. *Hum. Mol. Genet.* **24**, 5260-5269 (2015).

43   Iovino, M. *et al.* Early maturation and distinct tau pathology in induced pluripotent stem cell-derived neurons from patients with MAPT mutations. *Brain* **138**, 3345-3359 (2015).

44   Fong, H. *et al.* Genetic correction of tauopathy phenotypes in neurons derived from human induced pluripotent stem cells. *Stem cell reports* **1**, 226-234 (2013).

CHAPTER 6

45 Mertens, J. *et al.* Embryonic Stem Cell–Based Modeling of Tau Pathology in Human Neurons. *The American journal of pathology* **182**, 1769-1779 (2013).

46 Calafate, S. *et al.* Synaptic contacts enhance cell-to-cell tau pathology propagation. *Cell reports* **11**, 1176-1183 (2015).

47 Guo, J. L. & Lee, V. M. Neurofibrillary tangle-like tau pathology induced by synthetic tau fibrils in primary neurons over-expressing mutant tau. *FEBS Lett.* **587**, 717-723 (2013).

48 Hunsberger, H. C., Rudy, C. C., Batten, S. R., Gerhardt, G. A. & Reed, M. N. P301L tau expression affects glutamate release and clearance in the hippocampal trisynaptic pathway. *J. Neurochem.* **132**, 169-182 (2015).

49 Rocher, A. *et al.* Structural and functional changes in tau mutant mice neurons are not linked to the presence of NFTs. *Exp. Neurol.* **223**, 385-393 (2010).

50 Kuchibhotla, K. V. *et al.* Neurofibrillary tangle-bearing neurons are functionally integrated in cortical circuits in vivo. *Proceedings of the National Academy of Sciences* **111**, 510-514 (2014).

51 Mandelkow, E.-M., Stamer, K., Vogel, R., Thies, E. & Mandelkow, E. Clogging of axons by tau, inhibition of axonal traffic and starvation of synapses. *Neurobiol. Aging* **24**, 1079-1085 (2003).

52 Wagner, J. *et al.* Reducing tau aggregates with anle138b delays disease progression in a mouse model of tauopathies. *Acta Neuropathol.* **130**, 619-631 (2015).

53 Yoshiyama, Y. *et al.* Synapse loss and microglial activation precede tangles in a P301S tauopathy mouse model. *Neuron* **53**, 337-351 (2007).

54 Payne, N. L. *et al.* Application of human induced pluripotent stem cells for modeling and treating neurodegenerative diseases. *New biotechnology* **32**, 212-228 (2015).

55 Meneghello, G. *et al.* Evaluation of established human iPSC-derived neurons to model neurodegenerative diseases. *Neuroscience* **301**, 204-212 (2015).

56 Rodríguez-Martín, T. *et al.* Reduced number of axonal mitochondria and tau hypophosphorylation in mouse P301L tau knockin neurons. *Neurobiol. Dis.* **85**, 1-10 (2016).

57 Gamblin, T. C. *et al.* In vitro polymerization of tau protein monitored by laser light scattering: method and application to the study of FTDP-17 mutants. *Biochemistry* **39**, 6136-6144 (2000).

58 Nicholas, C. R. *et al.* Functional maturation of hPSC-derived forebrain interneurons requires an extended timeline and mimics human neural development. *Cell stem cell* **12**, 573-586 (2013).

59 Markram, H. *et al.* Interneurons of the neocortical inhibitory system. *Nature Reviews Neuroscience* **5**, 793-807 (2004).

60 Hanger, D. P., Anderton, B. H. & Noble, W. Tau phosphorylation: the therapeutic challenge for neurodegenerative disease. *Trends Mol. Med.* **15**, 112-119 (2009).

61 Trabzuni, D. *et al.* MAPT expression and splicing is differentially regulated by brain region: relation to genotype and implication for tauopathies. *Hum. Mol. Genet.* **21**, 4094-4103 (2012).

62 Hazra, A. *et al.* Inhibitory neuron and hippocampal circuit dysfunction in an aged mouse model of Alzheimer's disease. *PLoS One* **8**, e64318 (2013).

63 Krantic, S. *et al.* Hippocampal GABAergic neurons are susceptible to amyloid-β toxicity in vitro and are decreased in number in the Alzheimer's disease TgCRND8 mouse model. *J. Alzheimers Dis.* **29**, 293-308 (2012).

64 Bartos, M., Vida, I. & Jonas, P. Synaptic mechanisms of synchronized gamma oscillations in inhibitory interneuron networks. *Nat. Rev. Neurosci.* **8**, 45-56 (2007).

65 Mann, E. O. & Paulsen, O. Role of GABAergic inhibition in hippocampal network oscillations. *Trends Neurosci.* **30**, 343-349 (2007).

66 Lee, G. *et al.* Phosphorylation of tau by fyn: implications for Alzheimer's disease. *The Journal of neuroscience* **24**, 2304-2312 (2004).

67 Martin, L. *et al.* Tau protein phosphatases in Alzheimer's disease: the leading role of PP2A. *Ageing research reviews* **12**, 39-49 (2013).

68   Martin, L. *et al.* Tau protein kinases: involvement in Alzheimer's disease. *Ageing research reviews* **12**, 289-309 (2013).

69   Rose, T., Goltstein, P. M., Portugues, R. & Griesbeck, O. Putting a finishing touch on GECIs. *Front. Mol. Neurosci.* **7**, 88 (2014).

70   Berridge, M. J., Lipp, P. & Bootman, M. D. The versatility and universality of calcium signalling. *Nature reviews Molecular cell biology* **1**, 11-21 (2000).

71   Cornelissen, F. *et al.* Quantitation of chronic and acute treatment effects on neuronal network activity using image and signal analysis toward a high-content assay. *J. Biomol. Screen.*, 1087057113486518 (2013).

72   Paredes, R. M., Etzler, J. C., Watts, L. T., Zheng, W. & Lechleiter, J. D. Chemical calcium indicators. *Methods* **46**, 143-151 (2008).

73   Li, Y. & Tsien, R. W. pHTomato, a red, genetically encoded indicator that enables multiplex interrogation of synaptic activity. *Nat. Neurosci.* **15**, 1047-1053 (2012).

74   Jackson, R. E. & Burrone, J. Visualizing presynaptic calcium dynamics and vesicle fusion with a single genetically encoded reporter at individual synapses. *Front. Synaptic Neurosci.* **8** (2016).

75   Dodge Jr, F. & Rahamimoff, R. Co-operative action of calcium ions in transmitter release at the neuromuscular junction. *The Journal of physiology* **193**, 419 (1967).

76   Abuse, A., Woodson, A. P. B., Traynor, M. E., Schlapfer, W. T. & Barondes, S. H. Single-channel currents recorded from membrane of denervated frog muscle fibres. *Nature* **260**, 799-802 (1976).

77   Taketani, M. & Baudry, M. Advances in network electrophysiology. *US: Springer* (2006).

78   Detrez, J. R. *et al.* Image Informatics Strategies for Deciphering Neuronal Network Connectivity. *Adv. Anat. Embryol. Cell Biol.* **219**, 123-148, doi:10.1007/978-3-319-28549-8_5 (2016).

79   Rao, A., Cha, E. M. & Craig, A. M. Mismatched appositions of presynaptic and postsynaptic components in isolated hippocampal neurons. *The Journal of Neuroscience* **20**, 8344-8353 (2000).

80   Kraszewski, K. *et al.* Synaptic vesicle dynamics in living cultured hippocampal neurons visualized with CY3-conjugated antibodies directed against the lumenal domain of synaptotagmin. *The Journal of neuroscience* **15**, 4328-4342 (1995).

81   Kim, J. *et al.* mGRASP enables mapping mammalian synaptic connectivity with light microscopy. *Nat. Methods* **9**, 96-102 (2012).

82   Feng, L., Kwon, O., Lee, B., Oh, W. C. & Kim, J. Using mammalian GFP reconstitution across synaptic partners (mGRASP) to map synaptic connectivity in the mouse brain. *Nat. Protoc.* **9**, 2425-2437 (2014).

83   Druckmann, S. *et al.* Structured synaptic connectivity between hippocampal regions. *Neuron* **81**, 629-640 (2014).

84   Mahmoudi, S. & Brunet, A. Aging and reprogramming: a two-way street. *Curr. Opin. Cell Biol.* **24**, 744-756 (2012).

85   Miller, J. & Studer, L. Aging in iPS cells. *Aging (Albany NY)* **6**, 246 (2014).

86   Yamanaka, S. A fresh look at iPS cells. *Cell* **137**, 13-17 (2009).

87   Espuny-Camacho, I. *et al.* Pyramidal neurons derived from human pluripotent stem cells integrate efficiently into mouse brain circuits in vivo. *Neuron* **77**, 440-456 (2013).

88   Blondel, S. *et al.* Induced pluripotent stem cells reveal functional differences between drugs currently investigated in patients with hutchinson-gilford progeria syndrome. *Stem Cells Transl Med* **3**, 510-519 (2014).

89   Liu, G.-H. *et al.* Recapitulation of premature ageing with iPSCs from Hutchinson-Gilford progeria syndrome. *Nature* **472**, 221-225 (2011).

90   Shimamoto, A., Yokote, K. & Tahara, H. Werner Syndrome-specific induced pluripotent stem cells: recovery of telomere function by reprogramming. *DNA helicases: expression, functions and clinical implications*, 6 (2015).

91   Shi, Y., Kirwan, P., Smith, J., Robinson, H. P. & Livesey, F. J. Human cerebral cortex development from pluripotent stem cells to functional excitatory synapses. *Nat. Neurosci.* **15**, 477-486 (2012).

CHAPTER 6

92   Chen, C. *et al.* Role of astroglia in Down's syndrome revealed by patient-derived human-induced pluripotent stem cells. *Nature communications* **5** (2014).

93   Muffat, J. *et al.* Efficient derivation of microglia-like cells from human pluripotent stem cells. Report No. 1078-8956, (Nature Research, 2016).

94   Mungenast, A. E., Siegert, S. & Tsai, L.-H. Modeling Alzheimer's disease with human induced pluripotent stem (iPS) cells. *Molecular and Cellular Neuroscience* **73**, 13-31 (2016).

95   Tyzack, G., Lakatos, A. & Patani, R. Human Stem Cell-Derived Astrocytes: Specification and Relevance for Neurological Disorders. *Current Stem Cell Reports*, 1-12 (2016).

96   Rudy, C. C., Hunsberger, H. C., Weitzner, D. S. & Reed, M. N. The role of the tripartite glutamatergic synapse in the pathophysiology of Alzheimer's disease. *Aging Dis.* **6**, 131-148 (2015).

97   Bellucci, A. *et al.* Induction of inflammatory mediators and microglial activation in mice transgenic for mutant human P301S tau protein. *The American journal of pathology* **165**, 1643-1652 (2004).

98   Hong, S. *et al.* Complement and microglia mediate early synapse loss in Alzheimer mouse models. *Science* **352**, 712-716 (2016).

99   Zhang, Y., He, K., Wang, F., Li, X. & Liu, D. Notch-1 signaling regulates astrocytic proliferation and activation after hypoxia exposure. *Neurosci. Lett.* **603**, 12-18 (2015).

100   Cahoy, J. D. *et al.* A transcriptome database for astrocytes, neurons, and oligodendrocytes: a new resource for understanding brain development and function. *The Journal of Neuroscience* **28**, 264-278 (2008).

101   Puschmann, T. B. *et al.* Bioactive 3D cell culture system minimizes cellular stress and maintains the in vivo-like morphological complexity of astroglial cells. *Glia* **61**, 432-440 (2013).

102   Paşca, A. M. *et al.* Functional cortical neurons and astrocytes from human pluripotent stem cells in 3D culture. *Nat. Methods* **12**, 671-678 (2015).

103   Smith, I. *et al.* Human neural stem cell-derived cultures in three-dimensional substrates form spontaneously functional neuronal networks. *J. Tissue Eng. Regen. Med.* (2015).

104   Choi, S. H. *et al.* A three-dimensional human neural cell culture model of Alzheimer/'s disease. *Nature* **515**, 274-278 (2014).

105   Kim, Y. H. *et al.* A 3D human neural cell culture system for modeling Alzheimer's disease. *Nat. Protoc.* **10**, 985-1006 (2015).

106   Zhang, D. *et al.* A 3D Alzheimer's disease culture model and the induction of P21-activated kinase mediated sensing in iPSC derived neurons. *Biomaterials* **35**, 1420-1428 (2014).

107   Mertens, J. *et al.* APP processing in human pluripotent stem cell-derived neurons is resistant to NSAID-based γ-secretase modulation. *Stem cell reports* **1**, 491-498 (2013).

108   Hill, R. S. & Walsh, C. A. Molecular insights into human brain evolution. *Nature* **437**, 64-67 (2005).

109   Rakic, P. Evolution of the neocortex: a perspective from developmental biology. *Nature Reviews Neuroscience* **10**, 724-735 (2009).

110   Finlay, B. L. & Darlington, R. B. Linked regularities in the development and evolution of mammalian brains. *Science* **268**, 1578 (1995).

111   Fame, R. M., MacDonald, J. L. & Macklis, J. D. Development, specification, and diversity of callosal projection neurons. *Trends Neurosci.* **34**, 41-50 (2011).

112   Douglas, R. J. & Martin, K. A. Neuronal circuits of the neocortex. *Annu. Rev. Neurosci.* **27**, 419-451 (2004).

113   López-Bendito, G. & Molnár, Z. Thalamocortical development: how are we going to get there? *Nature Reviews Neuroscience* **4**, 276-289 (2003).

114   Kosik, K. S., Orecchio, L. D., Bakalis, S. & Neve, R. L. Developmentally regulated expression of specific tau sequences. *Neuron* **2**, 1389-1397 (1989).

115   Takuma, H., Arawaka, S. & Mori, H. Isoforms changes of tau protein during development in various species. *Developmental brain research* **142**, 121-127 (2003).
116   Suzuki, I. K. & Vanderhaeghen, P. Is this a brain which I see before me? Modeling human neural development with pluripotent stem cells. *Development* **142**, 3138-3150 (2015).
117   Imaizumi, Y. & Okano, H. Modeling human neurological disorders with induced pluripotent stem cells. *J. Neurochem.* **129**, 388-399 (2014).
118   Israel, M. A. *et al.* Probing sporadic and familial Alzheimer/'s disease using induced pluripotent stem cells. *Nature* **482**, 216-220 (2012).
119   Medina, M. & Avila, J. New perspectives on the role of tau in Alzheimer's disease. Implications for therapy. *Biochem. Pharmacol.* **88**, 540-547 (2014).
120   Gatz, M. *et al.* Role of genes and environments for explaining Alzheimer disease. *Arch. Gen. Psychiatry* **63**, 168-174 (2006).
121   Sanders, D. W. *et al.* Distinct tau prion strains propagate in cells and mice and define different tauopathies. *Neuron* **82**, 1271-1288 (2014).

CHAPTER 6
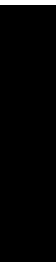
7

Summary - Samenvatting

In 2015 almost 50 million people worldwide suffered from dementia in which the performance of complex brain tasks gradually declines. In advanced stages patients need help with basic activities of daily living, which has an enormous socioeconomic impact. The underlying processes involved in complex tasks of the brain are organized by neuronal networks. Specialized structures called synapses are responsible for communication between neurons and networks.

The most common form of dementia is Alzheimer's disease (AD), which is a neurodegenerative disorder characterized by abnormal protein deposition in the brain and synaptic deficits. Extracellular aggregation of beta amyloid (plaques) and intracellular tangles of tau protein (neurofibrillary tangles) develop in the cortex and hippocampus (an important brain area involved in memory) in particular. The distribution of tau pathology in time and space correlates well with nerve cell degeneration and cognitive decline. Other neurodegenerative disorders called tauopathies show similar tau pathology.

The low accessibility of live human neurons for research forces researchers to use and develop representative models. Animal models have been indispensable for the current knowledge about the human brain, but the complexity of the human brain can hardly be mimicked. Despite the prevalence and high socioeconomic impact of these cognitive disorders there is inadequate knowledge about disease onset and mechanisms and no disease-modifying treatments are available. Most experts agree about the involvement of complex interactions between genetic and environmental factors in tauopathies, but clinical trials are afflicted by high attrition rates. Therefore, new research methods and therapeutic strategies have to be tested. The recent generation of pluripotent stem cells from human somatic cells enables the differentiation of patient-derived cells to almost all relevant cell types. This way, human neurons containing the complete genetic background of a patient can be studied *in vitro*. The aim of this thesis is exploration of the opportunities to use these human neuronal cells as a model for cognitive disorders, with tauopathies as a specific application.

The results of this thesis show a robust and reproducible differentiation protocol from stem cells towards human functional neuronal networks *in vitro*. Using various imaging based approaches networks were characterized further. Starting from this protocol two tauopathy models were proposed and neuronal networks were studied. In addition to the development of tau aggregation, other tauopathy-related phenotypes were identified which might be used for research concerning onset and progression of tau pathology and possible treatment options.

The presented data in this thesis show the potential to use the recently developed human stem cells to study processes involved in human brain function. The combination of different approaches seems inevitable, but comparison of this technology with previously described animal models can possibly replace animal studies and bridge the gap with the clinical manifestation of disease.

In 2015 leden wereldwijd bijna 50 miljoen mensen aan dementie, waarbij de mogelijkheid tot het uitvoeren van complexe taken door de hersenen geleidelijk afneemt. In vergevorderde stadia zijn patienten niet meer in staat om voor zichzelf te zorgen en dit heeft een enorme socio-economische impact. De complexe functies van het menselijk brein worden onder andere georganiseerd door connecties tussen individuele hersencellen, maar ook door neuronale netwerken. De communicatie tussen hersencellen verloopt via gespecialiseerde structuren, zogenoemde synapsen.

De meest voorkomende vorm van dementie is de ziekte van Alzheimer, een neurodegeneratieve ziekte gekenmerkt door de vorming van abnormale eiwit afzettingen in het brein en beschadiging van synapsen. Buiten de hersencellen ontstaan opeenhopingen van bèta amyloïd (plaques) en intracellulair ontstaan kluwens van het eiwit tau (neurofibrillaire kluwens). Met name de hersenschors en hippocampus (een hersengebied betrokken bij het geheugen) zijn aangedaan. Vooral de ophopingen van het eiwit tau correleren in tijd en locatie met neurodegeneratie en cognitieve achteruitgang. Andere neurodegeneratieve aandoeningen (tauopathiën) vertonen vergelijkbare vormen van tau pathologie.

Omdat levende menselijke neuronen nauwelijks toegankelijk zijn voor onderzoek, moet er gewerkt worden met representatieve modellen. Diermodellen hebben enorm bijgedragen aan de huidige kennis over het menselijk brein, maar de humane complexiteit kan moeilijk volledig worden nagebootst. Ondanks de prevalentie en de hoge socio-economische impact is er onvoldoende kennis over het ontstaan en de ziektemechanismen van veel van deze cognitieve aandoeningen en zijn er geen medicijnen beschikbaar waarmee de ziekten kunnen worden behandeld. De meeste experts zijn het er over eens dat tauopathie wordt veroorzaakt door een complex samenspel van genetische en omgevingsfactoren, maar klinische studies kampen met lage slagings-percentages. Daarom moeten nieuwe onderzoeksmethoden en therapeutische strategieën worden getest. Een recente ontwikkeling maakt het mogelijk patient-afgeleide cellen te bestuderen door somatische cellen te reprogrammeren tot pluripotente stamcellen welke vervolgens gedifferentieerd kunnen worden tot bijna elk relevant celtype. Hierdoor is het mogelijk om in vitro humane hersencellen te bestuderen met de volledige genetische achtergrond van de patient. Het doel van deze thesis is het onderzoeken van de mogelijkheden om deze humane hersencellen te gebruiken als model voor cognitieve aandoeningen, met specifieke aandacht voor tauopathiën.

De resultaten in deze thesis beschrijven een robuust en reproduceerbaar differentiatie protocol van stamcellen naar humane functionele neuronale netwerken *in vitro*. Door gebruik te maken van verschillende beeldvormings-technieken zijn de eigenschappen van deze netwerken verder gekarakteriseerd. Uitgaande van dit protocol werden twee tauopathie-modellen voorgesteld en neuronale netwerken werden bestudeerd. Naast de vorming van tau kluwens vonden we andere tauopathie-gerelateerde fenotypes die mogelijk gebruikt kunnen worden voor onderzoek naar de totstandkoming en voortgang van tau pathologie en de mogelijke manieren om de ziekten te behandelen.

De bevindingen van deze thesis laten zien dat het gebruik van de recent ontwikkelde humane stamcellen nieuwe mogelijkheden geeft om processen die zich afspelen in het menselijk brein te bestuderen. De combinatie van verschillende technieken lijkt onvermijdelijk, maar door de vergelijking te maken met eerder gebruikte diermodellen kan de technologie mogelijk leiden tot vervanging van diermodellen en een betere benadering van de klinische manifestatie van de ziektebeelden.

Scientific Curriculum Vitae

Jacobine Kuijlaars

Nieuwstraat 56
5571 BD Bergeijk
The Netherlands

jacobine_kuijlaars@hotmail.com

Education

1998 – 2005	Secondary education, SG Were Di Valkenswaard, The Netherlands
2005 – 2008	Biomedical Sciences BSc, Utrecht University, The Netherlands
2008 – 2010	Biomedical Sciences MSc, Utrecht University, The Netherlands Programme: Neuroscience and Cognition
2013 – 2017	Biomedical Sciences PhD, Physiology group BIOMED, Hasselt University and CNS department Janssen R&D Beerse, Belgium

Professional experience

2010 – 2012	Lab technician via VIB/KU Leuven at CNS department Janssen R&D, Beerse, Belgium Research project about the role of VEGF in depression.
2012 – 2013	Lab technician via Randstad Professionals at CNS department Janssen R&D, Beerse, Belgium Research project about the role of TNFα in depression.
2013 – 2017	PhD candidate at Hasselt University and CNS department Janssen R&D, Beerse, Belgium

List of publications

Steven Biesmans, Theo F. Meert, Jan A. Bouwknecht, Paul D. Acton, Nima Davoodi, Patrick De Haes, Jacobine Kuijlaars, Xavier Langlois, Liam JR. Matthews, Luc Ver Donck, Niels Hellings, Rony Nuydens (2013) Systemic immune activation leads to neuroinflammation and sickness behavior in mice. Mediators of inflammation. 2013:271359; doi: 10.1155/2013/271359.

Giulia Meneghello, An Verheyen, Max van Ingen, Jacobine Kuijlaars, Marianne Tuefferd, Ilse van den Wyngaert, Rony Nuydens (2015) Evaluation of established human IPSC-derived neurons to model neurodegenerative diseases. Neuroscience 301, p. 204-212.

Jan Detrez, Peter Verstraelen, Titia Gebuis, Marlies Verschuuren, Jacobine Kuijlaars, Xavier Langlois, Rony Nuydens, Jean-Pierre Timmermans, Winnok de Vos (2016) Image informatics strategies for deciphering neuronal network

connectivity. Advances in anatomy, embryology and cell biology - ISBN 978-3-319-28547-4 - 219, p. 123-148.

Jacobine Kuijlaars, Tutu Oyelami, Annick Diels, Jutta Rohrbacher, Sofie Versweyveld, Giulia Meneghello, Marianne Tuefferd, Peter Verstraelen, Jan R. Detrez, Marlies Verschuuren, Winnok H. De Vos, Theo Meert, Pieter J. Peeters, Miroslav Cik, Rony Nuydens, Bert Brône*, An Verheyen* (2016) Sustained synchronized neuronal network activity in a human astrocyte co-culture system. Scientific Reports 6, 36529; doi: 10.1038/srep36529. * contributed equally

Peter Verstraelen, Jan R. Detrez, Marlies Verschuuren, Jacobine Kuijlaars, Rony Nuydens, Jean-Pierre Timmermans, Winnok H. De Vos (submitted to Frontiers in Cellular Neuroscience) Dysregulation of microtubule stability impairs morphofunctional connectivity in cultivated neuronal networks.

Abstracts

Jacobine Kuijlaars, Patrick Vandormael, Cecilia Eklund, Frans Cornelissen, Bert Brone, Xavier Langlois, Rony Nuydens (2014) Implementation of calcium indicators to monitor network activity in vitro.
- *EURON workshop: New targets in neurodegenerative diseases: Emphasis on advances in Alzheimer's disease research. 31 August – 5 September 2014, Braga, Portugal (pitch talk).*

Jacobine Kuijlaars, Patrick Vandormael, Frans Cornelissen, Peter Verstraelen, Jan Detrez, Jean-Pierre Timmermans, Theo Meert, Xavier Langlois, Bert Brone, Rony Nuydens (2015) A toolbox to study synaptopathies in vitro.
- *EMBL Symposium: Mechanisms of Neurodegeneration. 14 - 17 June 2015, Heidelberg, Germany (poster presentation)*
- *School on Neurotechniques 2016: The toolbox for investigating the function of neural circuits. 15 – 19 February 2016, Padova, Italy (poster presentation).*

Jacobine Kuijlaars, Tutu Oyelami, Annick Diels, Sofie Versweyveld, Giulia Meneghello, Marianne Tuefferd, Peter Verstraelen, Jan Detrez, Marlies Verschuuren, Winnok de Vos, Theo Meert, Pieter Peeters, Miroslav Cik, Rony Nuydens, Bert Brône, An Verheyen (2016) Sustained synchronized neuronal network activity in a human astrocyte co-culture system.
- *Knowledge for Growth 2016. 26 May 2016, Ghent, Belgium (poster presentation).*

Dankwoord

Na 4 jaar aan dit project gewerkt te hebben ben ik blij met dit proefschrift als resultaat. Dit heb ik echter niet alleen volbracht en daarom zou ik graag via deze weg degenen die me hebben geholpen willen bedanken.

Graag wil ik mijn promoter prof. dr. Bert Brône bedanken voor de supervisie en coördinatie van dit project. Bert, bedankt voor het vertrouwen dat ik nagenoeg al het werk van mijn project mocht uitvoeren bij Janssen. De afstand tussen Beerse en Diepenbeek was dan misschien wel groot, maar ik mocht altijd langskomen of bellen. Dankzij jouw kritische kijk op de resultaten vanuit de fundamentele wetenschap in plaats van de benadering vanuit drug development heb ik een thesis geschreven waar ik trots op ben. Daarnaast wil ik mijn co-promoter bij Janssen, prof. dr. Theo Meert, bedanken voor zijn bijdrage aan dit proefschrift. Beiden bedankt voor de goede samenwerking tussen UHasselt en Janssen.

Een hele speciale 'dankjewel' voor mijn tweede co-promoter en dagelijkse supervisor dr. Rony Nuydens. Na het afronden van mijn master gaf jij mij de mogelijkheid om op het IWT-project bij Janssen te komen werken als laborant. Toen in 2012 een volgende IWT-project geschreven werd, heb je voor mij de mogelijkheid gecreëerd om me verder te ontwikkelen en hieraan als PhD kandidaat te beginnen. Rony, jouw kennis over microscopie, neurofysiologie en alle beschikbare technieken is enorm. Ik ben blij dat ik hierover veel van je heb kunnen leren. Bedankt voor je deskundige begeleiding, nieuwe ideeën, en goede collaboraties binnen je netwerk. Het was fijn dat ik altijd bij je binnen kon lopen met vragen of problemen. Bedankt voor de goede zorgen en mooie kansen die je me hebt gegeven.

Ik zou ook graag prof. dr. Hendrix, prof. dr. Lambrichts en prof. dr. Rigo willen bedanken voor het plaatsnemen in mijn doctoraatscommissie. Bedankt voor de opvolging van mijn doctoraat tijdens afgelopen 4 jaar en het verbreden van mijn blik op de resultaten door uw kritische commentaar. Daarnaast wil ik graag prof. dr. Ameloot en prof. dr. De Vos bedanken voor hun deelname in mijn doctoraatsjury en om mijn proefschrift kritisch na te lezen. Dr. Cowley, thanks a lot for being part of my jury and reading my thesis.

Beste An, zonder jou was dit proefschrift er misschien niet geweest. Jij hebt de IWT aanvraag mee geschreven wat de start was van dit project. En eigenlijk ben jij daarna degene geweest die al het werk met de iPSCs heeft gecoördineerd. Bij jou kon ik altijd terecht met praktische en wetenschappelijke vragen, al vanaf dat ik bij Janssen begon in 2010 heb ik heel veel van jou geleerd.

Daarnaast wil ik de rest van het iPSC team bedanken. Annick (en Danny), gelukkig hoefde ik niet al het celkweekwerk zelf te doen en kon ik altijd op jullie rekenen. Heel erg bedankt voor de hulp en gezelligheid!

En dan de collega's uit Antwerpen. Winnok, Peter, Jan, en Marlies, bedankt voor de beeldanalyse scripts, de snelle antwoorden op mijn vragen, de fijne samenwerking voor de mooie publicaties die we inmiddels hebben geschreven en bedankt voor jullie kritische blik op de projecten.

Hoewel ik de meeste tijd in Beerse heb doorgebracht wil ik ook graag de collega's van BIOMED in Diepenbeek bedanken voor de fijne sfeer op de dagen dat ik daar was. Patrick, zonder jou waren alle kloneringen en de optimalisatie van de tools in de eerste twee jaar van mijn doctoraat niet gelukt. Bedankt ook voor je kritische blik en de aangename samenwerking. Petra, van jou heb ik geleerd om te patchen (hoewel ik mijn skills niet echt verder heb ontwikkeld). Bedankt voor de gezellige babbels als ik op BIOMED was en de hulp als ik iets nodig had. Het onderwijsteam van Celcommunicatie/Celfysiologie wil ik graag bedanken voor de leuke lessen die ik in Diepenbeek heb mogen geven en de hulp die jullie daarbij hebben gegeven tijdens de voorbereidingen. Sophie, jij hebt veel stress voor mij ontnomen als er deadlines waren of als ik vragen had over het onderwijs of praktische zaken rondom mijn doctoraat. Heel veel succes met het afronden van jouw PhD project. Tot slot wil ik graag Stefanie en Veronique bedanken voor alle administratieve zaken rondom de Doctoral Schools en de afronding van mijn doctoraat.

Beste collega's van de afdeling Neuroscience bij Janssen, ook voor jullie een dikke merci. Bedankt voor de gezellige babbels, jullie interesse, de Belgische taal- en cultuurlessen, de hulp, en samenwerking in het lab. Bedankt ook aan de inmiddels vrij grote lunch-groep. Het was fijn om tussen de middag frustraties vanuit het lab kwijt te kunnen of gewoon te praten over iets anders dan het werk. Een aantal collega's wil ik graag nog specifiek noemen. Sofie, bedankt voor alle primaire culturen die je voor mij hebt gemaakt, ook al kwam mijn aanvraag soms pas op het laatste moment! Ines, bedankt om als collega in 'team Rony' altijd voor me klaar te staan. Tutu and Jutta, although I was supposed to be able to do some electrophysiology experiments myself, I am very happy that specialists like you helped me (even last minute) with the experiments for the paper. Dear Andreas, thank you for the collaboration on the iPSC project and your critical view on my work. Paula, Cindy en Ilse, bedankt voor alle bestellingen die jullie voor mij hebben gedaan! Hilde (en Leen en Mireille), hartelijk dank voor alle administratieve hulp die jullie de afgelopen 6,5 jaar hebben gegeven. Fijn dat ik met vragen altijd bij jullie kon binnenlopen. Tot slot nog een speciaal woordje voor de (oud)medebewoners van bureau 1K5. Astrid en Ingrid, hoewel jullie inmiddels zijn verhuisd wil ik jullie bedanken voor de rustige werkomgeving maar ook voor de mooie gesprekken die we altijd hadden. Daarvoor in de plaats kwamen Clara en Karolien. Bedankt voor de

gezellige en goede gesprekken en adviezen rondom mijn PhD project, proefschrift en de kleine die op komst is, vooral tijdens de laatste maanden waarin ik aan mijn bureau gekluisterd zat.

Naast degenen die direct betrokken waren bij mijn werk, wil ik ook graag vrienden en familie bedanken. Te beginnen met de (oud)-collega's, An, Eve, Lore en Liesbeth, die inmiddels vrienden zijn geworden. Hopelijk komen er nog heel veel doodles om weer een volgende koffieklets af te spreken. Familie en vrienden in Bergeijk, bedankt voor jullie interesse in mijn werk en de nodige ontspanning. Lianne, Emmely, Ischa en Eljo, bedankt voor de goede gesprekken over ons onderzoek, carrières en alle fijne dingen daar buiten, onder het genot van thee en heel veel lekkers. Dames uit Utrecht, jullie ken ik inmiddels al meer dan 10 jaar, vanaf het moment dat we aan de studie Biomedische Wetenschappen begonnen in Utrecht. Ook al zien we elkaar niet meer zo veel als toen, het voelt nog steeds zo vertrouwd en gezellig als toen. De borrels op zaterdag of zondag en de weekendjes weg, nu steeds vaker met de heren erbij, wil ik echt niet missen.

Sjef en Elly, wat is het fijn om elke dinsdagmiddag op tijd te "moeten" vertrekken van het werk om bij jullie aan tafel aan te mogen schuiven. Rik, Elvira en de mannen, bedankt voor alle mooie momenten die we nu al samen hebben mogen meemaken. Rudi, bedankt dat we de afgelopen jaren heel veel redenen hadden om weekendjes naar mooie bestemmingen in de bergen te boeken voor de nodige ontspanning.

Rick en Yvonne, jullie wil ik ook bedanken voor de gezelligheid in de Nieuwstraat en de hulp die altijd dichtbij was. Isolde, bedankt voor je interesse in mijn werk. Ik ben trots dat jij nu ook bent begonnen aan je promotie-project, heel veel succes en je weet dat je altijd bij mij om raad kan komen vragen. Bart, jij ook heel veel succes de komende jaren.

Pap en mam, wat ben ik blij dat jullie mij altijd hebben gesteund in wat ik graag wil doen, ook al is het niet altijd helemaal te volgen voor jullie. Bedankt voor alle hulp in en om huis, de interesse in mijn werk en de steun wanneer het nodig is. Jullie hebben me van vanalles ontzien, waardoor ik me op mijn werk kon focussen.

En last but not least, Hans, sorry voor al die vrijdagavonden waarop ik na een week hard werken op de bank in slaap viel. Je hebt mij altijd gesteund in wat ik doe en wil doen. Het is zo fijn om te zien dat jij trots op mij bent, ook al vind ik dat daar niet echt reden toe is. Inmiddels zijn we al heel wat jaren samen, maar het wordt nog elke dag beter. Jij bent mijn beste medicijn ;)